Functions of the translation factor eIF5A in cellular metabolism and transcriptional control

A dissertation submitted to qualify for the degree Doctor of Biomedicine and Biotechnology from Universitat de València

Marina Barba Aliaga

April, 2023

Supervisors:

Dr. Paula Alepuz Martínez and Dr. José Enrique Pérez Ortín

VNIVERSITAT DE VALÈNCIA

Dpto. Bioquímica y Biología Molecular

Instituto de Biotecnología y Biomedicina (Biotecmed)

Doctorado en Biomedicina y Biotecnología

PAULA ALEPUZ MARTÍNEZ, Doctora en Ciencias Químicas y Profesora Titular en el Departamento de Bioquímica y Biología Molecular de la Universitat de València,

y JOSÉ ENRIQUE PÉREZ ORTÍN, Doctor en Ciencias Biológicas y Catedrático en el Departamento de Bioquímica y Biología Molecular de la Universitat de València

INFORMAN:

Que Marina Barba Aliaga, graduada en Biotecnología por la Universidad Politécnica de Valencia ha realizado bajo nuestra dirección, el trabajo de Tesis Doctoral que lleva por título "Functions of the translation factor eIF5A in cellular metabolism and transcriptional control." Revisado el presente trabajo, expresan su conformidad para la presentación del mismo por considerar que reúne los requisitos necesarios para ser sometido a discusión ante el Tribunal correspondiente, para optar al título de Doctor en Biomedicina y Biotecnología con Mención Internacional por la Universitat de València.

Y para que conste, en cumplimiento de la legislación, firman el presente informe en Burjassot, a 26 de abril del 2023.

Fdo: Dra. Paula Alepuz Martínez

Fdo: Dr. José Enrique Pérez Ortín

Para la realización de esta Tesis Doctoral, Marina Barba Aliaga ha disfrutado de un contrato predoctoral FPU (referencia FPU17/03542) del Ministerio de Universidades.

Asimismo, este trabajo ha sido financiado por el Gobierno de España mediante los proyectos PID2020-120066RB-I00, PID2020-112853GB-C31 y BFU2016-77728-C3-3-P, y por la Generalitat Valenciana mediante los proyectos AICO-2020-086 y AICO-2019-088. Además, este trabajo se incluye dentro de la red de investigación europea TRANSLACORE Translational control in Cancer (COST Action CA21154).

A mis familias

AGRADECIMIENTOS

En estas líneas, me gustaría agradecer a todas las personas que se han cruzado en mi camino para hacer posible que esta tesis salga adelante y sin las cuales hubiese sido muy difícil conseguirlo.

En primer lugar, quisiera agradecer especialmente a mis directores de tesis, a los que admiro. Gracias a Paula y a José Enrique por abrirme las puertas de su laboratorio, por la confianza depositada en mí para la realización de esta tesis doctoral y por dedicar su esfuerzo y tiempo personal en la dirección de este trabajo. Paula, he disfrutado mucho trabajando a tu lado. Gracias por ayudarme en absolutamente todo y enseñarme todo lo que hoy sé. Gracias también por transmitirme tus ganas de luchar y animarme cuando me venía abajo. Para mí no solo has sido mi directora de tesis, sino también una persona en quien buscar consejo y apoyo en muchos otros ámbitos. José Enrique o como a mí me gusta llamarte, J.E, gracias por transmitirme tu pasión por la ciencia, por tener siempre respuestas para todo y por brindarme la oportunidad de crecer a tu lado tanto en lo profesional como en lo personal. Gracias a los dos por estar siempre al pie del cañón, por sacar tiempo para mí y por darme independencia para arriesgarme, cometer errores, aprender y mejorarme a mí misma.

No puedo olvidarme de agradecer a Pepe y a Toni por acogerme con los brazos abiertos en mis inicios y, sobre todo, por sacarme una sonrisa cuando más lo necesitaba.

A todos los profesores del departamento de Bioquímica y Biología Molecular que tanto me han ayudado estos últimos años, en especial a Maite Martínez, Inma Quilis, Patricia Casino, Lola Peñarrubia y Ana Perea por todos sus consejos. Gracias también a Juan Ramón Diosdado por haberme arreglado todo lo que no funcionaba y por solucionarme muchos problemas técnicos. Y, por supuesto, gracias a Mª Ángeles Tornero por ser un apoyo moral diario y por recordarme siempre que puedo con todo.

Gracias a todas las personas que han pasado por nuestro lab durante estos años. Gracias a María por darme una acogida tan cariñosa en mi primer año, y a mis compañeras Vanessa y Samoa por darme buenos momentos y poner las cosas siempre fáciles. Gracias a Lian por darme siempre su apoyo incondicional, su complicidad y su amistad. Este último año no hubiera sido lo mismo sin ti. También a todos los estudiantes que han pasado por aquí estos años, en especial, a Jorge, Javi, Tomás y Alba, por hacerme ver cuánto me gusta enseñar.

To Gaurav, thank you for being the best lab partner I could have ever wished for and for making these years so fun and special. I am extremely happy to have spent so much time by your side but even more to have you as my friend now.

To Brian Zid and his lab people specially to Yuko, Cynthia, Ximena and Juliette. Thank you for hosting me into your far, far away lab at UCSD and allow me to get into unknown worlds. Brian, thank you for your constant support and guidance and for showing me the meaning of

doing science for fun. My stay in San Diego was amazing thanks to you. A mis amigos Sonia, Quique y Rafa, gracias por hacer de esa estancia algo inolvidable.

A Paco, Sara, Raquel, Sheila, Marta y Cris gracias por haber compartido absolutamente todo. Todo lo que pueda escribir aquí se queda corto, pero gracias por todas las risas, cervezas, bailes y terapias grupales. Me habéis enseñado mucho y lo mejor que me llevo de estos años es, sin duda, la familia que hemos formado. Gracias por ser siempre mi temazo favorito en medio de tanto ruido.

Gracias a todos mis amigos por ser mi refugio. A Paula, Carlos, Celia, Irene y Elena por estar a mi lado desde siempre. A Paloma y Gigi, porque a pesar de no entender nada de lo que hago, siempre estáis para escucharme y apoyarme. Gracias a las dos por ser mi segunda familia y el oxígeno que muchas veces necesitaba.

A mi familia, a los que ya no están y en especial a mis padres por hacer de mí lo que hoy soy y por su eterno apoyo incondicional. Todo esto hubiera sido imposible sin vosotros. Gracias por intentar ayudarme siempre, hasta en lo que no podéis, y perdón por haber puesto las cosas difíciles en algunos momentos.

A todos los aquí mencionados, y muchos más, por haber sido la fuerza y el ánimo que flaqueaba en los momentos difíciles. ¡Muchísimas gracias a todos!

Preface

This dissertation was submitted in satisfaction of the requirements for the degree Doctor of Biomedicine and Biotechnology from Universitat de València and qualifies for an International Mention. This dissertation is structured in seven Chapters consisting of Introduction (1), Materials and Methods (2), four Chapters of Results and Discussion (3-6) and a General Discussion and Conclusions (7). As this thesis consists of both published and unpublished material, a detailed clarification for each chapter of results is provided for a better understanding of the scientific contribution.

Chapter 3 consists of published material as one research paper where the dissertation author is the primary author.

Chapter 4 consists of published material as two research papers and one additional review paper. The dissertation author is the primary author of the three publications.

Chapter 5 is currently being prepared for submission for publication. The dissertation author is the primary author of this material. The experimental work from this chapter was performed at Universitat de València and University of California San Diego (UCSD), where the dissertation author worked as a visiting PhD student for six months supervised by Dr. Brian M. Zid.

Chapter 6 consists of unpublished material.

Table of Contents

Table of Contents

LIST OF FIGURES

All schematic figures listed here were processed using BioRender software.

LIST OF TABLES

Abstract

Abstract

Eukaryotic translation initiation factor 5A (eIF5A) is an essential evolutionarily conserved protein with functions in the three stages of translation. eIF5A is codified by two similar but differentially expressed paralog genes, *TIF51A/TIF51B* and *EIF5A1/EIF5A2* in yeast and human respectively. Interestingly, eIF5A is the only known protein containing hypusine, an essential modification for its activity. Hypusination occurs post-translationally by the action of the two enzymes deoxyhypusine synthase (DHPS) and deoxyhypusine hydroxylase (DOHH). Once activated, eIF5A binds ribosomes to facilitate the translation of peptide motifs with consecutive prolines or combinations of prolines with glycine and charged amino acids. Beyond translation, eIF5A has been linked to other molecular functions and cellular processes such as nuclear mRNA export, proliferation, autophagy and apoptosis. The growing interest in eIF5A is related to its association with the pathogenesis of several diseases such as cancer, viral infection, diabetes and ageing. In this thesis we have used the model organism *Saccharomyces cerevisiae* and mammalian cell lines to gain fundamental knowledge on the functions of eIF5A in the cell. Here, we have identified and characterized two novel targets requiring eIF5A for translation, a new basic function for the factor and the molecular bases of the transcriptional regulation of the two eIF5A encoding genes.

Our results in yeast and mammalian cells demonstrated that hypusinated eIF5A is needed for the synthesis of mammalian collagen type I as translation stalls at collagenic tripeptide motifs, enriched in proline and glycine, under eIF5A deficiency. eIF5A inactivation by silencing RNAs or by DHPS inhibition reduced collagen I content and led to the retention of partially synthesized collagen I in the endoplasmic reticulum (ER), activating the ER stress response. The overproduction of collagen I protein in human hepatic stellate cells treated with the profibrotic cytokine TGF-β1 was found to be dependent on eIF5A. Therefore, the role of eIF5A as an anti-fibrotic agent is discussed here.

The transcriptional regulation of the two yeast eIF5A isoforms was investigated under different metabolic conditions. The gene expression of the two isoforms responded to the cellular energy demands and was found to be dependent on TORC1 and the heme-activated transcription factor Hap1. Under respiratory conditions, Hap1 induced *TIF51A* through direct binding to the promoter, while indirectly repressed *TIF51B* by inducing a set of transcription repressors. Conversely, when the respiration was impaired, Hap1 became a repressor to down-regulate *TIF51A* expression and, by reducing the level of *TIF51B* repressors, up-regulated the expression of this second eIF5A gene. Our results also demonstrated the essential role of the Tif51A isoform in the mitochondrial respiration. Indeed, depletion of Tif51A compromised respiratory growth and reduced oxygen consumption and mitochondrial membrane potential. A novel mechanism connecting eIF5A activity with mitochondria functions was revealed. We showed that eIF5A is required for the translation of the proline-rich region of Tim50, an essential protein of the TIM23 mitochondrial translocase complex that specifically recognizes mitochondrial protein precursors and mediates their import into mitochondria. Thus, eIF5A inactivation

inhibited mitochondrial protein import and caused non-imported precursors to aggregate in the cell, generating a specific mitochondrial stress response.

Finally, this work has uncovered a novel function of eIF5A at the transcription level. In addition to its cytoplasmic role in translation, eIF5A can be found in the nucleus and we showed that nuclear eIF5A participates in the transcriptional regulation of genes whose mRNAs require eIF5A for their translation. Although eIF5A had previously been found in the nucleus where it acts as a co-factor for specific viral mRNAs export, its function is not well understood. Our findings proved that eIF5A binds to chromatin and its absence increases the transcription of specific genes encoding proteins with eIF5A-dependent motifs, suggesting a transcriptional repressor effect on its targets. Therefore, our results indicated that eIF5A functions not only in translation but also in the control of mRNA synthesis to maintain protein homeostasis of its targets.

Glossary

+ Fe	Iron-sufficient condition
- Fe	Iron-deficient condition
α-SMA	α-smooth muscle actin
aa	Amino acid
ABC	ATP-binding cassette
ADP	Adenosine diphosphate
aIF5A	Archaeal initiation factor 5A
ALA	δ-aminolevulinate
ATF	Activating transcription factor
ATP	Adenosine triphosphate
BiP	Heavy chain binding protein
BPS	Bathophenanthrolinedisulfonic acid
BSA	Bovine serum albumin
CCCP	Carbonyl cyanide m-chlorophenyl hydrazone
cDNA	Complementary DNA
CDS	Coding sequence
ChIP	Chromatin immunoprecipitation
CHOP	C/EBO homologous protein
CHX	Cycloheximide
clonNAT	Nourseothricin
Col1a1	Collagen type I α1 chain
ColIV	Collagen type IV
COX	Cytochrome c oxidase, complex IV
CSD	Cold-shock domain
DAPI	4′,6-diamidino-2-phenylindole
DD	Dimerization domain
DFMO	Difluoromethylornithine
DHPS	Deoxyhypusine synthase
DMEM	Dulbecco’s modified Eagle medium
DMSO	Dimethyl sulfoxide
dNTPs	Deoxyribonucleoside triphosphates

DOHH	Deoxyhypusine hydroxylase
DTT	1,4-Dithiothreitol
ECM	Extracellular matrix
EDTA	Ethylenediaminetetraacetic acid
eEF	Eukaryotic elongation factor
EFP	Elongation factor P
eIF	Eukaryotic initiation factor
eIF5A	Eukaryotic translation initiation factor 5A
ER	Endoplasmic reticulum
eRF	Eukaryotic release factor
ERG	Ergosterol
ETC	Electron transport chain
FC	Fold change
FCS	Fetal calf serum
gDNA	Genomic DNA
G6PDH	Glucose-6-phosphate dehydrogenase
GAPDH	Glyceraldehyde-3-phosphate dehydrogenase
GC7	N^1-guanyl-1,7-diaminoheptane
GFP	Green fluorescent protein
Gly	Glycine
GRO	Genomic run-on
GRP	Glucose regulated protein
Hap1	Heme activated protein 1
HDAC6	Histone deacetylase 6
HIF-1α	Hypoxia-inducible factor 1 α
HIV-1	Human immunodeficiency virus type 1
HL	Half-life
HRM	Heme-responsive motif
HRP	Horseradish peroxidase
HSCs	Hepatic stellate cells
HSF1	Heat shock factor 1

HSP	Heat shock protein
hyp-eIF5A	Hypusinated eIF5A
IMS	Intermembrane space
IRE1	Inositol-requiring enzyme 1
kb	kilobase
kDa	kilodalton
LB	Lysogeny Broth
MDR	Multridrug resistance
MIA40	Mitochondrial intermembrane space import and assembly protein 40
MIM	Mitochondrial inner membrane
mitoCPR	Mitochondrial compromised import response
Mitoprotein	Mitochondrial protein
mitoTAD	Mitochondrial protein translocation-associated degradation
MM	Mitochondrial matrix
MOM	Mitochondrial outer membrane
mPOS	Mitochondrial precursor over-accumulation stress
MPP	Matrix processing peptidase
mRNA	Messenger RNA
mtDNA	Mitochondrial DNA
mtHSP	Mitochondrial heat shock protein
MTS	Mitochondrial targeting signal
NAC	Nascent chain-associated heteromeric complex
NGD	No-go decay
NLS	Nuclear localization signal
nLuc	Nanoluciferase
OD	Optical density
ODC	Ornithine decarboxylase
ONPG	Ortho-Nitrophenyl-β-D-galactopyranoside
ORF	Open reading frame
OXPHOS	Oxidative phosphorylation
P-body	Processing body

PAM	Presequence translocate-associated motor
PBS	Phosphate buffered saline
PCR	Polymerase chain reaction
PDI	Protein disulfide isomerase
PDR	Pleiotropic drug response
PEG	Polyethylene glycol
PERK	Pancreatic ER kinase
PI	PolyPro index
PKA	Protein kinase A
PNK	Polynucleotide kinase
Poly(A)	Polyadenylated
PolyPro	Polyproline stretch of more than two consecutive prolines
PPAR-γ	Peroxisome proliferator-activated receptor-gamma
PPI	Protein pause index
Pro	Proline
RA	RNA amount
RFP	Red fluorescent protein
RLU	Relative light unit
RNA Pol II	RNA Polymerase II
ROS	Reactive oxygen species
RPM	Repression module
RQC	Ribosome quality control
RQT	Ribosome QC trigger
RT-qPCR	Quantitative reverse transcription PCR
SAM	Sorting and assembly machinery
Sarkosyl	N-lauryl sarcosine sodium sulfate
SC	Synthetic complete medium containing glucose
SD	Standard deviation
SDH	Succinate dehydrogenase
SDS	Sodium dodecyl sulphate
SDS-PAGE	Sodium dodecyl sulphate polyacrylamide gel electrophoresis

SE	Standard error
SG	Stress granule
SGal	Synthetic complete medium containing galactose
siRNA	Silencing RNA
SPDS	Spermidine synthase
SPMS	Spermine synthase
SR	Synthesis rate
SSC	Saline sodium citrate
TANGO1	Transport and Golgi organization 1
TBS	Tris buffered saline
TCA	Tricarboxylic acid
TE	Tris Edta
TF	Transcription factor
TIM	Translocase inner membrane
TGF-β1	Transforming growth factor β1
TOM	Translocase outer membrane
TORC1	Target of rapamycin complex I
TR	Transcription rate
TRITC	Tetramethylrhodamine
tRNA	Transfer RNA
UPR	Unfolded protein response
UPRam	Unfolded protein response activated by mistargeting of proteins
UPRmt	Mitochondrial unfolded protein response
UTR	Untranslated region
WT	Wild-type
XBP1	X-box binding protein
Xpo	Exportin
YEP	Yeast extract-peptone
YNB	Yeast nitrogen base
YPD	Yeast extract-peptone-dextrose
YPEtOH	Yeast extract-peptone-ethanol

YPGal	Yest extract-peptone-galactose
YPGly	Yeast extract-peptone-glycerol

Chapter 1

Introduction

Eukaryotic initiation translation factor 5A (eIF5A) was discovered almost 50 years ago but is still enigmatic in many aspects. eIF5A is a small, ubiquitous and essential protein highly conserved across eukaryotes and archaea (Schnier *et al.*, 1991). eIF5A is a very abundant protein, it is found among the 100 most abundant proteins in *Saccharomyces cerevisiae* with approximately 273000 copies per cell, almost twice the number of ribosomes (approximately 187000 per cell) (Kulak *et al.*, 2014).

Originally isolated from ribosomal high-salt washes of rabbit reticulocytes, eIF5A was classified as a translation initiation factor based on its ability to stimulate the synthesis of methionyl-puromycin, a model assay for the first peptide bond formation (Kemper *et al.*, 1976; Benne and Hershey, 1978). At present, several subsequent reports have indicated that eIF5A main role is to promote translation elongation and to assist in termination (Jao and Chen, 2006; Zanelli *et al*, 2006; Gregio *et al.*, 2009; Saini *et al.*, 2009; Gutierrez *et al.*, 2013; Pelechano and Alepuz, 2017; Schuller *et al.*, 2017).

After decades of research, the secrets of eIF5A hypusine modification and its significance in eukaryotic life and human health are still being deciphered. It is now known that eIF5A is involved in different biological functions and participates in various human pathological conditions. For this reason, studying the molecular mechanisms by which eIF5A exerts physiological functions is important for dealing with human diseases and for the development of medical treatments.

1.1 The unique features of eIF5A

1.1.1 General features

Translation is the process by which the genetic information contained in the messenger RNA (mRNA) molecules is read by ribosomes to produce new proteins. Translation can be divided into three phases: initiation, elongation and termination. In the first step, eukaryotic initiation factors (eIFs) guide the ribosome assembly at the start codon with an initiator methionyl-tRNA bound in the P site. During elongation, ribosomes move along the mRNA, three nucleotides per step, and synthesize the encoded protein through the coordinated actions of eukaryotic elongation factors (eEFs) and aminoacyl-tRNAs. Finally, when ribosomes encounter a termination codon, eukaryotic peptide chain release factors (eRFs) promote the release of the nascent chain from the peptidyl-tRNA and the ribosome complex is dissociated into 40S and 60S subunits to begin a new round of translation.

Translation factors assist the three stages of protein synthesis. They interact with ribosomes and other components of the translation machinery and play key roles in promoting the different stages of protein synthesis. Some of these factors, rather than stimulating general protein synthesis, have specialized roles to facilitate the translation of specific mRNAs, as it is the case for the translation factor eIF5A (Kemper *et al.*, 1976; Benne and Hershey, 1978). Increased evidence supports its predominant role in elongation rather than initiation, as eIF5A inactivation stabilizes polysomes in the absence of cycloheximide and increases the average ribosomal transit time (Gregio *et al.*, 2009; Saini *et al.*, 2009). According to more recent findings, eIF5A is also involved in the termination stage through the stimulation of hydrolysis of peptidyl-tRNA catalysed by the termination factor eRF1 (Schuller *et al.*, 2017). The excess of eIF5A molecules over ribosomes agrees with the notion that eIF5A participates in most translation events. At present, eIF5A is primarily known as a translation elongation factor which promotes translation of

sequences rich in prolines and other problematic amino acids that stall the ribosome (Gutierrez *et al*., 2013; Pelechano and Alepuz, 2017; Schuller *et al*., 2017).

eIF5A is an essential protein and one of the few universally conserved translation factors (Figure 1.1). eIF5A shows an archaeal homolog (aIF5A) with strong similarity to eIF5A and a bacterial distant ortholog named elongation factor P (EF-P). Crystal structures from a variety of bacteria, archaea and eukaryotes have been solved and proteins show structural similarities (Kim *et al*, 1998; Peat *et al*, 1998; Yao *et al*, 2003; Hanawa-Suetsugu *et al*., 2004; Tong *et al*, 2009). This suggests a certain functional conservation among the eubacterial, archaeal and eukaryotic proteins in their role in protein synthesis.

eIF5A is in the top 50 highest expressed genes and among the 100 most abundant proteins in yeast cells (Kulak *et al*., 2014). Most eukaryotes express two eIF5A protein isoforms, which are highly conserved and differentially expressed (Jenkins *et al*., 2001). In yeast, the two isoforms are encoded by *TIF51A* (*HYP2*) and *TIF51B* (*ANB*1) genes. These two paralog genes encode proteins of 157 amino acid residues which share 90% sequence identity (15 non-identical and 7 non-similar amino acids) and >60% identity with human eIF5A (Figure 1.1) (Schnier *et al*., 1991). The expression of the two forms is reciprocally regulated by oxygen, being *TIF51A* preferentially expressed under aerobic conditions while *TIF51B* is exclusively expressed under anaerobic conditions (Lowry *et al*., 1986). Thus, Tif51A isoform is usually referred to as eIF5A in the context of *S. cerevisiae*.

In mammals, eIF5A is encoded by *EIF5A1* and *EIF5A2* paralog genes. *EIF5A1* encodes a protein of 154 amino acid residues while *EIF5A2* of 153 amino acids. Both proteins share 82% sequence identity (Figure 1.1). The isoform *EIF5A1* is constitutively expressed in all cells and tissues whereas *EIF5A2* is usually undetectable, except in a limited number of tissues (brain and testis) and certain cancer cells where it is highly expressed (Clement *et al*., 2006; Ning *et al*., 2020). Here, eIF5A1 is usually referred to as eIF5A in the context of higher eukaryotes.

Figure 1.1. Evolutionary homologs of eIF5A. Amino acid sequence alignment of genes encoding EF-P in *E.coli* (Ec-EF-P), eIF5A in archaeal *Saccharolobus solfataricus* (Ss – aIF5A), eIF5A in *Drosophila melanogaster* (Dm-eEF5), homologs Tif51A and Tif51B in *S. cerevisiae* (Sc) and eIF5A1 and eIF5A2 in *Homo sapiens* (Hs). Residues with an asterisk are conserved in all organisms and residues in purple are identical only in the eukaryotic eIF5A shown here. The 12 amino acid residues surrounding the lysine residue that becomes hypusinated (indicated by an arrow) are identical in all eukaryotic eIF5A homologs and is marked by a box.

1.1.2 Hypusine and other modifications

Remarkably, eIF5A is the sole protein in nature containing the unusual amino acid hypusine [N^{ε}-(4-amino-2-hydroxybutyl)-lysine] (Shiba *et al.*, 1971; Park *et al.*, 1981). Hypusination occurs post-translationally and exclusively in a specific lysine residue (Lys51 in yeast and Lys50 in human eIF5A) through the consecutive action of the key enzymes deoxyhypusine synthase (DHPS) and deoxyhypusine hydroxylase (DOHH). In the first step, DHPS conjugates the 4-aminobutyl group from the polyamine spermidine to the ε-amino group of the specific lysine residue of the eIF5A precursor. This generates the intermediate reaction deoxyhypusine, which does not accumulate and is irreversibly hydroxylated by DOHH, which converts the deoxyhypusine residue to hypusine (Park *et al.*, 2018). The hypusine-containing eIF5A is the biologically active and mature form of eIF5A (Figure 1.2). Consequently, intracellular hypusinated eIF5A correlates to eIF5A cellular activity.

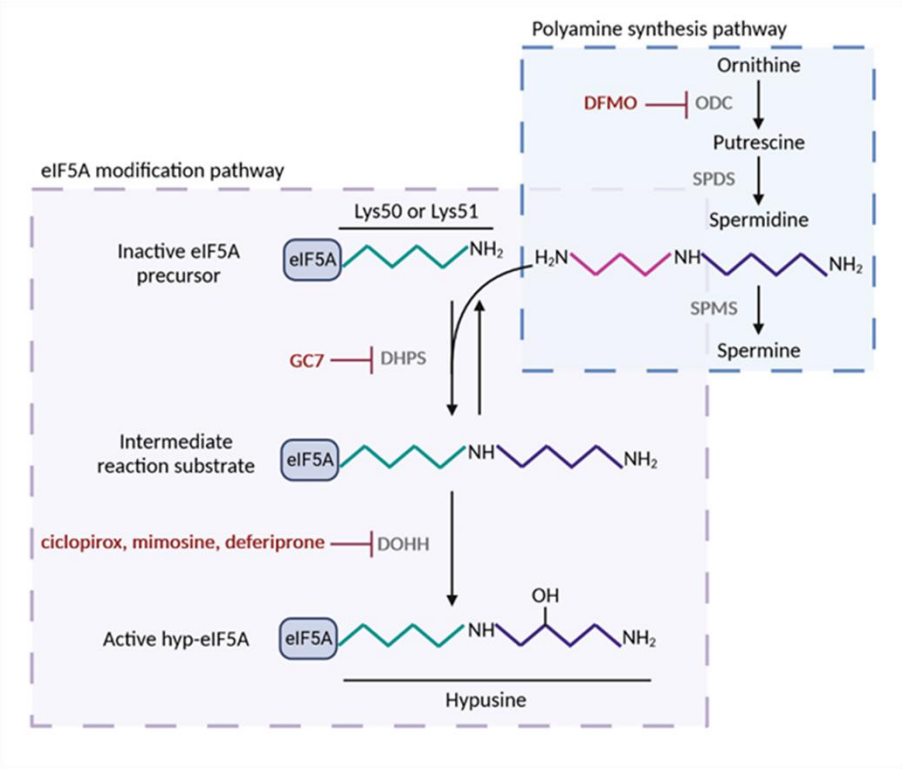

Figure 1.2. Polyamine-hypusine pathway and its pharmacological inhibitors. Spermidine substrate for eIF5A hypusination is obtained by the conversion of the polyamine ornithine in putrescine by the enzyme ornithine decarboxylase (ODC); spermidine is synthesized from putrescine by spermidine synthase (SPDS). Alternatively, spermidine is converted in spermine by spermine synthase (SPMS). Hypusine modification of Lys50 (human) or Lys51 (yeast) residue of eIF5A occurs by the addition of spermidine in two consecutive enzymatic reactions. First, deoxyhypusine synthase (DHPS) transfers the aminobutyl group of spermidine to the amino group of lysine, generating an intermediate substrate which does not accumulate. Second, deoxyhypusine hydroxylase (DOHH) adds a hydroxyl group and forms the hypusine residue of eIF5A, which confers the activity to the protein. Post-translational modification of eIF5A can be suppressed by inhibitors of DHPS and DOHH, as the commonly used competitive inhibitor of DHPS GC7 (N1-guanyl-1,7-diaminoheptane), but also by inhibition of ODC.

The hypusine synthesis pathway occurs in both archaea and eukaryotes. The two enzymes for hypusine synthesis (DHPS and DOHH) are highly conserved across eukaryotes and show high specificity for eIF5A, underscoring a vital function of eIF5A and its modification enzymes. DHPS is essential to all eukaryotes while DOHH to most of them (Park *et al.*, 2018). Besides, the lysine residue that is post-translationally modified to hypusine and the sequence flanking this site of hypusine modification are also highly conserved among archaea and eukaryotes (Figure 1.2) (Wolff *et al.*, 2007). However, bacterial EF-P is modified in a different way as DHPS and DOHH homologs are absent. Lys34 of EF-P is β-lysinilated instead and this modification is critical for EF-P activity (Aoki *et al.*, 2008).

Hypusination occurs irreversibly and is critical for eIF5A function and cell viability. However, partially modified deoxyhypusine eIF5A is functional in yeast, but not in higher eukaryotes, where the DOHH gene is essential (Park *et al.*, 2006). In fact, partially hypusinated isoform of eIF5A allows yeast cells to grow under normal conditions but it is no longer capable to perform specific cellular functions (Li *et al.*, 2014).

Considering the essential nature of this modification, hypusination is known to be one of the most critical functions of polyamines in cell growth and survival (Chattopadhyay *et al.*, 2008; Hyvönen *et al.*, 2012). Polyamines, including spermidine, are ubiquitous and essential for cell growth. These molecules interact with nucleic acids, acidic proteins and phospholipids and regulate a wide range of cellular activities at many levels (see review Igarashi and Kshiwagi, 2015). Therefore, polyamines are vital for cell growth, proliferation, differentiation and apoptosis although the molecular bases of their requirement are not fully understood. Among them, spermidine has an independent function as a source of hypusine although only a small fraction (1-2%) of it is metabolized to hypusine (Chattopadhyay *et al.*, 2008).

Although no inhibitors acting directly on eIF5A exist, its activity can be suppressed using compounds that inhibit DHPS and DOHH enzymes, separately or in combination with others (Figure 1.2). Pharmacological inhibition of eIF5A activity can be achieved by means of DHPS inhibitors such as GC7 (N1-guanyl-1,7-diaminoheptane), deoxyspergualin or semapimod; DOHH inhibitors such as ciclopirox, deferiprone or mimosine; or inhibitors of spermidine synthesis such as DFMO (difluoromethylornithine). Among them, GC7 is a spermidine analog and the most potent inhibitor of DHPS (K_i value for GC7, 0.01 μM, compared to K_m for spermidine, 4.5 μM) (Jakus *et al.*, 1993).

Even though eIF5A mainly exists in its hypusine-containing form, it is also phosphorylated and acetylated. Phosphorylation occurs in the Ser2 residue of the yeast protein (Klier *et al.*, 1993) and is not essential for cell viability or protein synthesis. In fact, the specific function of this post-translational modification remains unclear. Acetylation occurs in the Lys47 residue of yeast and mammalian eIF5A by acetyl transferase PCAF. Unlike hypusination, acetylation is a reversible modification catalysed by HDAC6 and SIRT2 deacetylases (Ishfaq *et al.*, 2012). Although occurring in close but different residues, hypusination and acetylation are mutually exclusive. Therefore, acetylation is only possible for unmodified eIF5A but not for hypusinated eIF5A. The role of acetylation remains unclear too but, importantly, it affects the intracellular localization of eIF5A in mammalian cells (Ishfaq *et al.*, 2012). Although eIF5A lacks a conventional nuclear import signal, acetylated eIF5A (least abundant form) accumulates in the nucleus whereas hypusinated eIF5A (most abundant form) is found in the cytoplasm (Lee *et al.*, 2009; Ishfaq *et al.*, 2012); suggesting that acetylation negatively regulates eIF5A activity in translation.

1.1.3 Mode of action in translation elongation

During translation elongation, ribosomes are faced with the challenge of forming 400 different peptide bonds and, although capable of making them all, not all reactions are equally favourable. Certain amino acids are classified as poor donors or acceptors as their peptide bonds are less efficiently formed. Among them, proline is considered as both poor peptidyl donor and poor peptidyl acceptor for the transferase reaction (Pavlov *et al.*, 2009). The fact that proline is a secondary amine (reactive nitrogen is found within a five-membered ring) explains its poor reactivity as an acceptor. Besides, its rigid geometric structure generated by the cyclic side chain creates entropic constraints and explains its slow kinetics as a donor (Pavlov *et al.*, 2009; Saha and Shamala, 2012). These two features combine to make the synthesis of Pro-Pro bonds slow, causing the ribosome to stall. Therefore, when peptide bond formation is slow, the E site tRNA naturally dissociates and the remaining unoccupied E site functions as a sensor for translation arrest. Both EF-P and eIF5A proteins are small and structurally resemble tRNA (Hanawa-Suetsugu *et al.*, 2004). EF-P and eIF5A bind strongly to the E site and rescue similarly stalled complexes (Rossi *et al.*, 2016).

eIF5A only binds to ribosomes in a hypusine-dependent manner (Zanelli *et al.*, 2006; Gutierrez *et al.*, 2013). eIF5A lies in the E site and extends its hypusine unstructured loop protruding from the N-terminal domain close to the acceptor stem of the P site tRNA. The hypusine moiety is then positioned proximal to the CCA-end of the peptidyl-tRNA and then, eIF5A stabilizes the conformation of the peptidyl-tRNA and promotes the proper alignment of substrates, enabling peptide bond formation between poor substrates (Melnikov *et al.*, 2016; Schmidt *et al.*, 2016). Therefore, eIF5A enhances peptide bond formation between consecutive proline residues (Gutierrez *et al.*, 2013) (Figure 1.3). Similarly, EF-P binds to the E site in a β-lysine-dependent manner and contacts the peptidyl-tRNA to stabilize an optimal geometry (Blaha *et al.*, 2009). Therefore, EF-P and eIF5A favour peptide bond formation at consecutive proline residues and alleviate ribosome stalling (Ude *et al.*, 2013; Doerfel *et al.*, 2013; Gutierrez *et al.*, 2013).

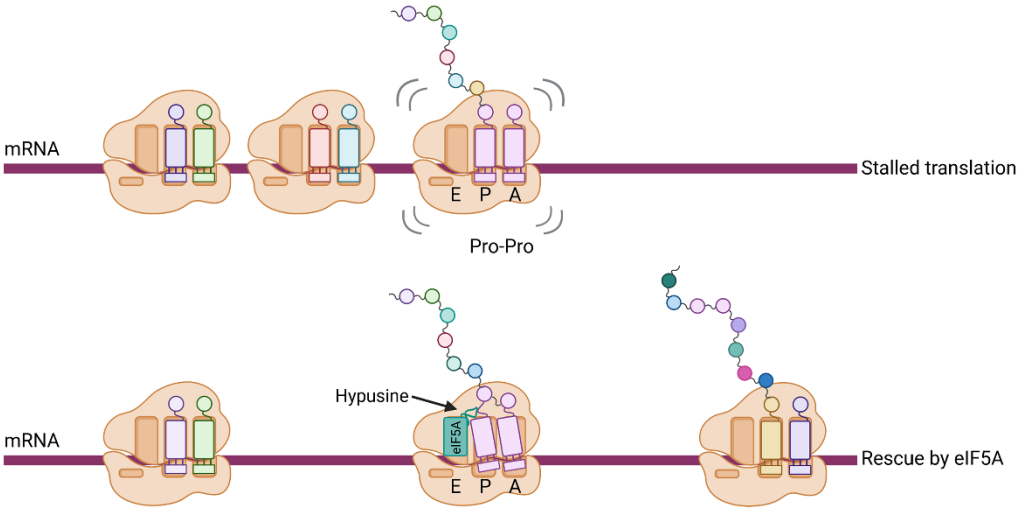

Figure 1.3. eIF5A function in the synthesis of Pro-Pro bonds. Under eIF5A deficiency, the peptide synthesis stalls in codons for two consecutive prolines with the A site containing the charged aminoacyl-tRNA (top). Binding of eIF5A to the E site positions the hypusine residue towards the acceptor stem of the P site peptidyl-tRNA, which favours a proper conformation for the synthesis of the peptide bond (bottom).

Recent studies have helped to elucidate the full range of amino acids and sequence motifs or triplets that require eIF5A for their efficient translation. The use of ribosome profiling (Schuller *et al.*, 2017) and 5PSeq (Pelechano and Alepuz, 2017) revealed considerable pausing at a wide spectrum of amino acid motifs (Table 1.1), including those containing proline but also glycine and charged amino acids (arginine, lysine, aspartic and glutamic). In fact, positively charged amino acids are believed to slow translation due to their interaction with the negatively charged ribosome exit tunnel (Charneski and Hurst, 2013). Notably, combinations of these problematic amino acids dramatically impair protein synthesis and establish a dependency on eIF5A for their translation.

Table 1.1. Top 43 tripeptide motifs associated with eIF5A-dependent ribosome pausing in *S. cerevisiae*. Individual strength pause values were extracted from 5PSeq analysis performed in Pelechano and Alepuz, 2017.

Tripeptide	Strength pause value	Tripeptide	Strength pause value
KPP	8.982	VPP	3.856
PPP	7.032	KPD	3.815
PGW	6.410	DYG	3.784
PPN	5.992	EGP	3.705
PPD	5.970	DDP	3.661
PDP	5.738	IPP	3.657
DPG	5.062	RYK	3.590
EPP	4.699	APP	3.499
PGG	4.672	DNP	3.438
DPP	4.636	GGQ	3.413
PPI	4.607	DPD	3.410
WKA	4.435	DRG	3.309
PGP	4.431	GWK	3.274
APD	4.395	DVG	3.183
KPG	4.324	PPG	3.014
PPL	4.256	LPP	2.848
PDI	4.233	GGA	2.827
PDG	4.195	DEG	2.780
EPG	4.193	GGG	2.631
QPP	4.143	KLK	2.367
RPP	3.955	RLK	2.365
PPA	3.912		

Many different proline-rich regions occur widely in eukaryotic proteins (Mandal *et al*., 2014) and have functional and structural roles in different cellular processes. In yeast, 12% of genes contain stretches of three or more consecutive proline residues while in humans 24% of genes contain at least three consecutive prolines. As the frequency of proline-rich motifs increases with biological complexity of eukaryotic organisms, this suggests the importance of proline-rich proteins and eIF5A for their translation across eukaryotic evolution. Proline-rich regions show unique structural features to form poly-L-proline type II helixes for example. This structure is usually located in disordered regions and allows a highly specific binding for other molecules. It is a structural element of fibrillar proteins and is functionally significant for protein-nucleic acid interactions (Mandal *et al.*, 2014). From here on and during all this thesis, repeats of three or more consecutive prolines are named polyPro regions.

1.1.4 Molecular functions

eIF5A mainly assists in the translation of only a subset of the overall mRNA population, which is its distinctive feature. In connection to its main role in translation, eIF5A can also be co-localized with endoplasmic reticulum (ER) where is associated to ribosomes bound to ER membrane and facilitates the co-translational translocation of some proteins into the ER (Shi *et al.*, 1996; Valentini *et al.*, 2002; Rossi *et al*., 2014). In this way, blocking eIF5A activation up-regulates the stress-induced chaperones in yeast (Rossi *et al.*, 2014) and leads to ER stress in mammalian cells (Mandal *et al.*, 2016).

However, there is a number of studies indicating that eIF5A is involved in processes that are not directly related to protein synthesis (Figure 1.4). eIF5A structural features suggest a potential to interact with nucleic acids. The C-terminal domain resembles the CSD (cold-shock domain), common in DNA and RNA-binding proteins, while the N-terminal carries the hypusine residue, which contains two positive charges and resembles spermidine, a molecule known to interact specifically with DNA or RNA. In this way, eIF5A has been reported to bind to some RNA molecules in a sequence specific manner (Xu *et al.*, 2004), although this function remains poorly understood. This is in line with findings linking eIF5A to assist with the transport of newly generated mRNAs from nucleus to cytoplasm (Xu *et al.*, 2011; Aksu *et al.*, 2016). Moreover, eIF5A mutants show a considerable impact on the balance between mRNA recruitment to ribosomes for translation and its degradation, pointing to a function of eIF5A in the steps of mRNA decay downstream of decapping (Zuk and Jacobson, 1998; Valentini *et al.*, 2002). Archaeal IF5A has also been described to play a role in RNA metabolism as a protein that associates with the ribosomes for translation but also exerts RNAse activity (Bassani *et al.*, 2019). Therefore, eIF5A seems to be a protein implicated in different steps of RNA metabolism, including both translation and degradation.

As previously stated, eIF5A assists the translation of a part of the global mRNA population and shows specific targets which contain critical motifs in their amino acids sequences. eIF5A plays a key role in many cellular processes due to the broad spectrum of cellular functions that their known direct targets present (Figure 1.4). The major implication resides in cell proliferation and animal development. eIF5A and its hypusination are essential for cell proliferation in eukaryotes and disruption of eIF5A or DHPS genes as well as inhibitors of DHPS cause growth arrest and strong anti-proliferative effects including apoptosis (Hanauske-Abel *et al.*, 1994; Chen *et al.*, 1996; Park *et al.*, 1997; Clement *et al.*, 2002;

Nishimura *et al.*, 2012; Sievert *et al.*, 2014; Levasseur *et al.*, 2019; Padget *et al.*, 2021). Additionally, eIF5A has been found critical for the induction and formation of cytoplasmic stress granules (SGs) in mammalian cells (Li *et al.*, 2010), which are formed in response to cellular stress that stalls translation initiation. In this way, eIF5A promotes the co-localization of aggregation proteins such as TDP-43 to SGs following arsenite treatment (Smeltzer *et al.*, 2021). eIF5A also mediates efficient autophagy in mammals via translation of the polyPro-containing autophagy master transcription factor TFEB and the ATG3 protein, which is involved in the lipidation of LC3B and formation of the autophagosome (Lubas *et al.*, 2018; Zhang *et al.*, 2019). Additionally, eIF5A plays an important role in cytoskeleton organization and cell shape (Zanelli and Valentini, 2005; Chatterjee *et al.*, 2006; Nguyen *et al.*, 2015). This is done through the translation of formins in eukaryotes. In yeast, eIF5A is needed for the translation of the polyPro-containing formin Bni1, involved in polarized growth during mating (Li *et al.*, 2014). Accordingly, a mechanistic connection has also been demonstrated between eIF5A and Diaphanous, the formin involved in actin-rich cable assembly during embryonic dorsal closure of *Drosophila* and migration of neural-stem cells (Muñoz-Soriano *et al.*, 2017). Thus, eIF5A has also been described to promote cell migration, invasion, and metastasis by controlling the expression of a set of key signalling molecules including RhoA and Rho-associated kinase, two cytoskeleton-regulatory proteins involved in promoting cell migration and metastasis (Fujimura *et al.*, 2015); by directly regulating MYC biosynthesis at specific pausing sites (Coni *et al.*, 2020); and by promoting the epithelial-mesenchymal transition (Xu *et al.*, 2013). eIF5A has also been implicated in regulating apoptosis but the mechanism involved seems tangled since this function appears opposite to the promotion of proliferation (Li *et al.*, 2004; Tan *et al.*, 2010; Caraglia *et al.*, 2013). Recently, it was found that eIF5A controls translation of the tumour suppressor and pro-apoptotic p53 gene expression, which contains polyPro motifs sensitive to the action of eIF5A (Martella *et al.*, 2020) and works as a transcription factor in charge of triggering a variety of antiproliferative programmes. This thesis further describes new molecular functions and direct targets of the translation factor eIF5A.

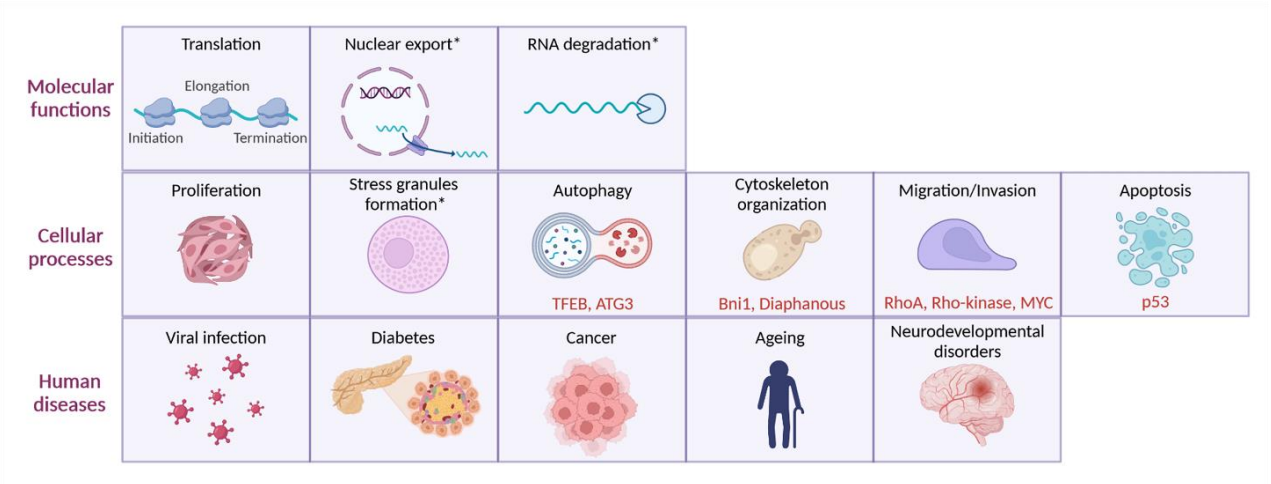

Figure 1.4. Molecular functions of eIF5A and cellular processes and diseases in which it is involved. Molecular functions of the translation factor eIF5A are highlighted at the top. eIF5A is involved in the three stages of translation and in other RNA metabolism-related functions. Asterisks indicate functions and processes in which the eIF5A function is not known in detail. Cellular processes directly related to translation of specific proteins containing eIF5A-dependent motifs are shown in the middle. eIF5A targets for their translation are shown in red letters. Human diseases in which eIF5A is involved are shown at the bottom.

1.1.5 Implications in human diseases

The essential role eIF5A plays in the stated cellular processes makes this protein to be implicated in the pathogenesis of a wide variety of human diseases including retroviral infection, diabetes, cancer, ageing and neurological disorders (Figure 1.4).

Increasing evidence suggests that eIF5A can play an important role in modulating virus replication. It has been defined as an essential co-factor of the human immunodeficiency virus type 1 (HIV-1) Rev transport factor. Through specific Rev binding, it participates in the translocation of unspliced viral mRNAs across the nuclear envelope (Ruhl *et al*., 1993) and can behave as a nucleocytoplasmic shuttle protein (Rosorius *et al.*, 1999). In this context, eIF5A was reported to interact with the mammalian nuclear exportin 1 (Xpo1/CRM1) (Rosorius *et al.*, 1999), and more recently, with exportin 4 (Xpo4) (Lipowsky *et al.*, 2000; Aksu *et al.*, 2016). Although HIV was the first virus suggested to require eIF5A, this factor also participates in the replication of other viruses such as the Marburg virus and Filoviruses Ebola virus (Olsen *et al.*, 2016).

A second human pathogenesis with a well-defined link to eIF5A is diabetes. Hypusinated eIF5A is expressed in mouse pancreatic islet β-cells and is responsible for the translation of cytokine induced transcripts as well as for the activation and proliferation of T helper cells in mouse models of diabetes (Maier *et al.*, 2010; Tersey *et al.*, 2014; Levasseur *et al.*, 2019).

As mentioned before, human eIF5A is encoded by two paralogous genes: *EIF5A1* and *EIF5A2*, which are expressed under different conditions. *EIF5A1* is ubiquitously expressed in all mammalian tissues and cell types, whereas *EIF5A2* shows restricted expression in healthy tissue, being almost undetectable, but is overexpressed in certain tissues or cancer cells. Overexpression of both eIF5A isoforms has been observed in several tumours and triggers cell migration, invasion, and cancer metastasis (see review Ning *et al.*, 2020 for details). As previously mentioned, eIF5A controls the translation of cancer-related proteins including the migration proteins RhoA and Rho-associated kinase, the oncogene MYC but also the tumour suppressor p53. Thus, the mechanism via which eIF5A functions in cancer is unclear as it seems to control proteins that promote and supress cancer. *EIF5A1* is overexpressed under the control of the myc oncogene (Coller *et al.*, 2000; Boon *et al.*, 2001) in some cancer tissues such as glioblastoma or adenocarcinomas of different localizations (Cracchiolo *et al.*, 2004; Mathews and Hershey, 2015; Nakanishi and Cleveland, 2016). While *EIF5A1* resides in a stable region of chromosome 17, *EIF5A2* resides in a region of chromosomal instability of chromosome 3 (3q26.2) and thus, can be subjected to changes in expression. Amplification and overexpression of this later gene are frequently associated with different cancer tissues such as ovarian, colorectal, bladder or liver, and can cause cellular transformation and metastasis (Guan *et al.*, 2001; Clement *et al.*, 2006; Xie *et al.*, 2008; Yang *et al.*, 2009; Tang *et al.*, 2010). Therefore, *EIF5A2* is the isoform considered as a potential oncogene and a diagnostic or prognostic marker (Jenkins *et al.*, 2001; Clement *et al.*, 2006) as its high expression is associated with poor survival, advanced disease stage, poor response to chemotherapeutic drugs and metastasis.

Inhibition of enzymes from the hypusine pathway provides the possibility of pharmacological control of eIF5A activity and therefore, opens opportunities in the clinic field. DFMO and GC7 treatments impair viral transcription and translation of Ebola virus (Olsen *et al*., 2016). Treatment with GC7 also improves glucose intolerance, insulin release and reduces β-cell mass loss (Maier *et al*., 2010; Robbins *et al*., 2010). GC7, used alone or in combination with other compounds, exerts strong antiproliferative effects and causes arrest of cell cycle progression in various cancers (Fang *et al*., 2018; Coni *et al*., 2020).

The role of eIF5A in ageing has also been extensively studied in the last decade. Hypusinated eIF5A levels and polyamines decline with age in yeast, and various *Drosophila*, mice and human tissues (Zhang *et al*., 2019; Liang *et al*., 2021). The polyamine spermidine serves as a unique substrate for eIF5A hypusination. Conversely, spermidine supplementation extended the lifespan of yeast, flies and worms, and human immune cells (Eisenberg *et al*., 2009). Spermidine enhances mitochondrial respiration and autophagy, delays aspects of brain ageing and improves cognitive functions (Hofer *et al*., 2021; Liang *et al*., 2021; Schroeder *et al*., 2021). However, mechanistic details of dietary spermidine effects remain elusive as brain function amelioration might be connected to higher autophagy or improved mitochondrial function independently of eIF5A. In addition, eIF5A is implicated in other processes which failure are also hallmarks of ageing such as long-term memory, adaptive immune response, cardiovascular function and mitochondrial function (see section 1.4). On one hand, eIF5A is overexpressed in mice Purkinje cells, the key neurons in the control of long-term memory (Luchessi *et al*., 2008). On the other hand, spermidine supplementation restores cardiac and mitochondrial function in mice (Eisenberg *et al*., 2016; Liang *et al*., 2021), improves memory T cell responses in mice (Puleston *et al*., 2014) as well as long-term β cell responses in mice (Zhang *et al*., 2019) and reduces the risk for cognitive impairment in humans (Schroeder *et al*., 2021). However, because of the long-term nature of these studies, the information is scarce.

Finally, genetic variants of eIF5A genes have been identified as the bases of certain rare neurodevelopmental disorders in humans (see review Park *et al*., 2021). Mutations in the hypusine pathway and eIF5A genes are associated to rare genetic disorders. Heterozygous *eIF5A* variants are associated with the Faundes-Banka syndrome, which is characterized by developmental delay, intellectual disability, microcephaly or craniofacial dysmorphism (Faundes *et al*., 2021). These variants impair eIF5A function and synthesis of polyPro-containing proteins. Similarly, biallelic variants in *DHPS* and recessive rare variants of *DOHH* show similar neurodevelopmental features (Ganapathi *et al*., 2019; Park *et al*., 2021). Interestingly, spermidine supplementation partially rescues some of the phenotypes characteristic of the Faundes-Banka syndrome (Faundes *et al*., 2021).

1.2. Molecular aspects of collagen metabolism

1.2.1 Functional classification of eIF5A-translation dependent proteins

As mentioned before, ribosome profiling and 5PSeq studies performed in temperature-sensitive *TIF51A* mutants revealed other non-polyPro motifs producing severe ribosome pauses upon eIF5A inactivation (Pelechano and Alepuz, 2017; Schuller *et al.*, 2017). Ontology classification of human proteins containing the highest levels of eIF5A-dependent motifs (Table 1.1) revealed various processes such as cytoskeleton organization, neuron development, cell differentiation, ER-coupled translation, extracellular matrix organization and collagen metabolism (Pelechano and Alepuz, 2017). Among them, collagen metabolism was the functional group showing the highest significant enrichment. Collagens contain abundant repetitions of non-polyPro eIF5A-dependent tripeptides such as PGP, PPG, DPG and EPG. Therefore, although the precise role of eIF5A in this process was not defined, it was tempting to speculate that eIF5A might be involved in the translation of the pausing motifs contained in these proteins. As the role of eIF5A in translating these specific motifs will be addressed in Chapter 3, general knowledge about collagen structure, metabolism and implications in diseases is detailed below.

1.2.2 Collagen structure

The extracellular matrix (ECM) works as a skeleton for cells to adhere, grow, interact and differentiate. Collagen is the major component and together with glycoproteins, glycosaminoglycans and proteoglycans forms the building blocks of the ECM. Collagen is essential in the ECM with functions in cell-cell interaction, tissue structure, cell adhesion and migration, cancer and angiogenesis and tissue repair (Kadler *et al*., 2007).

Vertebrates express 28 different collagens (Myllyharju and Kivirikko, 2001). The collagen family shares a common structural feature: a triple helical domain composed of X-Y-Gly tripeptide repeats where glycyl residues occupy every third position and proline or hydroxylated proline frequently occupy the first (X) and second (Y) positions (Brodsky and Persikov, 2005). The collagen mature protein is formed by three polypeptide α chains, held together by hydrogen bonds, each of them containing abundant repetitions of this triplet XYGly, although variable among the different collagen members, that enable the formation of the collagenous triple helix. Collagens can be heterotrimeric with different α chains or homotrimeric with identical α chains. In addition, collagen triple helical domains are flanked by non-triple helical domains (non-collagenous domains) at their N- and C-terminus. Once in the extracellular space they assemble into long fibrils and fibres that cross-link to one another and form highly organized polymers (Brodsky and Persikov, 2005).

Collagen I is the archetypal and most well-studied heterotrimeric collagen, which consists of two identical α1 chains and a third α2 chain, encoded by two different genes (*COL1A1* and *COL1A2* respectively). Collagen I constitutes more than 25% of human body total protein mass and is the major constituent of skin, ligaments, tendons, bone and various connective tissues where it provides mechanical strength and elasticity. Collagen I is synthesized only by a few cell types, including fibroblasts, osteoblasts and odontoblasts (Brodsky and Persikov, 2005).

1.2.3 Collagen synthesis pathway

Under physiological conditions, collagen I is a long-lived protein with high mRNA stability and highly regulated translation. Translation of the two polypeptides encoding collagen I occurs at discrete spots of the ER membrane to ensure effective folding into the triple helix. In fact, collagen mRNAs are directly targeted to the ER for their translation (Zhang and Stefanovic, 2016). When translating, nascent procollagen polypeptides are co-translationally inserted into the lumen of the ER and targeted to the secretory pathway (Figure 1.5).

Within the ER, a number of resident molecular chaperones and several co- and post-translational modification enzymes assist collagen folding and trimerization (Ito and Nagata, 2019). Prior to folding, the polypeptides undergo extensive hydroxylations and glycosylation (Hudson and Eyre, 2013). Additionally, chaperones such as heavy chain binding protein (BiP), protein disulfide isomerase (PDI) and Hsp47 bind the nascent collagen chain to help folding and prevent aggregation (Myllyharju and Kivirikko, 2004). Hsp47 is a molecular chaperone exclusively required by collagen (Koide *et al*., 2006). Then, the two α1 chains and one α2 chain assemble and fold into a triple helix proceeding from the C- to the N-terminus in a zipper-like manner (Figure 1.5).

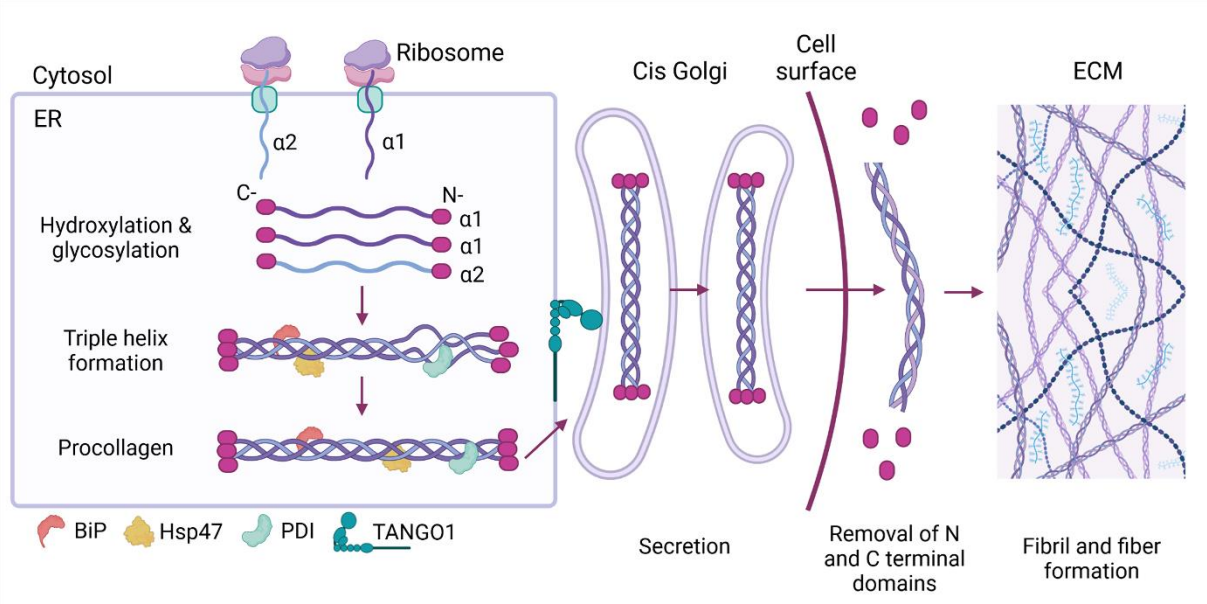

Figure 1.5. Collagen I synthesis pathway. Procollagen polypeptides are co-translationally inserted in the ER, where they are post-translationally modified and form a triple helical structure helped by additional enzymes and chaperones. Procollagen is transported to the cell surface via Golgi vesicles, helped by TANGO1 protein. Once secreted to extracellular space, the N- and C-terminal domains are removed, and fiber formation can occur by covalent crosslinking.

Once correctly folded, procollagens form rigid structures packed into large COPII vesicles and are transported to the cell surface via Golgi apparatus (Malhotra and Erlmann, 2015), although this mechanism is less understood than folding. As collagens are relatively large proteins, they require additional and specialized factors such as Transport and Golgi organization 1 (TANGO1) to be accommodated into small-diameter transport vesicles at ER exit sites (Saito *et al*., 2009; Maiers *et al*.,

2017). When the triple helices reach the extracellular space, its non-collagenous domains (N- and C-propeptides) are cleaved off by propeptidases (Figure 1.5). Then, triple helices are polymerized and arranged into fibrils and fibres, stabilized by covalent cross-links between lysine and hydroxylysine residues. These fibres show resistance to most proteases and can only be degraded by specific metalloproteases. Additional molecules are also bound to their surfaces such as glycoproteins, proteoglycans and plasma membrane receptors to finally form a large protein network in the ECM.

1.2.4 ER-stress and unfolded protein response (UPR)

Besides collagen, ER oversees the synthesis and folding of proteins destined for secretion, cell membrane, lysosomes, Golgi apparatus and other. As the capacity of the ER to process proteins is limited, misfolding or disruption of protein export results in intracellular accumulation and the induction of ER stress. ER stress is defined as an imbalance between the loading of new proteins and the organelle's ability to process them. ER stress activates the unfolded protein response (UPR) and may drive apoptosis (Wong and Shoulders, 2019).

The UPR consists of three signalling pathways which initially promote survival (Healy *et al*., 2009). The pancreatic ER kinase (PERK), activating transcription factor 6 (ATF6) and inositol-requiring enzyme 1 (IRE1) are three stress sensors maintained in an inactive state through the physical interaction with the ER chaperone-glucose regulated protein GRP78 in the ER lumen (Schroder and Kaufman, 2005). Upon cellular stress stimuli and buildup of unfolded proteins, GRP78 is dissociated and redirected to unfolded proteins, thus releasing and activating the three stress sensors (Figure 1.6):

1. PERK represses global translation through the phosphorylation of Ser51 on eukaryotic initiation factor 2 α (eIF2α) to reduce the load of new proteins being targeted into the ER. Conversely, the expression of the key transcription factor ATF4 increases, which is involved in the up-regulation of chaperones like BiP/GRP78 and proteins involved in resistance to oxidative stress or regulation of amino acid metabolism, which promote survival.
2. ATF6 relocates to the Golgi apparatus and is cleaved by specific proteases. Once active, ATF6 translocates to the nucleus and induces transcription of selective genes involved in protein folding (chaperones like BiP/GRP78 and GRP94), secretion and degradation to counteract ER stress.
3. IRE1 mediates the unconventional splicing of the transcription factor X-box binding protein (XBP1) which is up-regulated by ATF6. XBP1 translocates to the nucleus and targets various genes involved in the resolution of ER stress including $P58^{IPK}$ which binds and inhibits PERK, thus providing a negative feedback loop.

If the UPR signalling is successful in alleviating the ER stress, normal protein translation is resumed and the cell recovers, whereas if the stress is prolonged and unresolved, the ER function is impaired and cells undergo apoptosis. Here, ATF6, XBP1 and ATF4 transcription factors induce the transcription factor C/EBO homologous protein (CHOP) which promotes apoptotic cell death (Oyadomari and Mori, 2004) (Figure 1.6). CHOP leads to activation of caspase-3, translocation of Bax protein to the mitochondria and therefore, transmits the death signal to the mitochondria to promote the apoptotic pathway.

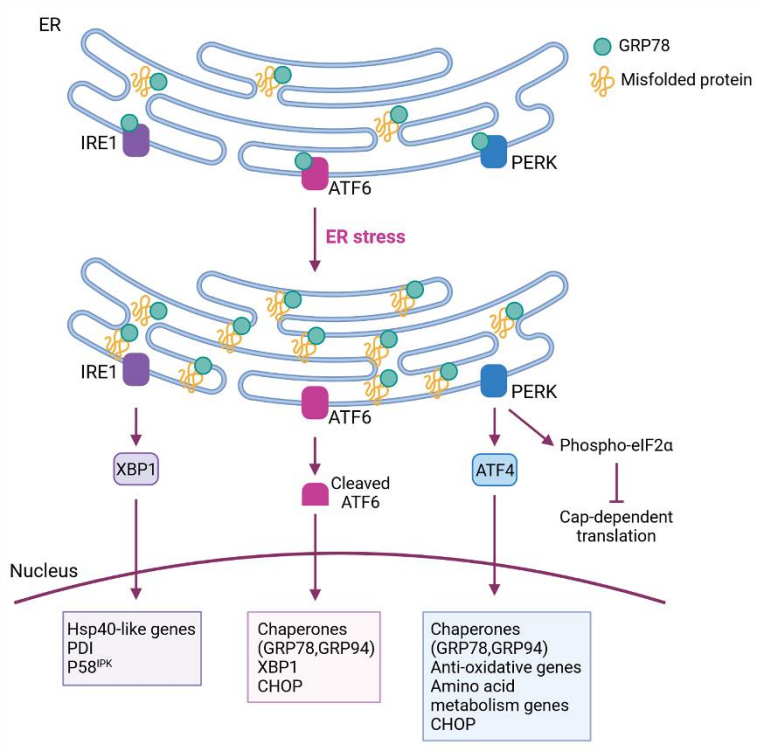

Figure 1.6. Schematic representation of the unfolded protein response (UPR) pathway. Misfolded proteins bind to GRP78 but when overloaded, GRP78 becomes limiting and the UPR response is activated through three arms, PERK, ATF6 and IRE1, which in turn activate different signalling pathways. The activation of the three sensors leads to general translation repression and to increased expression of effector genes involved in the resolution of ER stress. If the ER stress is chronic and unresolved, the transcription factor CHOP is activated by the three arms and triggers apoptosis via mitochondria.

1.2.5 Human diseases related to collagen synthesis

More than 1300 mutations, mainly autosomal dominant mutations, in collagen encoding genes have been characterized in humans (Myllyharju and Kivirikko, 2004). Some of them can lead to deficient and abnormal production of mature collagen and result in severe diseases, collectively termed collagenopathies. Some notable diseases include Alport syndrome (collagen IV), osteogenesis imperfecta (collagen I) and Kniest dysplasia (collagen II) (Jobling *et al*., 2014; Arseni *et al*., 2018). By contrast, excessive and uncontrolled synthesis and deposition of matrix proteins, especially collagen, culminates in fibrosis (Zeisberg and Kalluri, 2013).

Here we will focus on liver fibrosis, where the dominant matrix protein overproduced and deposited is collagen I, reaching up to several hundred-fold increase. As collagen I represents 80-90% of ECM proteins, hyperaccumulation and deposition of collagen fibrils disrupts normal liver tissue architecture and function. Liver fibrosis is the most common fibrotic disease and affects millions of people worldwide as it is involved in the development of most chronic liver diseases such as viral hepatitis, alcoholic liver disease and non-alcoholic fatty liver disease (Friedman *et al*., 2013; Kocabayoglu and Friedman, 2013). As most of existing treatments address disease symptoms rather than underlying causes, fibrotic diseases present a major health problem (Ricard-Blum *et al*., 2018; Weiskirchen *et al*., 2019).

Hepatic stellate cells (HSCs) are the main hepatic collagen-producing cells and effectors of liver fibrosis. They are found in a quiescent state in the perisinusoidal space and have specialized functions (Tsuchida and Friedman, 2017). Upon liver injury, hepatocytes and neighbouring cells release pro-fibrogenic and pro-inflammatory signals (growth factors, cytokines, chemokines…) which make HSCs undergo local activation and transdifferentiate into myofibroblasts (Figure 1.7). Among the pro-fibrogenic signals, the transforming growth factor beta 1 (TGF-β1) is considered the major pro-fibrogenic inducer. Activated HSCs show new features including increased proliferation, contractility and migration, but most importantly, they can synthesize and release ECM components such as collagen fibres and ECM-modifying enzymes to reduce the degradation of matrix proteins (Lee and Friedman, 2011; Kocabayoglu and Friedman, 2013; Iwaisako *et al*., 2014).

If the injury is resolved, the amount of myofibroblasts is reduced through apoptosis or reversion to quiescent state, and the fibrotic process is attenuated (Kisseleva *et al*., 2012; Troeger *et al*., 2012). On the contrary, if the injury persists, HSCs remain activated and the functional liver parenchyma is progressively replaced by fibrotic tissue. This impairs the architecture and functions of the liver to ultimately develop liver pathologies such as cirrhosis or hepatocellular carcinoma with an increased risk of mortality.

In Chapter 3 of this thesis, we provide insights to the relevance of eIF5A in the synthesis of collagen I under normal conditions and in the context of liver fibrosis.

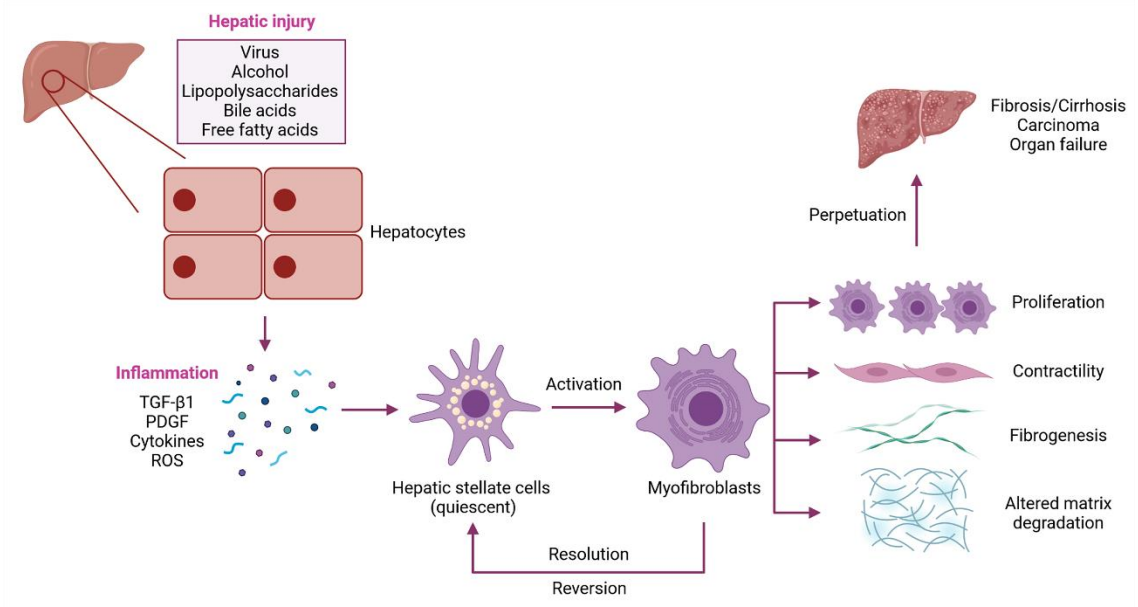

Figure 1.7. Cellular mechanism of liver fibrosis. Hepatocyte injury causes release of pro-inflammatory molecules from neighbouring cells, which drives HSCs activation and trans-differentiation into myofibroblasts. Myofibroblasts are able to proliferate, increase their contractility and modulate the ECM through excessive collagen I production and altered expression of degradation enzymes. If the injury is resolved, HSCs can revert to a quiescent state, while if injury is persistent, it may lead to severe pathologies such as cirrhosis or hepatic carcinoma.

1.3 Gene expression regulation upon metabolic changes

1.3.1 Transcriptional control of fermentative/respiratory metabolisms in *S. cerevisiae*

Yeast cells deal with a continuously changing environment, so the reconfiguration of cellular metabolism is important to adapt to external circumstances. *S. cerevisiae* is a facultative anaerobe and even under aerobic conditions prefers a fermentative rather than respiratory metabolism. Glucose fermentation is metabolized to ethanol and carbon dioxide and, although energetically less efficient than respiration in terms of ATP, allows cell activities and competitive growth to proceed at higher rates. During fermentation, most of the glycolytically produced pyruvate is converted to acetaldehyde, while a small fraction is translocated into mitochondria and used for the tricarboxylic acid (TCA) cycle (Gancedo, 1998; Santangelo, 2006; Zaman *et al*., 2008). Here, glycolysis and fermentation genes are induced, while genes encoding respiratory enzymes from the TCA, electron transport chain (ETC) and oxidative phosphorylation (OXPHOS) are subjected to glucose repression (Rolland *et al*., 2002; Schüller, 2003; Kayikci and Nielsen, 2015). However, non-fermentable substrates such as glycerol, ethanol or lactate, although slow down growth can also be used for energy production. A shift from fermentative to respiratory metabolism results in a massive reprogramming of gene expression, mainly exerted at transcriptional level, to induce genes from respiratory processes (TCA, ETC and OXPHOS). This gene expression reprogramming involves different signalling pathways, crosstalk between them and several transcription factors (Rolland *et al*., 2002; Schüller, 2003; Fendt and Sauer, 2010; Galdieri *et al*., 2010; Conrad *et al*., 2014; Kayikci and Nielsen, 2015).

High glucose levels promote fermentation and suppress respiration. Protein kinase Snf1 (homologous to mammalian AMP-activated kinase) is the master kinase of glucose derepression and has a dual role, both as an activator and repressor. High glucose levels render Snf1 dephosphorylated inactive and outside the nucleus through Glc7/Reg1 phosphatases. Meanwhile its major downstream target, the transcription factor Mig1, is maintained in the nucleus. Mig1, together with the Ssn6/Tup1 complex binds to and represses genes involved in respiration, gluconeogenesis and in the use of alternative carbon sources (Figure 1.8) (Rolland *et al*., 2002; Schüller, 2003; Hedbacker and Carlson, 2008; Kayikci and Nielsen, 2015). Additionally, high glucose also maintains the activity of protein kinase A (PKA) and target of rapamycin complex 1 (TORC1) which promote proliferation, through ribosome and translation machinery synthesis, and inhibit mitochondrial respiration. Although these two signalling pathways act conversely to that of Snf1, crosstalk between pathways to enable fine-tune regulation of cell processes has been documented (Shashkova *et al*., 2015).

Limited glucose or non-fermentative growth conditions render Snf1 kinase activated by phosphorylation (performed by three different kinases) and transferred to the nucleus. Together with its regulatory subunit Snf4 and alternative β-subunits Sip1, Sip2 and Gal83, Snf1 inhibits Mig1-mediated repression through its phosphorylation, subsequent dissociation from Ssn6/Tup1 and translocation to the cytoplasm (Rolland *et al*., 2002; Schüller, 2003; Hedbacker and Carlson, 2008; Kayikci and Nielsen, 2015). The release of glucose repression triggers the expression of respiratory genes such as components of the TCA cycle, ETC and OXPHOS (Figure 1.8). Derepressing these genes requires the transcription factor Hap1 and the transcription complex Hap2/3/4/5 (HAP complex), whose activities depend on heme cellular levels and are independent of PKA and Snf1 (Forsburg and Guarente, 1989; Zhang and Hach, 1999; Schüller, 2003; Zaman *et al*., 2009).

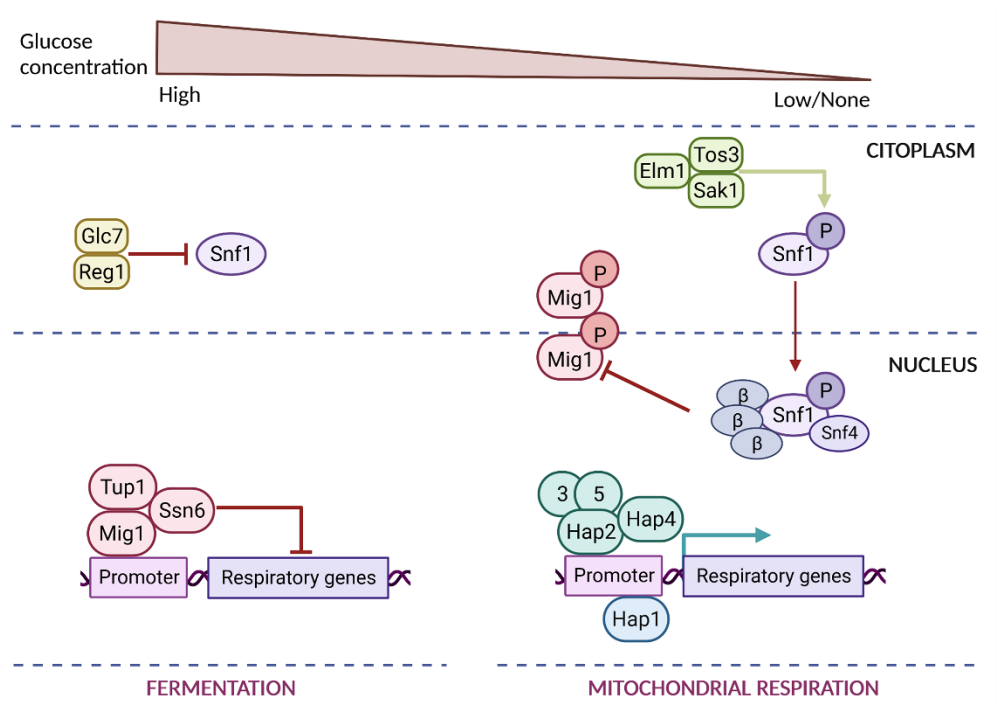

Figure 1.8. Yeast Snf1/Mig1 signalling pathway. Upon high glucose levels, Snf1 is inactivated by Glc7/Reg1 phosphatases and Mig1 is located in the nucleus where it recruits Ssn6/Tup1 complex and represses the expression of respiratory genes. Upon low glucose levels, Snf1 is activated by phosphorylation through Elm1, Tos3 and Sak1 kinases and localizes in the nucleus, where phosphorylates Mig1, which is translocated to the cytoplasm. The action of Hap1 and the HAP complex renders the expression of respiratory genes.

1.3.2 Hap transcription factors and their heme-mediated regulation

As previously mentioned, the Hap transcription factors constitute a global activator complex of respiratory genes. The heme activator protein 1 (Hap1) binds to DNA and activates transcription of genes required for respiration and control of oxidative damage in response to changes in oxygen or heme levels (Zhang and Hach, 1999). Hap1 is activated through heme binding, whose synthesis depends on the presence of oxygen, while inactive Hap1 upon heme deficiency functions as a transcriptional repressor.

Hap1 contains a DNA-binding domain with a C6 zinc cluster motif and a coiled-coil dimerization domain (DD) located near the N-terminus, a heme-binding domain with seven heme-responsive motifs (HRMs) and three repression modules (RPMs), and an acidic activation domain near the C-terminus (Figure 1.9-A). Hap1 binds as a dimer to asymmetric sites containing two CGG triplets (consensus binding sequence CGGnnnTAnCGG) with each zinc cluster motif contacting one CGG (Zhang and Guarente, 1994). HRMs and RPMS are responsible for coupling heme regulation with Hap1 activation/inactivation. Hap1 dimers are found associated to chaperone Hsp70 and co-chaperones Sro9 and Ydj1, mediated by the RPMs. Upon heme binding via HRMs, the Hap1 multichaperone complex associates to Hsp90, which causes conformational changes and leads to Hap1 activation (Hach *et al*., 1999; Hon *et al*., 2001).

During aerobiosis/respiration, heme concentration is high and activates Hap1 in the nucleus. Here, Hap1 works as an aerobic transcriptional activator of genes including: cytochrome c isoform 1 (*CYC1*), cytochrome c isoform 2 (*CYC7*), cytochrome c1 (*CIT1*), catalase (*CTT1*) and flavohemoglobin (*YHB1*). In addition, Hap1 activates transcription of *ROX1*, which represses the transcription of many hypoxia genes (Lowry and Zitomer, 1988; Zitomer and Lowry, 1992; Zitomer *et al*., 1997). Therefore, Hap1 directly activates aerobic genes while indirectly represses hypoxic genes. Under hypoxia, heme is not synthesized and Hap1 switches from activator to repressor. Its repressive activity through general repressors (Ssn6/Tup1) recruitment controls several genes such as *ROX1* and various *ERG* genes required for ergosterol biosynthesis (Zhang and Hach, 1999; Hickman and Winston, 2007). Additionally, Hap1 has recently been found to repress *ERG* genes under iron deficiency, a cell condition in which the heme synthesis is inhibited (Jordá *et al*., 2022).

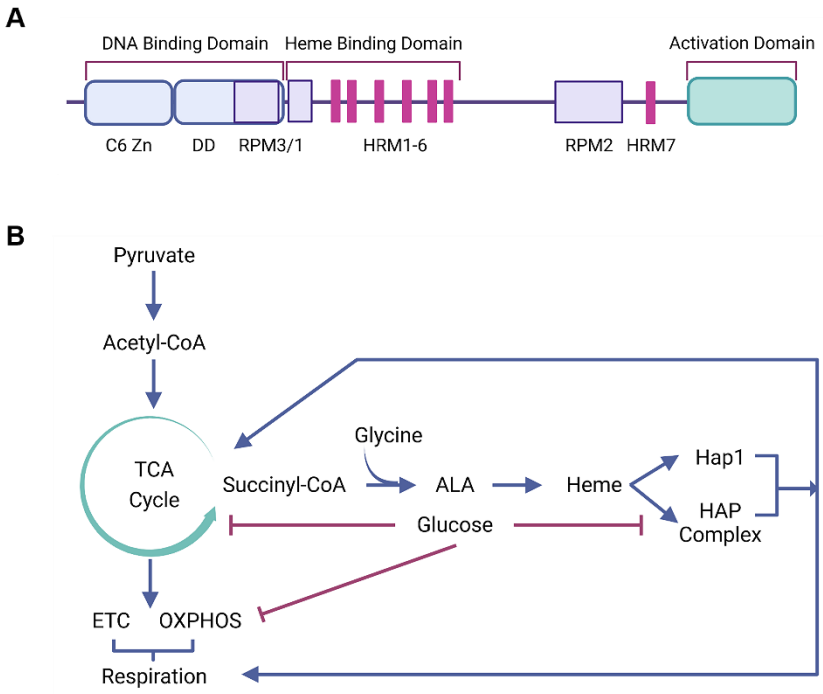

Figure 1.9. Domain structure of Hap1 protein, synthesis of heme and its role in the regulation of respiration. (A) Hap1 domain structure. The zinc cluster (C6 Zn) together with the dimerization domain (DD) constitute the DNA binding domain in the N-terminal region while the acidic activation domain is found in the C-terminus. The repression modules RPM1-3 and RPM2 repress Hap1 upon heme absence while the HRMs motifs mediate Hap1 activation. Adapted from Zhang and Hach, 1999. (B) Synthesis of heme requires succinyl-CoA to generate ALA, a key intermediate. Heme activates Hap1 and the HAP complex, which induce the expression of respiratory genes from TCA, ETC and OXPHOS. Glucose repression inhibits the expression of respiratory genes as well as the HAP complex. Adapted from Zhang *et al.*, 2017.

Besides Hap1, the HAP complex is the master regulator of mitochondrial respiration (see review Mao and Chen, 2019). The HAP complex binds to the CCAAT box through the constitutively expressed Hap2, 3 and 5 subunits. Hap4 is the co-activator subunit and is the only subunit whose expression is regulated. Hap4 mediates activation upon contacting the trimeric Hap2/3/5 complex already bound to its CCAAT site and then, activates the expression of TCA, ETC and OXPHOS genes (McNabb and

Pinto, 2005). Like Hap1, the HAP complex is activated by heme. Heme induces transcription of *HAP4*, through Cat8 and Hap1, and regulates its mRNA stability (Zhang *et al*., 2017; Bouchez *et al*., 2020); while glucose represses its expression (Figure 1.9-B).

Hence, heme plays an essential role as a signalling molecule in cell metabolism. Heme serves as a prosthetic group for respiratory enzymes working in electron transfer or redox reactions and thus, regulates mitochondrial biogenesis and growth (Bouchez *et al*., 2020). Also, heme works as a signalling molecule in oxygen sensing, transport and usage (Mense and Zhang, 2006). Heme is a tetrapyrrole containing a central iron, which synthesis requires eight enzymes. Heme synthesis starts and ends in mitochondria, with intermediate reactions occurring in cytosol, and is limited by metabolic flux into TCA cycle and availability of succinyl-CoA, oxygen and ferrous iron (Zhang *et al*., 2017). Heme synthesis requires the intermediate of TCA cycle succinyl-CoA and glycine to produce the key intermediate 5-aminolevulinic acid (ALA) (Figure 1.9-B). Thus, heme synthesis correlates with oxygen availability and is highly produced under aerobic conditions when the pyruvate flux into the TCA cycle is high. Though Hap1 and HAP complex activation, heme controls gene expression and induces metabolic transition from fermentation to respiration (Zhang *et al*., 2017). Conversely, under anaerobic growth conditions, metabolic flux into TCA cycle is insufficient for heme synthesis, which results in low activity of the HAP complex and repressor activity of Hap1.

1.3.3 Regulatory aspects of the two eIF5A isoforms

As previously introduced, most eukaryotes express two paralogous genes encoding two different eIF5A isoforms. These two genes show a clear differential expression pattern, suggesting a functional specialization despite both isoforms share more than 90% of amino acid sequence identity and produce very similar proteins (Figure 1.1).

In yeast, the expression of the two genes is reciprocally regulated by oxygen (Figure 1.10). Under aerobic conditions, *TIF51A* is highly expressed and essential, while *TIF51B* is poorly expressed being almost undetectable. *TIF51B* repression is achieved via the synergistic action of the two DNA-binding proteins Rox1 and Mot3 which recognize two operator regions through mechanisms that partially depend on the general repressor complex Ssn6/Tup1. The activation of these two repressors in the presence of oxygen and heme is produced via heme-bound Hap1 which recognizes the Hap1-binding sites at their promoters (Zitomer and Lowry, 1992; Zhang and Hach, 1999; Kastaniotis *et al*., 2000; Sertil *et al*., 2003; Klinkenberg *et al*., 2005). Rox1 and Mot3 repress then hypoxia genes, among which is found *TIF51B*. By contrast, under anaerobic conditions, *TIF51B* becomes highly expressed while *TIF51A* is down-regulated. Here, heme synthesis is deficient and Hap1 becomes a repressor of Rox1 and Mot3, triggering the induction of *TIF51B* (Figure 1.10) (Zitomer and Lowry, 1992; Hickman and Winston, 2007).

While the mechanism of *TIF51A* repression under anaerobiosis was unknown, it had been suggested to be positively regulated by Hap1 under oxygen conditions (Zitomer and Lowry, 1992). On the other hand, although the mechanism of *TIF51B* transcriptional regulation seemed to be quite understood, other transcriptional activators might be functioning as well under anaerobic growth (Figure 1.10). In Chapter

4 of this thesis, we study the transcriptional regulation of the two yeast eIF5A isoforms and describe the role of Hap1 as an activator/repressor for both.

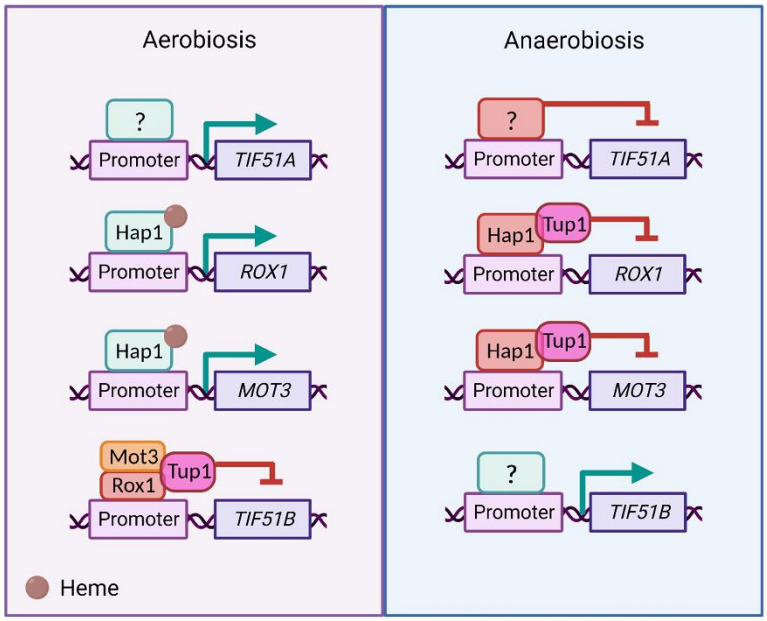

Figure 1.10. Current knowledge of the gene expression regulation of the two eIF5A isoforms in response to oxygen levels. Under aerobic conditions, *TIF51A* is activated by unknown transcriptional activators. Heme-bound Hap1 activates the expression of *ROX1* and *MOT3* which repress *TIF51B* through Tup1/Ssn6 recruitment (left panel). Under anaerobic conditions, *TIF51A* is repressed and Hap1 becomes a repressor as heme levels go down and down-regulates *ROX1* and *MOT3* expression. Due to Rox1 and Mot3 low levels, and possibly by additional transcription factors, *TIF51B* is up-regulated (right panel).

Human *EIF5A1* and *EIF5A2* also show a clear differential expression, with *EIF5A1* ubiquitously expressed in most cell types and *EIF5A2* only expressed in certain tissues (brain and testis) but overexpressed in many cancer cells (Jenkins *et al*., 2001; Clement *et al*., 2006; Ning *et al*., 2020). Despite knowledge on the mechanism of differential regulation is scarce, it has been documented that KRas signalling pathway up-regulates the two isoforms (Fujimura *et al*., 2014). *EIF5A1* is also positively regulated by p53 and NF-kappaB (Rahman-Roblick *et al*., 2007) whereas *EIF5A2* is induced under hypoxia via hypoxia inducible factor 1α (HIF-1α) (Li *et al*., 2014) and by Gli1 (Xu *et al*., 2015). The expression of the two human isoforms has also been connected to different metabolic outputs. For example, in human hepatocellular carcinoma samples, *EIF5A2* was upregulated and correlated with higher expression of glycolysis enzymes together with lactate dehydrogenase, promoting anaerobic glycolysis, the most common reprogramming of most cancer cells (Cao *et al*., 2017; San-Millán *et al*., 2017).

In this line, the differential regulation of the two eukaryotic eIF5A isoforms suggests that the first isoform (Tif51A/eIF5A1) would favour a respiratory metabolism whereas the second isoform (Tif51B/eIF5A2) would favour a fermentative/anaerobic metabolism. However, and despite the current information about this regulation, the molecular terms of how this gene expression is achieved remain unclear. In Chapter 4 of this thesis, we also study the transcriptional regulation of the two yeast eIF5A isoforms in response to different metabolic conditions.

1.4 Mitochondrial function

1.4.1 General aspects of the mitochondrial proteome synthesis

Mitochondria are complex eukaryotic organelles with endosymbiotic origin. They arise from a bacterial ancestor which was integrated by archaea and now are completely dependent on each other (Roger *et al*., 2017). Mitochondria are essential for energy production and macromolecular synthesis as they house key metabolic processes such as OXPHOS, ETC, TCA cycle, β-oxidation and lipid, amino acids, heme and Fe-S clusters synthesis. Besides this primary function, mitochondria also participate in other cellular processes including Ca^{+2} homeostasis and apoptosis (Vakifahmetoglu-Norberg *et al*., 2017). Given its essential role in cells, mitochondrial function is critical in health and disease and is a pivotal hallmark of ageing-related disorders (Balaban *et al*., 2005; Boengler *et al*., 2017).

Mitochondria have double membrane structure. The mitochondrial outer membrane (MOM) and mitochondrial inner membrane (MIM) delimit two aqueous spaces: the intermembrane space (IMS) and the mitochondrial matrix (MM). The mitochondrial proteome comprises about 1000 or 1500 proteins, in yeast and human respectively, to perform the abovementioned functions (Schmidt *et al*., 2010). *S. cerevisiae* mitochondrial genome (mtDNA) encodes 1% of these proteins, essentially seven enzymes (13 in human) of the respiratory chain and one ribosomal protein (Borst and Grivell, 1978). The other 99% is encoded in the nuclear genome, as a consequence of the gene transfer after the endosymbiotic process. Therefore, these mitochondrial proteins, herein termed mitoproteins, are synthesized by cytosolic ribosomes but need to be transported into the mitochondria where they fulfil their biological function (Morgenstern *et al*., 2017). As mitochondria is one of the most challenging destinations, mitoprotein targeting, recognition and import are key processes for the right mitochondrial function (Bykov *et al*., 2020).

Once synthesized on free ribosomes in the cytosol, mitoproteins associate with cytosolic chaperones from the Hsp40, Hsp70 and Hsp90 families. Chaperones bind to hydrophobic regions and keep mitoproteins in an unfolded and import-competent state as these are prone to aggregation and degradation when exposed to the cytosolic environment. Additionally, chaperones assist the docking and delivery of mitoproteins to specific receptors at the MOM for translocation (Hansen and Herrman, 2019). Therefore, when mitoproteins are translated in the cytosol, translocation to mitochondria occurs post-translationally (Figure 1.11).

Beyond cytosolic translation, translocation of mitoproteins can occur co-translationally as some mRNAs are located in the mitochondrial surface where mitoprotein synthesis can be coupled to their import (Figure 1.11). Co-translational import ensures that protein synthesis occurs where needed and allows quick responses to cell needs (Kellems *et al*., 1972; Williams *et al*., 2014; Gold *et al*., 2017; Tsuboi *et al*., 2020). Of all mitoproteins, the MIM proteins have the largest fraction of mRNAs located in the surface and co-translationally imported (Williams *et al*., 2014). In addition, mitochondrial mRNA localization can be constitutive or regulated depending on the metabolic state (Tsbuoi *et al*., 2020). Among the molecular factors targeting transcripts to the mitochondrial surface for proximal translation we find Puf3, an RNA-binding protein that interacts with a specific motif in the 3'UTR of some mRNAs encoding mitoproteins (García-Rodríguez *et al*., 2007; Saint-Georges *et al*., 2008); and the nascent chain-associated heteromeric complex (NAC), a chaperone that binds to ribosomes and nascent

polypeptides simultaneously in the ribosomal exit tunnel and also interacts with the MOM protein Om14 (Gamerdinger *et al*., 2019). Additional factors influencing mRNA localization have been recently identified. These include Larp, identified in *Drosophila*, is recruited by the protein complex MDI to the outer membrane where amplifies mRNA binding and local translation (Zhang *et al*., 2016); and SYNJ2BP, identified in human cells, which modulates levels of selected mRNAs on the mitochondrial surface in a stress-dependent manner (Qin *et al*., 2021).

The fact that many of the mRNAs localized show reduced association with the mitochondrial surface upon polysome dissociation (Eliyahu *et al*., 2010; Fazal *et al*., 2019), suggests that translation is needed for localization, and once ribosomes are engaged to mRNA, can be targeted to mitochondria. In fact, properties such as transcript length, low translation speed due to rare codons and ribosome stalling favour co-translational import (Tsuboi *et al*., 2020). Targeting signals are also found within the polypeptide chains. About 60% of mitoproteins contain a mitochondrial targeting sequence (MTS) in the N-terminal region, recognized by specific receptor proteins in the MOM and necessary to promote mRNA localization and protein targeting to mitochondria (Figure 1.11) (Vögtle *et al*., 2009). MTSs are cleaved upon import into the mitochondria and thus, are termed presequences. MTSs are of variable length, from 10-100 amino acid residues and form an amphipathic α-helix with a positively charged face and a hydrophobic face. The rest of the mitoproteins show different internal signals which lack consistent patterns and their nature remains elusive.

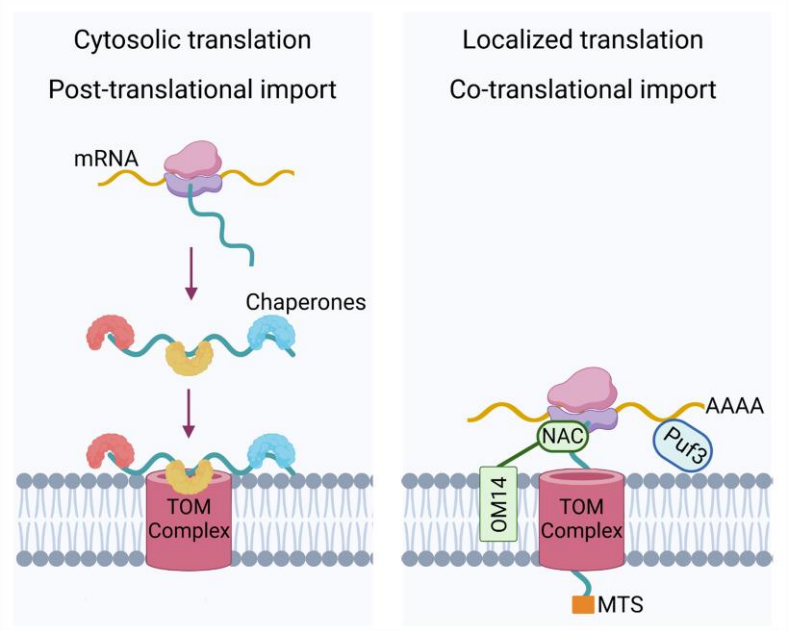

Figure 1.11. Location of mitoproteins translation affects their import mode. Cytosolic translation of mitoproteins exposes precursors to cytosolic environment, which recruits chaperones (Hsp40, Hsp70 and Hsp90) to prevent aggregation and targets them to the TOM translocase of the MOM. Then, import into mitochondria occurs post-translationally (left panel). However, localized translation in the mitochondrial surface renders co-translational import. Different factors impact the mRNA localization and translation machinery recruitment to mitochondria (NAC and Om14, Puf3 or N-terminal MTS among others; right panel).

1.4.2 Overview of the mitochondrial protein import system

Protein translocases in the outer and inner membrane mediate the import and sorting of mitoproteins into mitochondria (Figure 1.12). They cooperate closely with each other to ensure the exact targeting and maturation of mitoproteins. Seven machineries define five different but connected import pathways (for extensive review see Wiedemann and Pfanner, 2017; Lenkiewicz *et al*., 2022; Haastrup *et al*., 2023). The information detailed below belongs to yeast data, although most of the proteins show homologs in higher eukaryotes and humans.

- The translocase of the outer membrane (TOM) defines the first step of the import pathway and is considered the universal entry gate for nearly all mitoproteins. TOM recognizes different precursors in the cytosol and transfers them across the outer membrane. The TOM complex consists of three receptors (Tom20, Tom22 and Tom70), the transmembrane channel and central subunit Tom40 and three small subunits (Tom5, Tom6 and Tom7) (Figure 1.12). Tom20 is the master receptor for proteins containing N-terminal MTSs while Tom70 recognizes substrates containing hydrophobic regions. Tom22 is a central receptor and plays a structural role for the integrity of the complex. Tom40 forms the translocation pore and the small subunits Tom5, Tom6 and Tom7 mediate complex assembly and stabilization. After translocation through TOM, proteins are sorted to different pathways depending on their final destinations.

- The translocase of inner membrane (TIM) mediates the import of all matrix proteins and most inner membrane proteins. TIM is considered the major translocase as the biggest group of precursor proteins follows this pathway. TIM recognizes N-terminal MTSs and additional hydrophobic signals termed stop-transfer sequences. The TIM complex consists of the receptor Tim50, the central subunit Tim23 and the regulatory subunits Tim17 and Tim21 (Figure 1.12). TIM translocation is energetically driven by the electrical membrane potential. The receptor protein Tim50 regulates the gating of the channel, binds to MTS from precursors translocating from TOM complex and transfers them to the translocation pore Tim23. The regulatory subunit Tim21 physically links the TIM23 complex to the respiratory chain while Tim17 mediates the sorting and lateral release of inner membrane proteins that contain additional hydrophobic signals. The rest of mitoproteins which only contain an N-terminal MTS are routed to the matrix. Protein translocation into matrix requires ATP hydrolysis as a second energy source, which is powered by the presequence translocate-associated motor (PAM). Here, the mitochondrial heat shock protein 70 (mtHsp70) forms the core of the motor and is coupled to TIM23 through Tim44 (Figure 1.12). Additional Pam proteins (Pam16, Pam17 and Pam18) regulate its hydrolysing activity. PAM completes the process and mediates the release of the precursor mitoprotein into the matrix, where the MTS is removed by the action of the matrix processing peptidase (MPP).

- The translocase of inner membrane 22 (TIM22) mediates the import of mitochondrial metabolite carriers to the inner membrane. Precursors for this pathway consist of hydrophobic proteins with multiple α-helical transmembrane segments. TIM22 recognizes internal targeting elements, rich in hydrophobic residues, distributed over the primary sequence. The TIM22 complex consists of the central subunit Tim22, the receptor Tim54 and the additional Tim18-Sdh3 module (Figure 1.12). Translocation is also energetically driven by the membrane potential. Tom70 recognizes the precursors and delivers them to Tom40. Once in the IMS, they are directly transferred to the small Tim chaperone complex (Tim9-Tim10-Tim12) which prevents aggregation and recruits them to the Tim54 subunit. Tim54 delivers precursors to the Tim22 channel which drives their insertion into the inner membrane.

- The mitochondrial intermembrane space import and assembly protein 40 (MIA40) mediates the import of IMS proteins with cysteine motifs that form intramolecular disulfide bonds. Precursors for this pathway contain a signal with hydrophobic residues and a cysteine residue. Substrates cross the outer membrane through Tom40 and then bind Mia40, which facilitates their entry into the IMS. Mia40 works as an oxidative protein folding machinery and transfers a disulfide bond to precursors, leading to their oxidation (Figure 1.12). Mia40 thus promotes conformational stabilization and assembly of many IMS proteins.

- The sorting and assembly machinery (SAM) drives the import and insertion of β-barrel proteins into the outer membrane. SAM recognizes proteins with a β-hairpin element as a targeting signal in the C-terminus. The SAM complex consists of the membrane-integrated protein Sam50 and two peripheral proteins exposed to the cytosol, Sam35 and Sam37 (Figure 1.12). Substrates are synthesized by cytosolic ribosomes and translocated through Tom40. Once in the IMS, they are transferred to the small Tim chaperone complex (Tim9-Tim10-Tim12) which prevents aggregation and delivers them to Sam50. Finally, the SAM complex directs their membrane insertion.

- The MOM insertase mediates the import and insertion of α-helical proteins into the outer membrane. This complex recognizes proteins with targeting signals in transmembrane segments and consists of multiple copies of Mim1 and one copy of Mim2 (Figure 1.12). Although the molecular mechanism is not clear, it is known that Tom70 receptor cooperates with this complex but substrates do not cross through TOM and are directly inserted in the membrane. This complex promotes the efficient insertion of both single-anchored and polytopic proteins into the outer membrane.

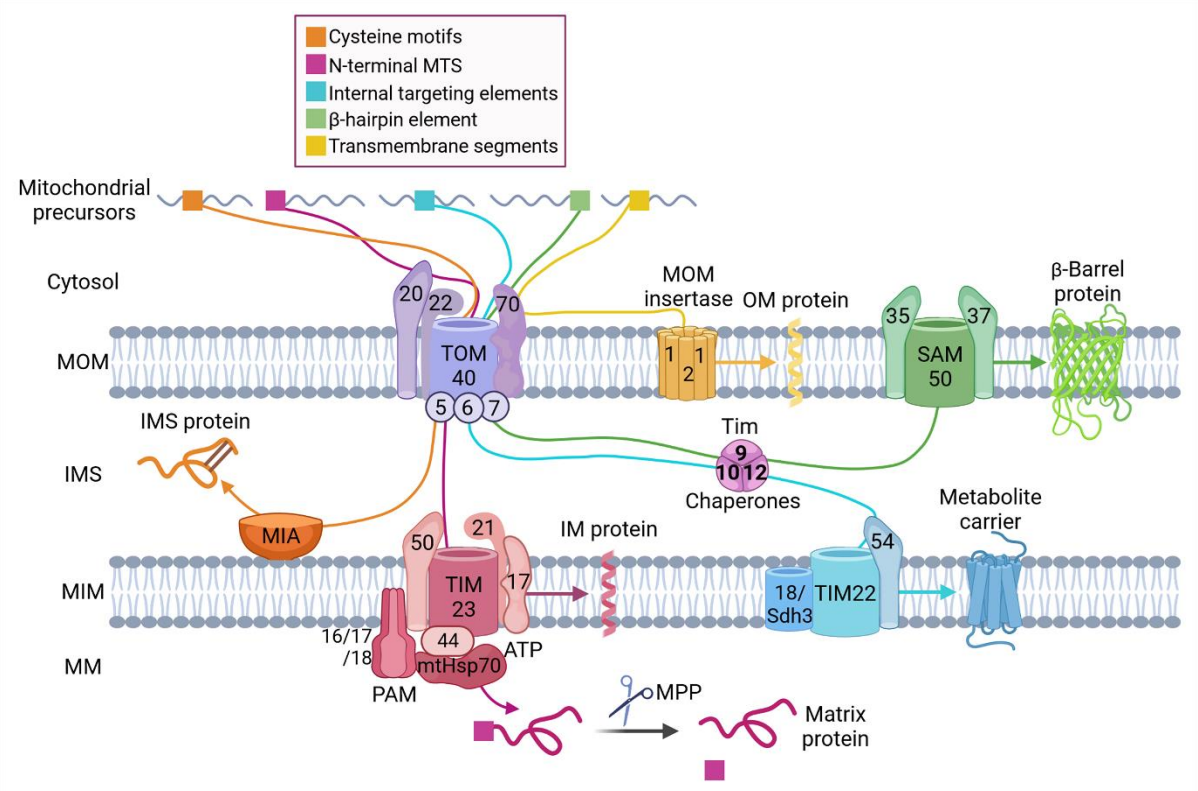

Figure 1.12. The mitochondrial protein import system. The mitochondrial protein import system consists of seven machineries, including TOM complex, TIM23 complex, PAM, TIM22 complex, MIA, SAM complex and MOM insertase. Mitochondrial precursors contain different targeting signals which are recognized by specific receptors in the TOM complex and then delivered to a specific import machinery depending on the final destination.

1.4.3 Cellular responses to compromised mitochondrial protein import

Mitochondrial fitness is manifested by optimal ATP levels, redox environment and maintenance of membrane potential. Stressful stimuli that decrease mitochondrial membrane potential, mutations in the components of translocases and defective or overloading precursors may lead to clogging of the translocases and mitochondrial import failure, which will impair essential mitochondrial functions (Boos *et al*., 2020). Import failure leads to proteotoxic effects both inside and outside the mitochondria, as unfolded precursors will accumulate on the translocases and in the cytosol, which is detrimental to cellular fitness and associated with various diseases. To avoid this, cells are equipped with several stress responses to increase the activity of chaperones and proteasome system in the cytosol, remove accumulated precursors from translocases and cytosol, and stabilize homeostasis (Figure 1.13). The mitochondrial quality control machineries described until now are:

- Mitochondrial protein translocation-associated degradation (mitoTAD) (Mårtensson *et al*., 2019). mitoTAD constitutively monitors the TOM complex to prevent clogging under non-stressed circumstances in yeast cells. The ubiquitin regulatory X (Ubx2) protein, which also functions in ER, specifically binds to the TOM complex and provides a docking site for the cytosolic AAA ATPase Cdc48. Upon the appearance of arrested precursors in the translocases

and accumulation of non-imported precursors in the cytosol, Ubx2 recruits Cdc48 and co-factors to the clogged complex and there, Cdc48 drives the extraction of translocation-arrested precursors from the translocation channel by ATP hydrolysis to further facilitate their proteasomal degradation (Figure 1.13). However, when the capacity of this pathway is exceeded, other responses are activated.

- Mitochondrial compromised protein import response (mitoCPR) (Weidberg and Amon, 2018). On prolonged clogging of translocases and accumulation of precursors in the cytosol of yeast cells, mitoCPR induces a Pdr3-dependent transcriptional response which entails the expression of several genes including multi-drug resistance genes, lipid metabolism related-proteins and NADPH-dependent enzymes. Among them, the up-regulation of Cis1 enhances the clearance of stalled unimported precursors from the TOM complex. Cis1, located at the MOM, recruits the AAA ATPase Msp1, which monitors the mitochondrial surface for aberrant proteins, to Tom70. There, Msp1 mediates the removal of unimported precursors, which are then ubiquitinated and degraded by the proteasome machinery (Figure 1.13).

- Mitochondrial precursor over-accumulation stress (mPOS) (Wang and Chen, 2015). Upon yeast mitochondrial damage and aberrant aggregation of non-imported precursors in the cytosol, mPOS response is triggered to balance the turnover of accumulated proteins and to limit the consequences of their mislocalization. Here, the abundance and activity of the proteasome is boosted and the synthesis of nascent mitoproteins is attenuated. The up-regulation of Nog2 and Gis2 proteins inhibit ribosome biogenesis at the level of nuclear export of ribosome components and thus, reduces general cytosolic translation (Figure 1.13).

- Unfolded protein response activated by mistargeting of proteins (UPRam) (Wrobel *et al*., 2015). UPRam is a yeast protective mechanism that, in response to defective import, regulates protein homeostasis through two arms (Figure 1.13). On one hand, UPRam enhances and improves the proteasomal activity to degrade the accumulated toxic precursors in the cytosol. On the other hand, UPRam mitigates protein translation through eIF2α phosphorylation to prevent further accumulation of non-imported precursors.

- Mitochondrial unfolded protein response (UPRmt) (Münch and Harper, 2016; Rolland *et al*., 2019). This response was initially characterized in *C. elegans*, where the transcription factor ATFS-1 harbours a mitochondrial presequence and a nuclear-localization signal. In healthy mitochondria, ATFS-1 is efficiently imported into the mitochondrial matrix and degraded. Upon import failure conditions, ATFS-1 translocates to the nucleus where it functions as a transcription factor and induces the expression of mainly mitochondrial chaperones and proteases while represses respiratory enzymes (Figure 1.13). UPRmt is not restricted to nematodes. In humans, ATF4 and ATF5 transcription factors have been proposed to function similarly (Quiros *et al*., 2017). Despite of no ATFS-1 homologs, yeast HAP-complex seems to play a comparable role through the repression of respiratory components upon protein import overload (Boos *et al*., 2019).

Although described as independent phenomena, the transcriptional regulation of these pathways seems to be integrated into one coordinated stress response which involves heat shock factor 1 (Hsf1) (Boos *et al*., 2019; Boos *et al*., 2020). Under non-stressed conditions, Hsf1 activity is repressed through binding to molecular chaperones while upon import stress, chaperones could be titrated away from Hsf1 through preferential binding to accumulated non-imported precursors. Then, Hsf1 could be activated and translocated to the nucleus to induce the expression of chaperones and Rpn4, the master regulator of components of the proteasome system. Rpn4 up-regulates the activity of the proteasome to degrade precursors in mitoTAD, mPOS and UPRam responses. Rpn4 also induces the transcription factor Pdr3, which stimulates the expression of Cis1 in the mitoCPR pathway (Figure 1.13). Therefore, although the exact molecular mechanism of Hsf1 activation by compromised protein import is unknown, Hsf1 arises as the primary initiator of most of the transcriptional responses connecting mitochondrial dysfunction and proteotoxic stress. Finally, if the abnormal protein accumulation exceeds the cellular degradation capacity, damaged mitochondria are targeted for degradation in lysosomes or vacuoles by mitophagy (Pickrell and Youle, 2015), a process involving the PINK1 and Parkin proteins.

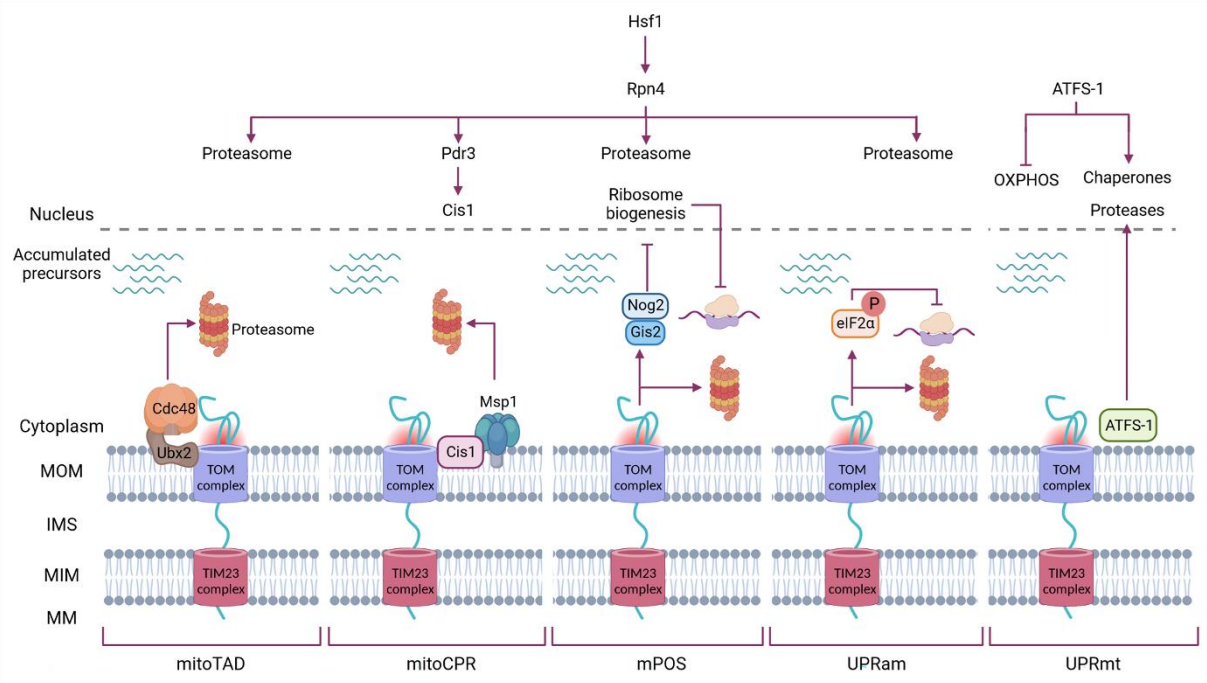

Figure 1.13. Mechanisms of quality control of clogged import system. Different responses are elicited by the cell upon failure of the import machineries and clogging of translocases. Mitochondrial precursors are accumulated in the cytosol and to avoid subsequent toxicity, the cell initiates different responses at transcriptional and post-transcriptional level, which include mitoTAD, mitoCPR, mPOS, UPRam and UPRmt. Hsf1 initiates the transcriptional remodelling in almost all the pathways through the activation of Rpn4, which induces the up-regulation of proteasome components and through Pdr3, the transcriptional activator in charge of the mitoCPR response.

1.4.4 Links between eIF5A and mitochondrial function

Connections between eIF5A, its hypusination enzymes, polyamines and mitochondrial function have been reported in the last years but the overall picture is not entirely clear.

Both a defect in and an excess of eIF5A produce deleterious effects on mitochondrial function. eIF5A overexpression increases reactive oxygen species (ROS) and Ca^{+2} influx in mitochondria, induces apoptosis and reduces mitochondrial membrane potential (Tan *et al*., 2010; Sun *et al*., 2010) while mutations in the *DOHH* gene lead to defects in mitochondrial morphology and distribution in *Schizosaccharomyces pombe* (Weir *et al*., 2004). Regarding disease contexts, a positive role of eIF5A in promoting mitochondrial activity has been established. These results point to eIF5A inhibition as a potential strategy to protect cells under situations of low oxygen availability that otherwise contribute to mitochondrial damage and cell death. For instance, GC7-mediated inhibition of eIF5A hypusination prevented anoxia-induced cell death in ischemia-induced renal injury and kidney transplation models (Melis *et al*., 2017). Here, GC7 treatment shifted metabolism towards anaerobic glycolysis, decreased the expression and activity of ETC and reduced the oxygen consumption and ROS production, resulting in a preservation of the mitochondrial function by reducing its activity (Melis *et al*., 2017; Giraud *et al*., 2020). In this line, GC7 treatment in an in vitro model of malaria infection prevented cardiac damage driven by hypoxia (Kaiser *et al*., 2020).

Interestingly, non-cytoplasmic localizations of eIF5A protein, including mitochondria, have been reported (Liu *et al*., 2012; Miyake *et al*., 2015; Pereira *et al*., 2016). One of the mRNA transcript variants of *EIF5A1* human gene shows an alternative start codon which generates a longer eIF5A isoform. Although less efficiently translated, this isoform contains a putative mitochondrial localization signal and renders its association to this organelle (Pereira *et al*., 2016).

Although eIF5A has been found to be essential for mitochondrial activity, the mechanism by which eIF5A affects mitochondrial function remains elusive. Until now, two alternative but related mechanisms have been described. First, eIF5A was reported to control the synthesis and activity of many mitoproteins of macrophage cells including ETC complex components, TCA enzymes (succinyl-CoA synthetase and succinate dehydrogenase) and TCA-feeding enzymes (pyruvate dehydrogenase) in a specific manner. The MTSs of some of them were sufficient to confer hypusinated eIF5A-dependent translation efficiency, suggesting that eIF5A might regulate mitochondrial respiration, at least in part, by promoting the translation of MTSs of some mitoproteins, which are rich in charged amino acids (Puleston *et al*., 2019). In connection with this, a mechanism for eIF5A-dependent translation of MTSs has been recently proposed in yeast. Zhang *et al*., 2022 reported how eIF5A promotes the translation of some respiratory proteins in response to oxygen levels and suggested a possible mechanism in which eIF5A and hypusine would favour a suitable interaction between the amino acids contained in the MTSs regions and the peptide exit tunnel, forcing the formation of the peptide bond in a proline-independent manner. However, mechanistic molecular details are still missing.

Chapter 5 of this thesis characterizes a specific molecular mechanism by which eIF5A impacts the import and synthesis of mitoproteins and thus, the mitochondrial function.

1.5 Translation elongation in gene expression regulation

1.5.1 Coordination of RNA metabolism with translation

Gene expression is defined as the production of the right amount of protein at the right time, effectively interacting with its cellular partners and targeted to the correct cellular compartment. Precise control of gene expression is essential for the healthy growth and development of all cellular organisms. The main steps of gene expression pathway comprise transcription, mRNA processing and decay, and translation. Although mostly independently studied, the integration or crosstalk between these four gene expression events exists and is fundamental for cells to finely tune gene expression to meet cellular demands and adapt to changing environmental stimuli.

Protein synthesis represents the most energy-consuming process in the cell and its careful regulation is essential for cell proliferation and survival (Stouthamer, 1973; Buttgereit and Brand, 1995; Wieser and Krumschnabel, 2001; Pérez-Ortín *et al*., 2019). The steady state pool of mRNAs available for protein synthesis is defined by the rates of transcription (mRNA synthesis) and decay.

Although transcription and translation are considered independent processes due to their distinct molecular mechanisms, timings and sites of action, different crosstalk factors coordinate transcription and post-transcriptional processes, including translation. Among them the heterodimer Rpb4/Rpb7, the Ccr4-Not complex or the exonuclease Xrn1 have been extensively described (Slobodin and Dikstein, 2020). The two RNA polymerase II (RNA Pol II) subunits Rpb4/Rpb7 impact transcription processivity and mRNA export. They associate with mature transcripts and accompany them to cytoplasm, where Rpb4 interacts with translation initiation factor eIF3 and promotes translation (Harel-Sharvit *et al*., 2010; Dahan and Choder, 2013). The Ccr4-Not complex regulates gene expression principally through the shortening of poly(A) tails of mRNAs or deadenylation. The Ccr4-Not complex also impacts transcription elongation through RNA Pol II binding and promotes the degradation of inefficiently translated mRNAs by monitoring decoding rates (Collart, 2016; Begley *et al*., 2019; Buschauer *et al*., 2020). Finally, the exoribonuclease Xrn1 is the major 5'-3' mRNA degradation enzyme in the cytoplasm. Xrn1 binds genes promoting transcription initiation and elongation (Haimovich *et al*., 2013; Medina *et al*., 2014; García-Martínez *et al*., 2021) but is also important for efficient translation of specific yeast genes and co-localizes with 40S and 60S fractions from polysomal gradients (Blasco-Moreno *et al*., 2019).

In addition, crosstalk between translation and mRNA decay is essential in gene expression regulation. The most prominent and well-described correlation between translation and mRNA stability is through codon optimality. Codon optimality takes into account several factors involved in translation elongation rate, including tRNA availability and demand, GC content, frequency of use in the genome and interactions with the ribosome exit tunnel (Reis *et al*., 2004; Pechmann *et al*., 2013; Gardin *et al*., 2014; Presnyak *et al*., 2015). Thus, stable transcripts are enriched in optimal codons and have faster elongation speed, whereas those enriched in non-optimal codons are unstable mRNAs with slower elongation speed (Chu *et al*., 2011; Gardin *et al*., 2014; Ingolia 2014; Hussman *et al*., 2015; Harigaya and Parker, 2016; Saikia *et al*., 2016; Weinberg *et al*., 2016; Hanson and Coller, 2018).

The dependence of mRNA stability on codon optimality immediately implicates the ribosome and translation elongation as a major regulator of mRNA turnover. Ribosomes elongate more slowly when

they need to find a rare cognate tRNA with low abundance compared to a commonly available tRNA (Presnyak *et al*., 2015; Yu *et al*., 2015; Yan *et al*., 2016). Slow elongation rates lead then to decreased protein synthesis and will determine the mRNA decay rate.

1.5.2 Ribosome collisions and surveillance pathways

Eukaryotic ribosomes translocate across the mRNA at an average rate of 3-10 amino acids per second. During translation elongation, ribosomes may encounter impediments imposed by a combination of mRNA sequence, damaged mRNA, secondary structures or tRNA availability, and pause (Doma and Parker, 2006; Letzring *et al*., 2010; Han *et al*., 2020). As multiple ribosomes are often concurrently translating on a single mRNA, the ribosome pause may lead to the upstream translating ribosomes reaching the paused one, resulting in ribosomes collision and eventually, in the formation of higher order ribosome structures. Although ribosome collisions are not inherently detrimental for the cell, prolonged stalling results in the production of truncated polypeptides and deleterious effects on cellular fitness. Thereby, the cell is able to distinguish between physiologic/benign and pathologic stalls to prevent the buildup of ribosomes on problematic mRNAs. Severity of ribosome collisions may determine the cellular response activated but how this works remains unclear (Meydan and Guydosh, 2020).

Stalled ribosomes signal quality control responses which, depending on the nature of the signal, may lead to translational repression, ribosome recycle, nascent polypeptide degradation and/or mRNA degradation (Inada, 2020; D'Orazio and Green, 2021). When ribosomes stall, the upstream ribosome collides into the stalled ribosome and forms a disome structure, that triggers the full cascade of ribosome quality control (RQC) events (Juszkiewicz *et al*., 2018; Ikeuchi *et al*., 2019). The leading ribosome is found in an unrotated state with an empty A site and a peptidyl-tRNA in the P site, whereas the upstream colliding ribosome is found in a rotated state with a peptidyl-tRNA in the A-P site and an uncharged tRNA in the P-E site (Figure 1.14). This interface is recognized by the E3 ubiquitin ligase Hel2 which ubiquitinates the key small subunit yeast ribosomal proteins S3 and S10. The ubiquitinated state forms an interface likely to recruit downstream RQC factors to set off ribosome rescue and proteolytic decay of nascent polypeptide. The ribosome QC trigger (RQT) complex consists of three factors, the RNA helicase Slh1, the ubiquitin-binding protein Cue3 and Rqt4, which induce ribosomal dissociation into small (40S) and large (60S) subunits (Matsuo *et al*., 2020). Once disassembled, the mRNA remains bound to the 40S subunit while the nascent polypeptide is bound to the 60S subunit. This latter complex binds to Rqc1, Rqc2 and to the E3 ubiquitin ligase Listerin (Ltn1). Rqc2 stimulates the C-terminal elongation of the stalled polypeptide by multiple alanyl and threonyl residues (CAT-tailing) and Ltn1 ubiquitinates the nascent polypeptide chain and targets it for proteasomal degradation. Vms1 helps in the release of the ubiquitinated polypeptide from the tRNA prior degradation (Figure 1.14) (Bengtson and Joazeiro, 2010; Shao *et al*., 2015; Brandman and Hegde, 2016; Joazeiro, 2019; Collart and Weiss, 2020; Inada, 2020).

Concurrently and coupled to RQC pathway, mRNAs are targeted for decay in a process broadly referred to as no-go decay (NGD), which also occurs when a ribosome stalls with an empty A site (Figure 1.14). Here, key protein adapters couple translation elongation status to mRNA degradation. First, the endonuclease Cue2 specifically targets and cleaves the mRNA generating two intermediates, the

upstream 5'NGD and the downstream 3'NGD, which are further degraded by the cytoplasmic exosome and Xrn1 exonuclease respectively (D'Orazio *et al*., 2019; Ikeuchi *et al*., 2019). Other proteins have been found implicated in mRNA decay on slowly elongating ribosomes such as Ccr4-Not complex (Buschauer *et al*., 2020). Activation of the NGD pathway is Hel2-dependent, suggesting that ribosome collision and empty A-site are required for mRNA degradation (Garzia *et al*. 2017, Juszkiewicz and Hegde, 2017).

The buildup of disomes upon Pro-Pro and other eIF5A-dependent motifs is common under normal conditions while the number of these structures is increased upon eIF5A depletion (Han *et al*., 2020). Whether these structures are targeted for ribosome quality control and mRNA degradation under eIF5A deficiency is still a question. Interestingly, eIF5A has been recently proposed as an RQC factor as it is required for efficient peptidyl transfer during CAT tailing and for stabilizing the CCA tail via its hypusine residue (Tesina *et al*., 2023).

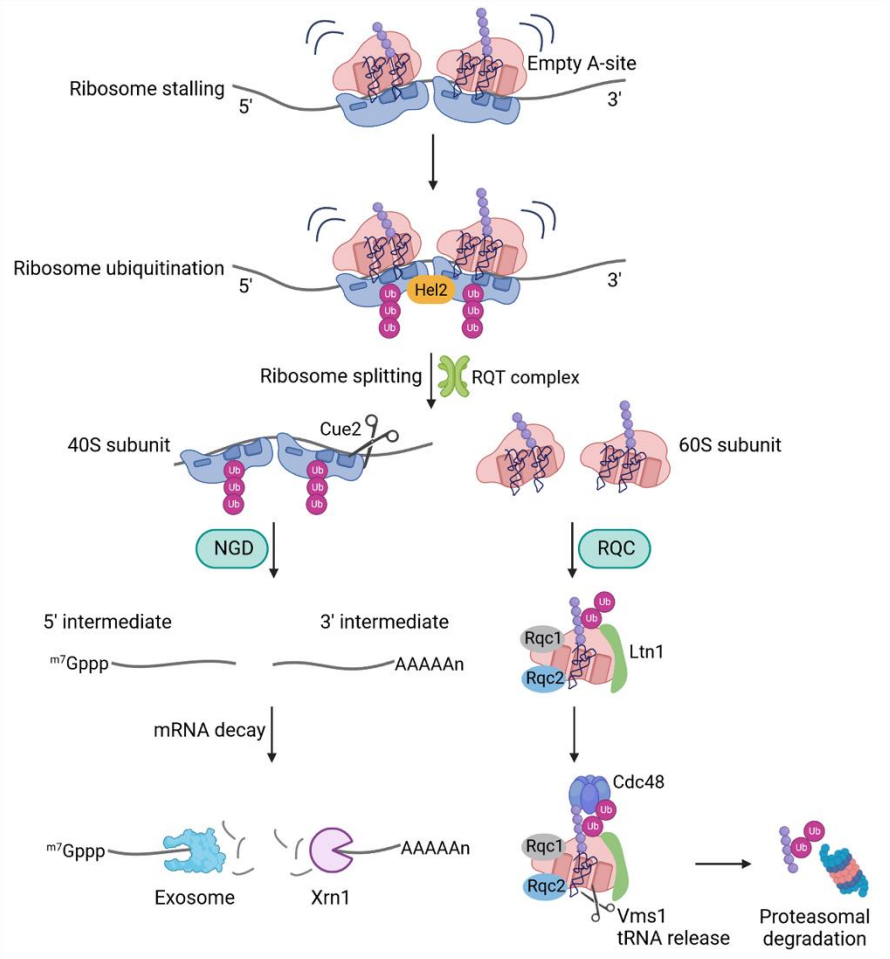

Figure 1.14. Ribosome quality control response on stalled ribosomes. Ribosome collisions and disome interface formation signal Hel2-dependent ubiquitination. Once S3 and S10 proteins are ubiquitinated, ribosome subunits are dissociated by the RQT complex and the nascent polypeptide chain is targeted for proteasomal degradation through the action of Rqc1, Rqc2, Ltn1, Cdc48 and Vms1 proteins. At the same time, no-go decay (NGD) is triggered for mRNA decay. The endonuclease Cue2 generates two types of mRNA intermediates further degraded by exosome and Xrn1 nucleases. The buildup of disomes upon Pro-Pro motifs with an occupied A site is rescued by eIF5A as shown in Figure 1.2 and avoids ribosome quality control and RNA decay responses.

1.5.3 Translation factors in transcriptional control

Although eukaryotic translation factors are classically defined by their cytoplasmic location to regulate protein synthesis, components of the translation apparatus have been found in the cell nuclei in various organisms, where they are involved in different processes associated to genome integrity control and nuclear stages of gene expression (transcription, mRNA processing and export) and thus, are regarded as moonlighting proteins (Kachaev *et al*., 2021). Their nuclear translocation is often involved in processes like stress response, oncogenesis and viral infection. Besides, different mechanisms are used to control nuclear localization of translation factors, such as post-translational modifications, although for many factors it remains unknown.

The participation of translation factors in transcriptional regulation has been reported. In this line, direct interactions of several translation factors with RNA polymerase and their subunits have been described. For instance, the yeast Rpb4/Rpb7 heterodimer interacts with eIF3 in the cytoplasm, once Rpb4 exits the nucleus associated to transcripts (Harel-Sharvit *et al*., 2010), and the human Rpb11 interacts with eIF3a, eIF3i and eIF3m (Proshkin *et al*., 2011). The human interactome of RNA Pol II shows the presence of eukaryotic initiation factors and multiple ribosomal proteins. Moreover, binding to transcription factors to regulate their subcellular localization and transcriptional activity, have also been reported. In mammals, eIF3e interacts with the transcriptional repressor Rfp and regulates the expression of 34 genes (Esteves *et al*., 2020); and eEF1A stimulates the Hsf1 which results in *HSP70* transcription during the heat shock response (Vera *et al*., 2014). Finally, some nuclear activities of translation factors in the nucleus are related to their ability to bind RNA molecules. For instance, human eIF4E associates to the mRNA encoding CDK1 and other oncogenes and mediates its export through the Xpo1/CRM1 system (Volpon *et al*., 2017).

Several studies have also described connections between eIF5A and processes related to gene expression occurring in the nucleus (Figure 1.15). The nuclear accumulation of eIF5A is regulated via acetylation, which is mediated by nuclear PCAD, HDAC6 and SIRT2 enzymes. Acetylation and hypusination occur in proximal Lys residues in a disordered loop structure and are considered mutually exclusive, so that hypusination determines cytoplasmic localization while acetylation determines nuclear localization (Lee et *al*., 2009). The export of mammalian eIF5A requires preferably exportin 4 (Xpo4) (Lipowsky *et al*., 2000; Aksu et al., 2016) and less frequently the general nuclear export receptor Xpo1/CRM1 (Rosorius *et al*., 1999). These two mammalian exportins lack obvious orthologs in yeast.

In the nucleus, eIF5A has been found highly associated with RNA Pol II in precursor neurons (Rafiee *et al*., 2023). eIF5A2 isoform also translocates to the nucleus and binds to the promoter region of the hypoxia inducible factor 1α (*HIF-1α*) gene under hypoxic conditions. The induction of *HIF-1α* allows the activation of a number of hypoxia-responsive genes and depends on the eIF5A2 levels (Li *et al*., 2014; Tariq *et al*., 2016). Additionally, following the induction of apoptosis in human cancer cells, acetylated eIF5A is translocated to the nucleus where it may have pro-apoptotic functions (Taylor *et al*., 2007). Although indirectly, eIF5A2 isoform also regulates the transcription of ageing genes in human neuroblastoma cells through the modulation of transcription factors associated to the unfolded protein response (Liu *et al*., 2023).

Regarding its RNA binding properties, as mentioned in section 1.1.5, eIF5A has been described as a co-factor for the nuclear export of HIV-1 transcription factor Rev and replication factor Rex RNAs (Ruhl *et al*., 1993). Via interaction with Xpo1/CRM1, eIF5A is essential for the export of these two viral RNAs and thus, impacts HIV-1 functions in transcriptional activation, viral export and replication in mammalian cells. eIF5A also mediates the export of the *NOS2* mRNA via Xpo1/CRM1 in an inflammatory mouse model of diabetes, contributing to the early pathogenesis of β cell dysfunction in response to cytokines (Maier *et al*., 2010). In addition, it was recently described that human eIF5A becomes deacetylated to induce the export of associated *TSC2* mRNA during anaerobiosis conditions. The export of this specific mRNA induces its translation in the cytoplasm and allows for corresponding metabolic changes to avoid acidosis-induced DNA damage (Balukoff *et al*., 2020)

Growing evidence indicates a role for eIF5A in the nucleus and thus, although poorly understood, suggests a relationship between its transcription and translation functions. However, a systematic study of eIF5A functions in the nucleus is lacking. Chapter 6 of this thesis explores the possibility of eIF5A as a moonlighting protein that functions not only in translation but also in transcription.

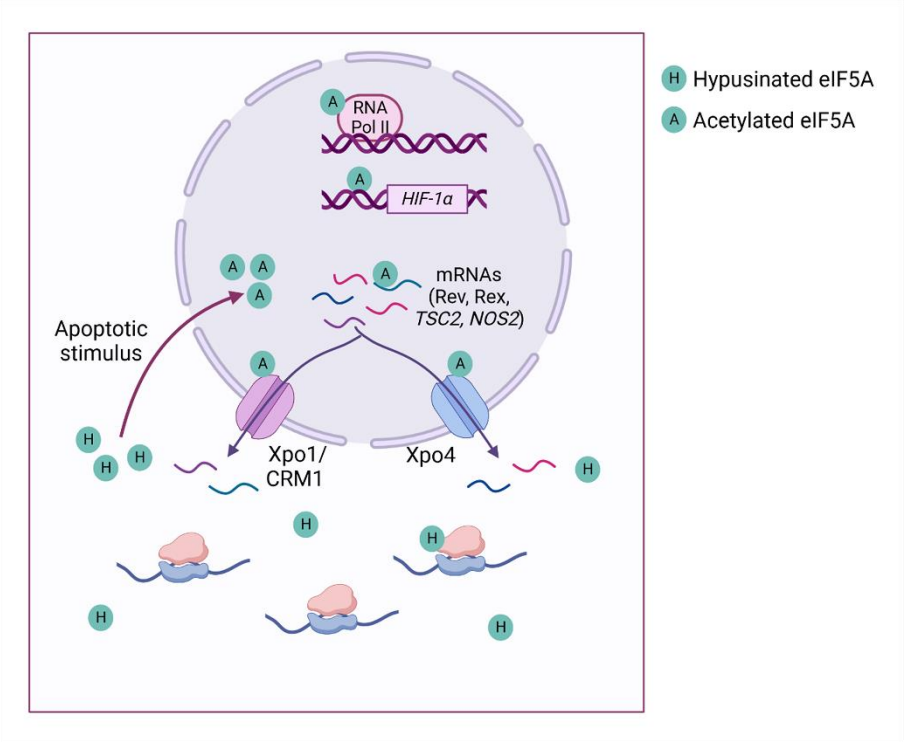

Figure 1.15. Nuclear functions of eIF5A. eIF5A in its hypusinated form assists translation in the cytoplasm whereas eIF5A in its acetylated form is found in the nucleus, where it plays different functions. eIF5A mediates the export of some HIV-1 mRNAs (Rev and Rex) and others like *TSC2* and *NOS2* under specific conditions. In addition, eIF5A has been found associated to RNA Pol II in neurons as well as bound to the promoter of *HIF-1α* under hypoxic conditions. In certain cancer cells and upon apoptosis induction, eIF5A translocates to the nucleus to exert pro-apoptotic functions.

General objectives of this thesis

In the context of the eukaryotic model organisms *Saccharomyces cerevisiae* and *Mus musculus*, this dissertation aims to characterize the functions of the translation factor eIF5A in different aspects of cellular metabolism and transcriptional control. For these purposes, this thesis has been divided into four results chapters corresponding to the following objectives:

1. To determine whether eIF5A is necessary for collagen synthesis in mammalian cells and to describe at the molecular level the causes of collagen translation blockade produced by eIF5A inhibition.

2. To elucidate whether gene expression regulation of the two eIF5A eukaryotic isoforms responds to the cellular metabolic status and the mechanisms involved in the regulation in *S. cerevisiae*.

3. To decipher the molecular mechanism by which eIF5A is essential for the cellular mitochondrial respiration in *S. cerevisiae* and how it affects the synthesis of mitochondrial proteins.

4. To investigate whether nuclear eIF5A is involved in transcriptional control and identify target genes, mechanisms and its putative contribution to the crosstalk between transcription and translation in *S. cerevisiae.*

Chapter 2

Materials and Methods

2.1 Microbiological techniques in *Saccharomyces cerevisiae*

2.1.1 Strains, buffers, reagents and growth media

All the *S. cerevisiae* strains used herein are listed in Table A1.1 (see Annex I for all the A1 Tables mentioned in the Materials and Methods section). Composition of all media, buffers and solutions used herein are listed in Table A1.2. References and trading houses of reagents and enzymes used in this study are listed in Table A1.3. Yeast cells were grown in either liquid YPD, YPGal, YPGly, YPEtOH, synthetic complete medium containing glucose (SC) or galactose (SGal). SC media lacking the indicated selection marker were used for selection of auxotrophic markers. All the media were autoclaved for 20 min at 121ºC before use.

Solid media were obtained by adding bacteriological agar to a final concentration of 2% to the liquid media before autoclave sterilization. For antibiotic resistance selection, Geneticin (Kanamycin) was added to a final concentration of 200 µg/mL while Nourseothricin (clonNAT) was added to a final concentration of 100 µg/mL. Antibiotics were filtered and added to the media after autoclave sterilization.

2.1.2 Growth conditions and treatments

Experimental assays were performed with cells exponentially grown for at least four generations until the required optical density at a wavelength of 600 nm (OD_{600}) at 30ºC with shaking at 190 rpm. Temperature-sensitive strains were grown at the permissive temperature of 25ºC until the required OD_{600} and transferred to the semi-permissive temperature (33ºC) or restrictive temperature (37ºC) for 4 h for complete depletion of eIF5A.

For certain experiments described in the text, different drugs were used and are summarised in Table A1.3. For iron-deficient (- Fe) conditions, bathophenanthrolinedisulfonic acid (BPS), a specific Fe^{+2} chelator, was added to a final concentration of 100 µM for 7 h. For electron transport chain (ETC)-deficient conditions, antimycin A, a specific inhibitor of complex III of ETC was added to a final concentration of 10 µg/mL for 6 h. For other experiments, the media were supplemented with 300 µg/mL of δ-aminolevulinate (ALA) and 25 µg/mL of hemin to increase the heme levels, with 200 ng/mL of rapamycin to inhibit the TORC1 complex, with 1 µM carbonyl cyanide m-chlorophenylhydrazone (CCCP) to uncouple the mitochondrial oxidative phosphorylation or with 0.5 mM auxin to achieve Tim23 depletion.

2.2 Microbiological and molecular biology techniques in *Escherichia coli*

2.2.1 Strains and growth conditions

Subcloning Efficiency™ DH5α Competent Cells with genotype: F- φ80lacZΔM15 Δ(lacZYA-argF)U169 recA1 endA1 hsdR17(rk-, mk+) phoA supE44 thi-1 gyrA96 relA1 λ- were used for experiments requiring bacterial cells (Table A1.3).

The Lysogeny Broth (LB) medium was used to grow *E. coli*. For LB agar plates, 2% of agar was added prior autoclave sterilization. Ampicillin (50 µg/mL) was filtered and added to the media after autoclave sterilization to select the bacteria with the plasmids containing the antibiotic-resistance gene.

2.2.2 *E. coli* transformation and plasmid extraction

The competent *E. coli* strain DH5α (see section 2.2.1 of Materials and Methods) was used for propagation of newly constructed and already verified plasmids. Transformation was made according to manufacturer's instructions. Briefly, cells were mixed with 1 µL of plasmid of interest and incubated on ice for 30 min. Then, heat shock was performed at 42ºC for 30 s followed by a second incubation on ice for 2 min. 1 mL of LB medium was added and samples were incubated at 37ºC for 1 h. 200 µL of transformed cells were spread onto LB plates supplemented with ampicillin and incubated overnight at 37ºC. Colonies were selected and incubated in 5 mL of LB liquid media supplemented with ampicillin at 37ºC overnight. For subsequent plasmid extraction, the GeneJET Plasmid Miniprep Kit was used following manufacturer's instructions. In the case of new constructs, plasmids from several individual colonies were analyzed by polymerase chain reaction (PCR, see section 2.3.1 of Materials and Methods) followed by DNA sequencing to check the position and sequence of the insert.

2.3 Molecular biology techniques in *Saccharomyces cerevisiae*

2.3.1 DNA-related molecular techniques

- Polymerase chain reaction (PCR)

PCR was used to amplify DNA fragments and generate disruption or tagging cassettes, to clone inserts and to test yeast transformants and constructed plasmids. The Taq DNA polymerase was used for conventional PCR whereas the Pfu ultra fusion high-fidelity polymerase was used for gene disruption, genomic tagging and plasmid construction (see below). Oligonucleotides used for PCR are listed in the Table A1.4. The PCR was performed in a Veriti™ 96-Well Fast Thermal Cycler (Thermo Fisher Scientific). PCR cycles generally consisted of an initial denaturing step at 95ºC 5 min, 30 amplification cycles divided in 3 steps (denaturation at 95ºC for 45 s, annealing at corresponding temperature for 45 s and elongation at 72ºC for 1 min per kb of PCR product) and a final extension step at 72ºC 10 min. Duration and temperatures depended on the DNA polymerase and oligonucleotides used as well as on the size to amplify.

- Agarose gel electrophoresis

DNA fragment size determination and separation, as well as the RNA quality control, were carried out in 1% agarose gels. Agarose was dissolved in the electrophoresis buffer 0.5x TBE. When the solution was tempered, 10 µL of SafeView nucleic acid stain were added per 100 mL. The Generuler DNA Ladder was used to estimate the size of DNA products. Nucleic acids were resuspended in DNA Gel Loading Dye and visualized under UV illumination using the Molecular Imager Gel Doc XR+ Imagining System (BioRad).

- Genomic DNA extraction

Genomic DNA (gDNA) was obtained from a 10 mL yeast overnight culture grown in YPD at 30ºC the corresponding temperature (25ºC or 30ºC). The culture was centrifuged at 3000 rpm for 5 min and washed with 10 Prep buffer. Then, cells were dissolved in 500 µL of 10 Prep buffer and transferred into a screw-cap tube already containing 500 µL of sterile glass beads and 500 µL of phenol:chloroform (1:1). Cells were mechanically broken using the Precellys 24 tissue homogenizer (Bertin Technologies) with 2 shaking cycles of 30 s at 6500 rpm each and centrifuged at 13000 rpm for 5 min. The aqueous phase was transferred into a fresh tube containing 500 µL of phenol:chloroform (1:1) and centrifuged again at 13000 rpm for 5 min. The aqueous phase was transferred into a fresh tube containing 500 µL of chloroform and centrifuged again at 13000 rpm for 5 min to eliminate organic residues. The aqueous phase was transferred into a fresh tube, and nucleic acids were precipitated with 2.5 volumes of cold 96% ethanol and 0.1 volumes of 3 M sodium acetate for 2 h at -80ºC. Following precipitation, each sample was centrifuged at 13000 rpm for 15 min, washed with cold 70% ethanol and the pellet was dissolved in 200 µL of 1x TE buffer. A volume of 3 µL of RNase A was added to eliminate the RNA contaminants during 30 min at 37ºC, followed by the addition of 10 µL of Proteinase K during 1 h at 65ºC to remove protein contaminants. DNA was then precipitated by adding 0.1 volumes of 3 M sodium acetate and 2.5 volumes of cold 96% ethanol. Finally, after centrifuging at 13000 rpm for 15 min and washing with cold 70% ethanol, the DNA pellet was dried and dissolved in 200 µL of 1x TE buffer.

- Obtention of new strains by gene disruption or genomic tagging

The disruption of genes as well as the tagging of the C-termini of genes of interest for protein quantification or visualization were carried out with a PCR-based genomic technique (see above). Plasmids from Longtine system (Longtine *et al.,* 1998) and others (listed in Table A1.6) were used as template for PCR reaction (see section 2.3.1 of Materials and Methods) using specific primers (listed in Table A1.4) containing 45 bases complementary to the gene of interest with an additional 18 bases complementary to the corresponding vector. The resulting cassette was transformed in the corresponding strains following the lithium acetate-based method (Gietz *et al.*, 1992) with modifications, that allowed auxotrophic or antibiotic resistance selection in the corresponding medium. Briefly, cells were grown until OD_{600} 1 and pelleted by centrifugation at 4400 rpm for 4 min. Cells were washed with distilled water and resuspended in 1 mL of water. Aliquots of 100 µl were used for each transformation, which were centrifuged 4 min at 4400 rpm. Then, 360 µl of transformation mix (240 µl PEG 3350 50%, 36 µl 1M LiAc, 50 µl single-strand carrier DNA 2 mg/mL, 34 µl DNA plus water) was added to each transformation tube and resuspended by vortexing. Finally, cells were incubated at 42ºC for 40 min. Transformants selected by antibiotic resistance were re-incubated for 2 h in YPD at 25ºC or 30ºC before plating in the selective medium. Selection plates were incubated at 25ºC or 30ºC for 2-3 days to select transformants. The genomic loss or integration was confirmed by gDNA conventional PCR (see above) and by plating in selective and non-selective media.

- Plasmid construction and integration

All plasmids used in this study are listed in Table A1.6. Fusions with *lacZ* under the control of a tetracycline-repressible operon (*tetO*$_7$) were constructed in the plasmid pCM179 (Garí *et al.*, 1997) while dual-luciferase reporter constructs were generated by cloning between the in-frame Renilla and firefly luciferase open reading frames (ORFs) in the plasmid pDL202 (Letzring *et al.*, 2010). pDL202 was kindly supplied by Elizabeth Grayhack (University of Rochester, Rochester, NY). The GAP-REPAIR homologous recombination method was used for cloning (Joska *et al.*, 2014). The DNA inserts for cloning were amplified by PCR (see above) using *M. musculus* cDNA or *S. cerevisiae* gDNA and oligonucleotides listed in Table A1.4. After PCR product purification (GeneJet Purification kit), the plasmid and the insert were digested with restriction enzymes according to manufacturer's instructions and isolated by gel purification (GeneJet Gel extraction kit) for subsequent ligation.

Fusions with nanoluciferase (nLuc) under the control of a tetracycline-inducible operon (*tetO*$_7$) were generated by cloning the corresponding ORF in the plasmid ZP446, derived from pAG306 vector. After amplifying the backbone by conventional PCR (see above), the parental plasmid was digested by restriction enzyme *Dpn*I (New England Biolabs) and linearized plasmid was isolated by gel purification (Zymo Research). The coding sequence (CDS) fragments for cloning were amplified by conventional PCR (see section 2.3.1 of Materials and Methods) from wild-type gDNA using oligonucleotides listed in Table A1.4. After PCR product purification (Zymo Research), the fragments of interest were inserted into linearized ZP446 using Gibson Assembly. The resulting nanoluciferase constructs were linearized by restriction enzyme *Not*I (New England Biolabs) and integrated into the genome of the corresponding cells by homologous recombination.

The integration of the nLuc constructed plasmids as well as the transformation of other centromeric plasmids encoding proteins of interest (listed in Table A1.6) were performed following the lithium acetate-based transformation method (Gietz *et al.*, 1992) in the corresponding strains as previously described (see previous section). Transformants were selected in the corresponding selective medium. Selective plates were incubated at 25ºC or 30ºC for 2-3 days to select transformants. The integration was confirmed by plating in selective and non-selective media.

- Chromatin immunoprecipitation (ChIP)

To perform chromatin immunoprecipitation analysis and thus determine enrichment of proteins bound to specific genes, a total volume of 50 mL was collected for each mid-log phase or post-exponential phase culture. The protein-chromatin cross-linking was made by adding 1.35 mL of 37% formaldehyde and incubating for 15 min at room temperature with occasional mixing. Then, a volume of 2.6 mL of 2.5 M glycine was added to each sample and incubated for 5 min to inactivate the formaldehyde. After centrifuging 4000 rpm for 4 min at 4ºC, cells were washed 3 times with 25 mL of cold Tris-buffered saline (TBS) pH 7.5 and flash frozen in liquid nitrogen.

Upon defrosting, pelleted cells were washed with 700 µL of lysis buffer, resuspended in 300 µL of lysis buffer and transferred into screw-cap tubes already containing 300 µL of glass beads. Cells were mechanically broken using the Precellys 24 tissue homogenizer (Bertin Technologies) with 2 shaking cycles of 30 s at 6500 rpm. Then, 300 µL of lysis buffer were added and glass beads were eliminated by centrifugation at 800 rpm for 1 min at 4ºC. Cell lysates were then sonicated in a chilled water bath using

Bioruptor (Diagenode) with 30 s on/off cycles during 12 min to generate chromatin fragments between 300-600 base pairs. Following sonication, cell lysates were cleared by centrifugation at 12000 rpm for 15 min at 4ºC. 20 µL of each supernatant were transferred into new tubes and maintained on ice (Input samples) while the rest of the supernatants (IP samples) were incubated for 3 h at 4ºC with magnetic beads Dynabeads™ Pan Mouse IgG or Dynabeads™ Sheep anti-rabbit IgG previously combined with the corresponding antibody (listed in Table A1.7). Following incubation, the liquid phase was removed using a magnetic rack, and three successive washes with PBS/Tween were performed. Following washings, 40 µL of elution buffer were added to elute the samples from the Dynabeads and incubated for 8 min at 600 rpm at 65ºC. A volume of 40 µL of supernatant was transferred into a new tube and the elution process was repeated. Finally, additional elution buffer was added to all supernatants (IP and Input samples) to a final volume of 100 µL. A subsequent 15 h incubation at 600 rpm at 65ºC was performed to reverse crosslinking.

To obtain the DNA, each sample was treated with 7.5 µL of Proteinase K at 37ºC during 1 h 30 min. Next, DNA was purified using the GeneJet Purification kit according to manufacturer's instructions. Specific binding of myc-tagged proteins (Hap1, Tup1 and Ssn6), RNA Pol II and eIF5A to DNA fragments was analyzed by quantitative PCR (qPCR, see section 2.3.2 of Materials and Methods) using specific primers listed in Tables A1.4 (ORF binding) and A1.5 (promoter binding). IP and Input samples were tested at 1/5 and 1/100 dilution respectively. To quantify the relative binding of proteins of interest to genes of interest, values were normalized first against an internal control (a DNA locus where the protein of interest was known not to be bound) and second, against the value obtained in the Input sample. Thus, the enrichments were represented as a percentage of Input.

2.3.2 RNA-related molecular techniques

- RNA extraction

Total RNAs were isolated from yeast cells following the phenol:chloroform protocol. A volume of a mid-log phase culture corresponding to 10 OD_{600} units was centrifuged at 4400 rpm for 4 min and the cell pellet was flash frozen and stored at -20ºC. Then, cells were resuspended in 500 µL of LETS buffer and transferred into a screw-cap tube already containing 500 µL of sterile glass beads and 500 µL of phenol:chloroform:isoamyl alcohol (125:24:1). Then, cells were mechanically broken using the Precellys 24 tissue homogenizer (Bertin Technologies) with 2 shaking cycles of 30 s at 6500 rpm each and centrifuged at 13000 rpm for 5 min at 4ºC. The aqueous phase was transferred into a new tube containing 500 µL of phenol:chloroform:isoamyl alcohol (125:24:1), centrifuged again and transferred then to a tube containing 500 µL of chloroform:isoamyl alcohol (25:1) to discard organic residues and phenol. The RNA from the aqueous phase was precipitated with 2.5 volumes of cold 96% ethanol and 0.1 volumes of 5 M LiCl overnight at -20ºC. After that, samples were centrifuged for 15 min at 13000 rpm at 4ºC and washed with cold 70% ethanol. The pellet was dried and dissolved in 200 µL of RNase-free milliQ water for 1 h at 30ºC for later RNA quantification and quality control with NanoDrop device (Thermo Fisher Scientific) and agarose gel electrophoresis respectively.

- Quantitative reverse transcription PCR (RT-qPCR)

The RT-qPCR was used to quantify the expression of mRNAs but also to analyze DNA-protein interactions following ChIP (see section 2.3.1 of Materials and Methods). For mRNA analysis, first, the DNA of each RNA sample was removed from 2.5 µg of RNA using the DNase I RNase-free for 15 min at 25ºC in a final volume of 25 µL. To inactivate the DNase I, a volume of 0.625 µL of 5 mM EDTA was added and incubated 10 min at 65ºC. For reverse transcription, 5 µL of DNA-free RNA were used in a final volume of 20 µL using an oligo $d(T)_{18}$ with the Maxima Reverse Transcriptase (200 U/µL) following manufacturer's instructions.

The qPCR reactions were carried out using the CFX96 TouchTM Real-Time PCR Detection System (BioRad) and 5 µL of SYBR Green Premix Ex Taq (Tli RNase H Plus) for a total reaction volume of 10 µL. A cDNA pool with all samples 1/10 diluted was made and serial dilutions (1/5, 1/10, 1/50, 1/100, 1/500 and 1/1000) were used to generate a calibration curve for each primer pair in each experiment. A volume of 2.5 µL of each cDNA sample (dilution depending on the studied gene) and 0.2 µL of each 10 µM primer were added to a final volume of 10 µL for RT-qPCR and ChIP-qPCR experiments. The list of primers designed to amplify gene fragments of interest are listed in Table A1.4. For amplification, the PCR conditions consisted of an initial denaturing step (95ºC for 3 min) and 40 amplification cycles (annealing at 95ºC for 10 s and extension at 55ºC for 30 s). After each cycle, the plate was read to determine the SYBR signal. The melting curves generated with each primer pair confirmed the specificity of the PCR reaction and the threshold (Ct) value of each sample was used to determine the amount of cDNA or DNA in each case by interpolation to the corresponding calibration curve. Endogenous actin mRNA levels were used for normalization.

- Polysome fractionation

For polysome fractioning, cells were grown at 25°C or 30°C to post-diauxic phase in SGal medium and transferred to 37°C for four hours for the experiments requiring temperature-sensitive strains. For cell extraction, a culture volume corresponding to an OD_{600} of 100 was chilled for 5 min on ice in the presence of 0.1 mg/mL cycloheximide (CHX). Cells were centrifuged at 4400 rpm for 3 min at 4°C and washed twice with 2 mL of lysis buffer. Cells were resuspended in 700 µL of lysis buffer and transferred to a 1.5 mL screw-cap tube already containing 500 µL of glass beads. Cells were mechanically disrupted by vortexing 8 times for 30 s with 30 s of incubation on ice in between. Then, lysates were cleared by centrifugation at 5000 rpm for 5 min at 4°C and the supernatant was recovered. After centrifugation at 8000 rpm for 5 min at 4°C, the RNA was recovered, and its concentration was estimated using a Nanodrop device (Thermo Fisher Scientific). Glycerol was added to all the samples to a final concentration of 5% and extracts were flash frozen and stored at -80°C. Samples of 10 A_{260nm} units were loaded onto 5-50% sucrose gradients and separated by ultracentrifugation for 2 h 40 min at 35000 rpm in a Beckman SW41Ti rotor at 4°C. Then, gradients were fractionated by isotonic pumping of 60% sucrose from the bottom and twenty-two 0.5 mL samples were recovered (workflow of the process is shown in Figure 2.1). The polysomal profiles were monitored by UV detection at 260 nm using a density gradient fractionation system (Teledyne Isco, Lincoln, NE). RNAs were extracted using SpeedTools Total RNA Extraction kit with the rDNAse treatment after the RNA elution step according to manufacturer's instructions. Specific mRNAs were analyzed by RT-qPCR (see section above) using

specific primers (listed in Table A1.4) and represented as a percentage of total. Three biological replicates were performed for each polysome profile, and a representative profile is shown.

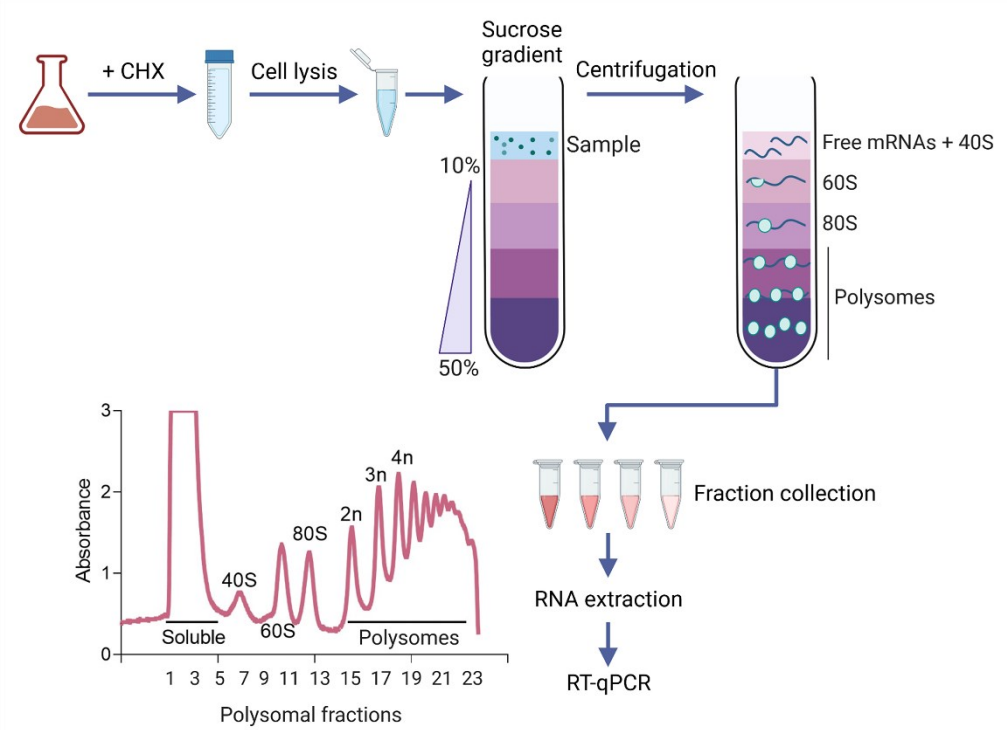

Figure 2.1. Workflow representation of the polysome fractionation protocol. The various steps of the protocol include cell lysis, sucrose gradient centrifugation, fractionation, RNA extraction and RT-qPCR. The general polysome profile represented shows, from lighter to heavier fractions, the soluble mRNAs, the total mRNAs bound to ribosomal subunits (40S and 60S), monosomes (80S) and polysomes.

2.3.3 Protein-related molecular techniques

- Western blotting assay

Protein extraction was performed in cells from mid-log phase cultures to identify and quantify the levels of yeast specific proteins. A cell culture volume corresponding to 5-10 OD_{600} units was centrifuged at 4400 rpm for 4 min and the cell pellet was flash frozen and stored at -20ºC. Upon defrosting, the cell pellets were washed with distilled water and then resuspended in 200 µL of 0.2 M NaOH. The samples were then incubated for 5 min at room temperature and subsequently centrifuged at 12000 rpm for 1 min. Then, samples were resuspended in 100 µL of 2x-SDS protein loading buffer and boiled 5 min at 95ºC. Afterwards, cell lysates were centrifuged at 3000 rpm for 10 min at 4ºC to remove cell debris and insoluble proteins and supernatants were transferred into fresh tubes and stored at -20ºC.

The soluble protein context in the extracts was quantified by an OD_{280} estimation using the Nanodrop device (Thermo Fisher Scientific) to load equal protein amounts per sample. After boiling the samples at 95ºC, a volume corresponding to approximately 80 µg of protein was separated by molecular weight in denaturing polyacrylamide gel electrophoresis (SDS-PAGE). The percentage of acrylamide:bis-acrylamide 37.5:1 of the gels was adjusted (8-15%) depending on the molecular weight of the proteins

to be analyzed. The MiniProtean Tetra Cell (BioRad) system was used with SDS Running buffer at 100 V during 2-3 h at room temperature. Once proteins were resolved together with 5 µL of molecular weight ladder per gel (PageRuler Prestained, Thermo Fisher Scientific), they were transferred onto a nitrocellulose membrane (Amersham Protran 0.45 µm NC, GE Healthcare). Transfer buffer was used in the Mini Trans-Blot Electrophoretic Transfer Cell (BioRad) system at 400 mA during 1 h with refrigeration. Then, the membranes were stained during 5 min with 0.5% Red Ponceau S staining solution to check that same amount of proteins was loaded in each lane. Ponceau S was removed with TBS-T pH 7.5 washings and the membranes were blocked with 5% skimmed in TBS-T for 1 h at room temperature. The primary antibodies (listed in Table A1.7) were incubated overnight at 4ºC and the appropriate horseradish peroxidase-conjugated secondary antibody was incubated during 1 h at room temperature, both in 5% skimmed milk blocking solution. The washings with TBS-T between antibodies and after secondary antibody incubation were made 3 times for 10 min.

Chemiluminiscent signals from bound antibodies were detected using the Amersham ECL Prime Western blotting detection kit (Sigma-Aldrich) following manufacturer's instructions and digitally analyzed using ImageQuant LAS 4000 software (GE Healthcare). Several exposure times per membrane were quantified using the ImageQuant TL 1D gel analysis (GE Healthcare). The intensity of bands was normalized against G6PDH bands.

- Fluorescence microscopy

For protein visualization under the microscope, yeast cells were grown to a post-diauxic phase in SGal medium, centrifuged, washed, and subjected to standard fluorescence and phase contrast microscopy.

For mitochondrial protein localization experiments, cells were imaged using an Eclipse Ti-E microscope (Nikon) with an oil-immersion x63 objective. Imaging was controlled using NIS-Elements software (Nikon). For mitochondrial aggregates co-localization experiments and mitochondrial membrane potential measurements, fluorescence images were acquired using an Axio Imager Z1 fluorescence motorized microscope equipped with a Plan Apochratic x63/1.4 oil-immersion objective and a 100 W mercury lamp (Carl Zeiss, Germany). Images were recorded with an AxioCam MRm digital camera (Carl Zeiss, Germany). The following excitation and emission wavelengths were used: 4′,6-diamidino-2-phenylindole (DAPI) (excitation 359 nm; emission 457 nm), GFP (excitation 475 nm; emission 509 nm), MitoTracker Red (excitation 578 nm; emission 600 nm), RFP (excitation 555 nm; emission 583 nm), mCherry (excitation 587 nm; emission 610 nm) and Nile Red (excitation 460 nm; emission 582 nm). The same exposure times were used to acquire all images. All the imaging analysis was performed on Image J software.

To analyze mitochondrial membrane potential, cells were incubated with 0.5 µM MitoTracker Red CMXRos for 30 min, washed and subjected to microscope. To analyze Pdr5 activity, cells were incubated with 3.5 µM Nile Red for 15 min, washed and subjected to microscope. To study nuclei localization, cells were incubated with 1 µg/mL DAPI for 30 min in the dark, washed and subjected to microscope. References and trading houses of microscopy probes used in this study are listed in Table A1.3.

- Determination of β-galactosidase activity

Yeast strains harbouring pCM179 plasmid and its derivatives (listed in Table A1.6) were used to perform the β-galactosidase assays. The *lacZ* gene encodes the β-galactosidase enzyme, which hydrolyses a lactose analogue (Ortho-Nitrophenyl-β-D-galactopyranoside, ONPG) resulting in the formation of yellow ortho-nitrophenol, spectrophotometrically detectable at A_{420}. This allows the study of the expression of the corresponding *lacZ*- fused genes.

Yeast cultures were grown at 25ºC in SC-URA medium with 2 µg/mL doxycycline to keep the $tetO_7$ promoter switched off. After reaching OD_{600} of 0.2, the cell culture was washed with medium lacking doxycycline, resuspended in fresh SC-URA medium to activate $tetO_7$ transcription and incubated at 25ºC or 37ºC for 6 h. Then, a volume corresponding to 1-5 OD_{600} units was centrifuged, and flash frozen in liquid nitrogen. Cells were resuspended in 1 mL of buffer Z and 700 µL were transferred into a new tube already containing 50 µL of 0.1% SDS and 50 µL of chloroform. Cells were permeabilized by vortexing during 10 s. The assay started by adding 200 µL of ONPG (4 mg/mL) to each sample and incubating at 30ºC with maximum shaking. The reaction was stopped after 5-30 min adding 350 µL of 1 M Na_2CO_3 and incubating the tubes on ice. Samples were centrifuged at high speed for 2 min and A_{420} was determined, as well as the OD_{600} using the original cell suspension in buffer Z. The β-galactosidase activity was calculated in Miller Units (one unit corresponds to 1 nmol of ONPG hydrolysed per min at 30ºC and pH 7.0):

$$\text{Miller Units} = (A_{420} \cdot 1000) / (OD_{600} \cdot \text{cell volume (mL)} \cdot \text{assay time (min)})$$

- Determination of dual-luciferase activity

The dual-luciferase assay was performed with yeast strains harbouring the plasmid pDL202 and its derivatives (listed in Table A1.6) following (Gutierrez *et al.*, 2013) procedure with some modifications. Briefly, yeast cells were grown at 33ºC in SC-URA medium to an OD_{600} of 0.8, harvested and flash frozen. Subsequently, cell pellets were resuspended in 200 µL lysis buffer and mixed with one volume of glass beads for further mechanical homogenization in a Precellys 24 tissue homogenizer (Bertin Technologies). Lysates were cleared by centrifugation at 12000 rpm for 5 min at 4ºC, and protein extracts were assayed for firefly and Renilla luciferase activity sequentially in a 96-well luminometer plate (Thermo Fisher Scientific) using a microplate luminometer (Thermo Fisher Scientific) and the Dual-Glo Luciferase Assay System. Manufacturer's instructions were followed. Finally, the firefly:Renilla luciferase ratio for each construct was calculated.

- Determination of translation elongation rates

The basic principle to measure translation elongation speed is based on the nanoluciferase induction and initially described by Schleif *et al.*, 1973. Yeast cells harbouring pAG306 series vectors were grown in at 25ºC in YPD medium to an exponential OD_{600} of 0.2 and then transferred to 37ºC for four h. Doxycycline was added to the culture to a final concentration of 10 µg/mL to induce the expression of the nLuc-fused gene in the pAG306 series vectors and pre-incubated for 5 min at room temperature. The nLuc activity was measured using furimazine as the nLuc highly specific substrate. A 90 µL volume of each culture and 10 µL of the furimazine (1/200 dilution were incubated in a Cellstar non-transparent white 96-well microplate for one h and the bioluminescence intensity was monitored with a Tecan Infinite 200 PRO plate reader every 30 s. For CHX-treated samples, 10 mg/mL CHX was added to reach

a final concentration of 50 µg/mL to stop the translation for 5 min. All the bioluminescence measurements were acquired at 460 nm, the peak emission wavelength of nLuc. The nLuc induction curve was constructed by plotting the nLuc activity against induction time and further linearized using a square-root plot (known as "Schleif plot") to estimate the minimum reaction time required for complete translation (Schleif *et al.,* 1973). The synthesis time of the first nLuc-fused protein (Tfirst) was estimated using the straight-line fit of the induction kinetics data and the reaction time of the nLuc reporter alone was subtracted. As a first estimate of the translation elongation rate (k) of each fused protein, the equation k = nLuc-fused protein length/Tfirst (aa/s) was used to calculate the time required for translating the different proteins of interest.

2.3.4 Determination of oxygen consumption rates

Saturated pre-cultures were used to inoculate new cultures in the appropriate medium (YPGal or SGal). Cells were grown at 25ºC or 30ºC until reaching OD_{600} of 1.5-2.0. A volume corresponding to 2 OD_{600} units was collected and washed with distilled water, resuspended in 1 mL of YEP medium supplemented with 2% ethanol and 3% glycerol, and transferred into an air-tight oxygen consumption chamber, magnetically stirred, and maintained at 30ºC. The oxygen content decline was monitored during 15 min using the model Oxyview 1 System (Hansatech) with an S1 Clark-type oxygen electrode following the manufacturer's protocol. The system consists of a platinum cathode (-) in contact with both the silver anode (+) through 3 M KCl, and the chamber on the top where cells were placed. A basal 0.7 V voltage difference occurs between the cathode and the anode, and when O_2 is present in the chamber it is reduced, and the voltage difference increases proportionally. First, the maximum voltage was established at 0.9 V using oxygen-saturated distilled water (0.28 µmol O_2 per mL at 20ºC). This maximum value was registered on a graph paper at the 180 mm horizontal division, and the minimum value, 0 µmol O_2 per mL, was situated at the 20 mm division. Second, vertical output speed of the register graph paper was established in 5 mm/min. Thereby, the horizontal changes in the recording corresponded to a decrease in the O_2 content of the solution in the chamber, and vertical changes corresponded to the time elapsed. In this way, it was possible to calculate the oxygen consumption rate per minute and per OD_{600}. The oxygen content declined was monitored for 15 min and respiratory rates were determined from the slope.

2.3.5 Determination of individual transcription rates and mRNA levels at genomic scale

To determine the transcription rate (TR) in the corresponding strains, a genomic run-on (GRO) was performed as originally described in (García-Martínez *et al.*, 2004). Briefly, wild-type and *tif51A-1* cells were grown to early mid-log phase at 25ºC overnight and then transferred to 37ºC for 4 h. A Coulter-Counter Z series device (Coulter Inc.) was used to calculate the number of cells per mL of culture. Culture volumes were adjusted so that approximately $6•10^8$ cells were harvested to perform the *in vivo* transcription. A second sample corresponding to 20 mL of cell culture was also harvested for total RNA extraction (see section 2.2.1 of Materials and Methods). Both pellets were flash frozen and stored at -20ºC. Upon defrosting, the cell pellet was washed in cold water and resuspended in 1 mL of 0.5% cold N-lauryl sarcosine sodium sulfate (sarkosyl) and transferred to a new tube. After permeabilization, cells were centrifuged at 6000 rpm for 1 min and the supernatant was removed. To perform the run-on, cells

were resuspended in 1.5 mL Eppendorf tubes with 115 µL of distilled water, 120 µL of 2.5x transcription buffer, 16 µL of ACG mix, 6 µL of 0.1 M DTT and 20 µL of [α-^{33}P]UTP (3000 Ci/mmol). The mixture was incubated at 30ºC for 5 min and 600 rpm shaking to allow transcription elongation. The transcription was stopped by adding 1mL of cold distilled water and the cells were collected by centrifugation at 6000 rpm for 1 min to remove the non-incorporated radioactive nucleotide. Then, total RNA was isolated following the phenol:chloroform protocol (see section 2.2.1 of Materials and Methods) and dissolved in 300 µL of RNase-free milliQ water. The RNA concentration was estimated using 1:100 dilutions by an OD_{260} measurement using a Biophotometer (Eppendorf). A 5 µL aliquot was used for specific radioactivity determination using the Tricarb scintillation counter (Perkin Elmer). Home-made macroarray nylon filters (García-Martínez *et al.*, 2004) were pre-hybridized for 1 h with 5 mL of hybridization solution at 65ºC. 300 µl of 2x hybridization solution were added to all the *in vivo* labelled RNA samples and mixed with 3 mL of hybridization solution. Macroarray filters were hybridized for 48 h in a roller oven at 65ºC. After the hybridization was completed, filters were washed once with 1x saline sodium citrate (SSC), 0.1% SDS for 10 min, and twice with 0.5x SSC, 0.1% SDS for 10 min at 65ºC. The macroarrays were vacuum-sealed with plastic and exposed to an imaging plate (BAS-MP, FujiFilm) for the desired time depending on the signal intensity (1-7 days). The imaging plate was read at 50 µm resolution in a phosphorimager scanner (FLA-3000, FujiFilm). Macroarrays were re-used for cDNA as well as for the rest of the replicates. For that purpose, filters were stripped by washing them for 5-10 min with boiling stripping solution (5 mM sodium phosphate buffer pH 7, 0.1% SDS).

For the second cell aliquot, total RNA was isolated following the phenol:chloroform protocol (see section 2.2.1 of Materials and Methods) and dissolved in 100 µL of RNase-free milliQ water. Approximately 50 µg of RNA were purified using the Quiaquick kit (Qiagen) following manufacturer's instructions and used for reverse transcription into cDNA. For that, 200 U of Maxima Reverse Transcriptase (200 U/µL), 3 µL of oligo $d(T)_{15}VN$ (500 ng/µL), 1 µL of RNaseOUT, 3 µL of 0.1 M DTT, 6 µL of 5x RT buffer, 1.5 µL of dNTP mix, and 4 µL of [α-^{33}P]dCTP (3000 Ci/mmol) were added to a final volume of 30 µL. The labelling reaction was incubated for 2 h at 50ºC and the reaction was stopped by adding 1 µL of 0.5 M EDTA. The labelled cDNAs were purified by a S300-HR MicroSpin column (Amersham Biosciences) so the non-incorporated radioactive nucleotide was removed. The hybridizations were performed as described previously for GRO except that cDNA samples were denatured at 95ºC for 5 min prior hybridization and a final concentration of 3.5 x 10^6/mL was employed. Microarray filters were hybridized for 24 h in a roller oven at 65ºC and the washings were done as previously mentioned. Both GRO and cDNA labelled samples belonging to the same sampling were successively hybridized against the same filter. Filters were swapped between the three replicates so the same samples from different experiments were hybridized in different microarrays (outline of the whole process is shown in Figure 2.2).

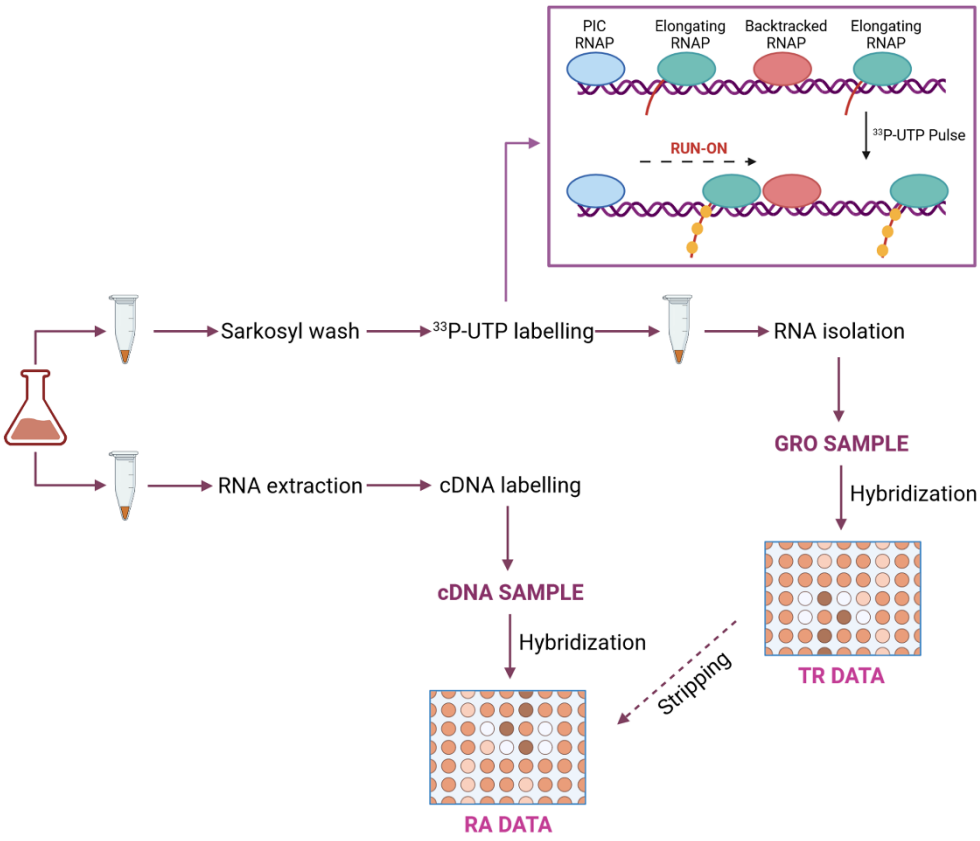

Figure 2.2. Workflow representation of the genomic run-on (GRO) method. Overview of the protocol explained in section 2.3.5. The protocol includes run-on analysis of one aliquot to determine the density of transcribing RNA polymerases and cDNA amount analysis of the second aliquot. Both samples were hybridized in the same DNA macroarray used first for GRO.

2.3.6 Total poly(A) RNA measurements

To determine the global mRNA amount (RA), a dot-blot procedure was used to determine the proportion of polyadenylated [poly(A)] mRNA per cell as previously described (García-Martínez *et al.*, 2004). Briefly, three different dilutions (67.5, 125 and 250 ng/µL) of the total RNA extracted from each sample were spotted on a nylon Hybond-XL filter (GE Healthcare), using a BioGrid robot (BioRobotics). Then, the RNA was cross-linked with the nylon using the GS GeneLinker (BioRad). Before hybridization, 1 µL of oligo $(dT)_{40}$ (10 µM) was radioactively labelled by incubating with 1 µL of polynucleotide kinase (PNK, 10 U/µL), 2 µL of 10x PNK buffer, 3 µL of [γ-^{32}P]ATP (3000 Ci/mmol) and 14 µL of RNase-free milliQ water at 37ºC for 1 h. The reaction was stopped by incubating the mixture at 70ºC for 10 min and purified using S300-HR MicroSpin column (Amersham Biosciences). Filter hybridization was performed at 42ºC for 24 h using the same procedure and solutions described in the section above. Sealing, exposure and scanning were performed as previously described. The proportion of poly(A) mRNA per µg of total RNA was calculated, and thus, per cell in each of the samples.

The relative proportion of poly(A) mRNA per µg of total RNA was calculated for each sample from the same dot-blot with regards to the reference sample was calculated: the quantified intensity signal (by

Image J software) was used as poly(A) RNA amount in each sample after dividing by the RNA amount in each well. This proportion was multiplied by the total RNA per cell and thus, a value of mRNA (mRNA/cell) concentration was obtained as a relative percentage of mRNA/cell with regards to the reference sample.

2.3.7 Quantification of hybridization signals and analysis procedures for genomic assays

These experiments were always done in triplicate to reduce the variability provided by differences in *in vivo* incorporation, RNA extraction and hybridization. The scanned microarray images from both GRO and cDNA experiments were quantified using Array Vision software (Imaging Research) taking the sARM density (after background substraction) as signal. Analysis of the data was performed as described (García-Martínez *et al.*, 2004). For GRO and cDNA analysis, values that were at least 1.2 times higher than the local background were taken as valid measurements. An average data set of three replicates for each sample was created using median absolute deviation normalization by ArrayStat software (Imaging Research Inc.). Both GRO and cDNA hybridizations were normalized within each experiment replicate by the global mean procedure. Average cDNA values for each gene were finally corrected by percentage of guanines present in each probe-coding strand while average TR values for each gene were corrected by percentage of uridines present in each probe-coding strand. For cDNA, normalization between samples was made using the amount of mRNA/cell (see previous section) to get relative values of mRNA copies/cell for each gene. These values were used for further analysis and comparisons.

2.4 Molecular biology techniques in *Mus musculus*

2.4.1 Culture and growth conditions

The fibroblast cell line was isolated from mouse kidney and immortalized by retroviral delivery of the SV40 large T (Benito-Jardon *et al.,* 2017). These cells were cultured in Dulbecco's modified Eagle medium (DMEM) containing 10% foetal calf serum (FCS) and 1% penicillin–streptomycin and maintained at standard conditions of 37ºC and 5% CO_2 in a humidified atmosphere. Subculturing was performed using 0.25% Trypsin-EDTA and subconfluent cell cultures of less than 10 passages were used for all the experiments. Cells were cultured with or without treatment with the DHPS inhibitor GC7 at the indicated concentration to deplete functional eIF5A (Park *et al.,* 1994). LX2 (immortalized cell line of HSCs) cells were gifted by Dr Scott L. Friedman, Icahn School of Medicine at Mount Sinai, New York, NY. These cells were cultured in DMEM with high glucose (Sigma-Aldrich), supplemented with 10% FCS, 2 mM L-glutamine, 50 U/mL penicillin and 50 µg/mL streptomycin in a humidified atmosphere with 5% CO_2 at 37ºC. For the experiment, cells were seeded in a six-well plate ($0.18 \cdot 10^6$ cells/well) 24 h before treatment and treated for 48 h with TGF-β1 (2.5 ng/mL), a well-known stimulator of proliferation and fibrogenesis, or its vehicle DMSO. GC7 was used at 30 µM alone or together with TGF-β1.

To measure cell viability, cells from suspension, PBS washes and fibroblast monolayer detached with trypsin were collected. A 4% Trypan Blue/PBS dilution was used to stain dead cells and the fibroblast population was analyzed by counting live and dead cells in a Neubauer chamber.

2.4.2 Silencing *DHPS* and *eIF5A* expression by siRNA in fibroblasts

A synthetic pool of silencing RNAs (siRNAs) was used to target and knock down DHPS or eIF5A expression according to the manufacturers' protocols. Briefly, $3 \cdot 10^4$ cells/well were seeded in a six-well culture plate 1 day prior to transfection until reaching 70–90% confluence. For *Dhps* silencing, 250 µL Opti-Mem I Reduced Serum Medium containing 7 µL Lipofectamine 3000 reagent and 10 µL of either *Dhps* or control siRNA, previously incubated together for 15 min at room temperature, were added to the culture. Cells were transfected and incubated for 72 h. For eIF5A silencing, the culture medium was replaced with transfection medium containing 6 µL transfection reagent and 12 µL of either *Eif5a1* or control siRNA, previously incubated together for 30 min at room temperature. The cells were transfected and incubated with the transfection mixture for 6 h, after which the transfection medium was replaced with 2× fibroblasts' usual medium. After 24 h, the medium was replaced with 1× usual medium and incubated until 72 h post-transfection. Finally, cells were collected by trypsinization for RT-qPCR and Western blotting analysis (see sections 2.4.3 and 2.4.4 of Materials and Methods respectively).

2.4.3 RNA-related molecular techniques

- Quantitative reverse transcription PCR (RT-qPCR)

To analyze mRNA levels, cells were washed twice with PBS and trypsinized. Then, total RNAs were isolated from fibroblasts using a PureLink RNA Mini Kit following manufacturer's instructions. The reverse transcription and quantitative PCR reactions were performed as previously detailed (see section 2.3.2 of Materials and Methods). Specific primers are listed in Table A1.4. Endogenous *Gapdh* mRNA levels were used for normalization.

2.4.4 Protein-related molecular techniques

- Western blotting assay

For Western blotting analysis of fibroblasts protein content, cells were washed twice with PBS and proteins were extracted in RIPA buffer for 15 min. The lysates were passed through a needle-coupled syringe 15-20 times and then transferred to a new tube and centrifuged at 12000 rpm at 4ºC for 5 min to remove the cell debris and insoluble proteins. Supernatant was collected and suspended in 2x-SDS protein loading buffer and stored at -20ºC. Protein content was quantified by and OD_{280} estimation in a Nanodrop device (Thermo Fisher Scientific), and 100 µg of each sample was loaded into 4-20% gradient precast SDS-PAGE gels (BioRad) to detect proteins from different molecular weights at the same time. To analyze protein expression in LX2 cells, whole-cell protein extracts were obtained by lysis of the cell pellets in complete lysis buffer. Immediately prior to their use, 1 mM DTT, 5 mM broad-spectrum serine, cysteine protease inhibitors (Complete MiniTM) and 0.05% detergent solution (NP-40 Surfact-

Amps™) were added. Samples were then vortexed twice at maximum speed (10 s), incubated on ice (15 min), vortexed again at maximum speed (30 s) and centrifuged (12000 rpm, 15 min, 4ºC). Electrophoresis, transference, protein immunodetection, exposure and quantification were performed as detailed previously (see section 2.3.3 of Materials and Methods). Specific antibodies and their dilutions are listed in Table A1.7.

- Immunofluorescence assay

For indirect immunofluorescence of fibroblasts, 12 mm glass coverslips were coated with 10 µg/mL laminin dissolved in PBS at 37ºC for 4 h until dried. Then, 10^3 cells were seeded onto the laminin-coated glass coverslips and cultured for 1 or 4 days at 37ºC in 3.5 mL of medium containing 30 µM GC7 or *Dhps* siRNA. After removing the medium, cells were washed twice with PBS and fixed with 4% paraformaldehyde for 10 min. Then, cells were washed four times with PBS and the coverslips were transferred to a 12-well plate. Here, cells were permeabilized with 0.1% Triton X-100 in PBS for 10 min and blocked for non-specific protein binding with 3% bovine serum albumin (BSA)/PBS for 1 h at room temperature. Cells were incubated with primary antibodies (listed in Table A1.7) diluted in 1% BSA/PBS overnight at 4ºC. Following primary antibody incubation, cells were washed three times with PBS and the corresponding secondary antibody (listed in Table A1.7) diluted in 1% BSA/PBS was incubated for 1 h at room temperature together with rhodamine-conjugated phalloidin coupled with tetramethylrhodamine (TRITC; 1:500, Sigma-Aldrich), used for actin filament counterstaining (in 1% BSA/PBS). Nuclei were counterstained with DAPI (1:10000 in PBS, Merck) for 7 min at room temperature. The PBS washings between antibodies, after secondary antibody and after DAPI incubation were made 3 times for 10 min. Glass coverslips were mounted onto crystal slides using gelvatol and kept at 4ºC overnight until dried.

Immunofluorescence images were acquired using an Olympus FLUOVIEW FV 1000 confocal microscope equipped with ×40 and ×60 objectives on a Nikon ECLIPSE E200. The same exposure times were used to acquire all images. Image analysis was carried out with ImageJ software and Photoshop CC 2019.

5. Statistical analysis

Every experiment was performed at least in three biological replicates. Data are expressed as the mean ± standard deviation (S.D). For GRO experiments, genomic data are presented as the median or mean ± standard deviation (S.E). Statistical evaluation was carried out with Microsoft Office Excel 2016. Significant differences between the control and treated or mutant cells were determined using Student's t-test (two tailed, paired) at a significance level of $p<0.05$. Significance levels of straight, potential, and logarithmic lines from GRO-related data were determined using Mann-Whitney test at a significance level of $p<0.05$.

Chapter 3

Hypusinated eIF5A is required for the translation of collagen

Chapter 3. Hypusinated eIF5A is required for the translation of collagen.

This work was published in:

1. Journal of Cell Science, volume 134 (Barba-Aliaga *et al.*, 2021). "Hypusinated eIF5A is required for the translation of collagen." The authors are Marina Barba-Aliaga*, Adriana Mena*, Vanessa Espinoza, Nadezda Apostolova, Mercedes Costell and Paula Alepuz[#].

*These authors contributed equally.

[#]Corresponding author.

Detailed author contributions: Marina Barba-Aliaga contributed to the great majority of experimental development with yeast cells and mouse fibroblasts, experimental design, data analysis and review. Adriana Mena executed the setting and preliminary experiments with mouse fibroblasts. Vanessa Espinoza executed preliminary experiments with yeast cells. Nadezda Apostolova conducted experiments with hepatic stellate cells. Mercedes Costell gave scientifical support in experiments requiring mouse fibroblasts. Paula Alepuz supervised the work and carried out the manuscript conceptualization, writing and review.

As previously introduced, eIF5A is required for the translation of mRNAs encoding peptide sequences with consecutive prolines as it facilitates the formation of peptide bonds. Upon eF5A depletion ribosomes also stall in tripeptide sequences combining proline with glycine and charged amino acids. A search in the human proteome identified that the extracellular matrix compartment is highly enriched in potential eIF5A targets (Pelechano and Alepuz, 2017). Among these proteins, collagens contain a high number of the so-called collagenic motifs (X-Y-Gly), with proline or hydroxylated proline frequently in the first (X) and second (Y) positions and glycine in the third, which enable the formation of the collagenous triple helix. Therefore, the presence of the Pro-Gly (PG) motifs in the collagen sequences makes them potential candidates for an eIF5A-dependent translation. Collagen is the most abundant protein in vertebrates, constituting more than 25% of human body weight. Collagens are essential in the ECM and function in tissue structure, development and remodelling, cell adhesion and migration, cancer and angiogenesis. In humans, deficient production of mature collagen can lead to severe diseases, collectively named collagenopathies. By contrast, excessive and uncontrolled synthesis of collagen results in fibrosis, a leading cause of morbimortality. This work provides new insights on the eIF5A requirement for the maintaining of collagen homeostasis and its production during fibrotic processes.

3.1 Mammalian collagens, but not other ECM proteins, are enriched in putative eIF5A-dependent non-polyPro containing peptides

A previous study showed that the gene ontology terms "ECM organization" and "collagen metabolism" were significantly enriched in the human proteins with a high content (>25) of eIF5A-dependent motifs (Pelechano and Alepuz, 2017). To determine whether only collagens or also other proteins of the mammalian ECM compartment contain a significant number of eIF5A-dependent tripeptides, and to identify which ones, we analyzed the amino acid sequence of the *Mus musculus* ECM proteins. ECM proteins are classified as fibrous proteins, proteoglycans, glycoproteins and other proteins (Frantz *et al.*, 2010), and we further subdivided fibrous proteins into collagens and others (Figure 3.1-A). We examined the abundance of the 43 tripeptide motifs with the highest score for eIF5A-dependent ribosome pausing (Table 1.1) (Pelechano and Alepuz, 2017) and found that, although the average distribution of eIF5A-dependent motifs in mouse ECM proteins was 22.6 motifs per protein, collagen had a much higher average frequency (86.0 motifs per protein) than the rest of the ECM protein groups (motifs per protein: 21.7 in non-collagen fibrous proteins, 9.4 in proteoglycans, 13.0 in other proteoglycans and 6.8 in others) (Figure 3.1-B). Additionally, collagens also contained different eIF5A-dependent motifs from the rest of the ECM proteins, such as the non-polyPro motifs PGP, PPG, EPG and DPG that constitute 78% of the motifs, whereas the well-known PPP (Dever *et al.*, 2018) was almost absent in collagen sequences (Figures 3.1-B,C). Those four non-polyproline eIF5A motifs appear in stretches in the collagenic regions of the polypeptide sequences that form the triple helix of the collagen proteins (Kadler *et al.*, 2007). These analysis point to mammalian collagens as putative targets of eIF5A during their translation.

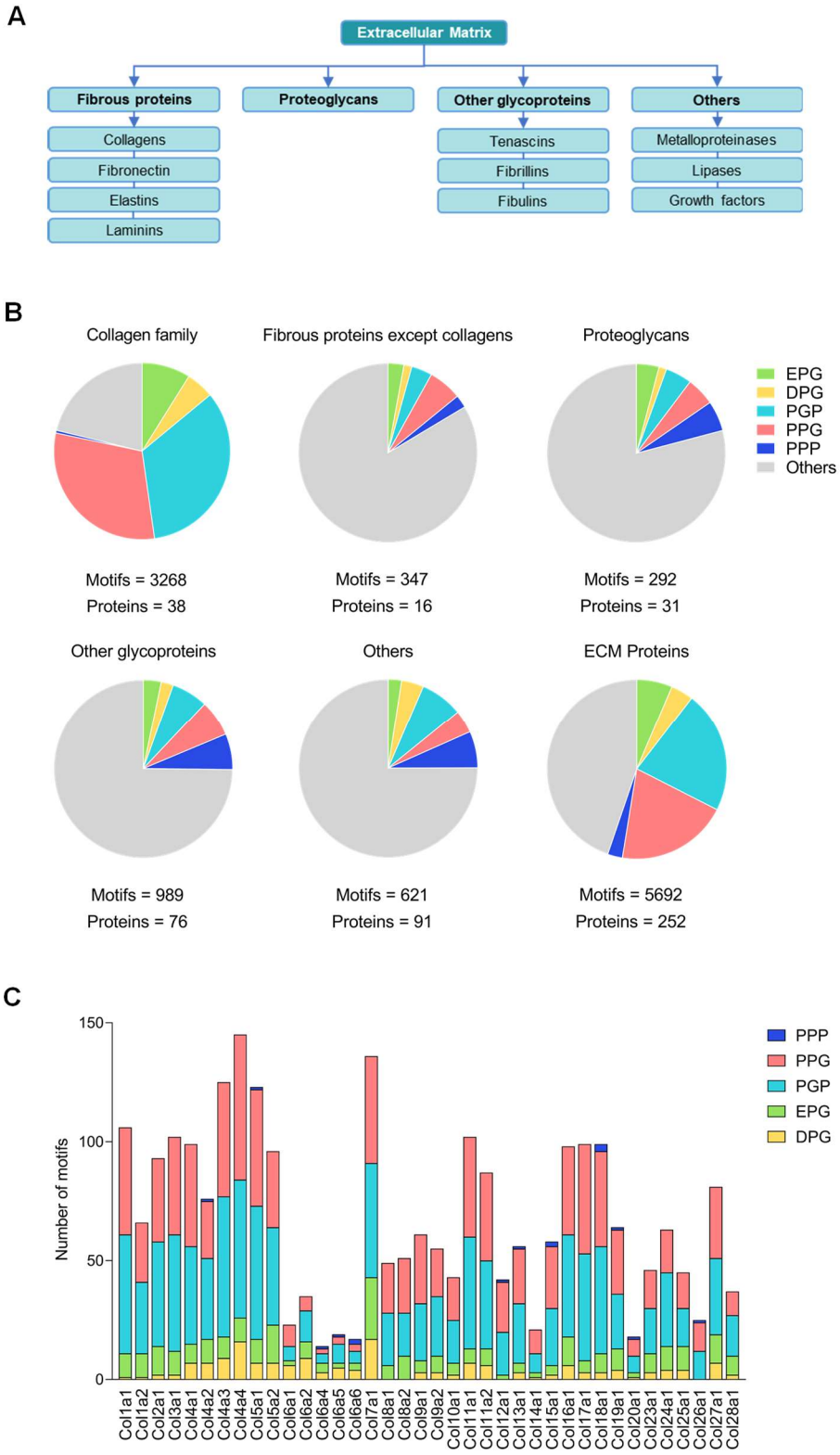

Figure 3.1. Distribution of eIF5A-dependent motifs in mouse extracellular matrix (ECM) proteins. (A) Classification of ECM proteins according to their structure and/or composition. (B) Distribution of the 43 highest-scoring eIF5A-dependent ribosome-pausing motifs (Pelechano and Alepuz, 2017) (polyPro PPP, collagenic EPG, DPG, PGP, PPG motifs and others) in the subtypes of mouse ECM proteins. (C) Number of eIF5A-dependent motifs in the mouse collagens.

3.2 eIF5A stimulates translation of collagenic motifs expressed in yeast cells

To gain molecular evidence supporting the role of eIF5A in the translation of collagenic sequences carrying putative eIF5A-dependent motifs, we followed two different approaches using *S. cerevisiae* cells. Human and yeast eIF5A proteins share >60% homology (Figure 1.1) and are functionally interchangeable (Schnier *et al.*, 1991; Schwelberger *et al.*, 1993). Yeast cells do not contain collagen, but heterologous expression of human collagen has been successfully achieved (Brodsky and Ramshaw, 2017). First, using a tetracycline-regulated (*tetO*$_7$) expression system (Garí *et al.*, 1997) to avoid the deleterious of constant collagen expression in yeast cells, we expressed the first 420 amino acids of mouse collagen type I α1 chain (Col1a1), containing 15 PPG, 15 PGP and four EPG motifs (Figure 3.2-A) fused to the β-galactosidase reporter. As a positive control of eIF5A-translation dependency, we constructed another fusion with a fragment of the yeast Bni1 protein containing three documented eIF5A-dependent polyPro sequences (Li *et al.*, 2014) (Figure 3.2-A).

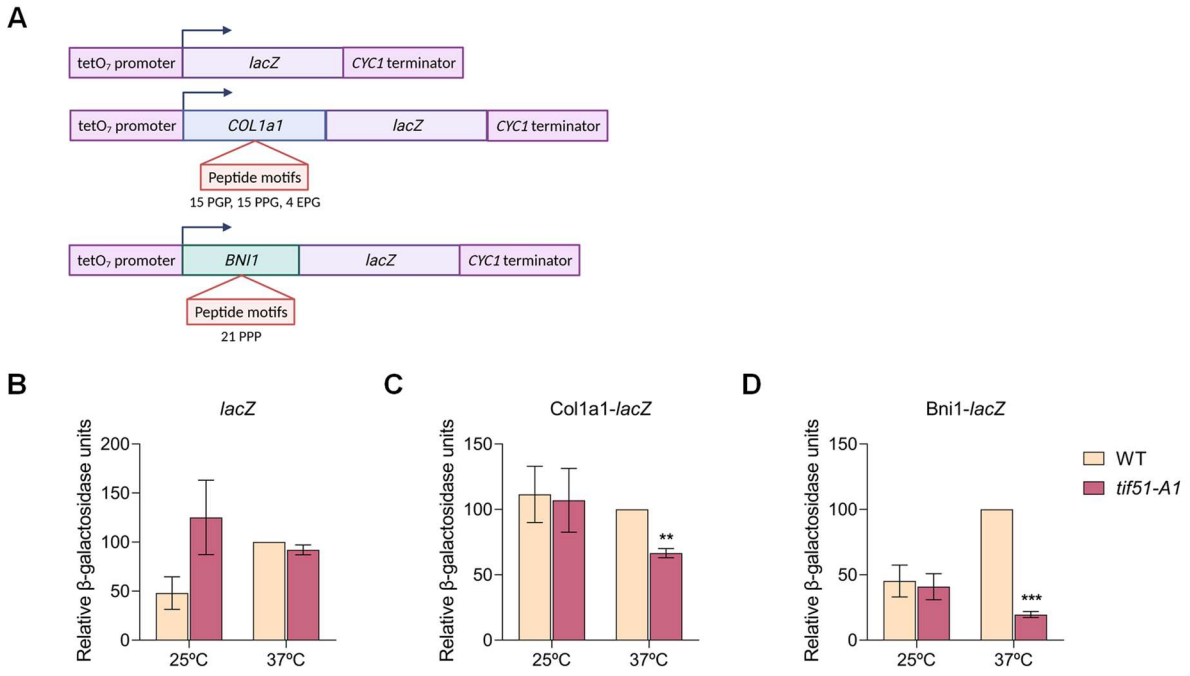

Figure 3.2. eIF5A depletion generates translation defects of collagen in yeast cells. (A) Scheme of the *lacZ* expression plasmid (pCM179) and derivative plasmids containing fusions between a fragment of mouse collagen type I α1 chain (Col1a1) with collagenic motifs or a fragment of the yeast polyPro protein Bni1 and the *lacZ* gene expressed under the control of the tetracycline-regulated *tetO*$_7$ promoter. (B-D) The plasmids illustrated in (A) were introduced into isogenic strains expressing wild-type or temperature-sensitive eIF5A-P83S (t*if51A-1*), and β-galactosidase activity was assayed. Data are presented as the β-galactosidase units relative to the units of wild-type at 37°C (given as 100 units). (B-D) Data are presented as mean ± SD from a minimum of three independent experiments. Statistical significance was determined using a two-tailed paired Student's t-test relative to corresponding wild-type cells. **p<0.01, ***p<0.001.

We analyzed the expression of non-fused *lacZ* gene, Col1a1-*lacZ* and Bni1-*lacZ* after inducing expression by incubating 6 h in tetracycline-free media in wild-type yeast cells and eIF5A temperature-sensitive mutant cells (*tif51A-1*) carrying a single point mutation (Pro83 to Ser) (Li *et al.*, 2011). β-galactosidase activity corresponding to Col1a1-*lacZ* and Bni1-*lacZ* was similar in wild-type and mutant cells when incubated at a permissive temperature (25ºC) (Figures 3.2-C,D). However, when incubated for 6 h at a restrictive temperature (37ºC), Col1a1-*lacZ* expression was reduced by 40% in the mutant with respect to the wild-type. A stronger reduction (80%) was observed in Bni1-*lacZ* (Figures 3.2-C,D). We did not observe any difference in the expression of non-fused *lacZ* between wild-type and mutant cells at 37ºC (Figure 3.2-B). These results indicate that eIF5A is required for the expression of the cloned Col1a1 fragment and confirm the strong requirement for the translation of the polyPro motifs of Bni1.

To further define the role of eIF5A in the translation of specific collagenic motifs, we used a second approach based on the use of the dual-luciferase reporter system developed in yeast cells (Letzring *et al.*, 2010). Dual-luciferase plasmids express a single mRNA that contains the *Renilla* luciferase at the 5' end and the firefly luciferase open reading frame (ORF) at the 3' end, joined in-frame by a short sequence from which the motifs to study can be cloned (Figure 3.3-A). In the dual-luciferase assay, a premature aberrant translation termination caused by the inserted motif, but without a stop codon, will result in a *Renilla* polypeptide without the C-terminal part containing the firefly luciferase. Although the synthesis of a truncated polypeptide may affect its stability, the detection of reduced firefly:*Renilla* luciferase ratio is indicative of motif-induced translation termination. For these analyzes, we used a plasmid with no insertions; a plasmid with consecutive optimal codons for proline inserted (10P) (Letzring *et al.*, 2010); and four plasmids we constructed with insertions of three non-consecutive repetitions of optimal codons for the polyPro motif PPP (3PPP), for the collagenic motifs PGP (3PGP) and EPG (3EPG), and for the control motif TQA (3TQA), for which ribosome pausing is not predicted upon eIF5A depletion (Pelechano and Alepuz, 2017) (Figure 3.3-A,B). We also constructed a dual-luciferase plasmid in which we inserted a short stretch of mouse collagen IV sequence (Col4a1) containing several PPG and PGP motifs (Figure 3.3-A,B). None of the resulting combinations of three amino acids in the inserted sequences, except the motif under investigation, were predicted to induce ribosome pausing by eIF5A depletion (Pelechano and Alepuz, 2017). Dual-luciferase reporter constructs were introduced into isogenic strains expressing wild-type eIF5A or temperature-sensitive eIF5A-S149P and grown at a semi-permissive temperature (33ºC) as described (Gutierrez *et al.*, 2013). We hypothesized that if eIF5A promoted translation of the inserted motifs in the dual-luciferase plasmid, then the firefly:*Renilla* luciferase ratio would be lower in the eIF5A-S149P mutant strain grown at 33ºC. As shown in Figure 3.3-C, the firefly:*Renilla* luciferase ratio for each construct was different depending on the cloned motif. The empty plasmid and the control TQA motif showed no difference in the firefly:*Renilla* luciferase ratio between the wild-type and eIF5A mutant. As previously reported (Gutierrez *et al.*, 2013), a very low ratio was observed for the 10P construct upon eIF5A depletion (Figure 3.3-C). Low ratios in the eIF5A mutant were also obtained with 3PPP, indicating that three non-consecutive polyPro tripeptide motifs are sufficient to impose a requirement for eIF5A, although without reaching the strong reduction observed with the longer polyPro motif (10P). Similarly, insertion of 3PGP and 3EPG and the Col4a1 fragment resulted in a lower luciferase ratio in the eIF5A mutant than in the wild-type (Figure 3.3-C). These results confirm that eIF5A promotes the translation of collagenic tripeptide motifs.

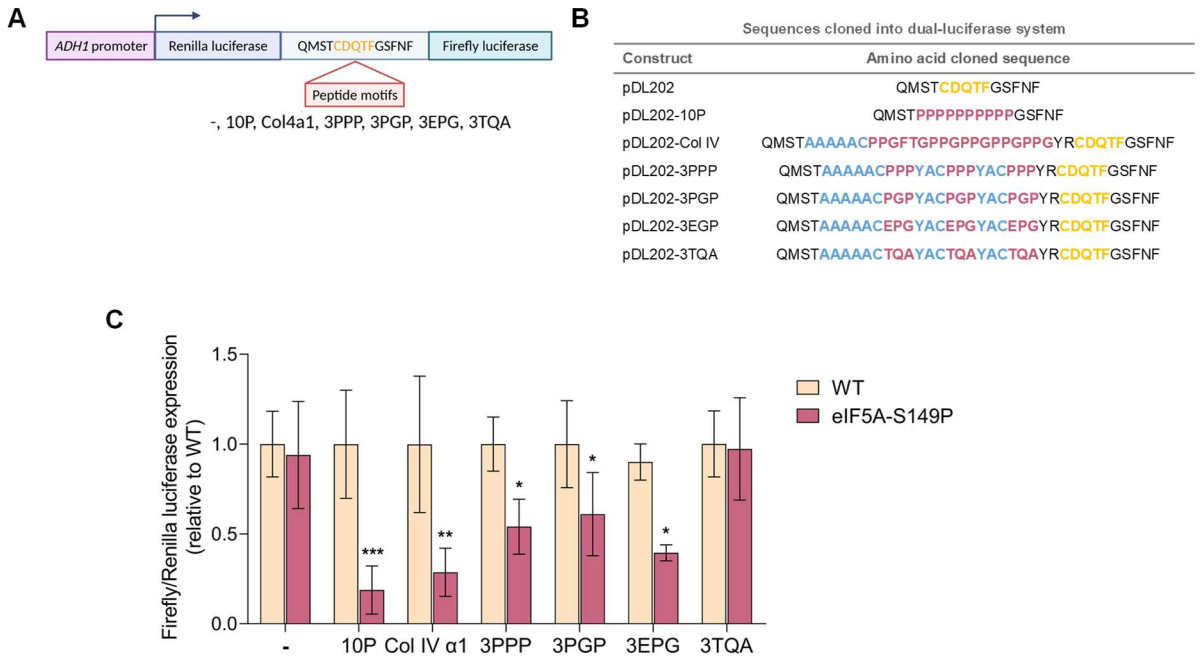

Figure 3.3. eIF5A stimulates translation of collagenic motifs in yeast cells. (A) Scheme of *Renilla*–firefly luciferase construct and peptide motifs inserted. Yellow and gray highlighted letters are flanking sequences to the insertion sites. (B) Sequences containing the tripeptide collagenic motifs cloned into the double luciferase reporter system (pDL202). Yellow and gray highlighted letters are flanking sequences to the insertion sites; red letters are polyPro (10P, 3PPP), collagenic motifs (3PGP, 3EPG), a mouse collagen IV fragment (Col4α1), and control motif (3TQA); blue letters are spacer sequences between motifs. (C) Dual-luciferase reporter constructs were introduced into isogenic strains expressing wild-type eIF5A or temperature-sensitive eIF5A-S149P and grown at semi-permissive temperature (33°C). Data are presented as mean ± SD from a minimum of three independent experiments. Statistical significance was determined using a two-tailed paired Student's t-test relative to corresponding wild-type cells. *p<0.05, **p<0.01, ***p<0.001.

3.3 Depletion of functional eIF5A in mouse fibroblasts reduces collagen protein levels

To investigate the role of eIF5A in collagen synthesis in mammalian cells, we used a mouse fibroblast line. Fibroblasts are prototypical collagen producer cells, and we focused on collagen I (Col1) because it is the most abundant collagen in animal tissue (Myllyharju and Kivirikko, 2001). Col1 is a heterodimer with two α1 chains and one α2 chain (see section 1.2.2 of Chapter 1). The Col1a1 subunit contains 50 PGP, 45 PPG, 10 EPG and one DPG motif (Figure 3.1-C). Using these mouse fibroblasts, we investigated the effect of inhibiting eIF5A hypusination with GC7, which acts as a competitive inhibitor of DHPS (Park and Wolff, 2018) and quantified Col1a1 levels. As seen in Figures 3.4-A and 3.4-B, treatment of fibroblasts with 30 µM or 65 µM GC7 reduced eIF5A hypusination and concomitantly lowered Col1a1 levels. A reduction in Col1a1 was already evident at 24 h of GC7 and was still visible at 96 h. Importantly, treatments with GC7 did not modify total eIF5A content, except for a slight reduction at 72 h (Figure 3.4-A).

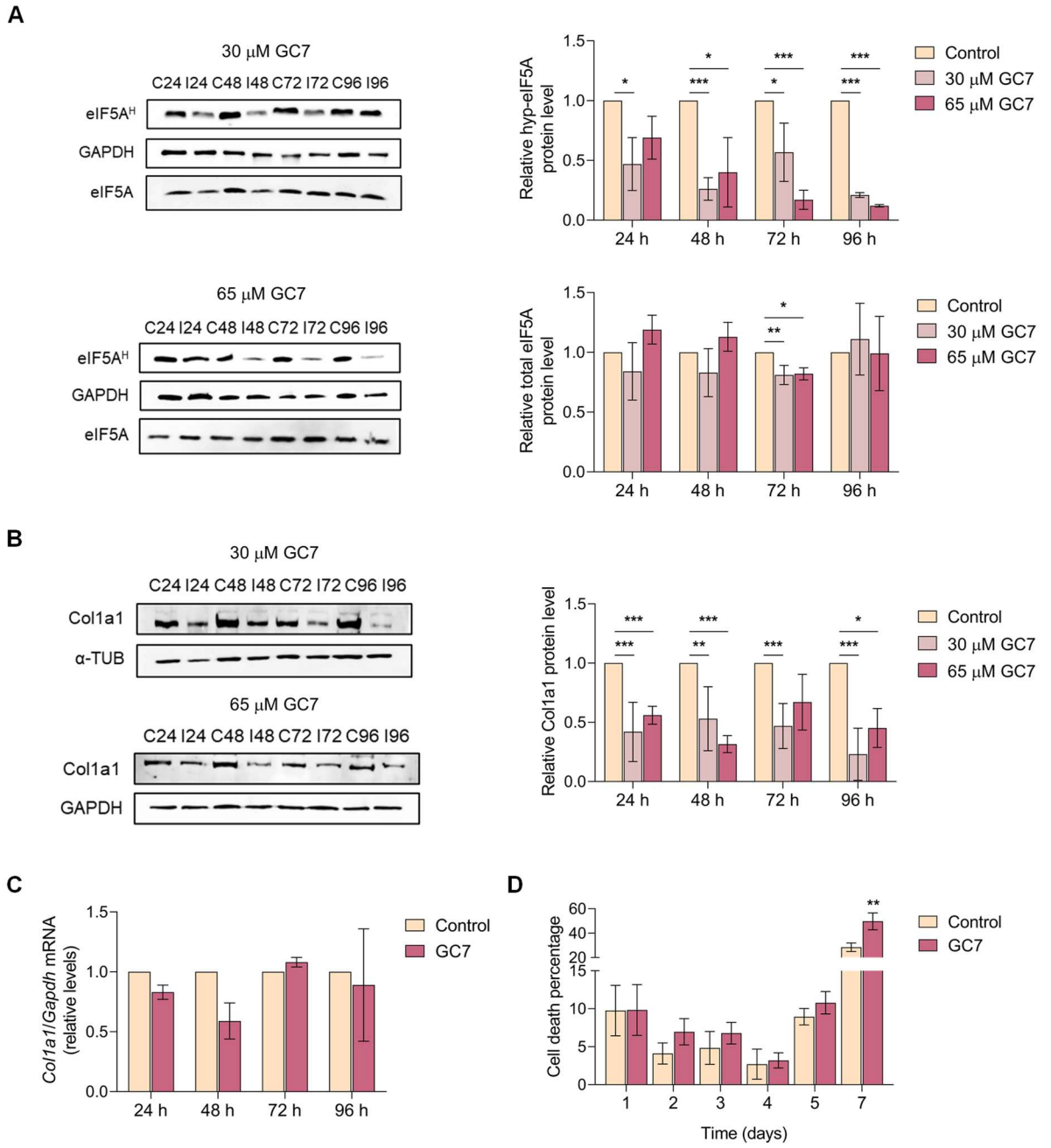

Figure 3.4. Depletion of functional eIF5A with GC7 reduces Col1a1 protein levels in mouse fibroblasts. **(**A,B) Western blotting (left) and quantification analysis (right) of hypusinated and total eIF5A (A) and Col1a1 (B) in fibroblasts at the indicated time points after 30 μM or 65 μM GC7 treatment. GAPDH or α-tubulin (α-TUB) was used as a loading control. A representative experiment is shown (n=6). (C) RT-qPCR analysis of expression of *Col1a1* at indicated time points after 30 μM GC7 treatment. No statistically significant difference was found. (D) Mouse fibroblast dead cell percentage at indicated time points after 30 μM GC7 treatment. (A-D) Data are presented as mean ± SD relative to untreated cells. Statistical significance was determined using a two tailed paired Student's t-test relative to the corresponding untreated cells. *p<0.05, **p<0.01, ***p<0.001.

Col1a1 synthesis is mainly regulated at the level of mRNA stability and translation (Zhang and Stefanovic, 2016). To investigate whether the effects of eIF5A depletion were attributable to a negative effect on Col1a1 translation rather than transcription, we quantified mRNA levels with GC7. No significant differences were observed in Col1a1 mRNA levels with GC7 (Figure 3.4-C), suggesting that the effect of eIF5A inhibition on Col1a1 occurs at translational level. Because eIF5A is an essential protein in eukaryotic cells, we also checked whether GC7 treatment reduced fibroblast viability. However, treatment with 30 µM GC7 up to 96 h (4 days) did not significantly reduce fibroblast viability when compared to control (untreated) cells (Figure 3.4-D). Low toxicity at 30 µM GC7 has also been described for human cells in culture (Xu *et al.*, 2014); therefore, we used this GC7 concentration in the following experiments.

Because off-target effects have been described for GC7 (Oliverio *et al.*, 2014), as an alternative to using GC7 to deplete functional eIF5A, we transfected mouse fibroblasts with *Dhps* siRNA to reduce the first enzymatic step of eIF5A hypusination. After 72 h, we observed a >50% reduction in *Dhps* mRNA levels and a similar reduction in hypusinated eIF5A (Figures 3.5-A,B). This depletion of functional eIF5A correlated with a >50% reduction in Col1a1 protein levels, whereas no reduction in *Col1a1* mRNA was observed (Figures 3.5-C,D).

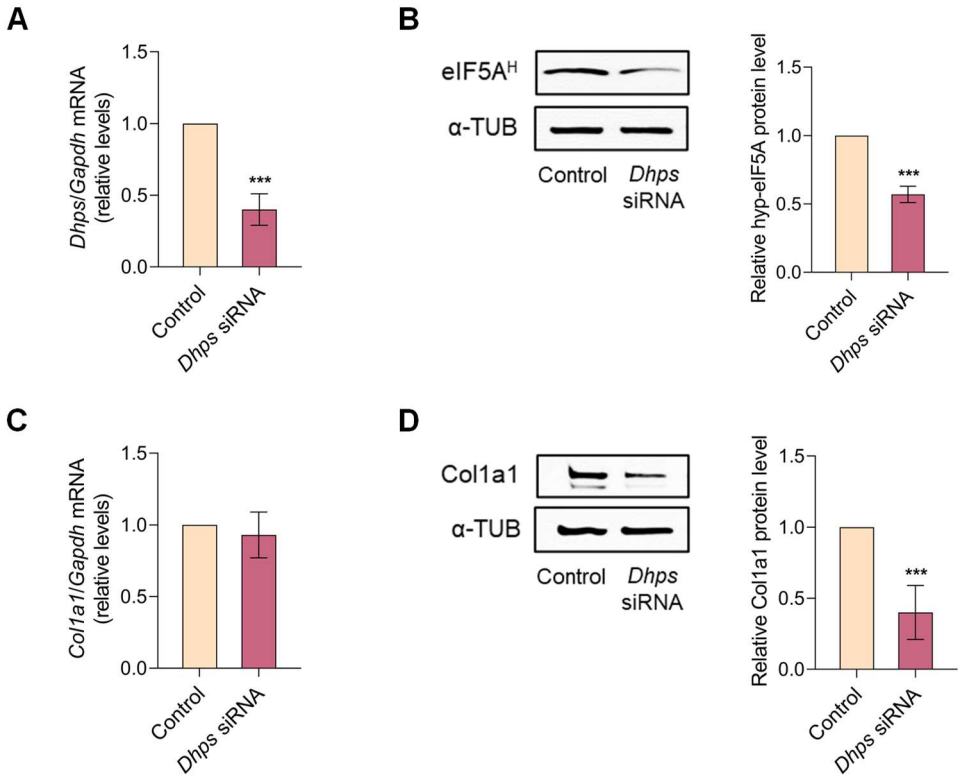

Figure 3.5. Depletion of functional eIF5A with *Dhps* siRNA reduces Col1a1 protein levels in mouse fibroblasts. (A) RNA expression analysis of *Dhps* after cell transfection with *Dhps* siRNA for 72 h. (B) Western blotting (left) and quantification of hyp-eIF5A (right) after cell transfection with *Dhps* siRNA for 72 h. α-Tubulin protein levels were used for normalization. (C) RNA expression analysis of *Col1a1* after cell transfection with *Dhps* siRNA for 72 h. (D) Western blotting (left) and quantification (right) of Col1a1 after cell transfection with *Dhps* siRNA for 72 h. α-Tubulin protein levels were used for normalization. A representative experiment is shown (n=5). (A-D) Data are mean ± SD relative to control cells. Statistical significance was determined using a two-tailed paired Student's t-test relative to scramble siRNA-transfected cells (control). ***p<0.001.

We then transfected mouse fibroblasts with *Eif5a1* siRNA to deplete *Eif5a1* mRNA, which is highly expressed in mammalian cells (Park and Wolff, 2018). The reduction in *Eif5a1* mRNA (50% at 72 h after transfection) was paralleled by a strong reduction in Col1a1 protein (70% compared to the control with scrambled siRNA) with, again, no change in *Col1a1* mRNA level (Figures 3.6-A-C).

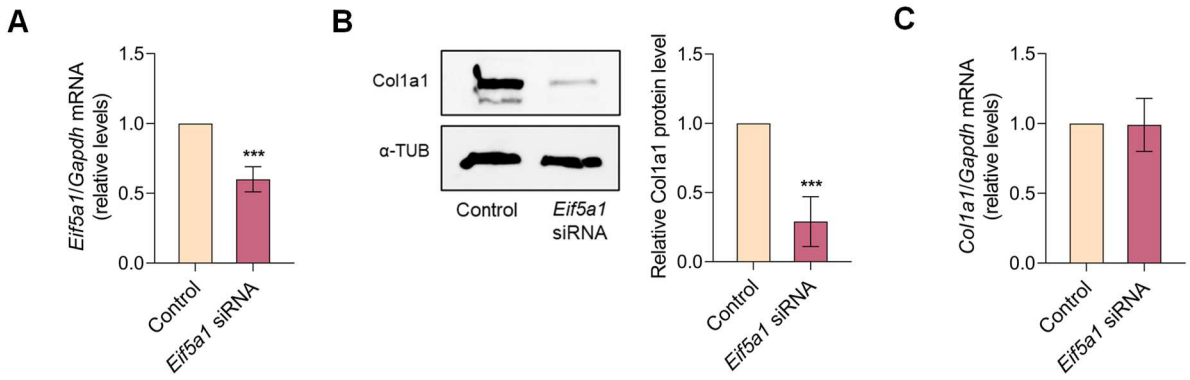

Figure 3.6. Depletion of functional eIF5A with *Eif51a1* siRNA reduces Col1a1 protein levels in mouse fibroblasts. (A) RNA expression analysis of *Eif5a1* after cell transfection with *Eif5a1* siRNA for 72 h. (B) Western blotting (left) and quantification (right) of Col1a1 after cell transfection with *Eif5a1* siRNA for 72 h. α-Tubulin protein levels were used for normalization. A representative experiment is shown (n=5). (C) RNA expression analysis of *Col1a1* after cell transfection with *Eif5a1* siRNA for 72 h. No statistically significant difference was found. (A-C) Data are mean ± SD relative to control cells. Statistical significance was determined using a two-tailed paired Student's t-test relative to scramble siRNA-transfected cells (control). ***p<0.001.

Together, these results show that hypusinated eIF5A is necessary to maintain high levels of Col1a1 protein in mouse fibroblasts and suggest a role for eIF5A in the translation of *Col1a1* mRNA.

3.4 Depletion of functional eIF5A in fibroblasts leads to an accumulation of Col1a1 in perinuclear regions

Translation of collagen polypeptides occurs in the ER, where the polypeptide chains are translationally and post-translationally modified to form the triple helix (see Malhotra and Erlmann, 2015; Zhang and Stefanovic, 2016; Sharma *et al.*, 2017 and section 1.2.3 of Chapter 1). To examine the effects of hypusinated eIF5A depletion on collagen synthesis, we analyzed Col1a1 distribution in mouse fibroblasts treated with 30 µM GC7. Immunostaining showed a lower Col1a1 signal in the treated fibroblasts than in untreated cells (Figures 3.7-A,B). Moreover, in the control cells, the Col1a1 signal was visualized as dots more concentrated in the perinuclear region but also distributed all over the cytoplasm. By contrast, although the GC7-treated fibroblasts showed a concentration of Col1a1-stained dots in the perinuclear region, suggesting localization in the ER, the signal was almost absent in the rest of the cytoplasm (Figure 3.7-C). Similar results of Col1a1 signal intensity reduction and predominant perinuclear localization were observed by depleting functional eIF5A in mouse fibroblasts with *Dhps* siRNA (Figures 3.7-D-F).

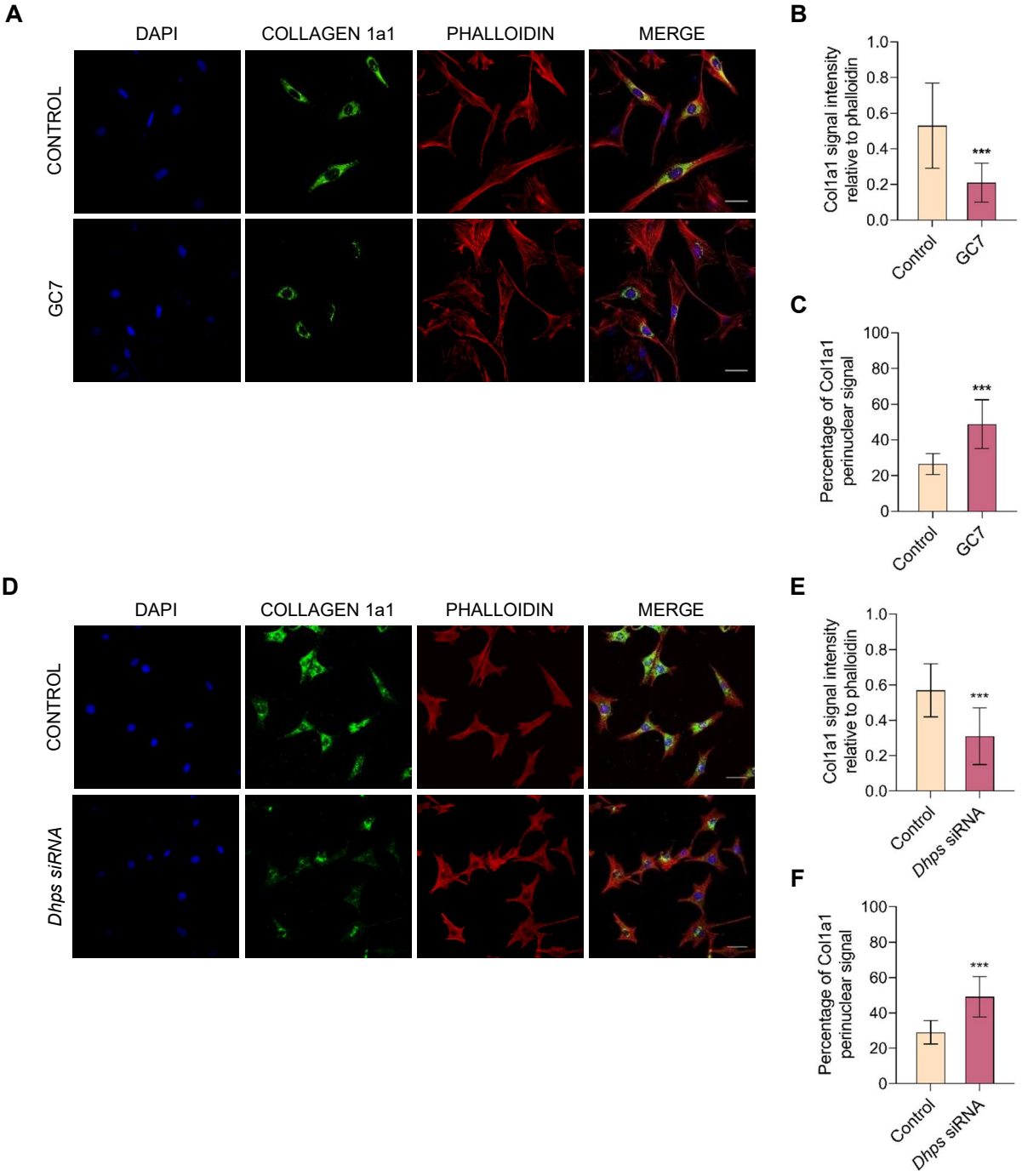

Figure 3.7. Mouse fibroblasts with hypusinated eIF5A depletion show lower Col1a1 signal accumulated in dots around the nuclei. (A) Confocal fluorescence microscopy images showing mouse fibroblasts at 96 h post-treatment with 30 μM GC7 stained with anti-Col1a1 antibody (green), DAPI (blue) and phalloidin actin (red). Scale bars: 40 μm. (B) Col1a1 intensity signal relative to phalloidin intensity signal quantification from A. (C) Quantification of Col1a1 perinuclear signal intensity with respect to total signal from A and expressed as a percentage. (D) Confocal fluorescence microscopy images of fibroblasts at 96 h post-treatment with *Dhps* siRNA and stained with anti-Col1a1 antibody (green), DAPI (blue) and phalloidin actin (red). Scale bars: 40 μm. (E) Col1a1 intensity signal relative to phalloidin intensity signal quantification from A. (F) Quantification of Col1a1 perinuclear signal intensity with respect to total signal from A and expressed as a percentage. (B,C,E,F) Data are mean ± SD from two independent experiments. Fluorescence signal was measured from at least 150 cells from two independent experiments. Statistical significance was determined using a two-tailed paired Student's t-test relative to control cells. ***$p<0.001$.

In order to clearly assign an ER localization to the Col1a1 dots observed in functional eIF5A-depleted fibroblasts, we co-visualized Col1a1 with Hsp47 (also known as SERPINH), the collagen-specific chaperone that aids during collagen folding and maturation (see Ito and Nagata, 2019 and section 1.2.3 of Chapter 1). In control, and GC7-treated fibroblasts, a similar Hsp47 perinuclear signal was observed (Figure 3.8-A). However, all Col1a1 signal co-localized with Hsp47 signal in GC7-tretated cells, whereas in control cells Col1a1 signal was distributed throughout the fibroblasts cells and part of the signal did not co-localize with Hsp47 signal. Again, these data suggest that Col1a1 is retained at the fibroblast ER upon functional eIF5A depletion.

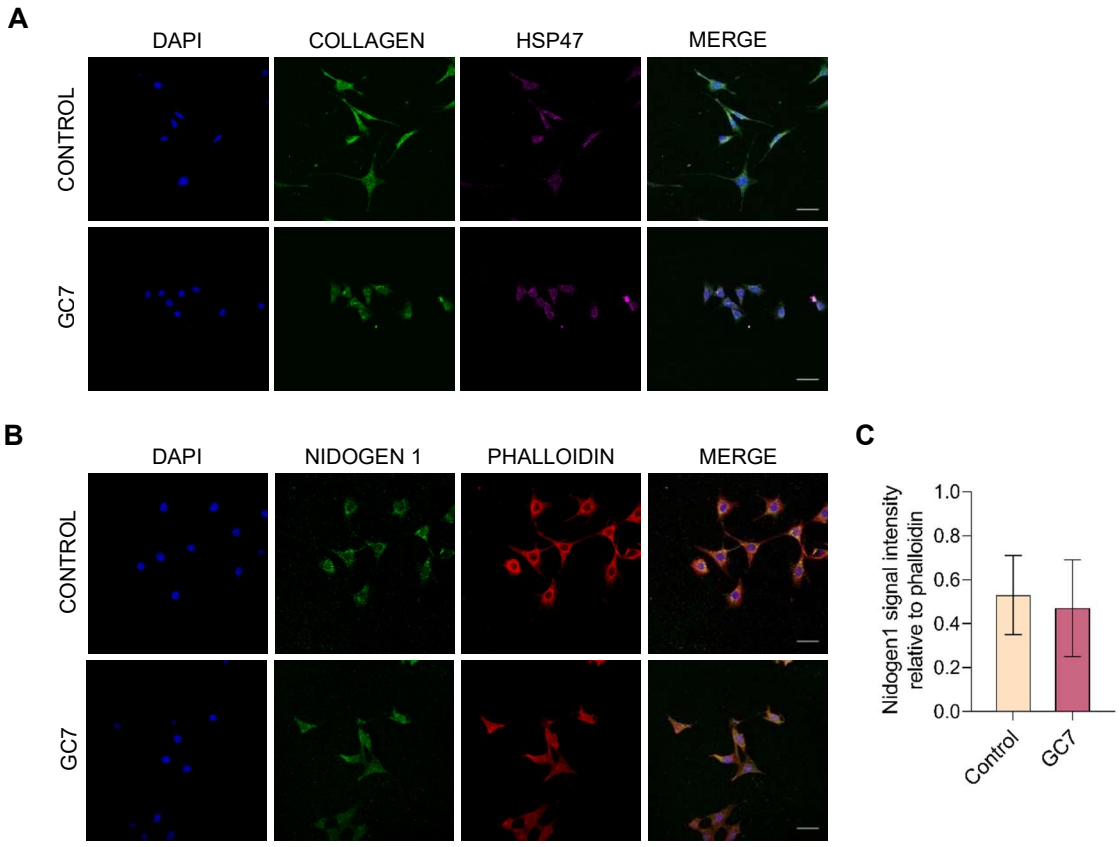

Figure 3.8. Depletion of functional eIF5A yields collagen type I α1 chain (Col1a1) co-localization with endoplasmic reticulum (ER) without affecting nidogen expression or localization. (A) Confocal fluorescence microscopy images showing mouse fibroblasts at 96 h post-treatment with 30 µM GC7 stained with anti-collagen type I α1 chain (Col1a1) antibody (green), anti-HSP47 antibody (magenta), and DAPI (blue). Scale bars: 40 µm. (B) Confocal fluorescence microscopy images showing mouse fibroblasts at 96 h post-treatment with 30 µM GC7 stained with anti-nidogen antibody (green), DAPI (blue), and phalloidin actin (red). Scale bars: 40 µm. (C) Nidogen intensity signal relative to phalloidin quantification from (A). Data are presented as mean ± SD from two independent experiments. Fluorescence signal was measured from at least 150 cells from two independent experiments. Statistical significance was determined using a two-tailed paired Student's t-test relative to control cells. No statistically significant difference was found.

Moreover, we also investigated whether the lack of functional eIF5A provokes a general defect in ER and the Golgi secretory pathway because a correlation between the function of eIF5A in translation and secretion has been described in yeast (Rossi *et al.*, 2014). With this aim, we visualized nidogen-1, which is a major component of basement membranes and ECMs (Mao *et al.*, 2020) and lacks eIF5A-dependent motifs. We observed no changes in nidogen-1 signal intensity and localization in GC7-treated fibroblast cells (Figures 3.8-B,C). This result supports the specific effect of eIF5A on collagen translation against a more general effect on ER translation and secretion, without excluding the possible specific effect of eIF5A in the ER-coupled translation of other proteins containing eIF5A-dependent motifs.

3.5 Depletion of functional eIF5A in fibroblasts generates ER stress

It is well documented that misfolding and accumulation of mutated collagen in the ER lead to ER stress and the induction of collagenopathies (Gawron, 2016). Thus, if the lack of functional eIF5A is hindering the translation of the Col1a1 collagenic segments, it would stall translating ribosomes at the ER membrane and trigger the ER stress response (see section 1.2.4 of Chapter 1). To test this, we analyzed the expression of several factors induced during the UPR that are activated in response to ER stress: the ER stress transducer ATF6, a transcription activator of genes involved in protein folding, secretion and degradation; the chaperone GRP78/BiP, a sensor of unfolded proteins in the ER; and CHOP, a proapoptotic factor induced upon severe ER stress (Hetz *et al.*, 2020; Oyadomari and Mori, 2004; Ron and Walter, 2007). A quick and transient induction of *Atf6*, *Bip* and *Chop* mRNA levels was observed after 24-48 h of GC7 treatment (Figure 3.9-A). Correspondingly, CHOP protein levels increased 100-fold at the same time in GC7-treated fibroblasts 24 h after GC7 treatment (Figure 3.9-B). Moreover, there was intense nuclear localization of CHOP protein in fibroblasts 24 h after GC7 treatment (Figures 3.9-C,D); which correlates with its previously described change from cytoplasmic to nuclear localization during stress (Oyadomari and Mori, 2004; Ron and Walter, 2007).

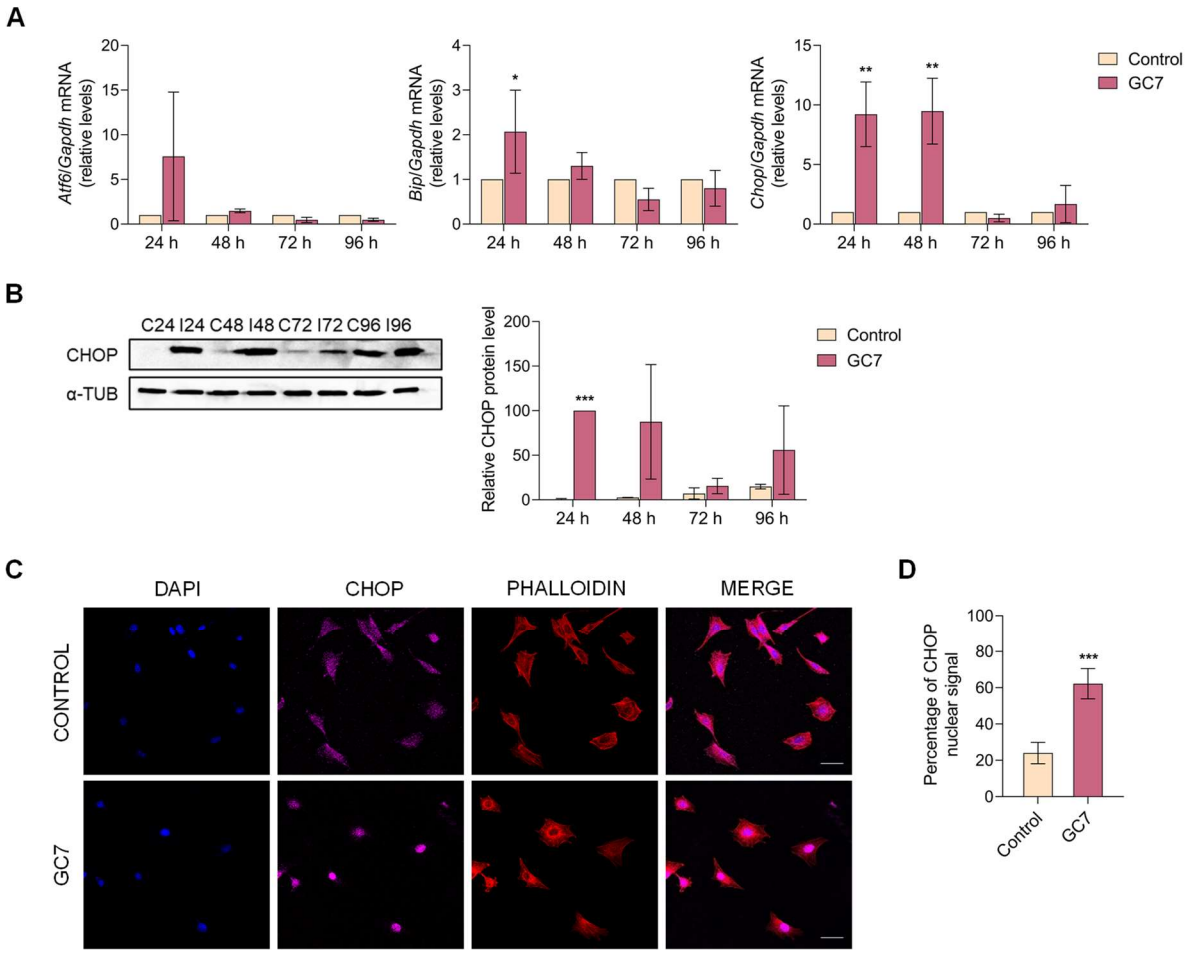

Figure 3.9. Depletion of functional eIF5A yields ER stress in mouse fibroblasts. (A) RT-qPCR analysis of the expression of *Atf6* (left), *Bip* (middle) and *Chop* (right) mRNA at the indicated time points after 30 µM GC7 treatment (n=5). (B) Western blotting (left) and quantification analysis (right) of CHOP protein levels at the indicated time points after 30 µM GC7 treatment. α-Tubulin was used as a loading control. A representative experiment is shown (n = 3). (C) Confocal fluorescence microscopy images showing fibroblasts after 24 h of treatment with 30 µM GC7 and stained with anti-CHOP antibody (magenta), DAPI (blue) and phalloidin actin (red). Scale bars: 40 µm. (D) Quantification of CHOP nuclear signal intensity with respect to total signal from C and expressed as a percentage. Fluorescence signal was measured from at least 150 cells from two independent experiments. (A,B,D) Data are mean ± SD. Statistical significance was determined using a two-tailed paired Student's t-test relative to corresponding untreated cells. *p<0.05, **p<0.01, ***p<0.001.

We confirmed in yeast that deletion of eIF5A was sufficient to induce the ER stress response (Figure 3.10), in agreement with previous results (Rossi *et al.*, 2014). Induced mRNA levels of ER stress markers (*SSB2, SSE1, HSP31*) were observed in the temperature-sensitive eIF5A mutant at restrictive temperature, whether expressing the Col1a1-*lacZ* construct or not. Moreover, we observed that expression of the Col1a1-*lacZ* construct in wild-type yeast cells also induced the ER stress response, probably due to the inability to obtain proper folding of the Col1a1 fragment fused to lacZ (Figure 3.10).

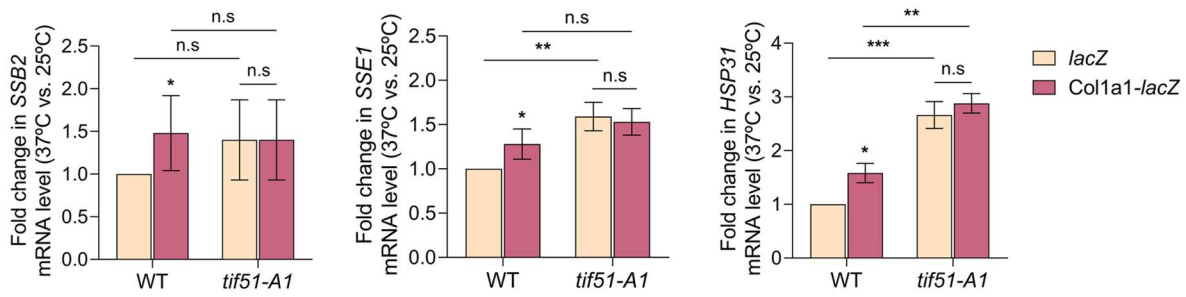

Figure 3.10. eIF5A inactivation induces the activation of ER stress markers in yeast cells. RT-qPCR analysis of the expression of the ER stress-related proteins encoded by *SSB2*, *SSE1* and *HSP31* after 6 hours growth at 25°C or 37°C in wild-type or temperature-sensitive eIF5A-P83S (*tif51A-1*) strains expressing a plasmid with a fusion between a fragment of mouse collagen type I α1 chain (Col1a1) containing collagenic motifs and the *lacZ* gene. *ACT1* mRNA levels were used as an internal control and ratio between expression at 37°C vs. 25°C relative to wild-type cells expressing *lacZ* is shown. Data are presented as mean fold change ± SD from a minimum of three independent experiments. Statistical significance was determined using a two-tailed paired Student's t-test relative to corresponding wild-type cells. *p<0.05, **p<0.01, ***p<0.001. n.s indicates no significant differences.

In sum, these results suggest that partially synthesized Col1a1 is retained at the ER in cells with a diminished amount of hypusinated eIF5A, causing a reduction in procollagen type I export from the ER to the Golgi complex. Either because there is an accumulation of translationally paused ribosomes at the ER or because partially synthesized Col1a1 peptides expose hydrophobic domains that may deplete components of the quality control system (Gawron, 2016), the UPR is induced in functional eIF5A-depleted cells. Additionally, a reduction in eIF5A may cause a defect in the ER-coupled translation of other proteins containing eIF5A-dependent motifs in yeast and mammalian cells.

3.6 Hypusinated eIF5A depletion inhibits *in vitro* TGF-β1-mediated fibrogenesis in human HSCs

Hepatic fibrosis is the most common fibrotic process, in which hepatic stellate cells (HSCs) are the major cellular type responsible for producing high levels of collagen (see section 1.2.5 of Chapter 1). HSCs in normal liver are quiescent and synthesize trace amounts of Col1, but an increase in the major profibrogenic inducer TGF-β1 (Meng *et al.*, 2016) results in the transdifferentiation of HSCs into myofibroblast-like cells, which acquire a strong contractile phenotype and secrete and remodel large amounts of Col1 (De Minicis *et al.*, 2007).

To assess the effect of eIF5A hypusination inhibition on Col1a1 production during hepatic fibrogenesis *in vitro*, LX2 cells, an immortalized cell line of human HSCs, were treated with TGF-β1 (2.5 ng/mL) for 48 h, or its vehicle (DMSO) with or without 30 μM GC7. We observed a 90% reduction in hypusinated eIF5A in GC7-treated cells compared to the corresponding controls of HSCs, treated with or without TGF-β1, while total eIF5A protein levels were not significantly changed (Figures 3.11-A,B). The level of hypusinated eIF5A was higher in TGF-β1-treated than in control cells, but the difference was not statistically significant. Importantly, Col1a1 protein was undetectable in GC7-treated HSCs under basal conditions. As expected, a huge increase in Col1a1 protein levels was observed in TGF-β1

treated cells, which was fully prevented by co-treatment with GC7 (Figures 3.11-A,C). We also analyzed *COL1A1* mRNA levels under these conditions to distinguish between transcriptional and post-transcriptional effects. A small increase in *COL1A1* mRNA levels was observed in TGF-β1-treated cells (Figure 3.11-D), in correlation with the profibrotic activation of HSCs, although most of the huge increase in Col1a1 protein level with TGF-β1 can be attributed to post-transcriptional effects. In GC7-treated cells we observed a slight reduction in *COL1A1* mRNA with and without TGF-β1 treatment, that does not explain the large drop in Col1a1 protein levels when active eIF5A is lacking (Figures 3.11-A,D). These results strongly suggest that eIF5A is required for Col1a1 synthesis during TGF-β1-mediated hepatic fibrogenesis.

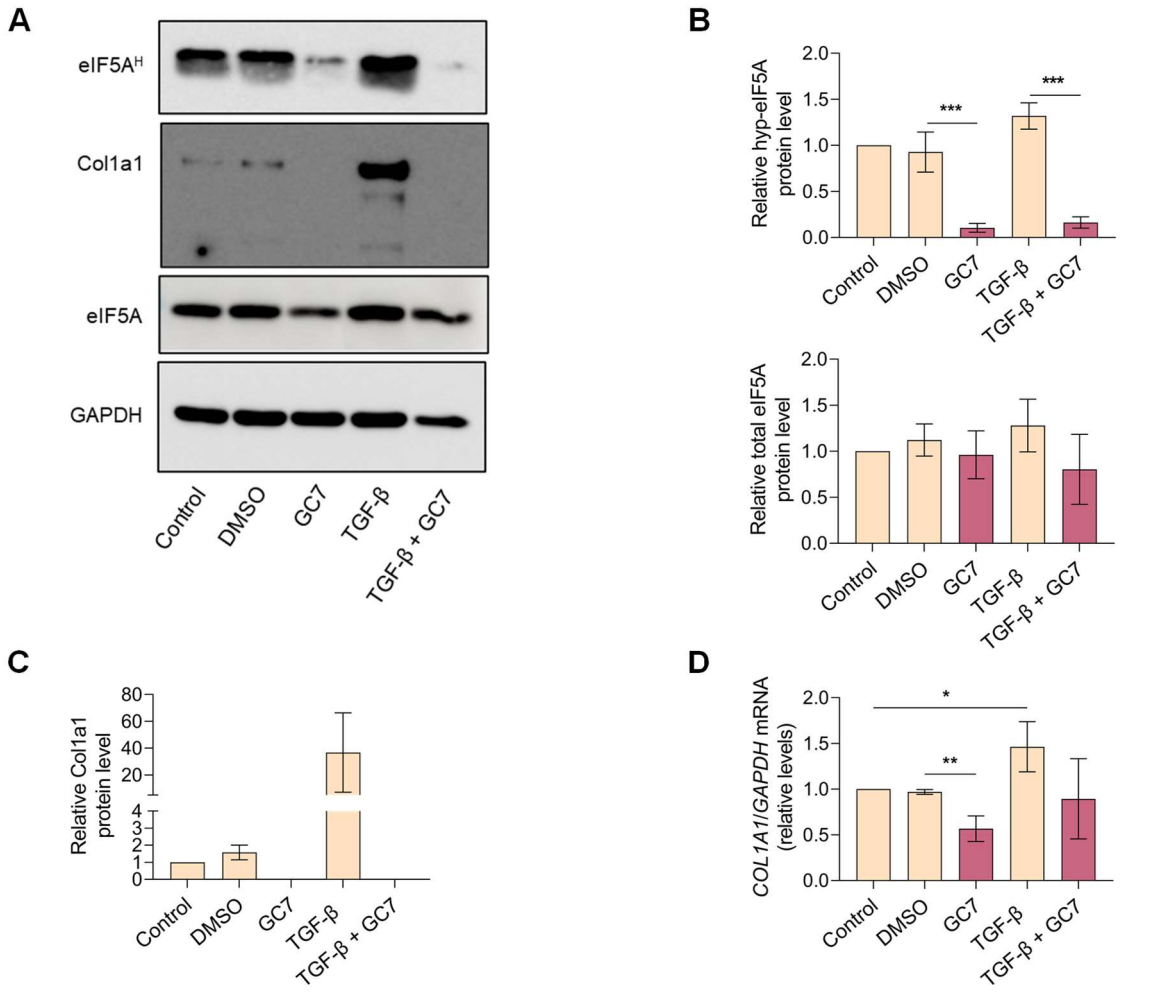

Figure 3.11. eIF5A is necessary for increased collagen production in cultured human hepatic stellate cells (HSCs) upon transforming growth factor-β1 (TGF-β1)-mediated fibrogenesis. (A) Western blotting analysis of Col1a1, hypusinated and total eIF5A in LX2 human HSCs untreated (control) or treated with 30 μM GC7 (GC7) or vehicle (DMSO) for 48 h. TGF-β1 (2.5 mg/mL) was used as a profibrogenic stimulus. GAPDH was used as a loading control. A representative experiment is shown. (B) Quantification analysis of the experiments in A showing hypusinated (n=3; top) and total (n=5; bottom) eIF5A protein levels. (C) Quantification analysis of the experiments in A showing Col1a1 protein levels (n=3). (D) RT-qPCR analysis of expression of *COL1A1* after 30 μM GC7 treatment of HSCs cells (n=3). (B-D) Data are mean ± SD relative to control cells. Statistical significance was determined using a two-tailed paired Student's t-test. *p<0.05, **p<0.01, ***p<0.001.

Additionally, we investigated further the effect of GC7 on the TGF-β transdifferentiation process in HSCs. This process involves the reprogramming of transcription with up-regulation of markers such as α-smooth muscle actin (ASMA) (De Minicis *et al.*, 2007) and also down-regulation of peroxisome proliferator-activated receptor-gamma (PPARG) in TGF-β-activated HSCs (De Minicis *et al.*, 2007; Hazra *et al.*, 2004). As expected, we observed an increase in *ASMA* mRNA and decrease in *PPARG* mRNA expression in TGF-β-treated HSCs (Figure 3.12). Interestingly, GC7-treated HSCs showed the opposite pattern, with significant reduction of ASMA mRNA and increase in PPARG mRNA, in cells incubated with or without TGF-β (Figure 3.12). These results suggest that inhibition of eIF5A hypusination yields antifibrotic effects as it not only reduced collagen synthesis but also inhibits the profibrotic transdifferentiation of HSCs.

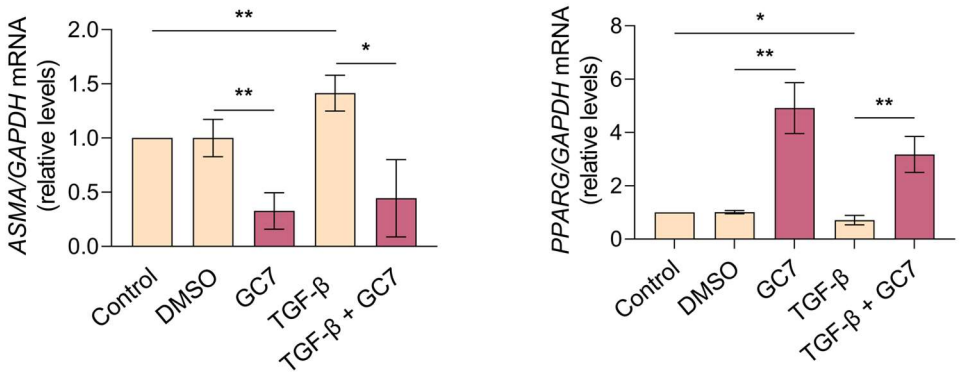

Figure 3.12. eIF5A depletion inhibits the profibrotic transdifferentiation in HSCs. RT-qPCR analysis of the expression of fibrotic markers *ASMA* mRNA (left) and *PPARG* mRNA (right) after 30 μM GC7 treatment of HSCs cells. Data are mean ± SD relative to control cells from three independent experiments. Statistical significance was determined using a two-tailed paired Student's t-test. *p<0.05, **p<0.01.

Discussion of Chapter 3

Expression of collagen, the most abundant protein in animals, is regulated at the level of transcription, mRNA stability and translation (Lindquist *et al.*, 2000). Our results here, using different approaches, provide evidence that eIF5A is essential for the translation of tripeptide motifs that are heavily present in collagens. In yeast, fusions of mouse Col1a1 fragments with β-galactosidase show low expression levels upon eIF5A depletion. In a dual-luciferase reporter system, PGP, PPG and EPG non-polyPro tripeptide motifs, abundant in collagens, stopped translation between *Renilla* and firefly luciferases when eIF5A is lacking. In mouse fibroblasts, depleting functional eIF5A by treatment with GC7 or by interfering with *Dhps* or *Eif5a1* siRNAs resulted in reduced Col1a1 levels, with no reduction in the *Col1a1* mRNA. In human HSCs, inhibiting eIF5A hypusination with GC7 eliminated the Col1a1 overproduction caused by profibrotic treatment with TGF-β1. Together, these results link eIF5A activity with translation of the PGP, PPG and EPG motifs that are highly abundant in the Col1a1 collagenic regions (Figure 3.13). The need for eIF5A in translating these non-polyPro tripeptide motifs has been suggested in yeast by ribosome profiling (Schuller *et al.*, 2017) and 5PSeq assays (Pelechano and Alepuz, 2017), in which it was noted that eIF5A depletion resulted in ribosomes stalling in these motifs. However, no physiological confirmation of a stop to translation causing the deficient protein synthesis in these motifs has been shown until now. Although our work has focused on the study of Col1a1, the existence of similar collagenic stretches in all collagens (Figure 3.1) suggests a similar dependency on eIF5A for the translation of the different collagens. Supporting this, a short polypeptide stretch of mouse Col4a1 containing several PPG and PGP motifs clearly stops translation in a yeast dual-luciferase system (Figure 3.3).

We observed that inhibition of eIF5A hypusination led to an accumulation of Col1a1 around the nuclei of mouse fibroblasts and provoked ER stress. Mutations in collagen, collagen-maturation enzymes or proteins that inhibit proper collagen folding, packing and secretion to induce ER stress and intracellular retention of collagen have been observed in collagenopathies, such as skeletal chondrodysplasia, osteogenesis imperfecta and osteoarthritis (Gawron, 2016). Intracellular retention of procollagen induces the ER stress proteins BiP and CHOP, which may lead to apoptosis (Schulz *et al.*, 2016). eIF5A has also been implicated in ER function. In yeast and HeLa cells, depletion of eIF5A causes ER stress and up-regulates stress-induced chaperones (Mandal *et al.*, 2016). We propose a direct role of eIF5A in facilitating ER-coupled collagen translation; similarly, eIF5A may facilitate the co-translational translocation into the ER of other proteins containing eIF5A-dependent motifs. Although most collagenopathies have a genetic etiology, with a mutation in a collagen or collagen-metabolism protein (Jobling *et al.*, 2014; Forlino and Marini, 2016; Marini *et al.*, 2017), it would be of interest to determine whether patients with a clinical, but not a genetic, diagnosis have defects in eIF5A expression. Interestingly, recent reports have linked impaired eIF5A function caused by the presence of human *EIF5A* or *DHPS* genetic variants with developmental and neurological rare disorders (Ganapathi *et al.*, 2019; Faundes *et al.*, 2021).

The excessive and uncontrolled synthesis of ECM proteins, mainly collagen type I, is the hallmark of fibrotic diseases; thus, the severity of the fibrotic disease depends on the amount of Col1 produced (Zhang and Stefanovic, 2016). Nearly 45% of all deaths in the developed world are attributed to chronic fibroproliferative diseases. Therefore, the demand for effective antifibrotic drugs will likely continue to

increase in the coming years (Wynn, 2008). In our study, using an *in vitro* model of fibrogenesis with human HSCs, TGF-β1 induced the expected huge increase in Col1a1 levels, which was almost completely abolished upon GC7 treatment. Additionally, we observed that GC7 inhibits the profibrotic transdifferentiation expression program of TGF-β1-activated HSCs. *In vivo* studies are required to confirm the profibrotic role of eIF5A and test whether down-regulation of eIF5A may be beneficial for the treatment of fibrosis of the liver and other organs.

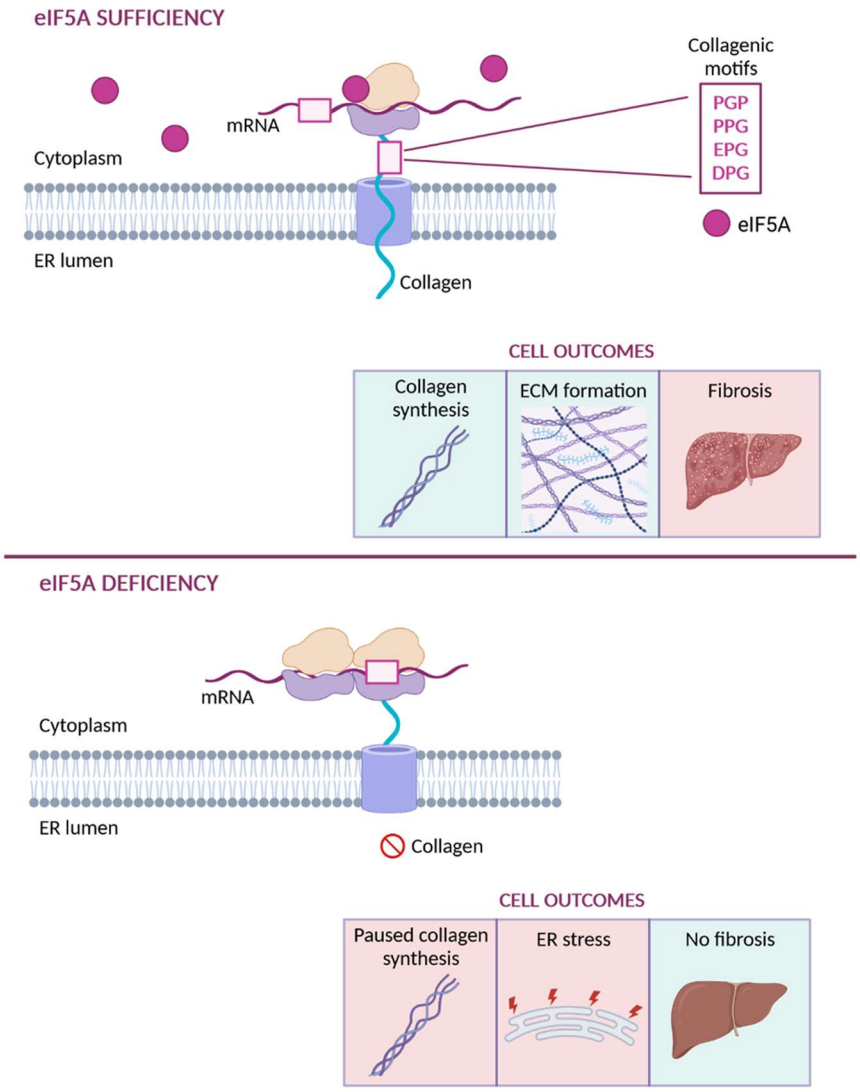

Figure 3.13. Model for eIF5A-mediated translation of collagen. During ER-coupled collagen translation, eIF5A, via its hypusine residue, assists the ribosome in translating mammalian collagen I protein at its PGP, PPG, EPG and DPG motifs. This increases the efficiency of collagen production and facilitates the formation of the extracellular matrix. In the absence of functional eIF5A, ribosomes stalls during translation, leading to ER stress and decreased collagen production which, in turn, will reduce fibrotic processes.

Chapter 4

eIF5A expression responds to cell metabolism and is regulated by Hap1 according to mitochondrial activity

Chapter 4. eIF5A expression responds to cell metabolism and is regulated by Hap1 according to mitochondrial activity.

This work was published in:

1. International Journal of Molecular Sciences, volume 22 (Barba-Aliaga *et al.*, 2021). "Yeast translation elongation factor eIF5A expression is regulated by nutrient availability through different signalling pathways." The authors are Marina Barba-Aliaga, Carlos Villarroel-Vicente, Alice Stanciu, Alba Corman, María Teresa Martínez-Pastor and Paula Alepuz[#].
   [#]Corresponding author.

   Detailed author contributions: Marina Barba-Aliaga contributed to the whole experimental development, and to experimental design, data analysis, review, manuscript conceptualization and writing. Carlos Villarroel-Vicente, Alice Stanciu and Alba Corman executed preliminary experiments. María Teresa Martínez-Pastor contributed to the experimental design of iron depletion experiments and revised the manuscript. Paula Alepuz supervised the work, experimental design, data analysis and carried out the manuscript conceptualization, writing and review.

2. FEBS Letters, volume 596 (Barba-Aliaga and Alepuz, 2022). "The activator/repressor Hap1 binds to the yeast eIF5A-encoding gene *TIF51A* to adapt its expression to the mitochondrial functional status." The authors are Marina Barba-Aliaga[#] and Paula Alepuz[#].
   [#]Corresponding author.

   Detailed author contributions: Marina Barba-Aliaga contributed to the whole experimental development and to experimental design, data analysis, review, manuscript conceptualization and writing. Paula Alepuz supervised the work, experimental design, data analysis and carried out the manuscript conceptualization, writing and review.

This work was included in the review:

3. International Journal of Molecular Sciences, volume 23 (Barba-Aliaga and Alepuz, 2022). "Role of eIF5A in mitochondrial function." The authors are Marina Barba-Aliaga[#] and Paula Alepuz[#].
   [#]Corresponding author.

   Detailed author contributions: Marina Barba-Aliaga and Paula Alepuz contributed to manuscript conceptualization, writing, review and editing.

As previously introduced, eIF5A is usually encoded by two highly homologous but differentially expressed genes in eukaryotes, even though no differences in molecular functionality between the two proteins have been found until now. One isoform is highly expressed under normal conditions, while the second one is only expressed in specific cell conditions or types. The human eIF5A1 isoform is abundant and implicated in some cancer types while the eIF5A2 isoform is absent in most cells but becomes overexpressed in many metastatic cancers (Ning *et al.,* 2020). In yeast, the two isoforms are reciprocally regulated by oxygen. The Tif51A isoform is the highly abundant isoform under aerobic conditions while the Tif51B isoform is poorly expressed. On the contrary, Tif51B is up-regulated and Tif51A is down-regulated when oxygen is limited (Zitomer and Lowry, 1992). Several reports have connected eIF5A to mitochondrial performance and suggested that both expression and activity of eIF5A are tightly linked to mitochondrial function. However, the specific molecular mechanism or whether eIF5A expression is regulated by the mitochondrial metabolism has not been determined yet. Mitochondrial activity and dynamics adapt to cellular energetic and metabolic demands and are regulated by the availability of, among other factors, oxygen, heme, iron and nutrient carbon source. Besides, its dysfunction is a hallmark of ageing and many human diseases. This work provides new mechanistic data on how gene expression of the two eIF5A isoforms is regulated by the cell metabolism and how their levels are adapted to the mitochondrial functional status.

4.1 The Tif51A isoform of yeast eIF5A is required for mitochondrial respiration

Saccharomyces cerevisiae preferentially consumes glucose as carbon source, but upon low glucose levels or deprivation and growth with non-fermentable carbon sources, many respiratory genes are highly induced for mitochondrial-dependent energy production. Previously, eIF5A, hypusination and polyamines had been described to participate in the mitochondrial function although the molecular mechanism was not outlined (see section 1.4.4 of Chapter 1). Here, we were interested in studying whether eIF5A is an essential protein for yeast respiration. To do so, we used partially or complete non-fermentable substrates as yeast carbon sources with different degrees of respiratory rates, such as galactose (intermediate respiration), glycerol and ethanol (complete respiration). Under these conditions, mitochondrial OXPHOS processes are required for cell growth and proliferation. At semi-restrictive temperature (34ºC), growth defects of the temperature-sensitive *tif51A-1* mutant, carrying a single (Pro83 to Ser) mutation in the yeast *TIF51A* gene, were found in these alternative carbon sources, whereas slight growth defects were observed in glucose medium. The *tif51A-3* mutant, carrying a double (Cys39 to Tyr, Gly118 to Asp) mutation, showed more severe defects while the *tif51B*Δ strain was not affected in media with galactose, glycerol or ethanol at 34ºC (Figure 4.1-A).

Next, we explored if eIF5A is essentially required for mitochondrial respiration. We measured the oxygen consumption rate in both wild-type and eIF5A temperature-sensitive mutant cells. The relative oxygen consumption in both mutant cells at restrictive temperature (37ºC) was significantly reduced compared to the wild-type, especially in the *tif51A-3* strain. Minor differences between wild-type and mutants were also observed at permissive temperature (25ºC) (Figure 4.1-B). This is in line with the expected slight loss of function given by the *TIF51A* mutations (Valentini *et al.*, 2002; Li *et al.*, 2011). Additionally, we investigated the implication of full hypusination (performed by both DHPS and DOOH enzymes) in the requirement of eIF5A for respiration. However, and contrary to Zhang *et al.*, 2022

results, we found no differences in the oxygen consumption between the wild-type and DOHH mutant cells (*lia1*Δ) (Figure 4.1-C).

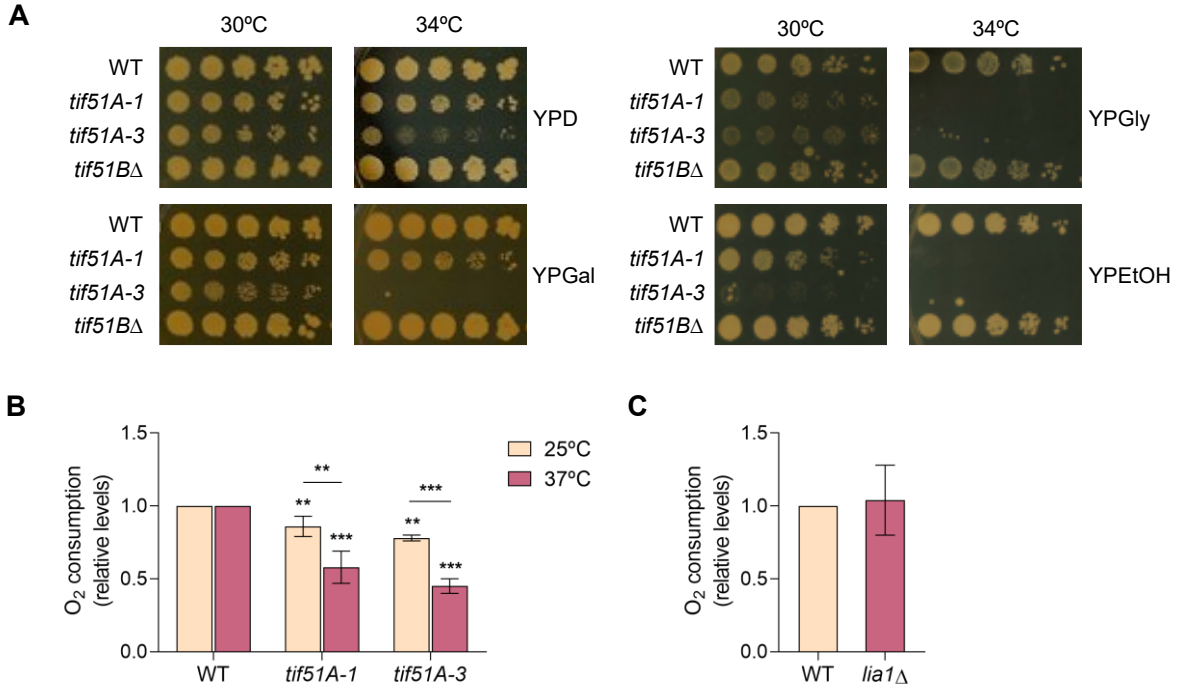

Figure 4.1. eIF5A yeast isoform Tif51A is required for respiration independently of hypusination. (A) Growth of the wild-type, *tif51A-1*, t*if51A-3* and *tif51B*Δ strains was tested in YEP medium containing 2% glucose (YPD), 2% galactose (YPGal), 2% glycerol (YPGly) or 2% ethanol (YPEtOH) at the indicated temperatures. (B, C) The wild-type, *tif51A-1* and t*if51A-3* (B) and wild-type and *lia1*Δ (C) strains were grown in YPGal at 25°C and transferred to 37°C for 4 h until an OD_{600} of 1.5–2 was reached. Relative oxygen consumption rates are shown. Data are presented as mean ± SD relative to wild-type from a minimum of three independent experiments. Statistical significance was determined using a two-tailed paired Student's t-test relative to corresponding wild-type cells. **p<0.01, ***p<0.001.

To increase our knowledge about the specific effects of eIF5A depletion in the mitochondrial function, we investigated the effects on mitochondrial membrane potential, distribution, and morphology. To do so, we used a MitoTracker fluorescent dye, which specifically accumulates at the mitochondria with the highest membrane potential inside the cell. Therefore, reduced staining indicates defects in membrane potential at the mitochondrial inner membrane caused by defective ETC and OXPHOS (Dimmer, 2014). Upon eIF5A depletion at restrictive temperature, the MitoTracker signal was decreased in *tif51A-1* and *tif51A-3* mutants, while increased in wild-type cells. Again, and in line with previous results, the membrane potential was already reduced in the two eIF5A mutants at permissive temperature (Figure 4.2-A). These results, suggest a strong loss of mitochondrial membrane potential under eIF5A deficiency, which is consistent with the strong drop in oxygen consumption already shown (Figure 4.1-B). To examine mitochondrial levels and morphology, we expressed in the yeast strains a mtGFP construct in which a mitochondrial targeting sequence guides GFP to the mitochondrial matrix independently of the mitochondrial membrane potential (Westermann and Neupert, 2000; Dimmer, 2014). We observed a similar reduction in GFP signal intensity at restrictive temperature in both wild-

type and *tif51A-1* strains, although the GFP signal was already significantly reduced in the *tif51A-1* strain at permissive temperature compared to the wild-type (Figure 4.2-B). Moreover, the distribution of the mitochondria in tubular networks was similar between both strains, with a slightly more discontinuous pattern in the *tif51A-1* cells (Figure 4.2-B). Therefore, a reduction in Tif51A protein levels generates a loss in the mitochondrial membrane potential which does not seem to entirely be a consequence of lower quantity of mitochondria or abnormal morphology and distribution. Altogether, these results highlight a specific role of Tif51A in sustaining the mitochondrial function.

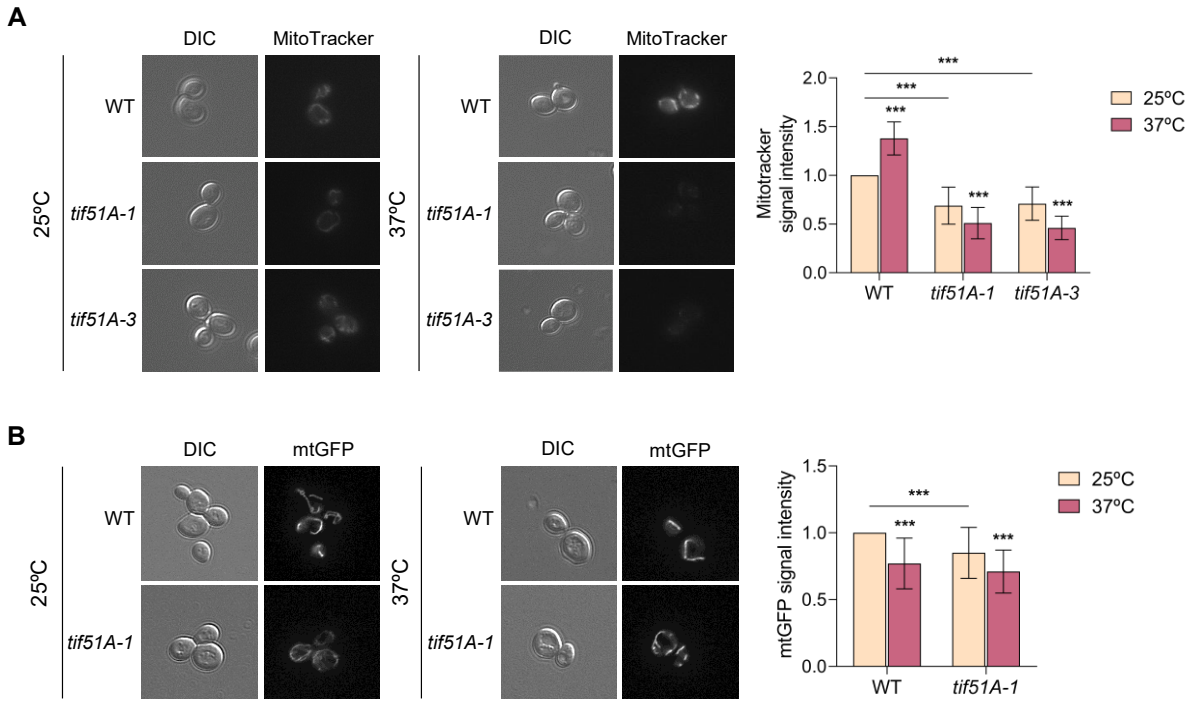

Figure 4.2. Depletion of the eIF5A respiratory isoform Tif51A reduces the mitochondrial membrane potential without severely affecting mitochondrial levels and morphology. (A) The wild-type, *tif51A-1* and t*if51A-3* strains were grown in SGal medium until post-diauxic phase at 25ºC, transferred to 25ºC or 37ºC for 4 h, and subjected to fluorescence and phase-contrast microscopy. Cells were incubated with Mitotracker prior microscopy to stain the mitochondria (left). Quantification of MitoTracker signal intensity relative to the value of the wild-type strain at 25ºC (right). (B) The wild-type and *tif51A-1* strains expressing mtGFP were grown in SGal medium lacking uracil as in (A) and subjected to fluorescence and phase-contrast microscopy (left). Quantification of mtGFP signal intensity as in (A) (right). (A,B) A representative image is shown. Fluorescent signal was quantified from at least 150 cells. Data are presented as mean ± SD from a minimum of three independent experiments. Statistical significance was determined using a two-tailed paired Student's t-test relative to the value at 25ºC. **p<0.01, ***p<0.001.

4.2 *TIF51A* expression drops during the diauxic shift while increases in the post-diauxic phase

We were interested in studying the gene expression regulation of the two eIF5A isoforms under fermentative and respiratory metabolisms. First, we assessed the expression of the two isoforms upon growth under non-fermentative conditions and observed regulation in opposite ways. While the mRNA levels of *TIF51A* significantly increased when growing under respiratory carbon sources, *TIF51B* levels lowered compared to glucose (Figure 4.3-A). Then, we aimed to investigate whether the previously observed up-regulation of *TIF51A* expression would also be reflected when the cells grown in glucose media underwent a metabolic shift from fermentation to respiration. To test this, we measured and compared the mRNA levels of the two eIF5A isoforms in the exponential and post-diauxic growth phases in a YPD batch culture for up to 4 days before reaching the stationary phase and entering the quiescent state (Figure 4.3-B). As seen in Figure 4.3-C the mRNA levels of *TIF51A* significantly increased to almost 2-fold after 48 h, while the *TIF51B* mRNA levels significantly and continuously decreased. To compare the regulation of eIF5A with that of another translation factor, we studied the expression of translation initiation factor eIF2A. Its mRNA levels were slowly and continuously lowering from 24 h (Figure 4.3-C), which agrees with previous results showing that the expression of most translation factors decreases as cells enter the post-diauxic phase and face the lack of glucose (DeRisi *et al.*, 1997). To confirm the transition to a respiratory metabolism, we also measured the expression of different respiration-related proteins including the TCA enzyme subunit SDH1, and the transcription factors Hap1 and Hap4, in charge of the upregulation of many TCA, ETC and OXPHOS genes under respiratory conditions. We observed a substantial increase in *SDH1* and *HAP4* expression after 24 h (Figure 4.3-D). Interestingly, *HAP1* also showed a 5-fold increase at 24 h and remained up-regulated for longer times (Figure 4.3-D). Finally, we also checked for possible variations in the eIF5A protein levels. Although the anti-eIF5A antibody cannot discriminate between the two isoforms, we found that the eIF5A protein level dropped to almost undetectable levels after 24 h of growth in YPD, which corresponds to the diauxic shift. However, initial levels were rescued at 72 h (Figures 4.3-E,F). This result may reflect on one hand, the observed reduction in *TIF51B* expression but, given the much higher *TIF51A* expression under basal conditions (Schnier *et al.*, 1991) and the slight drop in *TIF51A* mRNA levels at this point, this scenario suggests the down-regulation of Tif51A at translation or protein stability levels.

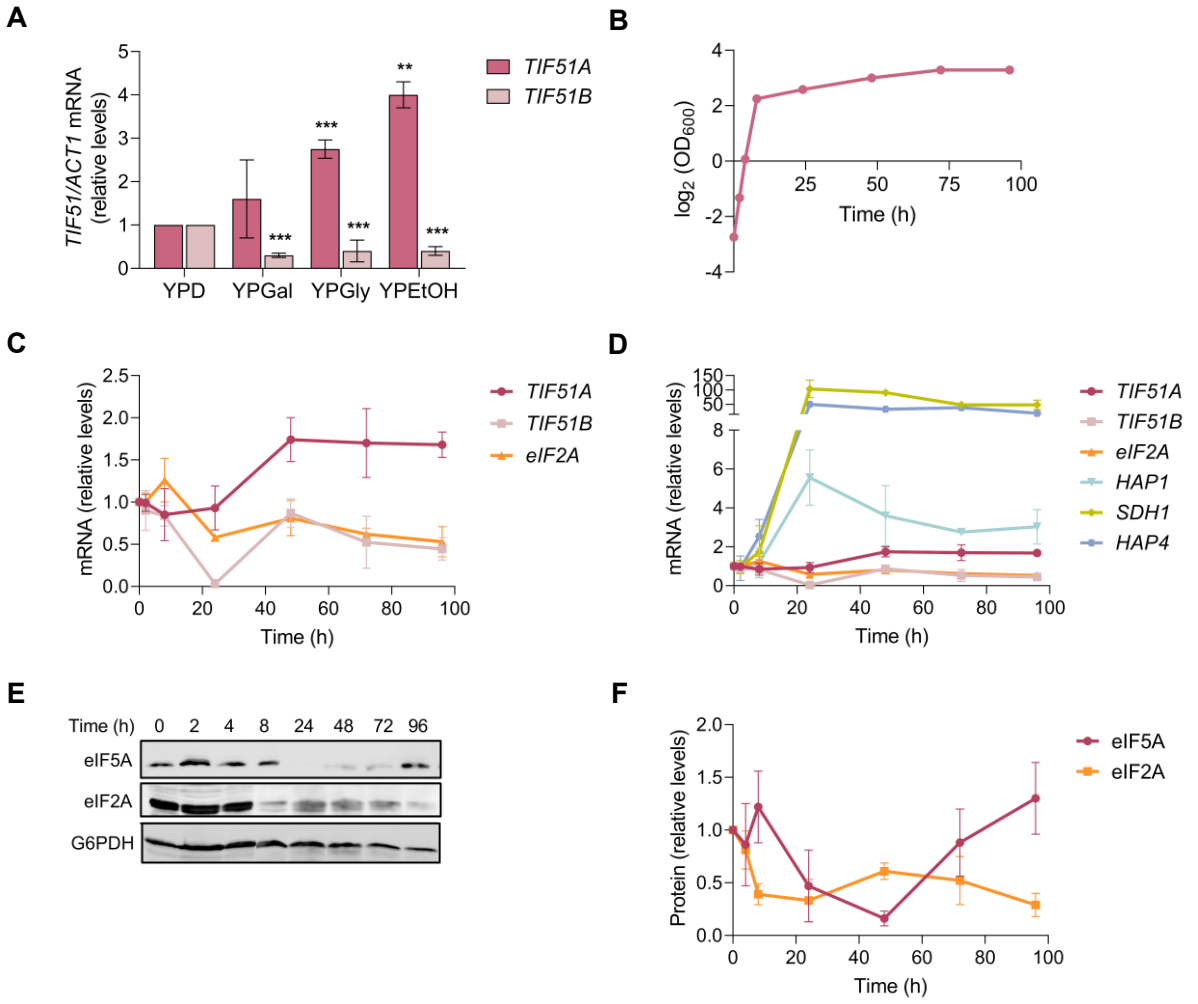

Figure 4.3. Tif51A expression drops during glucose exhaustion but recovers in the post-diauxic phase. (A) The wild-type cells were grown in YPD, YPGal, YPGly or YPEtOH to the exponential phase. Relative *TIF51A* and *TIF51B* mRNA levels were determined by RT-qPCR. (B) The wild-type cells were grown in YPD medium for 96 h and OD_{600} was measured, and cells collected at the indicated time points. (C) Relative *TIF51A*, *TIF51B* and *eIF2A* mRNA levels were determined by RT-qPCR. (D) Relative *TIF51A*, *TIF51B, eIF2A, HAP1, SDH1* and *HAP4* mRNA levels were determined by RT-qPCR. (E,F) A representative western blotting experiment (E) and quantification analysis (F) of the eIF5A and eIF2A protein levels in the wild-type cells at the indicated time points. G6PDH protein levels were used as loading controls. (A,C,D,F) Data are presented as mean ± SD relative to glucose or time 0 from a minimum of three independent experiments. Statistical significance was determined using a two-tailed paired Student's t-test relative to glucose condition. **p<0.01, ***p<0.001.

4.3 Glucose availability and TORC1 regulate eIF5A expression

In an effort to understand the eIF5A regulation during the diauxic shift when the glucose level drops, we decided to study the conceivable TORC1-mediated regulation. Like most organisms, yeast coordinates the protein biosynthetic capacity to nutrient availability through the TORC1 signal transduction pathway. Under unfavourable growth conditions, such as glucose deprivation, TORC1 is inactive, which leads to a slow reduction in translation and synthesis of ribosomal components (Cardenas *et al.*, 1999; Hardwick *et al.*, 1999; Proud, 2002).

First, we confirmed that TORC1 signalling inhibition by rapamycin treatment led to the rapid and pronounced down-regulation of the two eIF5A isoforms and of that of eIF2A (Figure 4.4-A). Likewise, upon TORC1 deactivation, the protein levels of both eIF5A and eIF2A translation factor significantly lowered (Figure 4.4-B).

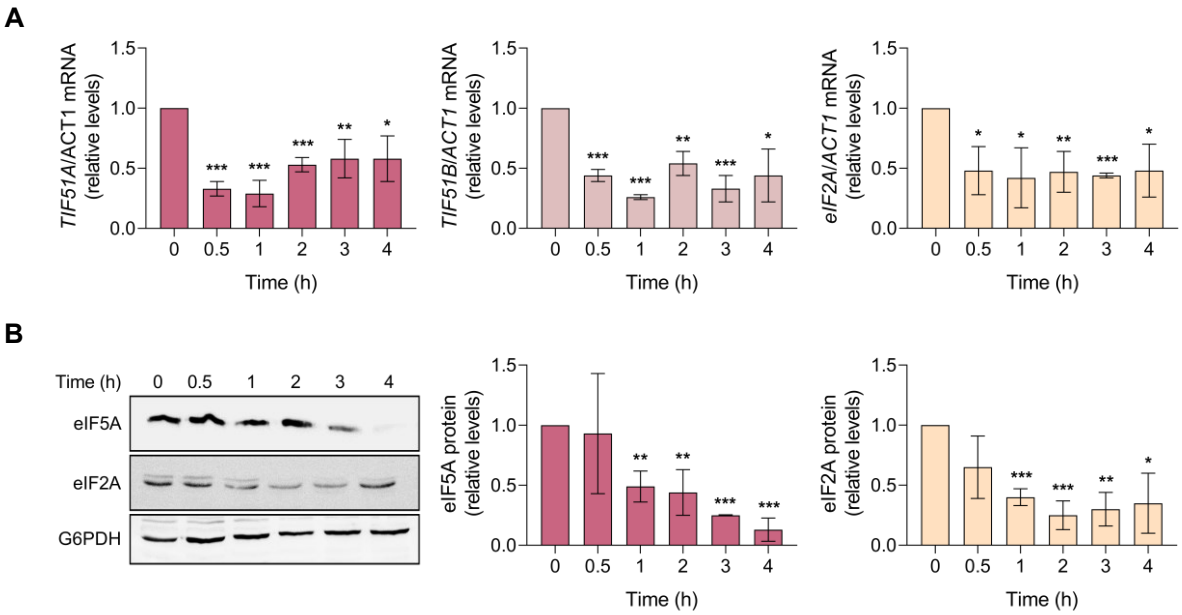

Figure 4.4. eIF5A expression is regulated by TORC1 pathway. (A) The wild-type cells were exponentially grown in YPD medium with the addition of 200 ng/mL rapamycin for 4 h. (A) Relative *TIF51A*, *TIF51B*, and *eIF2A* (from left to right) mRNA levels were determined by RT-qPCR. (B) Western blotting and quantification analysis of proteins eIF5A and eIF2A (from left to right). G6PDH protein levels were used as loading controls. A representative experiment is shown. (A,B) Data are presented as mean ± SD relative to time 0 from a minimum of three independent experiments. Statistical significance was determined using a two-tailed paired Student's t-test relative to time 0. *p<0.05, **p<0.01, ***p<0.001.

To further prove the regulation upon glucose availability, we studied the mRNA levels of *TIF51A* in three different scenarios: (1) glucose concentration drops from 2 to 0.1%; (2) glucose concentration rises from 0.1 to 2%; (3) the same increase in glucose concentration as (2) but supplemented with rapamycin. The results showed that *TIF51A* mRNA levels lowered after a drop in glucose concentration to 0.1% but were rescued when glucose was added back to the cells at regular levels (Figures 4.5-A,B). Furthermore, in the presence of rapamycin, adding 2% glucose did not rescue the higher levels reached in scenario 2, which implied a TORC1-mediated response to glucose availability (Figure 4.5-C). No significant differences were found between *TIF51A* and *eIF2A* mRNA levels in the three scenarios, meaning that both translation factors are regulated in the same way upon changes in nutrient accessibility (Figure 4.5).

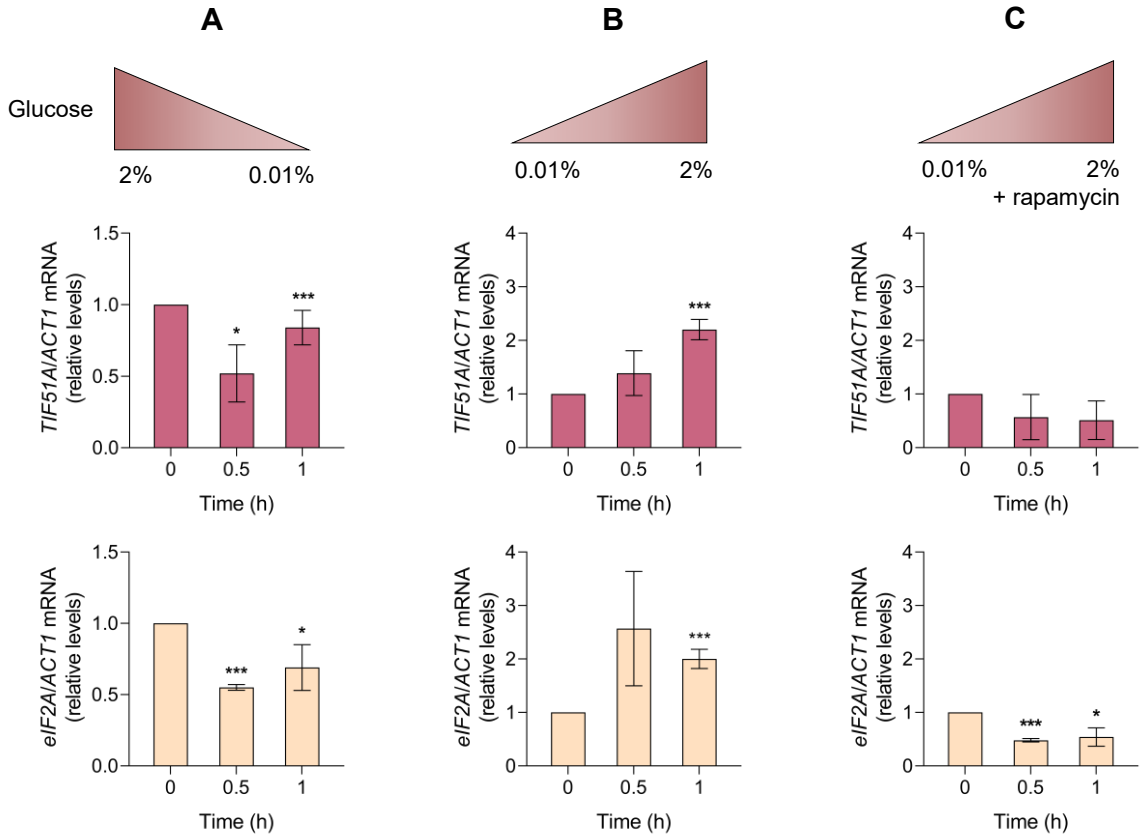

Figure 4.5. *TIF51A* expression is regulated by glucose concentration through TORC1. (A) The wild-type cells were exponentially grown in YEP medium containing 2% glucose and transferred to YEP medium containing 0.1% glucose for 1 h. (B,C) The wild-type cells were exponentially grown in YEP medium containing 0.1% glucose and transferred to YEP medium containing 2% glucose without (B) or with (C) the addition of 200 ng/mL rapamycin for 1 h. (A-C) The relative *TIF51A* (middle) and *eIF2A* (bottom) mRNA levels were determined by RT-qPCR. Data are presented as mean ± SD relative to time 0 from a minimum of three independent experiments. Statistical significance was determined using a two-tailed paired Student's t-test relative to time 0. *p<0.05, ***p<0.001.

4.4 Hap1 is constitutively bound to the *TIF51A* promoter and acts as a transcriptional activator under respiration

As previously described, *TIF51A* expression was induced in cells grown under non-fermentable carbon sources, used for the oxidative metabolism of mitochondria. Here, we aimed to investigate the mechanism exerted to reach different modulations in eIF5A abundance. According to literature (Zitomer and Lowry, 1992; Hickman and Winston, 2007), Hap1 was one of the possible candidates regulating eIF5A activation and thus, influencing respiration. Hap1 responds to heme cellular levels and is involved, together with the Hap2/3/4/5 complex in the metabolic reprogramming between the two alternative physiological states: fermentation and respiration (see section 1.3.1 of Chapter 1). We first asked if Hap1 was required for the up-regulation of *TIF51A* expression under respiratory conditions. Hence, we used a *hap1*Δ mutant and observed that the mRNA levels of *TIF51A* were not increased when grown under non-fermentable sources (Figure 4.6-A). On the contrary, we observed that the repression of *TIF51B* expression produced under respiration, was not compromised in the absence of Hap1 (Figure 4.6-B), suggesting that *TIF51B* expression is repressed by an additional Hap1-independent mechanism. Additionally, we also studied the mRNA levels of *TIF51A* in a *hap1*Δ mutant grown in a YPD batch culture for days. We observed how the *TIF51A* mRNA levels remained constant or were even slightly lowered in *hap1*Δ (Figure 4.6-C), pointing out the specific requirement of Hap1 for inducing *TIF51A* after a shift from fermentation to respiration.

Then, we aimed to investigate whether Hap1 regulation over *TIF51A* was direct. *TIF51A* presents a putative Hap1-binding site at the promoter at -571 bp of the transcription start site (Figure 4.6-D) with the consensus Hap1-binding sequence CGGataTAttCGG (Zhang and Guarente, 1994). Using chromatin immunoprecipitation (ChIP) in a yeast strain with an N-terminal 3myc-tagged Hap1, we studied Hap1 binding to three regions of the promoter and observed a strong signal for Hap1 binding to the *TIF51A* promoter centred on the Hap1 consensus sequence (region 2) under both respiratory and fermentative conditions (Figure 4.6-E). Weaker Hap1 ChIP signals were also detected in the surrounding 1 and 3 regions, probably since chromatin fragmentation in ChIP assays produced a variable range of size fragments around 400 bp, therefore allowing PCR amplification of regions 1 and 3. A weaker ChIP signal was also observed at the already described targets. Hap1 binds to the promoter of the transcriptional repressor *ROX1* at the consensus Hap1-binding sequence tGGaacTAcCGG, as well as to the promoter of *CYC1*, which encodes the ETC electron carrier cytochrome c, at the consensus Hap1-binding sequence CGGggtTtaCGG (Figure 4.6-E). Only a background signal was detected at *TIF51A*, *ROX1* and *CYC1* with the non-tagged strain (Figure 4.6-E). These results confirm the constitutive binding of Hap1 to the *TIF51A* promoter region, which increases Tif51A protein levels in conditions of high mitochondrial activity.

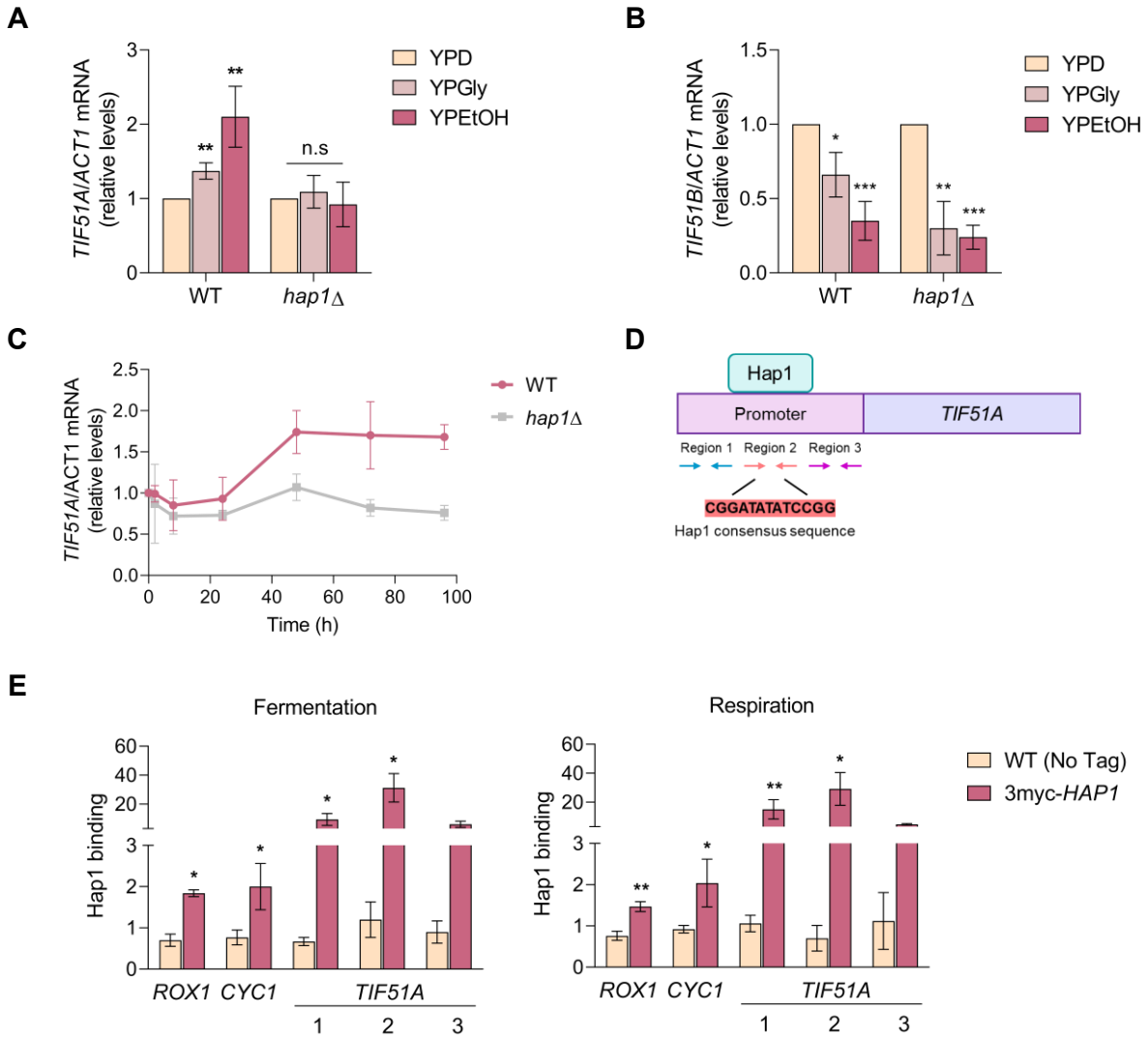

Figure 4.6. Hap1 is constitutively bound to *TIF51A* promoter and induces expression under respiration conditions. (A,B) The wild-type and *hap1*Δ strains were grown in YPD, YPGly or YPEtOH to the exponential phase. Relative *TIF51A* (A) and *TIF51B* (B) mRNA levels were determined by RT-qPCR. The results are expressed relative to each strain in YPD. (C) The wild-type and *hap1*Δ cells were grown in YPD medium for 96 h and samples were collected at the indicated time points. Relative *TIF51A* mRNA levels were determined by RT-qPCR. The results are expressed relative to time 0. (D) Scheme of Hap1 binding to the promoter of *TIF51A*. (E) ChIP analysis of Hap1 recruitment in wild-type (No Tag) and tagged Hap1 wild-type strains grown in YPD (fermentation) or YPEtOH (respiration). ChIP of Hap1 was performed using the antibody anti-myc. The ChIP DNA was used to quantify the binding to the promoters of *ROX1*, *CYC1* and *TIF51A* genes by qPCR. The percentage of the signal obtained in each ChIP sample with respect to the signal obtained with the DNA from the corresponding whole cell extract was calculated. (A-C,E) Data are presented as mean ± SD from a minimum of three independent experiments. Statistical significance was determined using a two-tailed paired Student's t-test relative to glucose condition or wild-type cells. *p<0.05, **p<0.01, ***p<0.001.

4.5 Hap1 activates *TIF51A* expression upon increased metabolic flux into the TCA cycle and heme cellular levels

The above-stated experiments reveal a Hap1-mediated *TIF51A* regulation under respiratory conditions. Hap1 is known to respond to both heme and non-fermentable energy. Heme synthesis starts in mitochondria and is limited by TCA and succinyl-CoA availability. Therefore, marked pyruvate transport into mitochondria results in high heme levels and, thus, enhanced Hap1 activity (see Zhang *et al.*, 2017 and section 1.3.2 of Chapter 1). To better understand the regulation of eIF5A by Hap1, we investigated whether the heme levels and flux into the TCA cycle are critical for *TIF51A* transcriptional regulation. We first examined the *TIF51A* expression in wild-type, *hap1*Δ, *mpc1*Δ and *pda1*Δ cells. Mpc1 is a pyruvate transporter localised in the inner mitochondrial membrane, while Pda1 is a subunit of the pyruvate dehydrogenase complex which catalyses the conversion of pyruvate into acetyl-CoA in mitochondria. We established the expression of *SDH1* as an additional control, which is induced under respiratory conditions. We observed that both *TIF51A* and *SDH1* expression levels in galactose medium were significantly lowered in all the mutant cells compared to the wild-type (Figure 4.7-A). These results indicate that the metabolic flux into the TCA cycle regulates eIF5A expression, by regulating Hap1 expression.

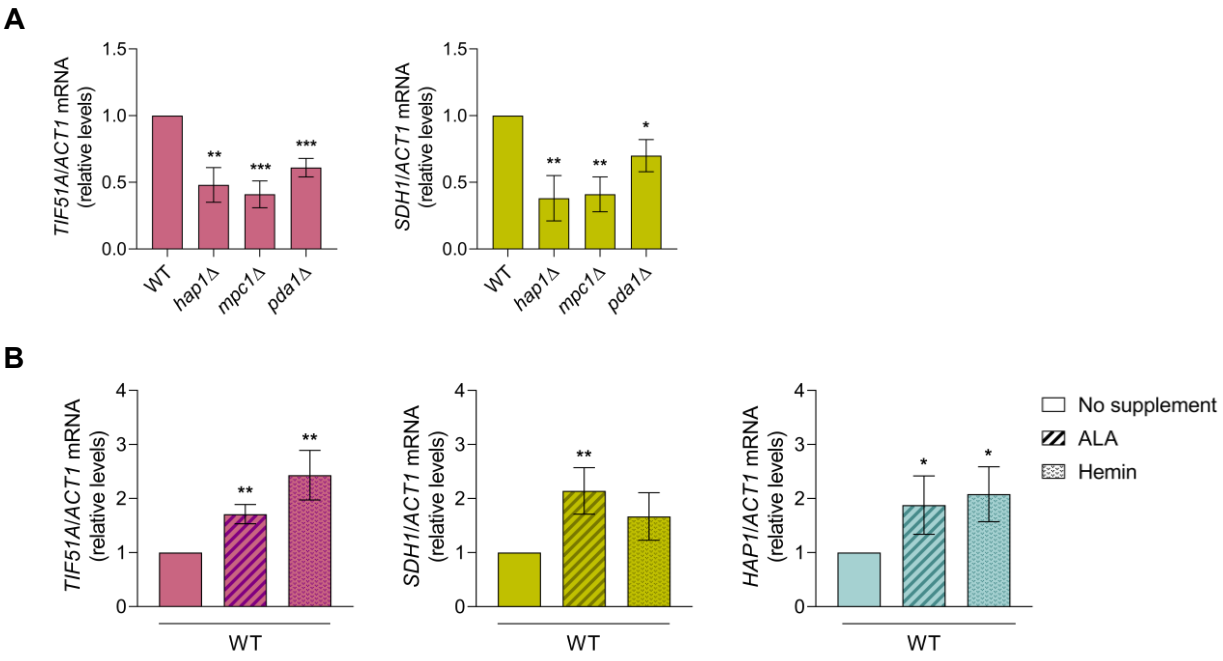

Figure 4.7. eIF5A expression is regulated by the metabolic flux into the TCA cycle and heme cellular levels. (A) The wild-type, *hap1*Δ, *mpc1*Δ and *pda1*Δ strains were grown in YPGal for 24 h. Relative *TIF51A* and *SDH1* mRNA levels were determined by RT-qPCR. The results are expressed relative to the wild-type value. (B) The wild-type cells were grown in YPD with or without the addition of ALA (300 µg/ml) or hemin (25 µg/ml) for 24 h. Relative *TIF51A*, *SDH1* and *HAP1* (from left to right) mRNA levels were determined by RT-qPCR. The results are expressed relative to the value for the no supplement condition. (A,B) Data are presented as mean ± SD from a minimum of three independent experiments. Statistical significance was determined using a two-tailed paired Student's t-test relative to corresponding wild-type or no supplement condition. *p<0.05, **p<0.01, ***p<0.001.

To determine whether the heme levels are limiting for *TIF51A* transcription, we added 5-aminovulenic acid (ALA, the second metabolite of the heme biosynthesis pathway; Figure 1.9-B) or hemin (heme derivative) to the cells grown in rich media containing glucose. We found that the addition of extracellular ALA or hemin increased *TIF51A* expression almost 2-fold, and a similar increase was observed for *HAP1* and *SDH1* expression (Figure 4.7-B). These results suggest that *TIF51A* transcription is regulated by heme and by the metabolic flux into the TCA cycle through the transcription factor Hap1.

4.6 Hap1 represses *TIF51A* expression under iron starvation by recruiting the co-transcriptional repressor Tup1

Respiration is a highly iron-consuming process as both the TCA cycle and ETC require iron and heme in many steps. Indeed, during iron starvation, cells are unable to grow under non-fermentable carbon sources. Iron deficiency in *S. cerevisiae* involves a metabolic remodelling, which is achieved by changes in gene expression at the transcriptional and post-transcriptional levels to prioritise iron-dependent essential cellular processes over non-essential processes, including in these last ones the mitochondrial respiration (Ramos-Alonso *et al.*, 2020). We hypothesized that under iron starvation, respiration inhibition would also involve the down-regulation of *TIF51A* expression. To test this possible iron-dependent activity of eIF5A, the mRNA levels of the two isoforms were determined under iron sufficiency and deficiency. Iron starvation caused by the addition of the iron chelator BPS (Bathophenanthrolinedisulfonic acid) significantly affected the expression of the two isoforms. While *TIF51A* expression decreased in a time-dependent manner, *TIF51B* expression increased almost 4-fold (Figure 4.8-A). Next, we determined if eIF5A regulation under iron deficiency was based on a Hap1-dependent transcriptional mechanism. We first analyzed the expression of *TIF51A* under iron sufficiency or deficiency in the wild-type and *hap1*Δ mutant cells. We found that for *hap1*Δ cells the *TIF51A* mRNA levels remained unchanged and transcriptional regulation was lost, which identify Hap1 as responsible for eIF5A regulation under iron deficiency (Figure 4.8-B). This result suggests that Hap1 may have dual actions, as an activator under respiratory conditions and as a repressor under non-respiratory conditions. This dual activity has already been reported for Hap1 and its regulation of the ergosterol biosynthetic (ERG) genes, which are activated by heme-bound Hap1 under aerobic growth but repressed by heme-unbound Hap1 under hypoxic conditions. In this case, Hap1 is constitutively associated to ERG promoters and executes its repressor activity by recruiting the co-repressor factor Tup1 (Hickman and Winston, 2007). We explored whether *TIF51A* regulation by iron follows a Hap1-dependent mechanism to that of ERG genes. First, we confirmed the constitutive Hap1 binding to the *TIF51A* promoter under iron availability and deprivation (Figure 4.8-C). Again, the signal of the association of 3myc-Hap1 with *TIF51A* chromatin was stronger than that observed for its association with the *CYC1* promoter (Figure 4.8-C).

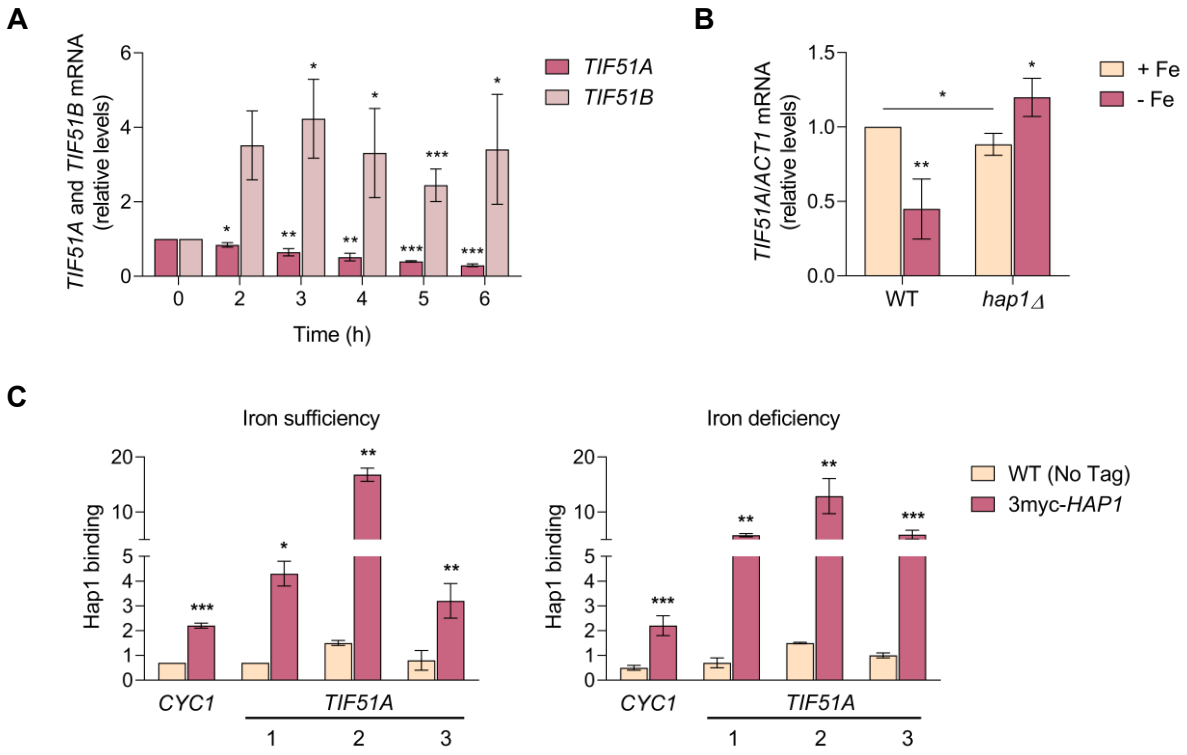

Figure 4.8. Hap1 acts as a transcriptional repressor of *TIF51A* under iron deficiency. (A) The wild-type cells were grown in SC medium with the addition of 100 µM BPS for 7 h and samples were collected at the indicated time points. Relative *TIF51A* and *TIF51B* mRNA levels were determined by RT-qPCR. The results are expressed relative to time 0. (B) The wild-type and *hap1*Δ strains were grown in SC medium with or without the addition of 100 µM BPS for 7 h. Relative *TIF51A* mRNA levels were determined by RT-qPCR. The results are expressed relative to the wild-type without treatment. (C) ChIP analysis of Hap1 recruitment in wild-type (No Tag) and tagged 3myc-Hap1 wild-type strains grown as in (B). ChIP of Hap1 was performed using the antibody anti-myc. The ChIP DNA was used to quantify the binding to the promoters of *CYC1* and *TIF51A* genes by qPCR. The percentage of the signal obtained in each ChIP sample with respect to the signal obtained with the DNA from the corresponding whole cell extract was calculated. (A-C) Data are presented as mean ± SD from a minimum of three independent experiments. Statistical significance was determined using a two-tailed paired Student's t-test relative to corresponding wild-type cells, non-treated cells or time 0. *p<0.05, **p<0.01, ***p<0.001.

Next, we checked whether *TIF51A* repression under iron starvation was dependent on the repressor complex Ssn6/Tup1. We observed that the reduction in *TIF51A* mRNA levels under iron starvation was completely lost in a *tup1*Δ yeast strain, whereas *TIF51A* repression was fully achieved in a *ssn6*Δ strain (Figure 4.9-A). Although it was unexpected that the two proteins forming the Ssn6/Tup1 complex would have unequal contribution to *TIF51A* repression, they do have different effects in other systems, such as the glucose repression of maltose metabolism (Lin *et al.*, 2014). Then, using a Tup1-13myc-tagged strain, we studied the binding of Tup1 to the *TIF51A* promoter and observed that Tup1 gave a low ChIP signal at the promoter under iron sufficiency, but a strong signal under iron deficiency. Tup1 recruitment was dependent on the presence of Hap1, and the association was stronger at region 2 containing the consensus Hap1-binding sequence (Figure 4.9-B). These results suggest that, under iron deficiency, constitutively bound Hap1 represses *TIF51A* by recruiting the Tup1 co-repressor protein, which is known to repress gene expression by interacting with chromatin-modifying histone deacetylases and basal transcription machinery components (Wu *et al.*, 2001; Zaman *et al.*, 2001; Fleming *et al.*, 2014).

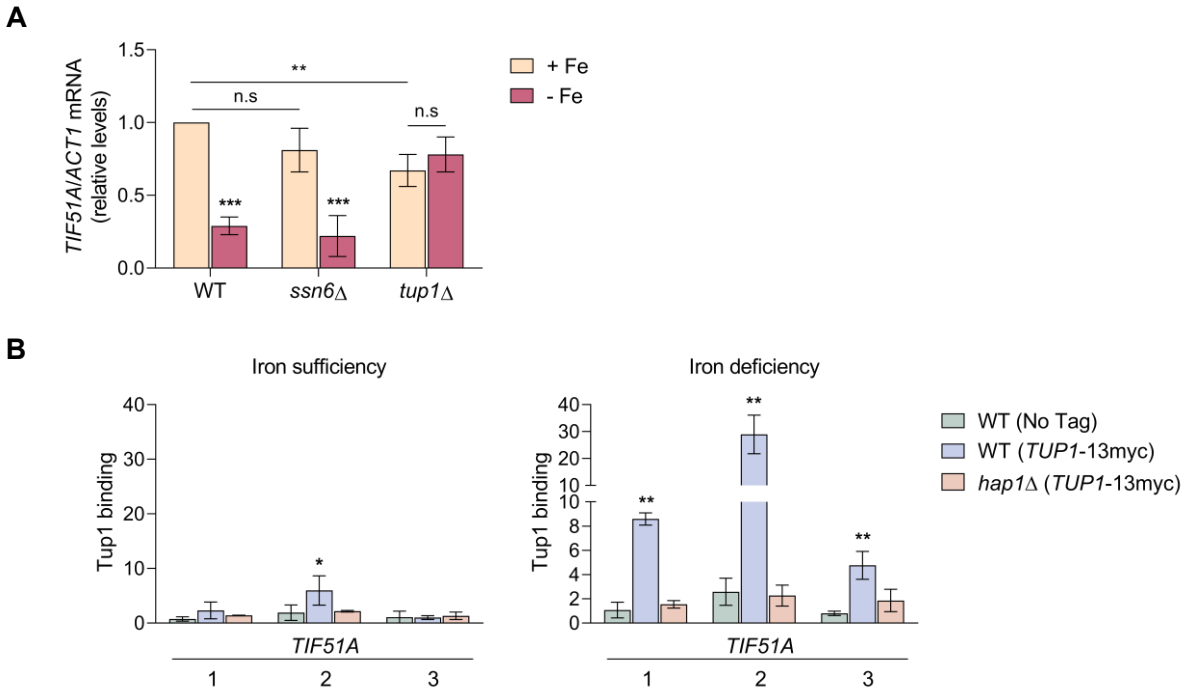

Figure 4.9. Hap1 acts as a transcriptional repressor recruiting Tup1 to *TIF51A* promoter under iron starvation. (A) The wild-type, *ssn6*Δ and *tup1*Δ strains were grown in SC medium with or without the addition of 100 µM BPS for 7 h. Relative *TIF51A* mRNA levels were determined by RT-qPCR. The results are expressed relative to wild-type strain under iron sufficiency. (B) ChIP analysis of Tup1 recruitment in wild-type (No Tag) and Tup1-13myc wild-type and *hap1*Δ tagged strains grown as in (A). ChIP of Tup1 was performed using the antibody anti-myc. The ChIP DNA was used to quantify the binding to the three regions of the promoter of *TIF51A* gene by qPCR. The percentage of the signal obtained in each ChIP sample with respect to the signal obtained with the DNA from the corresponding whole cell extract was calculated. (A-B) Data are presented as mean ± SD from a minimum of three independent experiments. Statistical significance was determined using a two-tailed paired Student's t-test relative to corresponding wild-type cells or non-treated cells. *p<0.05, **p<0.01, ***p<0.001.

4.7 Hap1 indirectly regulates *TIF51B* expression through direct *ROX1* and *MOT3* activation and Tup1-mediated repression in response to the respiratory status

The regulation of the eIF5A-encoding gene *TIF51B* is an illustrative example of the modulation of hypoxic gene expression by oxygen cellular levels. This regulation is controlled by the heme- and Hap1-dependent Rox1 and Mot3 proteins, which synergistically repress *TIF51B* expression under normoxia by recruiting the general repressor complex Ssn6/Tup1. Under hypoxia, Hap1 becomes a repressor of *ROX1/MOT3*; thus, a drop in these repressors upregulates *TIF51B* expression (see Lowry and Lieber, 1986; Lowry and Zitomer, 1988; Sertil *et al*., 2003; Klinkenberg *et al.*, 2005 and section 1.3.3 of Chapter 1). Although this *TIF51B* regulatory mechanism has been extensively described for normoxic/hypoxic conditions, it is still not fully documented with respect to Hap1 binding to genes. Regarding *TIF51B* expression under iron deficiency, we found that Hap1 was also important for its regulation as the induction occurring in the wild-type was lost in Hap1-deficient cells (Figure 4.10-A).

We asked if the lack of heme, caused by limited iron availability, converts Hap1 in a repressor that downregulates *ROX1*/MOT3, which is necessary for inducing *TIF51B*. Iron starvation generated a drop in the expression of *ROX1* and *MOT3*, suggesting that Hap1 shifted from an activator to a repressor of these genes (Figure 4.10-B). As expected, we observed that *ROX1* and *MOT3* expression was reduced in a *hap1*Δ strain under iron sufficiency and their repression under iron deficiency was lost in a *hap1*Δ mutant (Figure 4.10-B). Moreover, the co-repressor function of Tup1 was confirmed for *TIF51B* expression under iron availability and for *ROX1* and *MOT3* under iron starvation (Figures 4.10-A,B). Interestingly, in the *hap1*Δ strain, *TIF51B* was slightly up-regulated under iron sufficiency, whereas the up-regulation was much higher in a *tup1*Δ, suggesting the existence of a Hap1-independent and Tup1-dependent repression of *TIF51B* acting under sufficient iron and oxygen conditions (Figure 4.10-A). This residual *TIF51B* activation in the *hap1*Δ strain may also be due to the continued presence of low levels of *ROX1* and *MOT3* expression in *hap1*Δ under iron sufficiency (Figure 4.10-A).

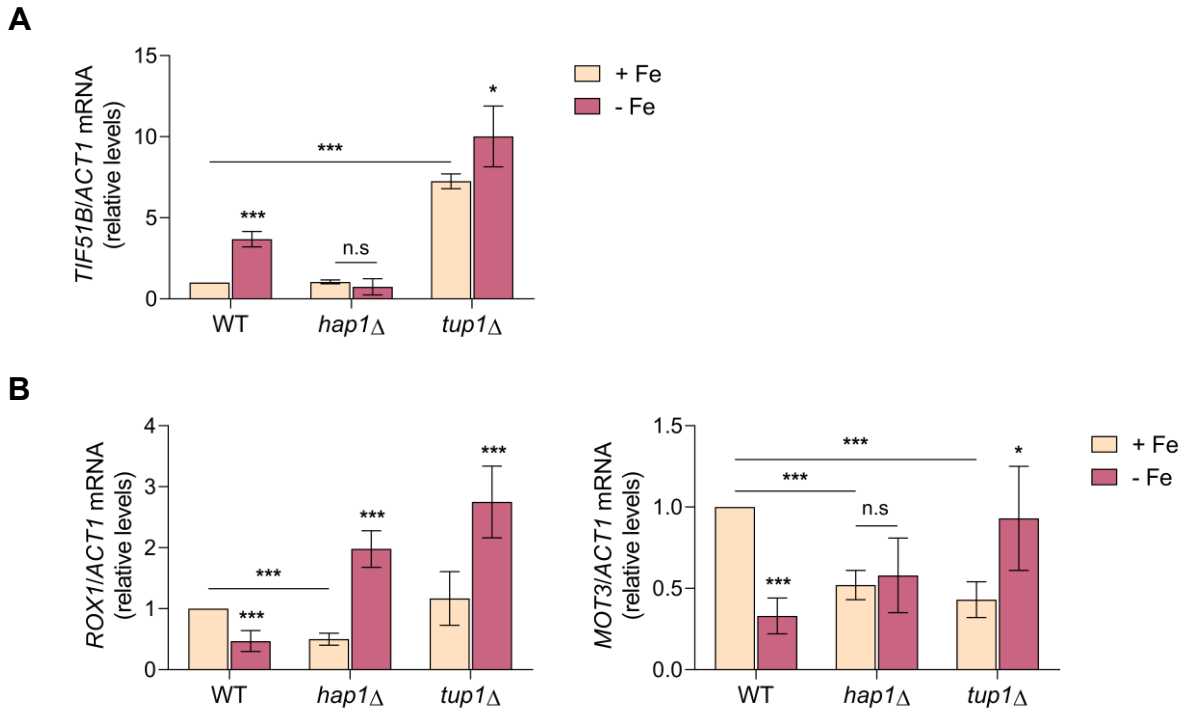

Figure 4.10. Hap1 acts through Rox1/Mot3-Tup1 to repress *TIF51B* expression under iron sufficiency. (A,B) The wild-type, *hap1*Δ and *tup1*Δ strains were grown in SC medium with or without the addition of 100 µM BPS for 7 h. Relative *TIF51B* (A), *ROX1* and *MOT3* (B) mRNA levels were determined by RT-qPCR. Data are presented as mean ± SD from a minimum of three independent experiments and relative to wild-type strain under iron sufficiency. Statistical significance was determined using a two-tailed paired Student's t-test relative to corresponding non-treated cells. *p<0.05, ***p<0.001.

Using the 3myc-HAP1 strain and ChIP analysis, we observed that Hap1 binds to the promoter of the repressor *ROX1* at the consensus Hap1-binding sequence tGGaacTAcCGG, as well as to the promoter of *MOT3* at the consensus Hap1-binding sequence tGGcgaTAaCGG. The binding occurs in both iron-sufficient and iron-deficient conditions, with a higher ChIP signal for the *MOT3* promoter (Figure 4.11-A). We next investigated the dependency on Hap1 of Tup1 repressor binding and observed that Hap1 recruits Tup1 to *ROX1* and *MOT3* promoters only under iron scarcity, whereas Tup1 binds to the *TIF51B* promoter only under iron sufficiency in a Hap1-dependent manner (Figure 4.11-B). This last result is consistent with the requirement of Hap1 for *ROX1* and *MOT3* expression under iron sufficiency (Figure 4.10-A). Together, these results show the *in vivo* regulation of *TIF51B* expression by iron through the constitutive binding of Hap1 to *ROX1* and *MOT3* to act as an activator/repressor factor. Moreover, the results confirm that iron regulation of *TIF51B* uses the same Hap1/Tup1-mediated mechanism proposed for oxygen regulation, pointing to the mitochondrial function as the common nexus of both regulations.

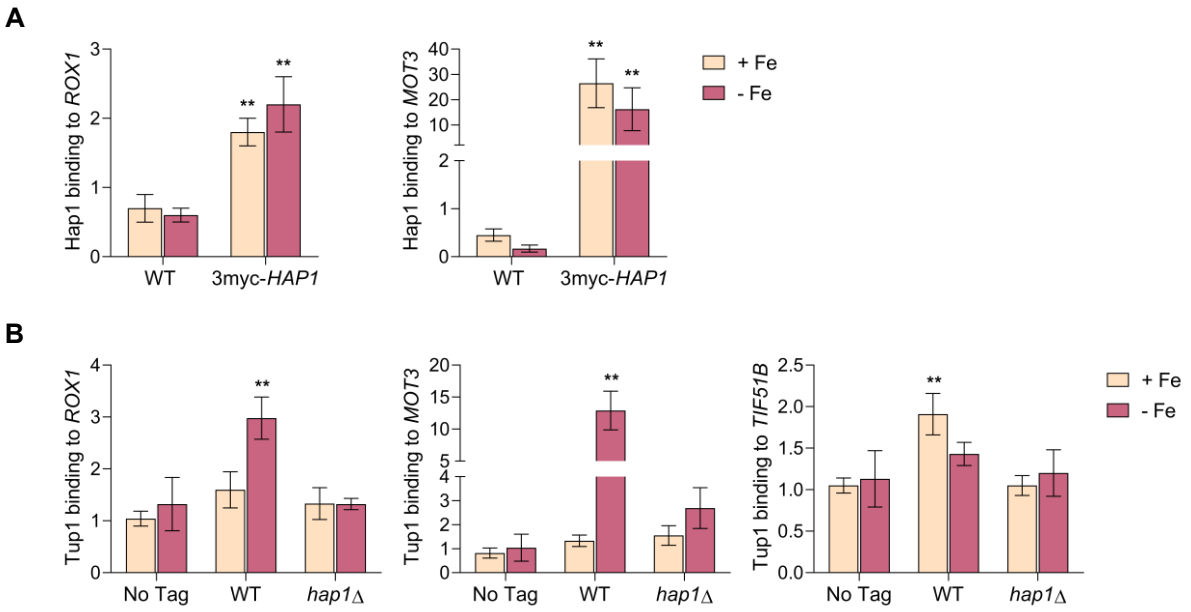

Figure 4.11. Hap1 acts through Rox1-Tup1 to repress *TIF51B* expression under iron sufficiency. (A) ChIP analysis of Hap1 recruitment in wild-type (No Tag) and 3myc-Hap1 tagged wild-type strains grown in SC medium with or without the addition of 100 µM BPS for 7 h. ChIP of Hap1 was performed using the antibody anti-myc. The ChIP DNA was used to quantify the binding to the promoter of *ROX1* (left) and MOT3 (right) genes by qPCR. (B) ChIP analysis of Tup1 recruitment in wild-type (No Tag) and Tup1-13myc wild-type and *hap1*Δ tagged strains grown as in (A). ChIP of Tup1 was performed using the antibody anti-myc. The ChIP DNA was used to quantify the binding to the promoter of *ROX1*, *MOT3* and *TIF51B* genes by qPCR. (A,B) The percentage of the signal obtained in each ChIP sample with respect to the signal obtained with the DNA from the corresponding whole cell extract was calculated. Data are presented as mean ± SD from a minimum of three independent experiments. Statistical significance was determined using a two-tailed paired Student's t-test relative to corresponding wild-type or no tag cells. **p<0.01.

4.8 Acute inhibition of mitochondrial respiration results in Hap1-dependent but Tup1-independent *TIF51A* repression

Results obtained until here suggest that the expression of both eIF5A-encoding genes responds to the mitochondrial activity status of the cell, which depends on the availability of oxygen, iron, heme and type of carbon source. Therefore, we investigated whether an acute disruption of mitochondrial respiration would result in the regulation of both eIF5A isoforms, promoting the expression of the fermentative isoform (Tif51B) and the inactivation of the respiratory isoform (Tif51A). To test this, we incubated yeast cells with antimycin A, which inhibits the activity of the ETC at the level of the cytochrome bc_1 (complex III), and analyzed first, the expression of the isoform A. Results showed that *TIF51A* mRNA levels were decreased when ETC activity was compromised (Figure 4.12-A). In line with previous results, the *TIF51A* regulation was lost in a *hap1*Δ strain and treatment with antimycin A resulted in an even higher expression of this eIF5A isoform (Figure 4.12-A). As previously mentioned, external addition of ALA (the second metabolite of the heme biosynthetis pathway) or hemin (a heme derivative) increases heme cellular levels, HAP transcription and *TIF51A* expression. Therefore, we investigated if the negative Hap1-dependent regulation of *TIF51A* under antimycin A treatment could

be reversed by the external addition of ALA and hemin. Figure 4.12-B shows a partial recovery of *TIF51A* expression after the combined treatment of antimycin A with ALA or hemin.

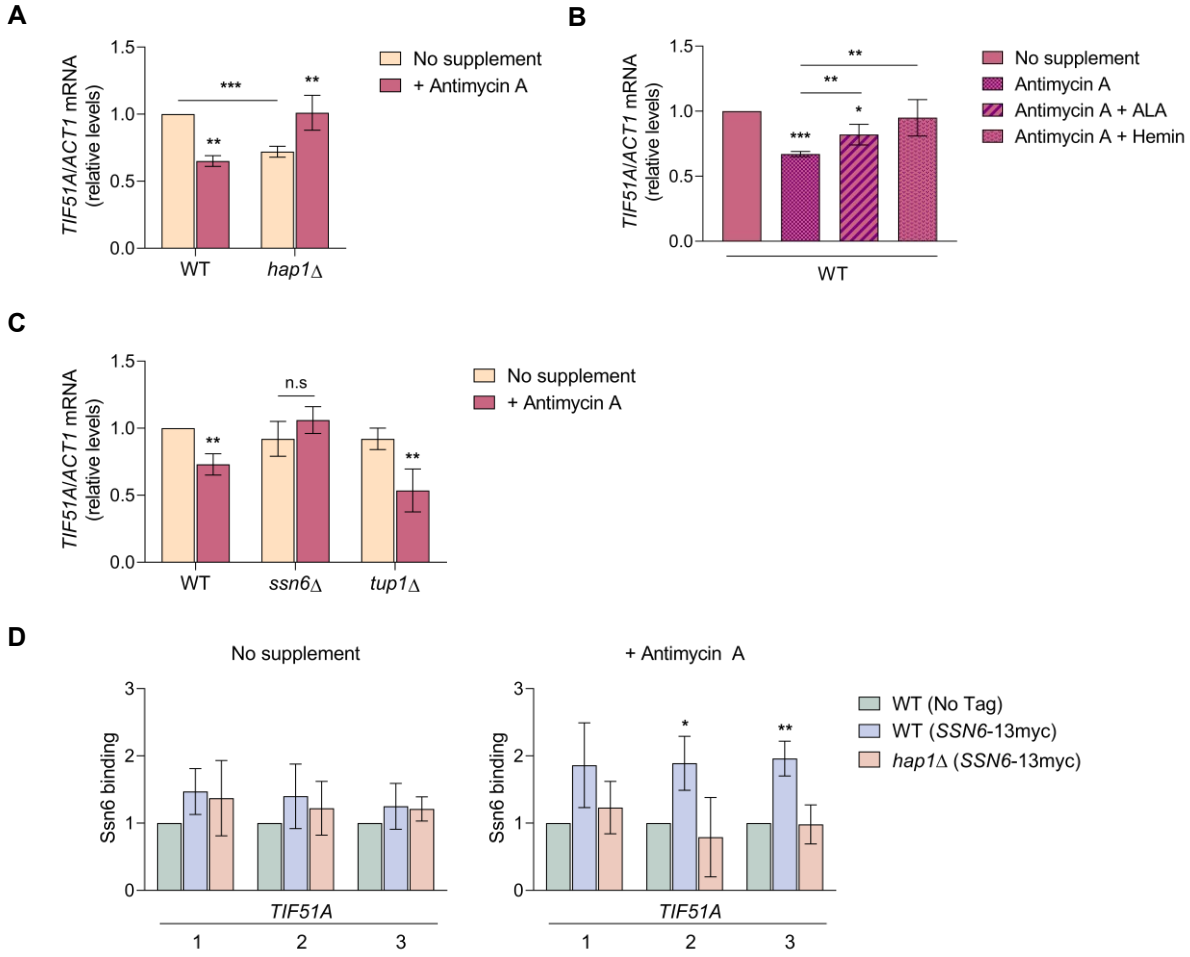

Figure 4.12. Inhibition of mitochondrial respiration down-regulates *TIF51A* expression dependently of Hap1 and Ssn6. (A-C) The wild-type and *hap1*Δ (A), only wild-type (B) and wild-type, *ssn6*Δ and *tup1*Δ (C) strains were grown in SC medium with or without the addition of 10 µg/ml Antimycin A for 6 h. In (B) medium was supplemented with ALA (300 µg/ml) or hemin (25 µg/ml). (A-C) Relative *TIF51A* mRNA levels were determined by RT-qPCR. Results are presented relative to wild-type strain without supplement. (D) ChIP analysis of Ssn6 recruitment in wild-type (No Tag) and Ssn6-13myc wild-type and *hap1*Δ tagged strains grown as in (A). ChIP of Ssn6 was performed using the antibody anti-myc. The ChIP DNA was used to quantify the binding to the three regions of the promoter of *TIF51A* gene by qPCR. The percentage of the signal obtained in each ChIP sample with respect to the signal obtained with the DNA from the corresponding whole cell extract was calculated. (A-D) Data are presented as mean ± SD from a minimum of three independent experiments. Statistical significance was determined using a two-tailed paired Student's t-test relative to corresponding wild-type or non-treated cells. *p<0.05, **p<0.01, ***p<0.001.

Next, we checked whether Tup1 was involved in this *TIF51A* repression, as occurs during iron depletion. However, inhibition of *TIF51A* in a *tup1*Δ strain was similar to that in wild-type. By contrast, lack of the repressor Ssn6 eliminated the antimycin A repression (Figure 4.12-C). These results again suggest the direct regulation of Hap1 over *TIF51A* in response to the mitochondrial respiration status, although in this case Ssn6 and not Tup1 seems to be involved in the repression that occurs with inhibited respiratory activity. Indeed, a low Ssn6-13myc binding signal to the *TIF51A* promoter was observed upon antimycin A treatment (Figure 4.12-D). Altogether, these results are consistent with antimycin A lowering the lowering the ETC and OXPHOS energetic balance and, subsequently, heme metabolism and levels. This causes the conversion of heme-unbound Hap1 into a repressor of *TIF51A*, which can be partially reversed by increasing heme cellular levels through the addition of heme precursors.

Regarding *TIF51B* expression, we found that the levels of *TIF51B* mRNA increased when ETC activity was compromised with antimycin A, although it seemed to be independent on Hap1 (Figure 4.13-A). Similar to the regulation observed with iron, *TUP1* deletion up-regulated *TIF51B* mRNA levels without antimycin A supplementation, which confirms once again the co-repressor function of Tup1 under normal conditions. Besides, the levels further increased with antimycin A supplementation (Figure 4.13-A). No major changes with respect to wild-type results were obtained in a *ssn6*Δ strain, suggesting a non-relevant contribution of this protein to the regulation of *TIF51B* (Figure 4.13-A).

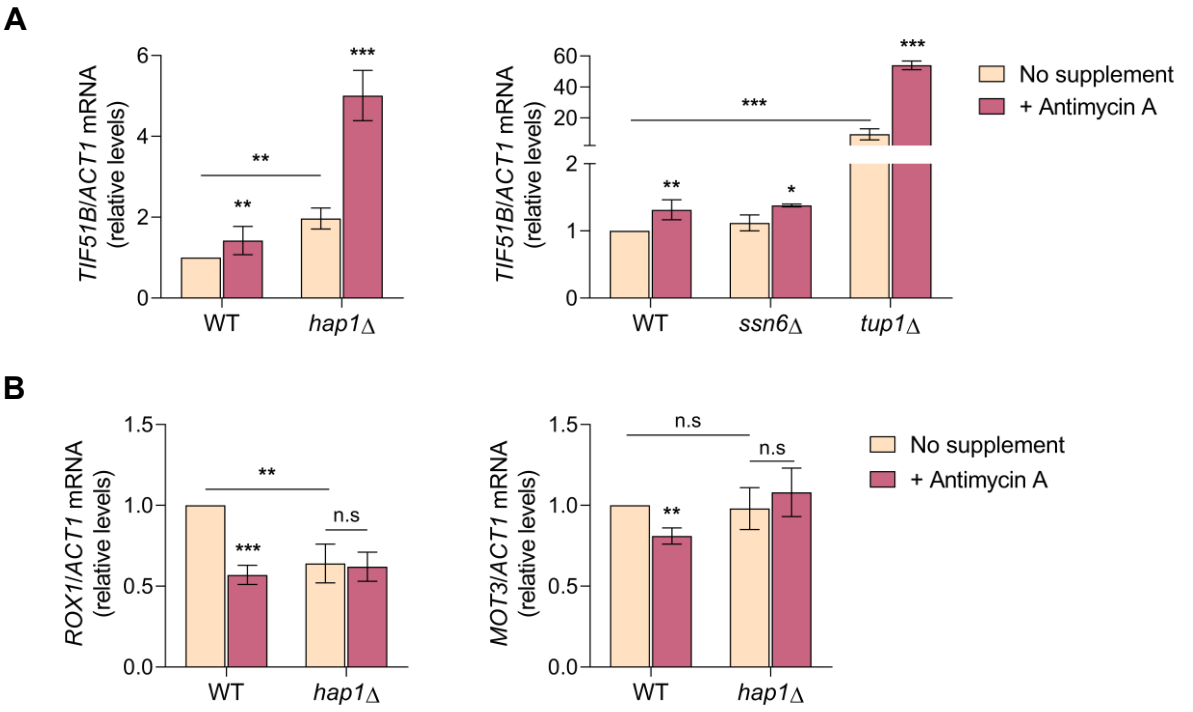

Figure 4.13. Inhibition of mitochondrial respiration up-regulates *TIF51B* expression. (A) The wild-type and *hap1*Δ (left) and wild-type, *ssn6*Δ and *tup1*Δ strains (right) were grown in SC medium with or without the addition of 10 µg/ml Antimycin A for 6 h. Relative *TIF51B* mRNA levels were determined by RT-qPCR. (B) The wild-type and *hap1*Δ were grown as in (A). Relative *ROX1* and *MOT3* mRNA levels were determined by RT-qPCR. (A,B) Data are presented as mean ± SD from a minimum of three independent experiments relative to the wild-type without supplement. Statistical significance was determined using a two-tailed paired Student's t-test relative to corresponding non-treated cells. *p<0.05, **p<0.01, ***p<0.001.

As expected for a respiration-deficient condition, treatment with antimycin A also led to a significant drop in the expression of *ROX1* and *MOT3* (Figure 4.13-B). This result indicates again the shift of Hap1 from an activator to a repressor of these genes as the expression is reversed in a *hap1*Δ mutant. It also supports the repressor function of Hap1 when respiration is deficient and heme levels are compromised. Because Hap1 represses *ROX1* and *MOT3*, the levels of *TIF51B* partly increase on treatment with antimycin A although an independent regulation is taking place too (Figure 4.13-A). As previously seen under iron-deficient conditions, the levels of *TIF51B* were upregulated under normal conditions in the *hap1*Δ and more so in the *tup1*Δ strain. Again, these results are in agreement with the hypothesis of a partial Hap1-dependent repression of *TIF51B* expression under respiration and the existence of an additional activation mechanism, aside from relief from Hap1-Tup1-mediated repression, under non-respiration conditions.

Discussion of Chapter 4

Unicellular and multicellular systems must deal with a continuously changing environment. Thus, adapting and redirecting the cellular metabolism to external circumstances is important. The most known example of metabolic adaptation is the so-called Warburg effect, by which most tumour cells sustain aerobic glycolysis with glucose fermentation into lactate to meet their bioenergetic and anabolic demands (Warburg *et al.*, 1927; Kroemer and Pouyssegur, 2008; Heiden *et al.*, 2009). It has been proposed that all high proliferating cells adapt their metabolism to facilitate the uptake and incorporation of nutrients into the biomass needed to produce a new cell (aerobic glycolysis) over the promotion of high-efficient ATP-synthesis in the quiescent state (mitochondrial OXPHOS). Understanding how cells adapt their metabolism to meet demands is relevant as wrong adaptation can have pathological consequences. In this thesis we propose a mechanism of eIF5A gene expression regulation in response to cellular metabolism.

Here, we have addressed how eIF5A expression is regulated to adapt it to the metabolic requirements. Like other translation factors (Cardenas *et al.*, 1999; Hardwick *et al.*, 1999; Proud, 2002), we have demonstrated a positive regulation by TORC1 signalling activated under abundant nutrient conditions. In this context, eIF5A functions to facilitate the cytoplasmic translation of the genes encoding proteins with specific amino acids (Pelechano and Alepuz, 2017; Schuller *et al.*, 2017), although other molecular functions for eIF5A have been described (Zanelli and Valentini, 2007). Although eIF5A is a highly expressed protein and has been described as one of the 100 most abundant proteins in proliferating cells (Hukelmann *et al.*, 2016), the expression of its most abundant isoform (Tif51A) increases 2- to 4-fold under respiratory conditions. Under continuous low glucose or under respiratory conditions, the Tif51A isoform is up-regulated by Hap1 to promote other functions different to cytoplasmic translation and related to promote mitochondrial function. Thus, Tif51A depletion compromises growth under non-fermentative carbon sources, reduces oxygen consumption and mitochondrial membrane potential (Figures 4.1 and 4.2). Furthermore, our results suggest, contrary to others in yeast and mammals (Puleston *et al.*, 2019; Zhang *et al.*, 2022), that full hypusination would not be necessary to promote respiration. Chapter 5 of this thesis illustrates one of the possible molecular mechanisms for eIF5A control of the mitochondrial function.

The main outcome of this study was the clearly differential regulation of *S. cerevisiae* eIF5A isoforms. A model summarising the results is shown in Figure 4.14. Their opposite regulation by oxygen had been previously documented, with *TIF51A* being repressed and *TIF51B* activated during hypoxia/anaerobiosis, when heme-dependent Hap1 activity controls *TIF51B* repressors Rox1 and Mot3 expression (Zitomer and Lowry, 1992; Zhang and Hach 1999; Kastaniotis *et al.*, 2000; Sertil *et al.*, 2003; Klinkenberg *et al.*, 2005; Hickman and Winston, 2007). Here, we have identified Hap1 as the main factor controlling *TIF51A* expression in response to the mitochondrial functional status through the binding to the putative Hap1-binding sequence (CGGataTAttCGG) at the *TIF51A* promoter. The heme-binding activator protein Hap1, together with the Hap2/3/4/5 complex is responsible for the up-regulation of many mitochondrial biogenesis and respiration genes. The control of the two eIF5A isoforms by Hap1 at the transcriptional level, allows the opposite regulation of the two paralog genes with only one factor, similar to its function as both activator and repressor of ERG genes under oxygen availability/active mitochondria or under hypoxia/inactive mitochondria, respectively (Hickman and

Winston, 2007). Under respiratory conditions, heme-bound Hap1 directly activates *TIF51A* expression while indirectly represses *TIF51B* expression through the activation of the Rox1 and Mot3 repressors. Here, Hap1 binds to the respective and already described consensus sequences at the *ROX1* and *MOT3* promoters and activates transcription, resulting in the Rox1 and Mot3 repressors becoming available for *TIF51B* repression through Tup1 recruitment. Conversely, under respiratory inhibition, heme cellular levels decrease and Hap1 becomes a repressor. Heme-unbound Hap1 directly represses *TIF51A* expression through the recruitment of Ssn6 or Tup1 co-repressors while indirectly activates *TIF51B* expression through the repression of the Rox1 and Mot3 repressors. Here, Hap1 recruits the Tup1 co-repressor to the *ROX1* and *MOT3* promoters, down-regulates their expression, and consequently up-regulates *TIF51B* expression. Additionally, a Hap1-independent up-regulation of *TIF51B* under iron starvation was observed, suggesting the existence of another regulatory mechanism.

Remarkably, the transcription factor Hap1 has been found to work as a mitochondrial sensor for the expression of eIF5A in *S. cerevisiae*. Hap1 contains three different functionality distinct domains: a zinc finger-like DNA-binding domain, an acidic activation domain and a heme regulatory domain. Heme binding increases Hap1 transcriptional activity by controlling the interaction of Hap1 with specific Hsp proteins, which seem to stimulate its repressor activity (Zhang and Hach, 1999; Lan *et al.*, 2004; Hickman and Winston, 2007). However, Hap1 shows no homologs in mammalian cells. Instead, two classes of nuclear transcriptional regulators are involved in mitochondrial biogenesis and respiration in mammals. These comprise DNA-binding transcription factors including NRF-1 and NRF-2 and nuclear coactivators encoded by PGC-1 and related family members (Scarpulla, 2002). The possibility of one of these factors acting together with the eukaryotic conserved repression system Ssn6/Tup1 to mediate a similar regulation of the eIF5A1 and eIF5A2 human isoforms cannot be ruled out and should be the focus of future research activity. Alternatively, hypoxia-inducible factor 1 α (HIF-1α) is considered the master regulator of oxygen homeostasis and controls the metabolic adaptation of mammalian cells to hypoxia. HIF-1α regulates the expression of hundreds of human genes involved in cellular energy metabolism, iron metabolism, vasomotor control and angiogenesis (Semenza, 2007). Interestingly, the promoter region of human *EIF5A2* gene contains two HIF-1α binding sites. Hence, whether the oxygen-regulated HIF-1α transcription factor regulates the expression of *EIF5A2* could be addressed in the future. In turn, eIF5A has also been identified as essential for the expression of HIF-1α (Tariq *et al.*, 2016), suggesting a bidirectional regulation between these two proteins. Although the mechanism underlying this retroactive regulation is yet to be elucidated, eIF5A2 activity could be involved in HIF-1α transcriptional expression under hypoxia as it binds to the *HIF-1α* promoter in cancer cells (Li *et al.*, 2014). Therefore, the up-regulation of the second eIF5A isoform observed in the cancer context (Ning *et al.*, 2020) could be: on one hand, induced by HIF-1α activity and on the other hand, meant to activate HIF-1α and control the expression of many genes involved in the survival to hypoxic environments as that of the tumour microenvironment, thus promoting the adaptation towards a fermentative metabolism.

This thesis describes the molecular mechanism oppositely regulating the expression of the two yeast eIF5A-encoding genes, but also indicates the cell's need to increase the levels of the respiratory eIF5A isoform, Tif51A, while decreasing the fermentative eIF5A isoform, Tif51B, in response to cellular mitochondrial activity requirements. However, we were not able to completely elucidate whether the increase in Tif51A and decrease in Tif51B is the cause or consequence of higher mitochondrial activity. The mitochondrial monitoring mechanism connected to eIF5A regulation makes it tempting to speculate

that the differential expression of the two eIF5A isoforms promotes, in each case, differential metabolic outcomes with the respiratory isoform Tif51A promoting respiration and the fermentative isoform Tif51B promoting aerobic glycolysis. Up to date, there has been no evidence to support this in *S. cerevisiae*, although it has been described that the human isoform eIF5A2 promotes aerobic glycolysis in human hepatocellular carcinoma (Cao *et al.*, 2017), which is precisely the metabolic reprogramming occurring in most cancer cells (San-Millán and Brooks, 2017). The difference in the amino acid sequences between Tif51A and Tif51B proteins (15 nonidentical and 7 nonsimilar amino acids) probably gives rise to partially different cellular functions still unknown.

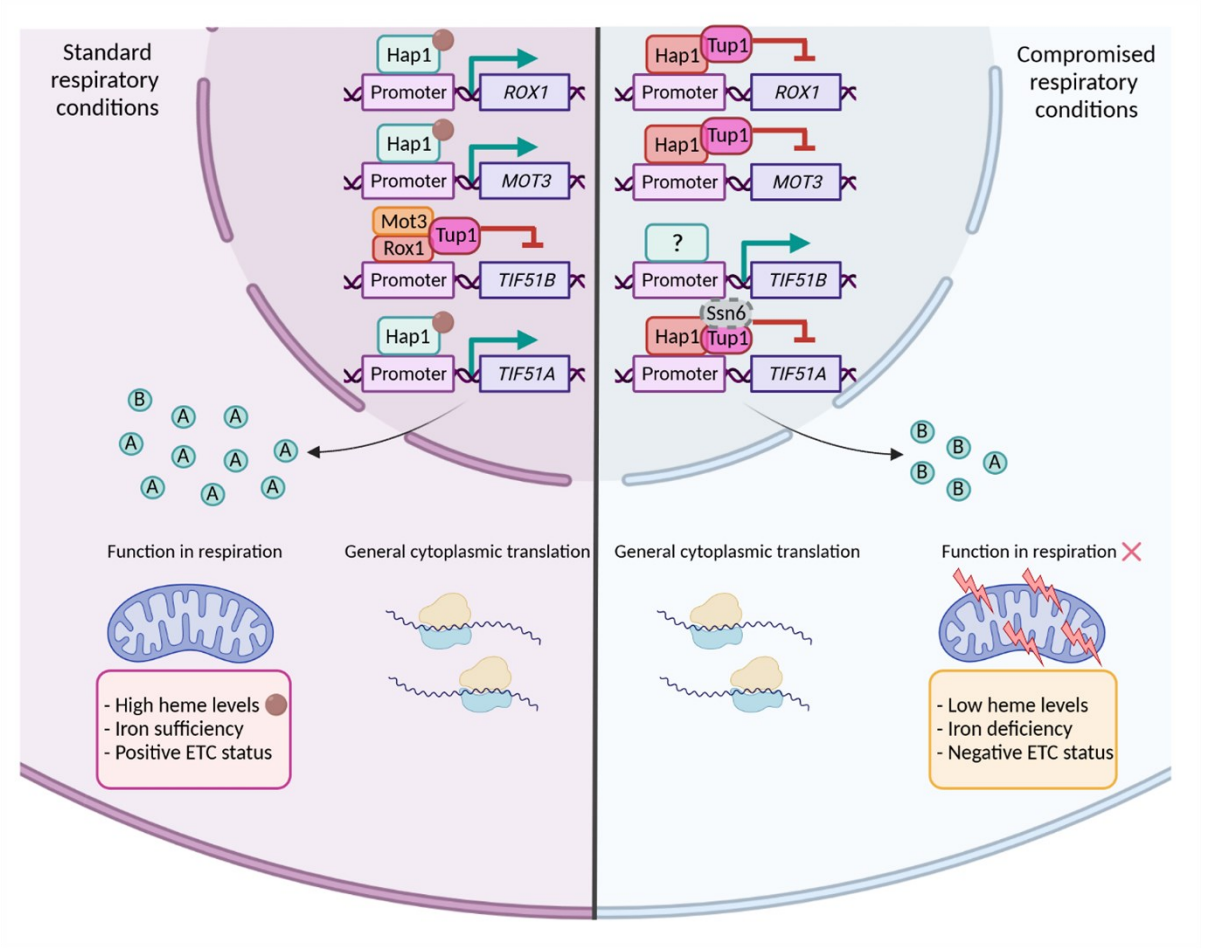

Figure 4.14. Model of the gene expression regulation of the two eIF5A isoforms in response to mitochondrial functional status. Under standard respiratory conditions, *TIF51A* expression is increased *via* regulation by Hap1, which binds directly to the consensus sequence contained in the *TIF51A* promoter. In tandem, Hap1 activates the expression of *ROX1* and *MOT3*, which repress *TIF51B* expression through Tup1 recruitment. Hap1 is active owing to the presence of high heme levels. eIF5A expression facilitates both cytoplasmic translation and supports respiratory metabolism. Under compromised respiratory conditions, Hap1 becomes a repressor as heme levels go down and *TIF51A* expression is down-regulated through the recruitment of Tup1 or Ssn6 by Hap1, while *TIF51B* expression is increased due to a down-regulation of *ROX1* and *MOT3 via* Hap1. The down-regulation of the eIF5A respiratory isoform Tif51A triggers the weak mitochondrial function.

Chapter 5

eIF5A controls mitochondrial protein import and synthesis

Chapter 5. eIF5A controls mitochondrial protein import and synthesis.

Chapter 5, in full, is currently being prepared for manuscript submission under the title: "eIF5A controls mitochondrial protein import and synthesis". The authors are Marina Barba-Aliaga, Cynthia Rong, Vanessa Bernal, Brian Zid[#] and Paula Alepuz[#].

[#]Corresponding author.

Detailed author contributions: Marina Barba-Aliaga contributed to the great majority of experimental development, experimental design, data analysis and manuscript writing. The whole experimental data shown in this dissertation was carried out by Marina Barba-Aliaga. Cynthia Rong contributed to part of experimental development. Vanessa Bernal performed the proteomic experiment and data analysis which are found only in the manuscript. Brian Zid and Paula Alepuz supervised the work and the manuscript conceptualization and writing.

The tight gene expression regulation of the two eIF5A isoforms (described in Chapter 4) in response to the cellular metabolic status highlights the essential role of eIF5A (Tif51A isoform) in the mitochondrial function. Mitochondria are complex organelles with endosymbiotic origin which play central functions in eukaryotic cellular homeostasis as they are the main energy producers, but also participate in other functions such as lipid metabolism, inflammation, apoptosis, or Ca^{+2} homeostasis. Besides, mitochondrial dysregulation is a pivotal hallmark of ageing-related disorders. eIF5A deficiency negatively affects the mitochondrial activity as the oxygen consumption rate decreases but also the expression of many proteins involved in the tricarboxylic acid (TCA) cycle and the electron transport chain (ETC) is reduced (Puleston *et al.*, 2019; Zhang *et al.*, 2022). In this line, our proteomic analysis (data not shown here but detailed in the manuscript mentioned above) reveals mitochondria as one of the functional categories most strongly affected under eIF5A deficiency and proteins from TCA, ETC, mitochondrial transport systems and ATP synthase subunits are found significantly reduced. Since not all downregulated proteins contain the well-characterized eIF5A-dependent motifs, other mechanisms have been suggested to link eIF5A to mitochondrial function. In this line, a mechanism in which hypusinated eIF5A is required for the translation of the N-terminal regions of some mitochondrial proteins, in a proline-independent manner, has been proposed (Zhang *et al.*, 2022). eIF5A was reported to promote the proper positioning of amino acids forcing a favourable interaction with the peptide exit tunnel to stimulate translation. In this Chapter, we describe a novel molecular mechanism by which eIF5A is essential for the mitochondrial activity. This mechanism relies on the eIF5A-dependent translation of Tim50, the receptor of the mitochondrial inner membrane translocase complex TIM23.

5.1 eIF5A is necessary for the translation of *TIM50* mRNA encoding the mitochondrial inner membrane receptor of the TIM23 complex

Tim50 is an essential protein conserved among fungi, plants and humans. Tim50 is the receptor component of the mitochondrial inner membrane translocase complex TIM23 and recognizes the N-terminal MTS-containing proteins after emerging from the TOM complex (see Mokranjac *et al.*, 2009; Chaudhuri *et al.*, 2021 and section 1.4.2 of Chapter 1). We were interested in its potential role as an eIF5A target as it contains polyPro stretches in its amino acid sequence. Thus, Tim50 sequence shows a region in the first half of the protein containing 14 prolines and 7 of them are consecutive (Figure 5.1-A left).

To test whether the *TIM50* mRNA sequence shows eIF5A-dependency for its translation, we used a reporter construct integrated in the *URA3* locus, consisting of a *tetO7* inducible promoter and a nanoluciferase (nLuc) reporter ORF for measuring protein synthesis. We fused three different versions of the Tim50 DNA sequence to the nLuc reporter: the first one expressing the wild-type *TIM50* sequence, the second one expressing *TIM50* with a deletion of the 7 consecutive prolines (Tim50Δ7Pro) and the third one expressing *TIM50* without the region containing the 14 prolines (Tim50Δ14Pro, deletion from 137 aa to 254 aa) (Figure 5.1-A right). After inducing expression, we analyzed the protein synthesis by incubating for 1 h in tetracycline-supplemented media in wild-type yeast cells and eIF5A temperature-sensitive mutant cells (*tif51A-1*), carrying a single point mutation (Pro83 to Ser) (Li *et al.*, 2011). After analysing the protein synthesis along time, it was observed that the *tif51A-1* mutant showed a 3-fold reduction in the synthesis of Tim50 at restrictive temperature compared to the wild-type strain, suggesting Tim50 as an eIF5A target for translation elongation (Figure 5.1-B). To test whether the decrease in protein synthesis is due to the presence of a high number of prolines in Tim50 sequence, we analyzed the other two Tim50 versions containing deletions of 7 and 14 prolines respectively. Results indicated that after removing the proline-rich region of Tim50, protein synthesis is rescued in the *tif51A-1* mutant at 37°C and reaches similar protein levels to the wild-type strain (Figures 5.1-C,D). Considering that final protein abundance is determined by both mRNA levels and translation, we confirmed that the lower protein levels were not attributed to *TIM50* transcription, as the mRNA levels were not reduced in the *tif51A-1* mutant at permissive nor restrictive temperatures (Figure 5.1-E).

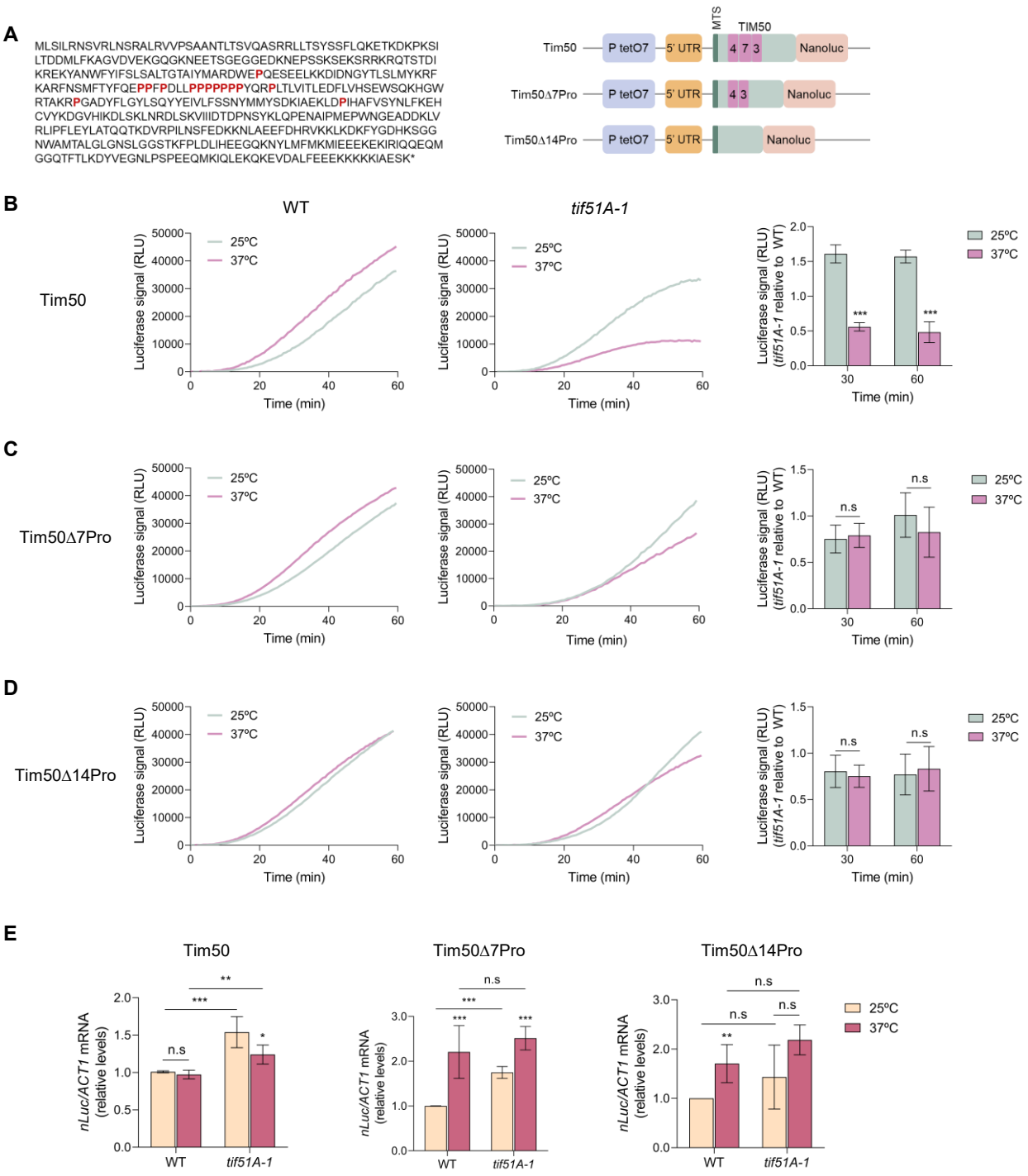

Figure 5.1. Tim50 translation depends on eIF5A due to its proline-rich sequence. (A) Scheme showing Tim50 protein sequence and nanoluciferase reporter constructs used in this study. (B-E) Wild-type strain (left) and *tif51A-1* (middle) expressing the wild-type Tim50 (B), Tim50Δ7Pro (C) or Tim50Δ14Pro (D) were cultured in YPD until early exponential phase and then transferred to 25ºC or 37ºC for 4 h. After addition of doxycycline to induce luciferase expression, the luminescence levels generated by the nanoluciferase after the addition of the furimazine substrate were measured along time. (B-D) A representative experiment is shown. Quantification of the Tim50 protein levels is shown in the right. (E) nLuc mRNA relative levels were determined by RT-qPCR and expressed relative to wild-type cells at 25ºC. (B-E) Results are presented as mean ± SD from at least three independent experiments. The statistical significance was measured by using a two-tailed paired Student t-test relative to 25ºC. *p < 0.05, **p < 0.01, ***p < 0.001. n.s indicates no significant differences.

These inducible reporter assays enabled us to calculate the time needed for translation elongation through the region upstream of the nLuc reporter gene (Masser *et al.*, 2016). By using the Schleif plotting technique (Schleif *et al.*, 1973; Zhu *et al.*, 2016), we compared the amount of time needed to detect luciferase signal from a reporter only expressing nLuc and the other three reporters and then, we obtained the time required for ribosomes to translate each of the three Tim50 versions. We found that the time required for translating a wild-type *TIM50* mRNA was significantly increased in the *tif51A-1* mutant at restrictive temperature (Figure 5.2-A). If a cell needs approximately 2 minutes to generate one full Tim50 polypeptide, upon eIF5A depletion, the ribosomes need almost 4 minutes to achieve the complete translation of this mRNA. However, the synthesis time required for translating *TIM50Δ7Pro* and *TIM50Δ14Pro* mRNAs were almost identical to those in the corresponding wild-type strain (Figure 5.2-A).

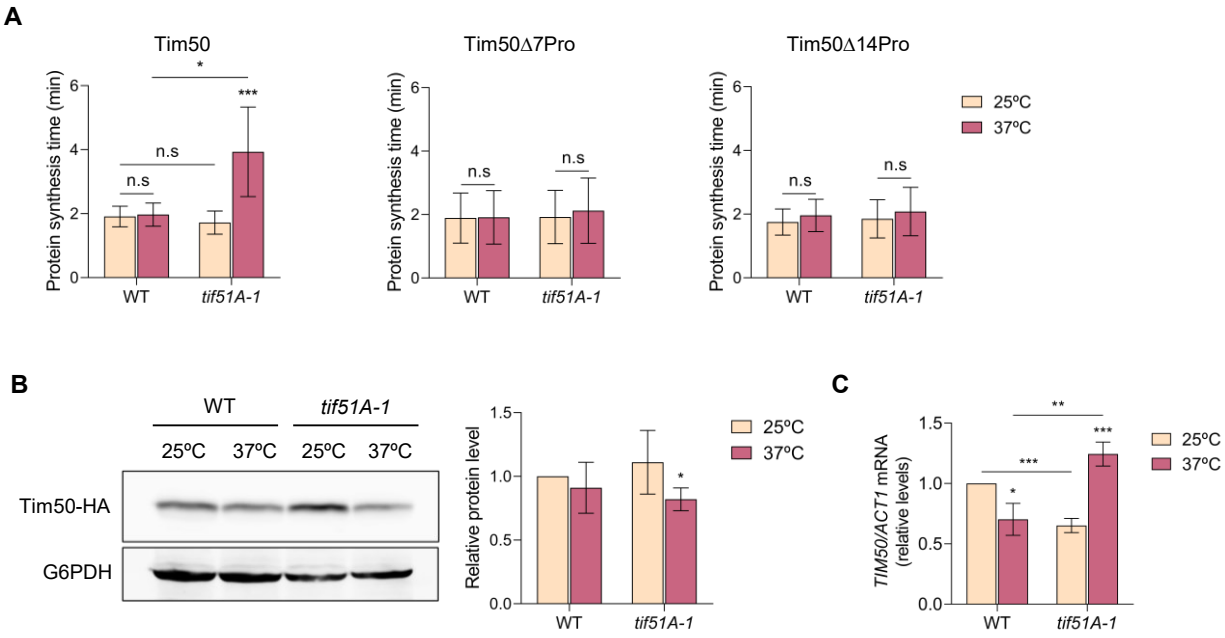

Figure 5.2. Lack of eIF5A extends the time required for the translation of Tim50 proline-rich sequence. (A) Full protein synthesis time was calculated for wild-type strain and *tif51A-1* expressing the wild-type Tim50 (left), Tim50Δ7Pro (middle) or Tim50Δ14Pro (right). (B,C) Wild-type strain and *tif51A-1* expressing Tim50-HA were cultured in SGal medium at 25ºC until reaching post-diauxic phase and transferred to 25ºC or 37ºC for 4 h. (B) Tim50 protein levels were determined by western blotting (left) and quantified (right). G6PDH levels were used as loading control. A representative image is shown. (C) *TIM50* mRNA relative levels were determined by RT-qPCR. (A-C) Results are presented as mean ± SD from at least three independent experiments. The statistical significance was measured by Student t-test relative to 25ºC. *p < 0.05, **p < 0.01, ***p < 0.001. n.s indicates no significant differences.

Besides using an artificially designed reporter construct, we also analyzed the protein levels of endogenous Tim50 protein. To do this we fused Tim50 ORF to 3-HA in its C-terminus and analyzed its protein levels by western blotting. We found a slight but significant decrease of Tim50 protein levels in the *tif51A-1* mutant cells at restrictive temperature (Figure 5.2-B) with no decrease in mRNA levels (Figure 5.2-C). As expected, differences were not as pronounced as in the nLuc reporter assays, where

de novo protein synthesis is measured. Here, the Tim50 protein produced before eIF5A was depleted is still present as the Tim50 protein half-life is approximately 9.6 h (Christiano *et al.*, 2014), which makes it difficult to measure large differences regarding newly protein produced.

Together, these results indicated that Tim50 downregulation in the *tif51A-1* mutant was due to a decrease in translation because ribosomes slow down or stall along the proline-rich region of its sequence. Thus, these data strongly suggest that *TIM50* mRNA translation is directly dependent on eIF5A.

5.2 Tim50 and Tim50-dependent mitoproteins aggregate outside the mitochondria in the absence of eIF5A

As previously mentioned, Tim50 is needed for the entry of many different mitoproteins to the mitochondrial inner membrane (MIM) or to the mitochondrial matrix (MM). We wondered if Tim50 translation downregulation upon eIF5A depletion could affect protein localization of mitoproteins requiring Tim50 for their MTSs recognition. First, we fused Tim50 ORF to the green fluorescent protein (GFP) and analyzed its cellular localization by using fluorescence microscopy, since Tim50 is also a TIM23/Tim50-import target. We carried out the experiments at post-diauxic growth phase using a galactose-based media, in which cells mainly perform respiration (Fendt and Sauer, 2010) and the expression of eIF5A is induced by the transcription factor Hap1 (see Chapter 4 for details). We also used a construct expressing the ATPase subunit Su9 fused to mCherry as a fluorescence marker to detect the cellular mitochondrial network. We observed that Tim50 perfectly localizes in the mitochondria in the wild-type strain at both temperatures. However, we found the presence of Tim50 foci which do not co-localize to the mitochondria in the *tif51A-1* mutant at restrictive but not at permissive temperature (Figure 5.3-A left). The number of cells containing more than one of these Tim50 aggregates was found to be significantly increased in the *tif51A-1* mutant compared to the wild-type strain (Figure 5.3-A right). Second, we fused Tom70 ORF to GFP and analyzed its cellular localization. Tom70 is part of the TOM complex, placed in the mitochondrial outer membrane (MOM) and shows no TIM23 complex dependency for its entrance to mitochondria. We did not find any difference for Tom70 protein localization between the wild-type and the *tif51A-1* mutant (Figure 5.3-B). Third, we decided to study different TIM23 complex substrates destined for different final locations within mitochondria (Filipuzzi *et al.*, 2017). Cytochrome c isoform 1 (Cyc1) is involved in the transfer of electrons during cellular respiration, targets the intermembrane space (IMS) and does not present any of the known eIF5A-dependent motifs in its sequence. Yta12 is an m-AAA protease component required for the degradation of misfolded or unassembled proteins. Yta12 targets the MIM and contains nine consecutive prolines in its sequence, so it could be considered as a potential eIF5A target for its translation. Ilv2 is an acetolactate synthase involved in the synthesis of isoleucine and valine. Ilv2 targets the MM and shows a few eIF5A-dependent motifs in its sequence, none of them containing consecutive prolines. We fused these three protein ORFs to GFP and analyzed their cellular location. Figures 5.3-C-E show that at restrictive temperature Cyc1, Yta12 and Ilv2 are localized in the mitochondria in the wild-type strain but, in the *tif51A-1* mutant they also form aggregates, which do not co-localize to the mitochondria. Although Ilv2 has been described to accumulate as one big aggregate in the nucleus upon protein import failure (Shakya *et al.*, 2021), we found that in the absence of eIF5A, this protein accumulates in multiple and distributed foci, similarly to the misslocalized aggregates of Tim50, Cyc1 and Yta12. To remark

that, although Su9 has been described as a TIM23 substrate (Filipuzzi *et al.*, 2017) and targets the MIM, we found this protein unaffected in the absence of eIF5A as its fluorescent signal shows a continuous pattern as expected for the mitochondrial network.

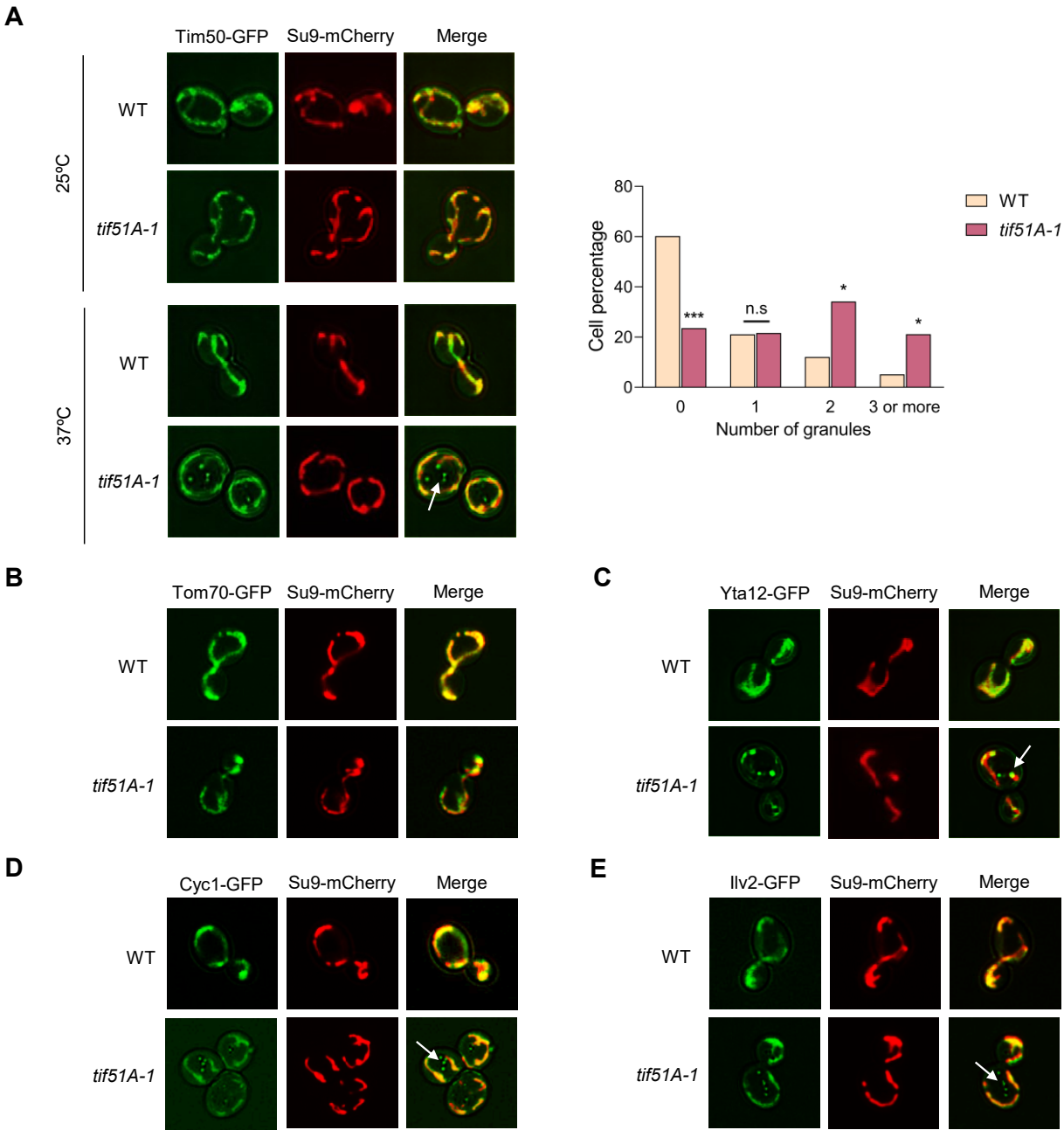

Figure 5.3. eIF5A deficiency generates protein aggregates of Tim50 and other Tim50-dependent mitoproteins. (A) Wild-type strain and *tif51A-1* expressing Tim50-GFP and Su9-mCherry were cultured in SGal medium at 25ºC until reaching post-diauxic phase, transferred to 25ºC or 37ºC for 4 h and then subjected to fluorescence microscopy. Quantification of cells presenting 0, 1, 2, 3 or more Tim50 aggregates at 37ºC from at least 150 cells from three independent experiments is shown (right). The statistical significance was measured by using a two-tailed paired Student t-test with respect to wild-type strain. *p < 0.05, ***p < 0.001. n.s indicates no significant differences. (B-E) Wild-type strain and *tif51A-1* expressing Tom70-GFP (B), Yta12-GFP (C), Cyc1-GFP (D) or Ilv2-GFP (E) were cultured as in (A). (A-E) A representative image is shown.

These results suggest that translation downregulation of Tim50 upon eIF5A depletion triggers a failure in the TIM23 complex and thus, reduces the translocation and import of proteins to the mitochondria. These non-imported proteins seem to form aggregates outside the mitochondria. The results also highlight differences between mitoproteins regarding their Tim50-dependency for import and localization. It is highly likely that mitoproteins localizing in the outer membrane, such as Tom70, are less sensitive to TIM23 complex activity than mitoproteins targeting the IMS (Cyc1), MIM (Yta12) and MM (Ilv2).

Because failure of protein import upon eIF5A depletion seems to be the cause for the appearance of mitoprotein aggregates outside the mitochondria, we tried to reproduce this effect using the oxidative phosphorylation uncoupler carbonyl cyanide m-chlorophenylhydrazone (CCCP) to dissipate the membrane potential. Together with ATP hydrolysis, the membrane potential is the driving force for the translocation of proteins through the TIM23 complex. Therefore, CCCP treatment prevents mitochondrial protein import (Wrobel *et al.*, 2015; Schäfer *et al.*, 2022). We used different doses of CCCP and studied the effect on localization of Tom70, Cyc1 and Tim50 proteins fused to GFP. We found that low CCCP doses (1 µM) were able to reproduce the phenotype observed in the *tif51A-1* mutant as Cyc1 and Tim50 formed aggregates while Tom70 was unaffected (Figure 5.4). Interestingly, we found that Su9 protein was also affected and formed isolated foci, suggesting that under this treatment the activity of the TIM23 complex is more broadly affected and more proteins show reduced import. On the other hand, high CCCP doses (10 µM) disrupted and collapsed the mitochondrial network morphology creating a general effect by which all the tested proteins showed dispersed fluorescence (Figure 5.4).

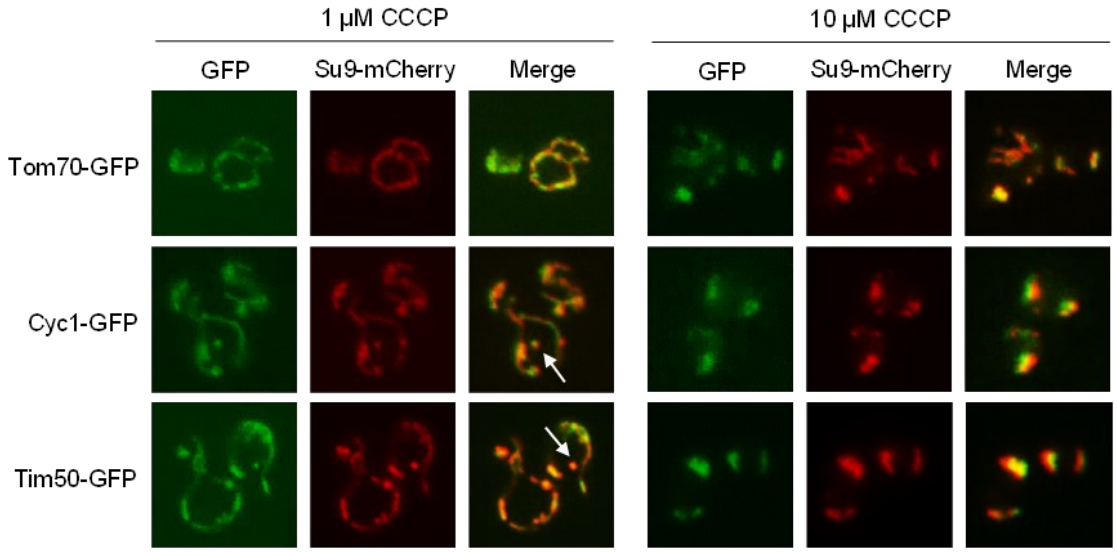

Figure 5.4. Membrane potential uncoupling upon low CCCP doses leads to protein aggregates of Tim50 and other Tim50-dependent mitoproteins. Wild-type strain expressing Tom70-GFP (up), Cyc1-GFP (medium) or Tim50-GFP (down) was cultured in SGal medium until reaching post-diauxic phase at 30ºC, treated with 1 µM or 10 µM CCCP for 2 h and subjected to fluorescence microscopy. A representative image is shown from three independent experiments.

5.3 Cytosolic aggregates of Tim50 and Tim50-dependent mitoproteins formed upon eIF5A depletion co-localize with Hsp104

Next, we asked about the intracellular localization and composition of these eIF5A-dependent mitoprotein foci. There have been described different cellular destinations for mitoproteins aggregates including the cytosol and nucleus (Shakya *et al.*, 2021). DAPI staining of the cells indicated that Tim50 and Cyc1 aggregates were not co-localizing in the nucleus and thus, seemed to be part of the cytosol (Figures 5.5-A,B).

We then asked if chaperones such as Hsp42 or Hsp104 could be controlling the accumulation of non-imported mitochondrial precursors in granules. The small heat shock protein Hsp42 and the disaggregase Hsp104 belong to the cytosolic chaperone system. While Hsp42 helps in the formation of aggregates in the cytosol, Hsp104 helps in aggregation but also binds to aggregated or misfolded proteins in the cytosol and disentangle them in an ATP-dependent manner (Sanchez and Lindquist, 1990; Gates *et al.,* 2017; Hill *et al.*, 2017). We fused Hsp42 and Hsp104 ORFs to RFP in strains already expressing Tim50-GFP and analyzed its cellular localization (Figures 5.5-C-E). We found that only 20% of the Tim50 aggregates did co-localize with Hsp42 (Figures 5.5-C,D) while almost 75% of them colocalized with Hsp104 (Figures 5.5-D,E). Additionally, Cyc1 aggregates also showed a high percentage of co-localization with Hsp104 (Figures 5.5-F,G), pointing out that Hsp104 works as the main disaggregase of the non-imported cytosolic mitoproteins found in the *tif51A-1* mutant. Besides, the mRNA levels of Hsp104 were considerably upregulated in the *tif51A-1* mutant at restrictive temperature compared to the wild-type strain (Figure 5.5-H), pointing out the exposure of the mutant cells to stress by increased protein aggregation and, consequently, the overloaded chaperone capacity (Hill *et al.*, 2017). Interestingly, the *tif51A-1* mutant displayed a significant increased mean diameter of Hsp104-bound foci at restrictive temperature compared to the wild-type strain (Figure 5.5-I), although the number of aggregates per cell did not increase (1 on average). Probably, the higher increase in size of Hsp104-bound aggregates under eIF5A deficiency is, at least in part, due to the accumulation of several Tim50-dependent mitoproteins (Cyc1, Yta12, Ilv2…) within these structures.

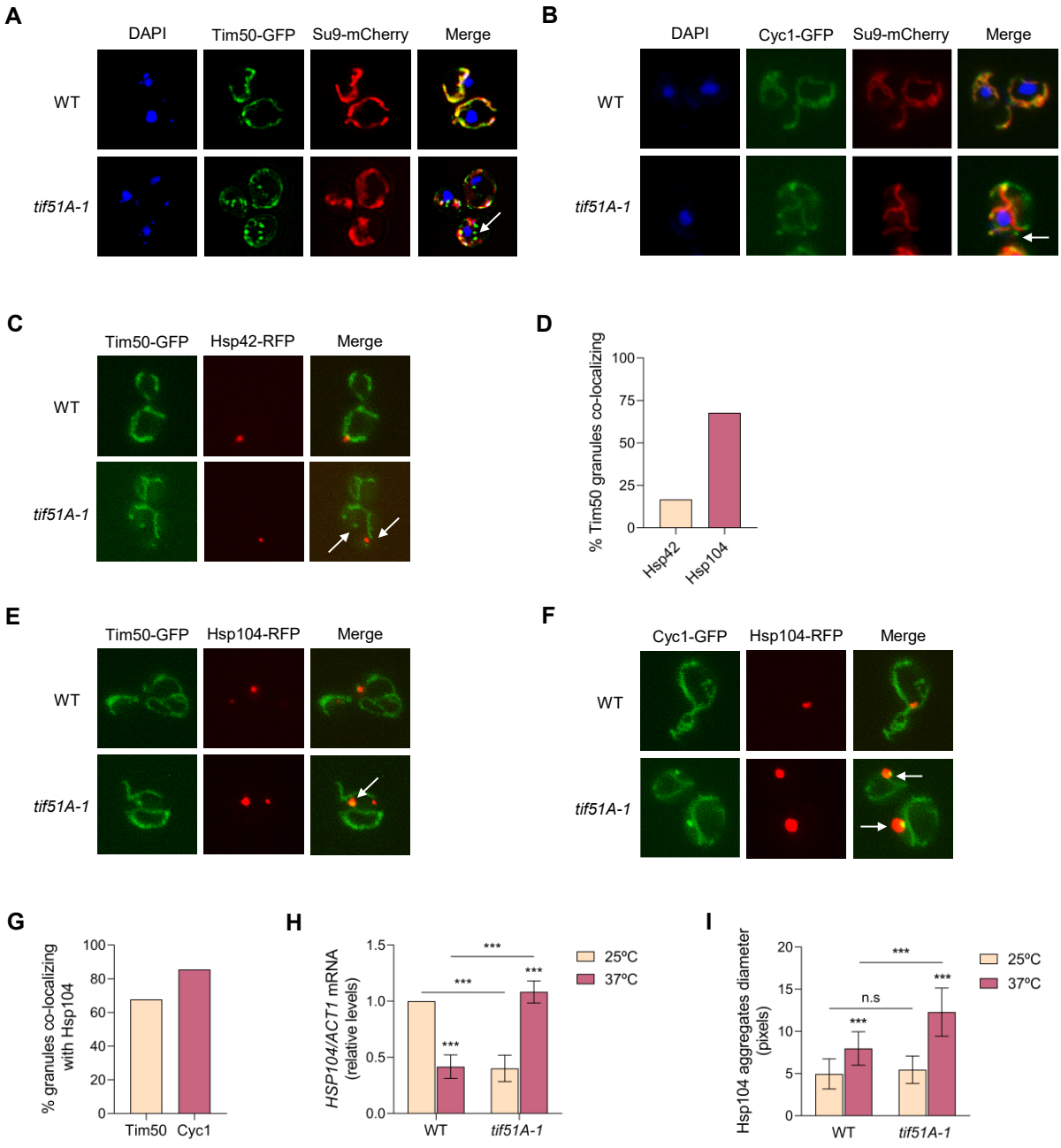

Figure 5.5. Tim50 and other Tim50-dependent mitoproteins aggregate in the cytosol with Hsp104. (A,B) Wild-type strain and *tif51A-1* expressing Tim50-GFP (A) or Cyc1-GFP (B) and Su9-mCherry were cultured in SGal medium until reaching post-diauxic phase at 25ºC, transferred to 37ºC for 4 h and then subjected to fluorescence microscopy. Cells were incubated for 30 mins with DAPI prior microscopy to stain the nuclei. (C) Wild-type strain and *tif51A-1* expressing Tim50-GFP and Hsp42-RFP were cultured as in (A). (D) Quantification of Tim50 aggregates co-localizing with Hsp42 and Hsp104 from at least 150 cells from three independent experiments. (E,F) Wild-type strain and *tif51A-1* expressing Tim50-GFP (E) or Cyc1-GFP (F) and Hsp104-RFP were cultured as in (A). (A-C,E,F) A representative image is shown. (D) Quantification of Tim50 and Cyc1 aggregates co-localizing with Hsp104 as in (D). (H) Analysis of *HSP104* mRNA relative levels by RT-qPCR at the indicated temperatures relative to wild-type cells at 25ºC. (I) Quantification of Hsp104 aggregates diameter in wild-type strain and *tif51A-1* at the indicated temperatures from (E) and (F) as in (C). (H,I) Results are presented as mean ± SD from three independent experiments. The statistical significance was measured by using a two-tailed paired Student t-test relative to 25ºC. ***p < 0.001. n.s indicates no significant differences.

In conclusion, the results showed that blocking Tim50-dependent mitoproteins translocation into the mitochondria by eIF5A depletion yields mitoprotein accumulation in specific deposits in the cytosol. These deposits are sequestered by the chaperone-mediated quality control system, mainly by Hsp104, which seems to be a mechanism used by the cells to survive the proteotoxic stress arising from the accumulation of non-imported precursor proteins.

5.4 eIF5A depletion generates mitochondrial stress

When the translocation and import of mitoproteins is affected, cells can initiate different responses to cope with the stress generated by the mitochondrial defects in order to maintain cellular homeostasis (see review Song *et al.*, 2021 and section 1.4.3 of Chapter 1). Several responses have been described over the last years including the termed mPOS (mitochondrial precursor over-accumulation stress) (Wang and Chen, 2015), mitoCPR (mitochondrial compromised protein import response) (Weidberg and Amon, 2018), UPRam (unfolded protein response activated by mistargeting of proteins) (Wrobel *et al.,* 2015) and mitoTAD (mitochondrial protein translocation-associated degradation) (Mårtensson *et al.,* 2019). We found, that among all the different stress response pathways previously mentioned, the mitoCPR was significantly induced (Figures 5.6-A,B). This response relies on the Pdr3-mediated transcriptional activation of different genes related to the multidrug resistance (MDR) response, lipid metabolism and transport. The Pdr3-induced expression of Cis1, among others, recruits the AAA-protease Msp1 to the TOM translocase to mediate the removal of accumulated mitoproteins upon import failure (Weidberg and Amon, 2018). Analyzes of the mRNA expression showed significant up-regulation of *PDR3* and the Pdr3-responsive genes *GRE2, PDR1, PDR5, PDR15* and *CIS1* in the *tif51A-1* mutant at restrictive temperature, being *CIS1* and *PDR5* the most induced ones (Figure 5.6-B).

Similar mRNA induction of the mitoCPR genes was found in a wild-type strain treated with low doses of the uncoupler CCCP as well as in a Tim23 auxin-degron strain (treated with auxin for 6 h) (Figures 5.6-C,D). In both cases, as well as under eIF5A deficiency, *CIS1* and *PDR5* were the most strongly and significantly induced genes. Altogether, these results point towards a compromised import of Tim50-dependent mitoproteins upon eIF5A depletion which triggers an import surveillance mechanism mediated by Pdr3 to cope with the accumulation of precursor proteins outside the mitochondria.

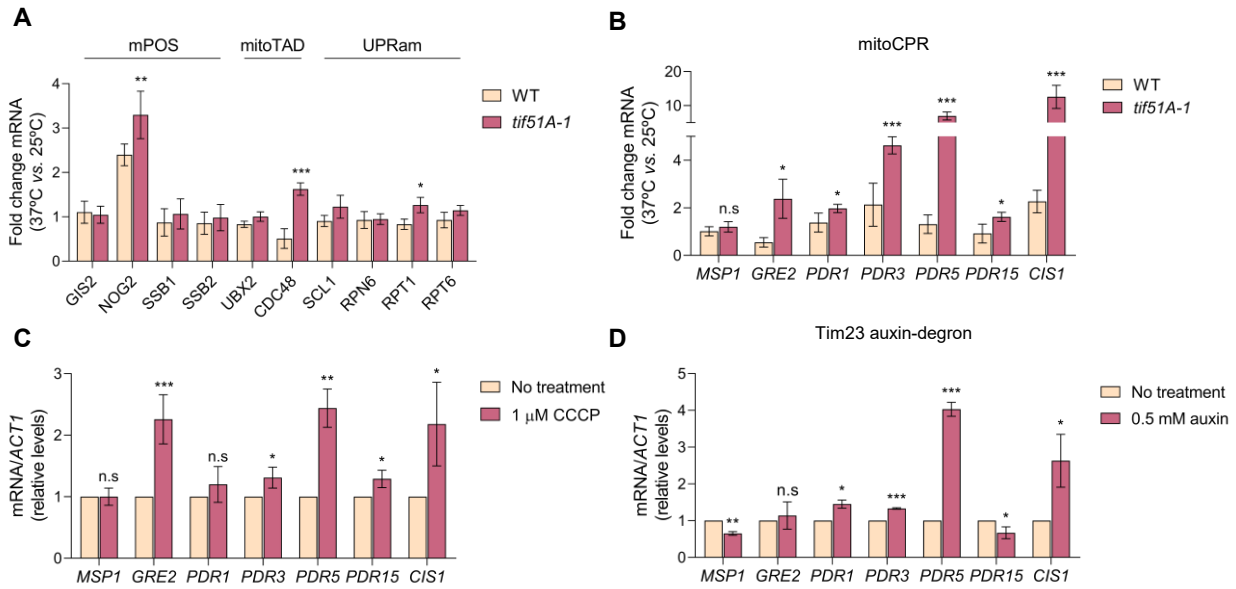

Figure 5.6. Mitochondrial import failure by eIF5A or Tim23 depletion and membrane potential uncoupling induces mitoCPR stress. (A-B) Wild-type strain and *tif51A-1* were cultured in SGal medium at 25ºC until reaching post-diauxic phase, transferred to 25ºC or 37ºC for 4 h. Fold change mRNA relative levels from specific genes were determined by RT-qPCR. (C) Wild-type strain was cultured in SGal at 30ºC until reaching post-diauxic phase and treated with 1 μM CCCP for 2 h. mRNA relative levels from mitoCPR genes were determined by RT-qPCR. (D) Tim23 auxin-degron strain was cultured as in (B) and treated with 0.5 mM auxin for 6 h. mRNA relative levels from mitoCPR genes were determined by RT-qPCR. (A-D) Results are presented as mean ± SD from three independent experiments. The statistical significance was measured by using a two-tailed paired Student t-test relative to wild-type or untreated cells. *p < 0.05, **p < 0.01, ***p < 0.001. n.s indicates no significant differences.

PDR5, the second most strongly induced mitoCPR gene in the *tif51A-1* mutant, encodes an evolutionary conserved ATP-binding cassette (ABC) membrane transporter involved in the MDR. When induced by Pdr3, Pdr5 is observed in the plasma membrane, where it mediates the efflux of xenobiotics, as well as in the vacuole, where it is degraded (Sarkadi *et al.*, 2006). We fused Pdr5 ORF to GFP and analyzed its cellular localization by fluorescence microscopy. We found that the levels of Pdr5 were almost non-detectable in the wild-type strain at both temperatures as well as in the *tif51A-1* strain at permissive temperature. However, at restrictive temperature, Pdr5 protein levels were significantly induced in the *tif51A-1* strain and could be observed at their expected cellular locations (Figures 5.7-A,B). Then, we added Nile Red, a Pdr5 specific substrate which stains lipid granules, to the cell cultures. We observed red fluorescent signal inside the cells in all the conditions tested except for the *tif51A-1* mutant at restrictive temperature, indicating that high Pdr5 pumping activity excludes the Nile Red from these cells (Figures 5.7-C,D). Altogether, these results demonstrate that the compromised mitochondrial import, caused by a reduction in Tim50 protein levels upon eIF5A depletion, induces the Pdr3-mediated mitoCPR response. This response is activated as a mechanism to reduce the driven toxicity from accumulated mitoprotein precursors to restore cellular homeostasis.

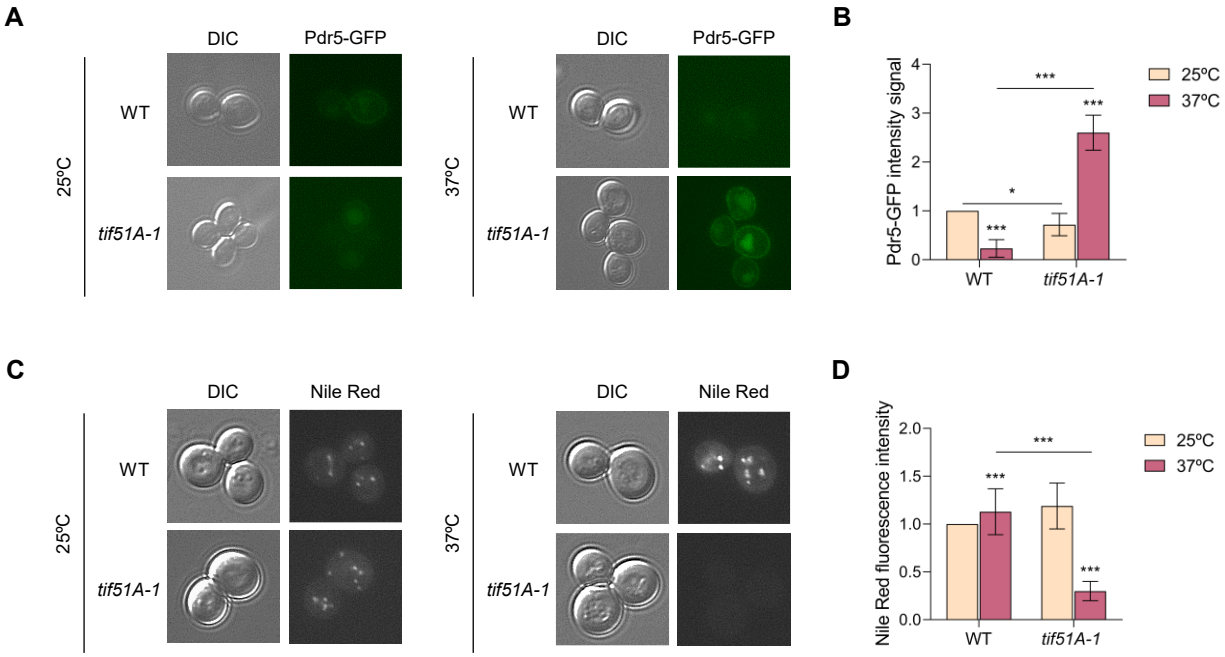

Figure 5.7. eIF5A deficiency induces Pdr5 expression. (A) Wild-type strain and *tif51A-1* expressing Pdr5-GFP were cultured in SGal medium until reaching post-diauxic phase at 25ºC, transferred to 25ºC or 37ºC for 4 h and then subjected to fluorescence microscopy. A representative image is shown. (B) Quantification of Pdr5-GFP fluorescent signal from at least 150 cells. (C) Wild-type strain and *tif51A-1* were incubated as in (A) and then, cells were incubated with Nile Red substrate for 15 min prior to microscopy. A representative image is shown. (D) Quantification of Nile Red fluorescent signal from at least 150 cells. (B,D) Results are presented as mean ± SD relative to wild-type at 25ºC from three independent experiments. The statistical significance was measured by using a two-tailed paired Student t-test relative to 25ºC. *$p < 0.05$, ***$p < 0.001$.

5.5 Translation of mitochondrial proteins is connected to eIF5A activity

Translation of some mRNAs can occur at the mitochondrial surface in the proximity of the TOM complex, located there with the help of targeting factors (see section 1.4.1 of Chapter 1). These mRNAs are preferentially the ones codifying for MIM proteins originated from the endosymbiont genome (Williams *et al.*, 2014) and may always be at the mitochondrial surface or change their location depending on the cellular metabolic state (Tsuboi *et al.*, 2020). Here, active ribosomes synthesize the proteins that are co-translationally imported mainly through TOM and TIM23 complexes (Kellems and Butow, 1972; Williams *et al.*, 2014; Gold *et al.*, 2017). Translation in the proximity of the mitochondria has been shown to enhance protein synthesis (Tsuboi *et al.*, 2020), suggesting a positive feedback between co-translational import of mitoproteins and the translation of the corresponding mRNAs.

We wanted to investigate whether the protein import failure caused by reduced TIM23 complex activity upon eIF5A depletion may trigger an effect in the translation of co-translationally and Tim50-dependent imported proteins. To test this, we used the nLuc reporter assay previously described and monitored the protein synthesis of Tim50-independent and Tim50-dependent mitoproteins, whose mRNAs are found in the mitochondrial surface and proteins are co-translationally imported through the TOM complex (Williams *et al.*, 2014). We did not find significant differences in protein synthesis between the *tif51A-1* mutant and the wild-type strain at restrictive temperature for the nLuc reporter alone, which targets

the cytosol, neither for Tom70, which targets the MOM, although its synthesis was slightly reduced (Figure 5.8-A). For the Tim50-dependent proteins Cyc1 and Cox5a, targeted to the IM and MIM respectively, luciferase fusions indicated that production of the two proteins was significantly affected at restrictive temperature in the *tif51A-1* strain (Figure 5.8-B).

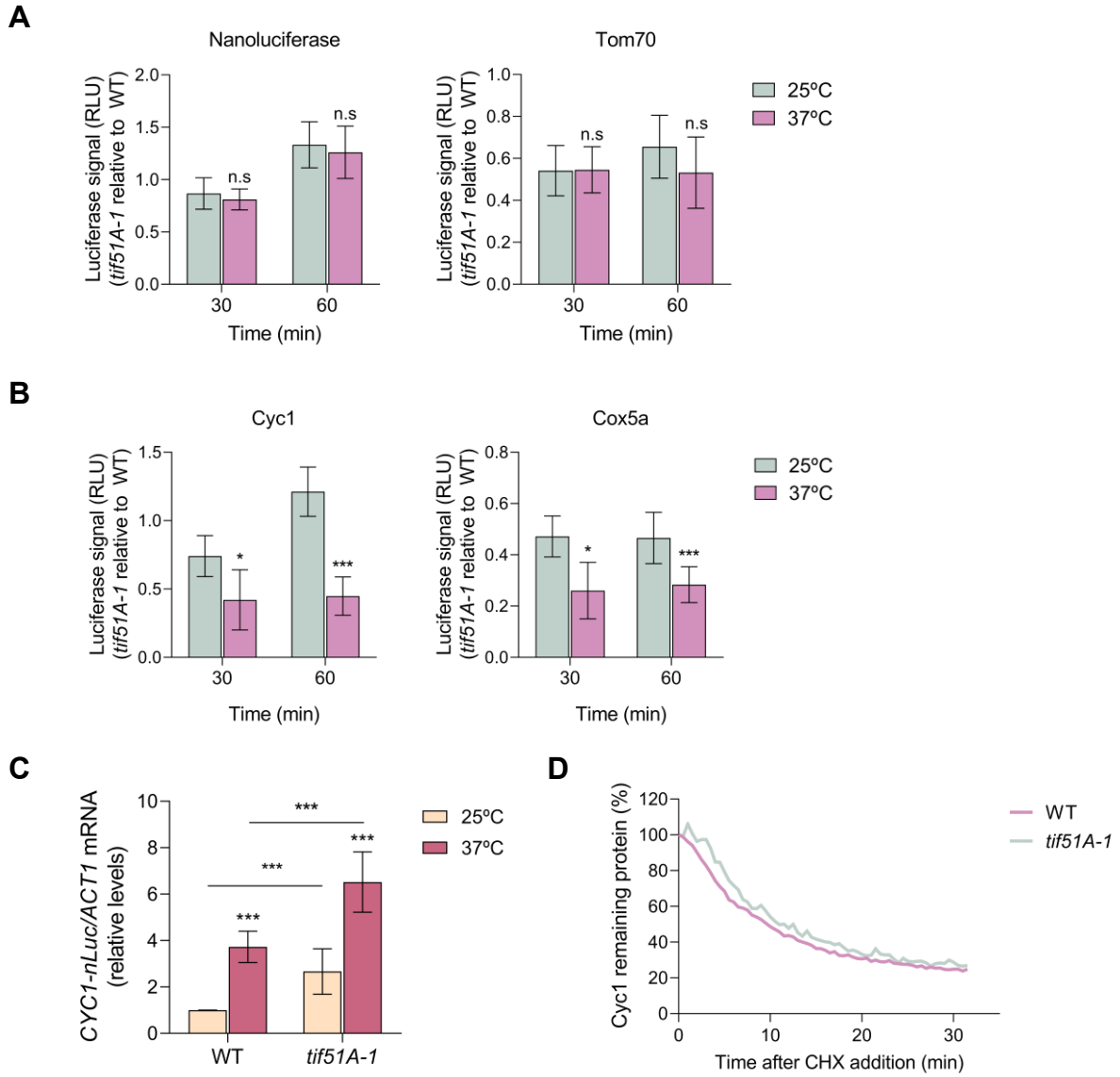

Figure 5.8. Translation of Tim50-dependent mitoproteins is highly sensitive to eIF5A deficiency. (A,B) Wild-type strain and *tif51A-1* expressing nLuc alone (A, left) or nLuc fusions with Tom70 (A, right), Cyc1 (B, left), Cox5a (B, right) were cultured in YPD until early exponential phase and transferred to 25ºC or 37ºC for 4 h. After addition of doxycycline to induce nLuc, the luminescence levels generated by the addition of the furimazine were measured along time and protein was quantified. (C) Wild-type strain and *tif51A-1* expressing Cyc1-nLuc were grown as in (B), one hour after addition of doxycycline *CYC1-nLuc* mRNA relative levels were determined by RT-qPCR and expressed relative to wild-type cells at 25ºC. (D) Wild-type strain and *tif51A-1* expressing Cyc1-nLuc were grown as in (B) and 30 min after addition of doxycycline, CHX (50 µg/mL) was added, and nLuc signal was monitored for an extra hour. Data were normalized against luciferase signal before CHX addition and represented as % of remaining protein. A representative experiment is shown. (A,B,C) Results are presented as mean ± SD from three independent experiments. The statistical significance was measured by using a two-tailed paired Student t-test relative to 25ºC condition. *p < 0.05, ***p < 0.001. n.s indicates no significant differences.

We confirmed that *CYC1* mRNA induction was taking place at similar levels in both strains, so differences in protein levels were not associated to differences in transcription (Figure 5.8-C). Using translation shut down by cycloheximide (CHX) treatment, we monitored Cyc1-nLuc activity over time and found no differences in the protein decay rate between both strains at restrictive temperature (Figure 5.8-D). Taken together, we interpret these results so that eIF5A depletion affects the translation of Tim50-dependent mitoproteins, as transcription and degradation were unaffected.

Then, we attempted to investigate if the import failure produced by a decrease in membrane potential also leads to synthesis reduction of Tim50-dependent proteins. Consistent with our previous results, we found that upon low CCCP doses, synthesis of Tim50-independent proteins (nanoluciferase, Tom70) was not significantly affected while the synthesis of the Tim50-dependent protein Cyc1 was significantly decreased (Figure 5.9-A). On the other hand, high CCCP doses led to a significant decreased synthesis of all tested proteins, pointing to a more global effect in which the cell might be responding to not just a failure in protein import but to a wider mitochondrial dysfunction, including loss of membrane potential, reduced ATP synthesis and arrested cell growth (Figure 5.9-A). In this line, a significant reduction of polysomes due to less initiation events was observed under high CCCP doses, while treatment with low CCCP doses displayed no translational differences with non-treated wild-type cells (Figures 5.9-B-D).

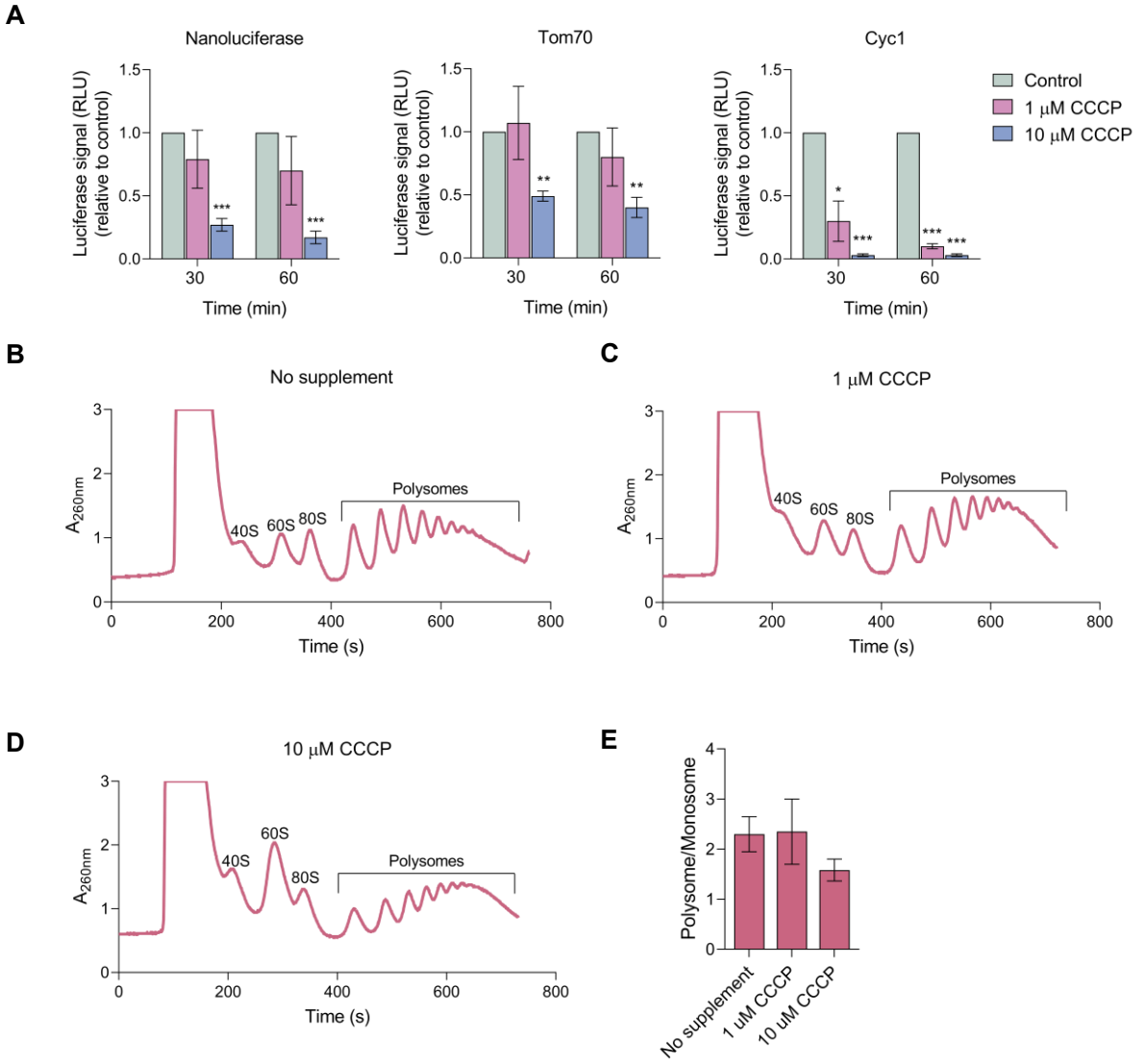

Figure 5.9. Translation of Tim50-dependent mitoproteins is highly sensitive to membrane potential uncoupling. (A) Wild-type strain was cultured in YPD and treated with 1 μM or 10 μM CCCP for 2 h. After addition of doxycycline to induce luciferase expression, the luminescence levels generated by the nanoluciferase reaction with furimazine were measured along time and protein was quantified relative to control cells. (B-D) Polysomes profiles were obtained for wild-type cells cultured in SGal at post-diauxic phase non-treated (B) or treated with 1 μM (C) or 10 μM (D) CCCP for 2 h. (E) The mean polysomes/monosome ratio is represented for each condition. (A,E) Results are presented as mean ± SD from a minimum of two independent experiments. No significant differences were found. (A,E) The statistical significance was measured by using a two-tailed paired Student t-test relative to wild-type strain non-treated. *$p < 0.05$, **$p < 0.001$, ***$p < 0.001$.

These findings point to an inhibition of some mitoproteins synthesis in response to decreased Tim50 levels and compromised mitochondrial protein import. We decided to further investigate this downregulation at the translational level. For this, we obtained polysome profiles for the two strains at permissive and restrictive temperatures and determined the distribution of specific mRNAs among the different polysomal fractions. Importantly, global translation was found unaffected in both strains at both temperatures and polysomes were maintained (Figures 5.10-A,B). To analyze the distribution of short length-RNAs along the fractions, we divided the polysome profiles in three different sections corresponding to monosomal fractions (M), fractions occupied by mRNAs with 2 or 3 ribosomes (2n-3n) and the rest of the polysomal fractions (P). For long length-RNAs we used the sections corresponding to monosomal fractions (M), fractions with 2 to 8 ribosomes (2n-8n) and the rest of the polysomal fractions (P) (Figure 5.10-C). In agreement with unaffected global translation, we found no differences in the ratios P/2n-3n and P/2n-8n between the two strains at permissive and restrictive temperatures (Figures 5.10-D,E).

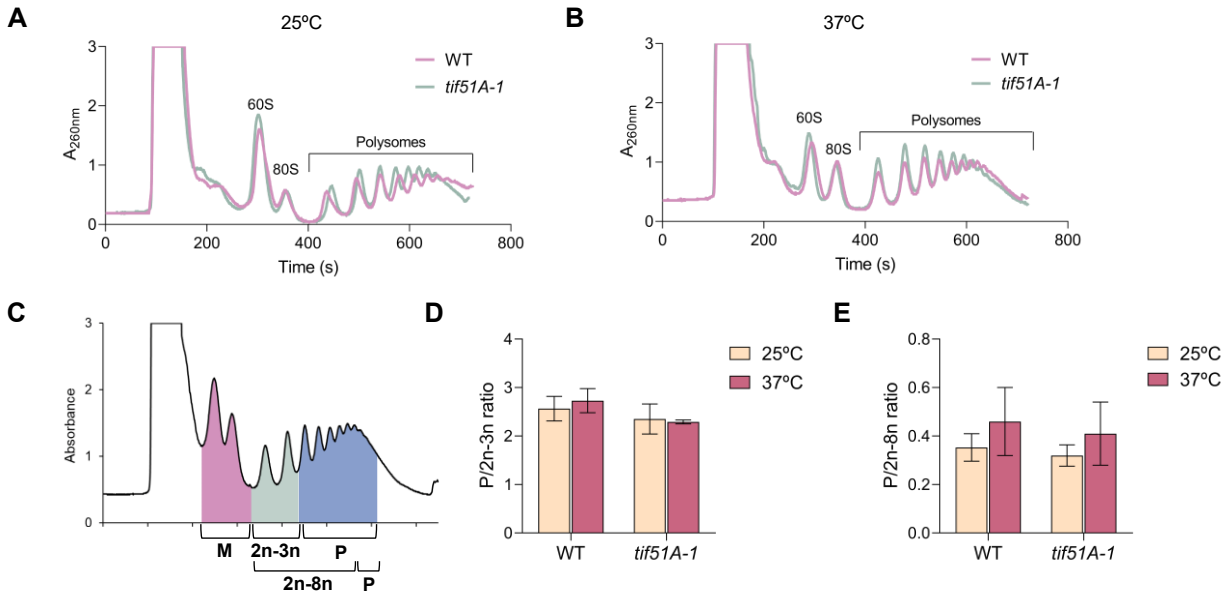

Figure 5.10. General translation is not affected upon eIF5A depletion. (A,B) Polysomes profiles were obtained for wild-type and *tif51A-1* strains cultured in SGal at 25ºC (A) or 37ºC (B) for 4 h. (C) Scheme with the employed area divisions for calculations. (D) The mean polysomes/2n-3n ratio (P/2n-3n) is represented for each strain at both temperatures. (E) The mean polysomes/2n-8n ratio (P/2n-8n) is represented for each strain at both temperatures. (D-E) Results are presented as mean ± SD from three independent experiments. The statistical significance was measured by using a two-tailed paired Student t-test relative to wild-type strain. No significant differences were found.

We analyzed the translation stage of several mRNAs localized or not at the mitochondrial surface and whose encoded proteins are destined to different localizations in the cell (Table 5.1). We first addressed the translation of *CYC1*, *COX5A, SDH2* and *TIM50* mRNAs, encoding Tim50-dependent proteins targeting the IM, MIM, MM and MIM, respectively. These four mRNAs are found in the mitochondrial surface and their proteins are co-translationally imported through the TOM complex (Williams *et al.*, 2014). Our results showed that for the wild-type strain, all the tested mRNAs were greatly associated with the heavy polysomal fractions at both temperatures. However, *CYC1, COX5* and *SDH2* mRNA abundance shifted to earlier fractions in the *tif51A-1* strain at restrictive but not at permissive temperature (Figures 5.11-A-C). The increased association to disome and trisome peaks indicated fewer translating ribosomes per mRNA. As expected, *TIM50* mRNA abundance also shifted to earlier fractions in the mutant at 37°C, as its translation is stalled upon eIF5A depletion due to the presence of consecutive prolines (Figure 5.11-D).

Then, we decided to analyze *TOM70* and *TOM20* mRNAs, which target the MOM and are also found in the surface of mitochondria (Williams *et al.*, 2014). According to previous results, these two mRNAs were predicted to behave as Tim50-independent mitoproteins. However, *TOM70* and *TOM20* also showed a significant shifting to earlier fractions in the *tif51A-1* strain at restrictive temperature (Figures 5.11-E,F), suggesting a general translation downregulation for the TOM translocase proteins too. We used the polysome profile of the actin (*ACT1*) as non-mitochondrial and not eIF5A-regulated mRNA and observed that it was highly associated with polyribosomes in both strains at both temperatures (Figure 5.11-G).

To broaden our study, we analyzed the translation status of other mRNAs encoding mitochondrial proteins but showing distinct features than the previously ones analyzed (Table 5.1). *PET9* mRNA encodes a transporter of the MIM and is a known substrate for TIM22 complex (Koehler *et al.*, 1998; Okamoto *et al.*, 2014). *HSP10* and *SDH8* mRNAs encode for a chaperone and assembly enzyme of the MM and are predicted Tim50-dependent mitoproteins. Contrary to the rest of the mRNAs previously analyzed, these two last mRNAs are not attached to the mitochondrial surface (Williams *et al.*, 2014), so they are translated in the cytosol prior import. However, we found that *PET9, HSP10* and *SDH8* mRNA abundance shifted to earlier fractions in the *tif51A-1* strain at restrictive temperature (Figures 5.12-A-C). These results suggested that translation of mitochondrial proteins was generally decreased upon eIF5A depletion, and the effect was not quantitatively correlated with the Tim50-dependency for import, submitochondrial localization nor mRNA localization. To clearly demonstrate that proteins reaching mitochondria, but not other locations were specifically affected under eIF5A deficiency, we studied the translation of the constitutively expressed *RPP2B, eIF2A* and *EFT2* mRNAs encoding a ribosomal protein and translation initiation and elongation factors, respectively, localized in the cytosol. We also studied the *ARF1* mRNA, which encodes a protein involved in vesicle formation and localized in Golgi. We found that the translation of these four mRNAs remained unaffected in the mutant strain at restrictive temperature compared to the wild-type strain (Figures 5.12-D-G). This is in agreement with the finding that global translation is not affected in the *tif51A-1* mutant (Figure 5.10).

Table 5.1. mRNAs analyzed by polysome fractionation

Gene	Length (bp)	eIF5A-dependent motifs	RNA mitochondrially localized	Protein localization	Tim50-dependency for import
CYC1	330	0	yes	IM	yes[1]
COX5A	462	1	yes	MIM	yes[1]
SDH2	801	1	yes	MM	yes
TIM50	1431	9	yes	MIM	yes[1]
TOM20	552	2	yes	MOM	no
TOM70	1854	4	yes	MOM	no[1]
PET9	957	4	yes	MIM	no[2]
HSP10	321	0	no	MM	yes
SDH8	417	1	no	MM	yes
ACT1	1437	2	no	Cytosol	no
RPP2B	333	1	no	Cytosol	no
eIF2A	1929	7	no	Cytosol	no
EFT2	2529	8	no	Cytosol	no
ARF1	546	3	no	Golgi	no
		Pelechano & Alepuz, 2017	**Williams *et al.*, 2014**		**1. This study** **2. Koehler *et al.*, 1998; Okamoto *et al.*, 2014**

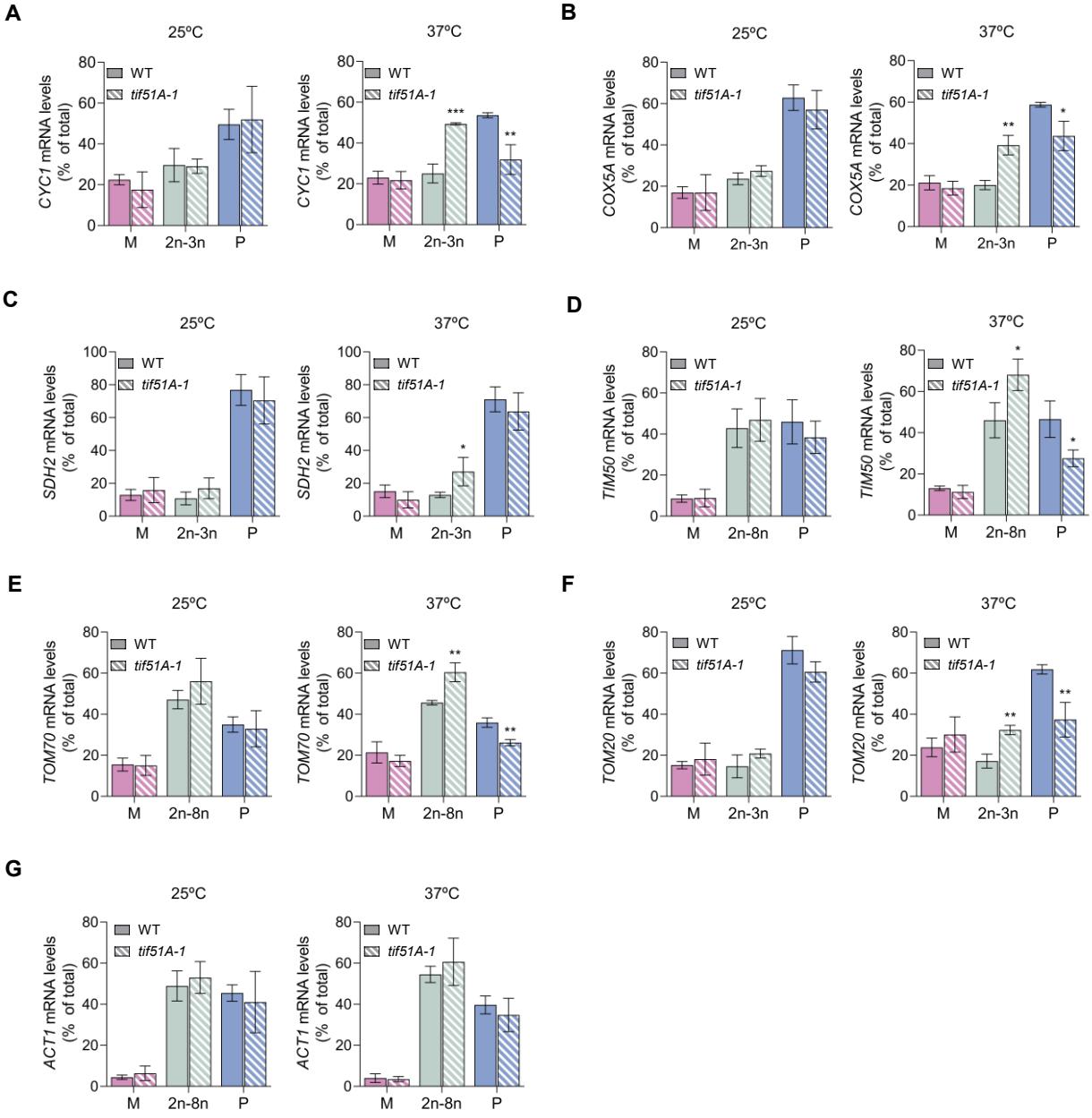

Figure 5.11. Translation of mitochondrial proteins is affected upon eIF5A depletion (part I). Polysomes profiles were obtained for wild-type and *tif51A-1* strains cultured in SGal at 25ºC or 37ºC for 4 h. The RNA from individual fractions of the polyribosome profiles was extracted and the mRNA levels of *CYC1* (A), *COX5A* (B), *SDH2* (C), *TIM50* (D), *TOM70* (E), *TOM20* (F) and *ACT1* (G) were analyzed by RT-qPCR in the corresponding sections at permissive (left) and restrictive temperature (right). (A-G) Results are presented as mean ± SD from three independent experiments. The statistical significance was measured by using a two-tailed paired Student t-test relative to wild-type strain. *$p < 0.05$, **$p < 0.001$, ***$p < 0.001$.

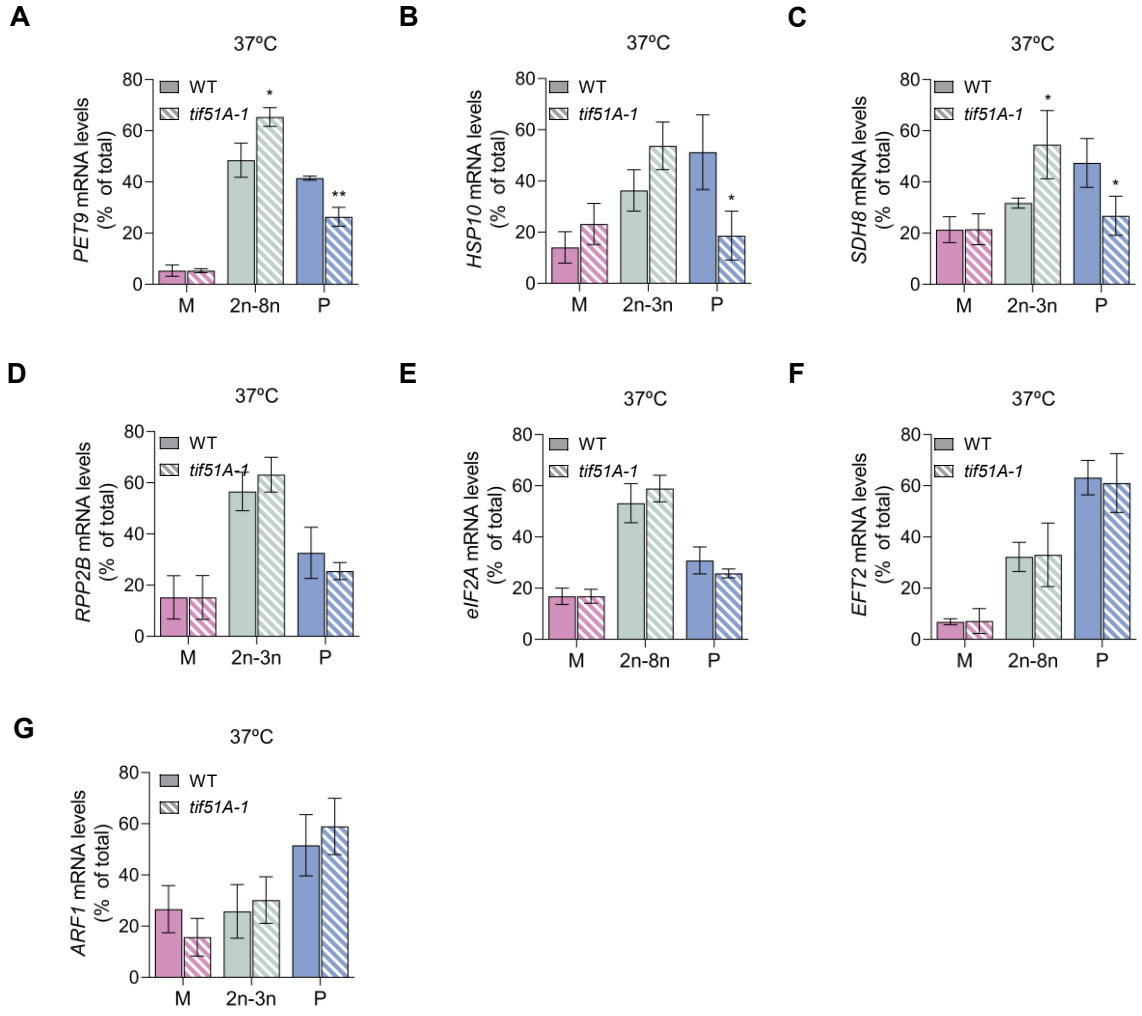

Figure 5.12. Translation of mitochondrial proteins is affected upon eIF5A depletion (part II). Polysomes profiles were obtained for wild-type and *tif51A-1* strains cultured in SGal at 25ºC or 37ºC for 4 h. The RNA from individual fractions of the polyribosome profiles was extracted and the mRNA levels of PET9 (A), *HSP10* (B), *SDH8* (C), *RPP2B* (D), *eIF2A* (E), *EFT2* (F) and *ARF1* (G) were analyzed by RT-qPCR in the corresponding sections at restrictive temperature. (A-G) Results are presented as mean ± SD from three independent experiments. The statistical significance was measured by using a two-tailed paired Student t-test relative to wild-type strain. *$p < 0.05$, **$p < 0.001$, ***$p < 0.001$.

Altogether, these data indicate that translation of mitochondrial proteins is generally reduced upon eIF5A depletion, as the association of multiple ribosomes to all the tested mRNAs encoding proteins targeting the mitochondria is diminished in a uniform manner. The obtained results point towards a specific mechanism highly dependent on the mitochondrial function and connected to eIF5A to highly reduce the synthesis of mitochondrial proteins. However, with our current data we cannot discern if this eIF5A-mediated mechanism is linked to the dysfunction of reduced TIM23/Tim50-dependent import upon eIF5A depletion.

5.6 Deletion of Tim50 proline stretch in eIF5A mutant does not rescue mitochondrial respiration but cancels the mitoCPR response induction and restores translation of mitoproteins

Herein, we have demonstrated how upon eIF5A depletion, Tim50 translation stalls in the polyPro stretch and its protein synthesis is decreased. This leads to reduced activity of the TIM23 complex translocase and generates specific import defects for Tim50-dependent mitoproteins, which accumulate and aggregate in the cytosol. Therefore, we asked if a restore in the Tim50 protein levels would alleviate the import collapse and its derived effects. To test this, we generated two strains expressing the endogenous Tim50 protein without the region containing the 7 consecutive prolines of its sequence (Tim50ΔPro), the first one in a wild-type (BY4741) background and the second one in a *tif51A-1* mutant background. In these strains, the endogenous *TIM50* gene is mutated so that the only source of Tim50 protein for the cell is the Tim50ΔPro and eIF5A-independent version.

Surprisingly, the functionality of the Tim50ΔPro version was shown to be almost unaffected. We observed very slight growth differences of the wild-type strain containing full Tim50 or Tim50ΔPro in glycerol media (Figure 5.13-A), although the proline-rich region is found in the presequence-binding groove of the Tim50 IMS domain, which functions in receiving the proteins in the TIM23 complex (Li and Sha, 2015). Therefore, the proline-rich region is not essential for cell viability under the respiratory conditions tested and thus, for the proper mitochondrial import. However, the substitution of the endogenous Tim50 by the Tim50ΔPro, whose translation is eIF5A-independent (Figures 5.1-B-D), did not rescue the growth of the *tif51A-1* mutant under glycerol at semi-permissive temperature (Figure 5.13-A). This result highlights the idea that Tim50 is not the only mechanism linking eIF5A to mitochondrial function. In fact, when we checked the accumulation of the membrane potential-dependent dye MitoTracker red, we observed that the *tif51A-1* Tim50ΔPro mutant still shows a decrease in the membrane potential at restrictive temperature (Figures 5.13-B,C); meanwhile, in the wild type Tim50ΔPro the membrane potential was preserved, confirming the functionality of this Tim50 version but pointing to Tim50-independent negative effects on mitochondrial function upon eIF5A depletion.

Additionally, we studied if the restore of Tim50 translation upon eIF5A depletion by the removal of the proline stretch would rescue other mitochondrial-related phenotypes. We found that the mRNA levels of the most induced mitoCPR genes (*PDR3, PDR5* and *CIS1*) were significantly decreased in the *tif51A-1* Tim50ΔPro mutant (Figure 5.13-D). Importantly, we found that in the *tif51A-1* strain harbouring Tim50ΔPro, the protein synthesis of Cyc1 and Cox5a was restored at restrictive temperature (Figure 5.13-E). Therefore, these two results strongly suggest that decreased Tim50 translation and derived import failure upon eIF5A depletion is the primary event that drives the mitoCPR induction and signals to a reduction in the translation of Tim50-dependent proteins. Thus, if the Tim50 protein levels are restored (in Tim50ΔPro), so is the protein import across the TIM23 complex and so is the translation of mitoproteins highly dependent on this system.

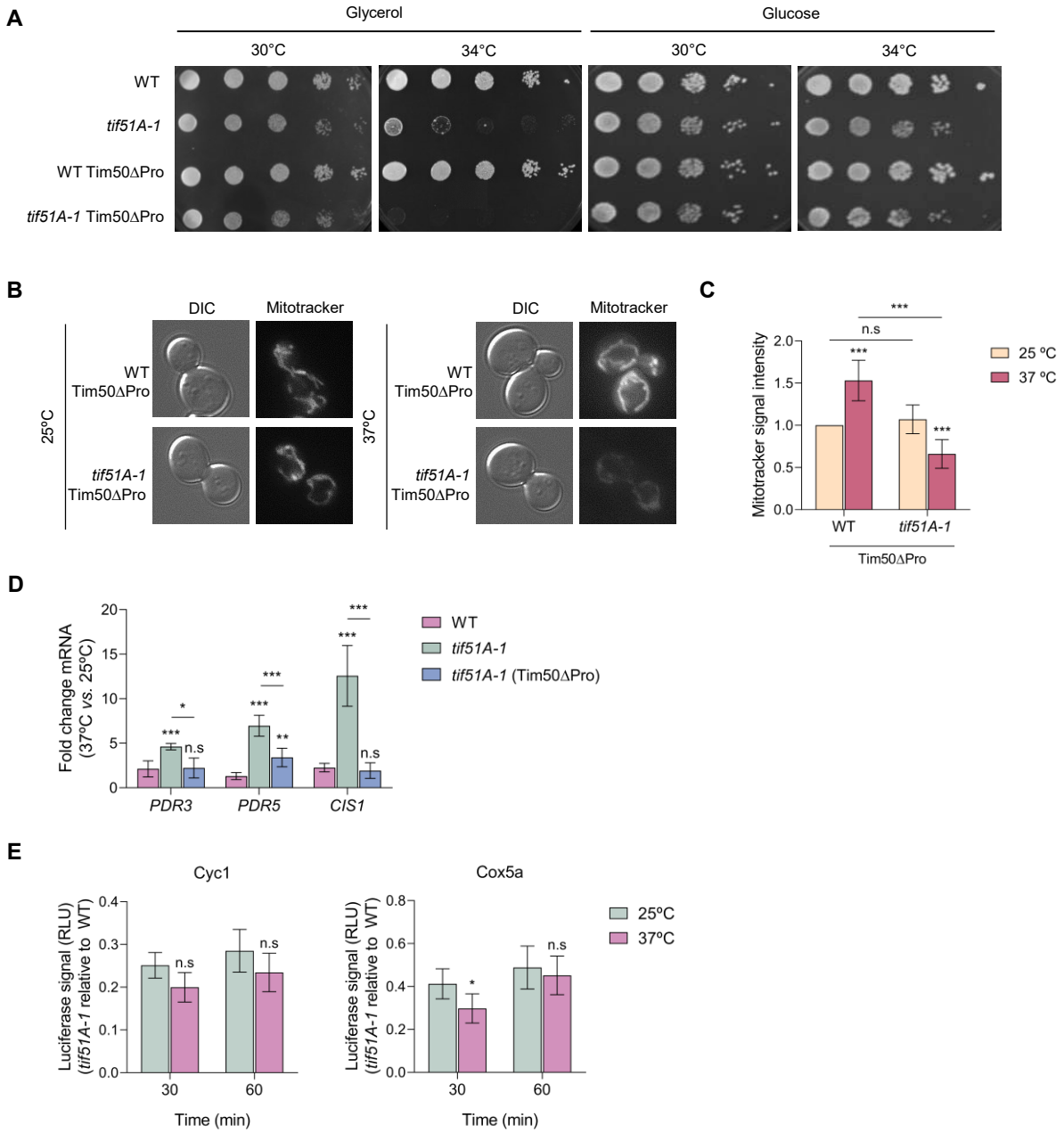

Figure 5.13. Restoring Tim50 levels in eIF5A mutant does not rescue mitochondrial respiration but cancels other mitochondrial-related phenotypes. (A) Growth of the wild-type, *tif51A-1,* wild-type Tim50ΔPro and *tif51A-1* Tim50ΔPro was tested in YPGly and YPD at the indicated temperatures. (B) Wild-type strain and *tif51A-1* carrying Tim50ΔPro were cultured in SGal medium until reaching post-diauxic phase at 25ºC, transferred to 25ºC or 37ºC for 4 h and subjected to phase contrast and fluorescence microscopy. Cells were incubated for 30 mins with MitoTracker prior microscopy to stain the mitochondria. A representative image is shown. (C) Quantification of MitoTracker fluorescent signal from at least 150 cells relative to wild-type cells at 25ºC. (D) Wild-type strain, *tif51A-1* and *tif51A-1* Tim50ΔPro were cultured as in (B). mRNA relative levels from mitoCPR genes were determined by RT-qPCR. (E) Wild-type strain and *tif51A-1* carrying Tim50ΔPro and expressing Cyc1-nLuc (left) or Cox5a-nLuc (right) were cultured in YPD until early exponential phase and transferred to 25ºC or 37ºC for 4 h. After addition of doxycycline to induce nLuc, the luminescence levels generated by the nLuc after the addition of the furimazine were measured along time and protein was quantified. (C-E) Results are presented as mean ± SD from three independent experiments. The statistical significance was measured by using a two-tailed Student t-test relative to WT or 25ºC. *p < 0.05, **p < 0.001, ***p < 0.001. n.s indicates no significant differences.

Discussion of Chapter 5

In this chapter we have described one of the possible molecular mechanisms by which eIF5A is essential for the mitochondrial function and activity. We have shown that eIF5A is necessary for the translation of the proline-rich region of Tim50 protein, which is part of the TIM23 complex and essential for the recognition and sorting of mitoproteins into the mitochondrial inner membrane and matrix. Tim50 and Tim23 proteins expose conserved soluble domains into the IMS that interact with each other, and this interaction is essential for protein translocation by the complex (Gevorkyan-Airapetov *et al.*, 2009). Thereby, if one of the two proteins is downregulated, it will affect the functional state of the whole complex and its translocating function. Through the modulation of Tim50 translation and thus, the activity of the TIM23 complex, eIF5A specifically impacts the import of Tim50-dependent proteins targeting the MIM and MM and some targeting the IMS. Upon eIF5A depletion, the mitochondrial import of Tim50-dependent proteins is compromised, so it is expectable that the translocase becomes clogged. We have seen that different non-imported mitochondrial proteins aggregate in the cytosol as a consequence of reduced import provoked by the lack of eIF5A, and consequent depletion of Tim50, or when the MIM is depolarized upon CCCP treatment. Interestingly, it has been recently demonstrated that decreased mitoprotein uptake with CCCP causes the stall of translocating proteins in the outer membrane (Schäfer *et al.*, 2022). A response for the clearance of stalled proteins in the mitochondrial surface has been shown to be mediated by the mitoCPR response, which induces, through the transcription factor Pdr3, the coordinated action of Cis1 and Msp1 to promote the degradation of arrested precursor proteins (Weidberg and Amon, 2018). We have shown here that compromised protein import upon eIF5A depletion, low doses of CCCP treatment or auxin-inducible degradation of Tim23, activate the mitoCPR response. Altogether, our results demonstrate that low levels of eIF5A causes mitochondrial stress by reducing the TIM23/Tim50-dependent protein import (Figure 5.14).

Our results also indicate that the accumulation of Tim50-dependent non-imported precursors in specific deposits in the cytosol is buffered by cytosolic chaperones, mainly Hsp104, to relieve the proteotoxic stress. The induction of Hsp104 at RNA level and its colocalization with mitoprotein aggregates might indicate that Tim50-dependent proteins escape, at some extend, proteolytic degradation and then, the chaperone system is activated to efficiently alleviate the cell toxicity arising in the cytosol (Hill *et al.*, 2017). Our results are in line with the recent description of the cytosol as a place with capacity to store mitochondrial precursor proteins in dedicated storage granules that are controlled by the cytosolic chaperone system, with Hsp104 binding the N-terminal presequences of mitoproteins (Krämer *et al.*, 2023). Besides, the observed Pdr5 induction upon eIF5A depletion seems indicative of a cellular detoxification effort to eliminate toxic substrates accumulating in the cytosol in a context of protein aggregates accumulation.

To rescue the cytosolic proteostasis upon mitochondrial import failure, the cell usually activates Hsf1 and Rpn4 transcription factors to induce, among others, chaperones and the proteasome system, respectively, to clear the accumulated precursors (Wrobel *et al.*, 2015; Boos *et al.*, 2019;). Although the activation of Hsf1 upon eIF5A depletion is not confirmed, our results indicate it is highly likely. Hsf1 targets such as Hsp104 are induced under eIF5A depletion conditions, and Hsp70 could be titrated away from Hsf1 through preferential binding to non-imported precursor mitoproteins, allowing the release and activation of functional Hsf1 (Krakowiak *et al.*, 2018). The transcriptional induction of Rpn4 would

be responsible for the upregulation of the ubiquitin-proteasome system but it would also induce the expression of Pdr3 and thus, the mitoCPR response (Boos *et al.*, 2019) until clogging is solved.

Upon prolonged mitochondrial dysfunction, the stress response is usually accompanied by cytosolic translation attenuation to reduce the synthesis of precursors and the protein load to translocases. General translation is known to be downregulated upon treatment with multiple mitochondrial stressors such as defective mitochondrial biogenesis (Wrobel *et al.*, 2015), clogger expression (Boos *et al.*, 2019), oxidative stress (Topf *et al.*, 2018) and mitochondrial depolarization with high CCCP doses (Schäfer *et al.*, 2022). Herein, we found that eIF5A depletion specifically down-regulates the translation of mitochondrial proteins. While general cytosolic translation remained unaffected, translation of proteins targeting mitochondria, co- or post-translationally, was affected. These results suggest that loss of TIM23 functionality might be driving a translocation clogging at the TOM complex which may stall translation of most mitochondrial proteins, independently of their strict import dependency on Tim50. Accordingly, rescue of the Tim50 protein levels in eIF5A mutant by replacing the endogenous copy with an eIF5A-independent Tim50ΔPro version, yielded the recovery of the translation of Tim50-dependent mitoproteins. Thus, the translation apparatus switches to respond directly and specifically to compromised import by decreasing the load of mitochondrial proteins. This finding suggests for the first time a tight connection between mitoprotein import and translation and that, among the different responses exerted by the cell to cope with the import failure, there is a specific signal coupling the functional status of TIM23 complex (and probably of the TOM complex as a consequence) to translation (Figure 5.14). Further work will be needed to describe the mechanistic connection between the clogging of the mitochondrial import systems and the translation of the mRNAs producing the specific loading cargos of these systems. We tried to decipher whether the mRNA localization at the mitochondrial surface was relevant for this translation regulation, as indicative of a physical proximity related mechanism. However, on the basis of the specific mRNAs investigated here, described as mitochondrial localized or not (Williams *et al.*, 2014) but showing translation down-regulation upon eIF5A depletion, we cannot support such a relation. Nevertheless, since the mRNA localization to the mitochondria seems to be constitutive for some mRNAs but regulated under specific conditions for others (Tsuboi *et al.*, 2020), it cannot be excluded that most if not all mitoprotein mRNAs are located in the proximity of the mitochondria under some circumstances.

The presented results herein highlight the idea that multiple mechanisms, besides Tim50 regulation, link eIF5A to mitochondrial function. Thus, recovery of Tim50 function with the eIF5A-independent Tim50ΔPro version was not sufficient to rescue growth of eIF5A mutant in respiratory media nor to fully recover the MIM potential. In the last years it has been proposed that eIF5A is necessary for the translation of specific mitoproteins with the specificity residing in the amino acid sequences at their N-terminal/MTS sequences, especially those ones with weak interactions with the peptide exit tunnel (Puleston *et al.*, 2018; Zhang *et al.*, 2022). Here, we added a new molecular mechanism explaining why eIF5A is essential for the mitochondrial function, although the recognition of the N-terminal/MTS sequences by the TIM23/Tim50 import system may alternatively explain the reduction of many mitoprotein levels already documented in other works.

Human Tim50 sequence contains 27 prolines, none of them are consecutive nor accumulate in a specific region as in *S. cerevisiae's* Tim50. In future studies, it would be of interest to examine if Tim50 is a true eIF5A-target for its translation in higher eukaryotes. In humans, Tim50 downregulation and derived import failure is associated to neurodegeneration and several genetic disorders (Sugiyama *et al.*, 2007; Shahrour *et al.*, 2017) whereas Tim50 overexpression has been observed in some cancer cell lines. The upregulation of Tim50 activity may increase protein import and mitochondrial function, promoting cell growth and metastasis (Sankala *et al.*, 2011; Gao *et al.*, 2016; Zhang *et al.*, 2019). Furthermore, defective mitochondrial protein import has been demonstrated in various diseases such as cancer, Parkinson's and Huntington's disease (Yano *et al.*, 2014; Di Maio *et al.*, 2016; Kang *et al.*, 2018; Nicolas *et al.*, 2019). The specific eIF5A-mediated mechanism of Tim50 modulation and therefore, mitochondrial protein import regulation described here may be important for understanding the molecular bases of pathologies where mitochondrial protein uptake fails. Lack or defects in eIF5A protein or its post-translational modification enzymes could raise as one of the underlying causes of impaired uptake in disease contexts. Thereby, eIF5A and its well-characterized hypusination precursor spermidine, could be considered as potential candidates to potentiate the activity of mitochondrial import machineries in compromised cells.

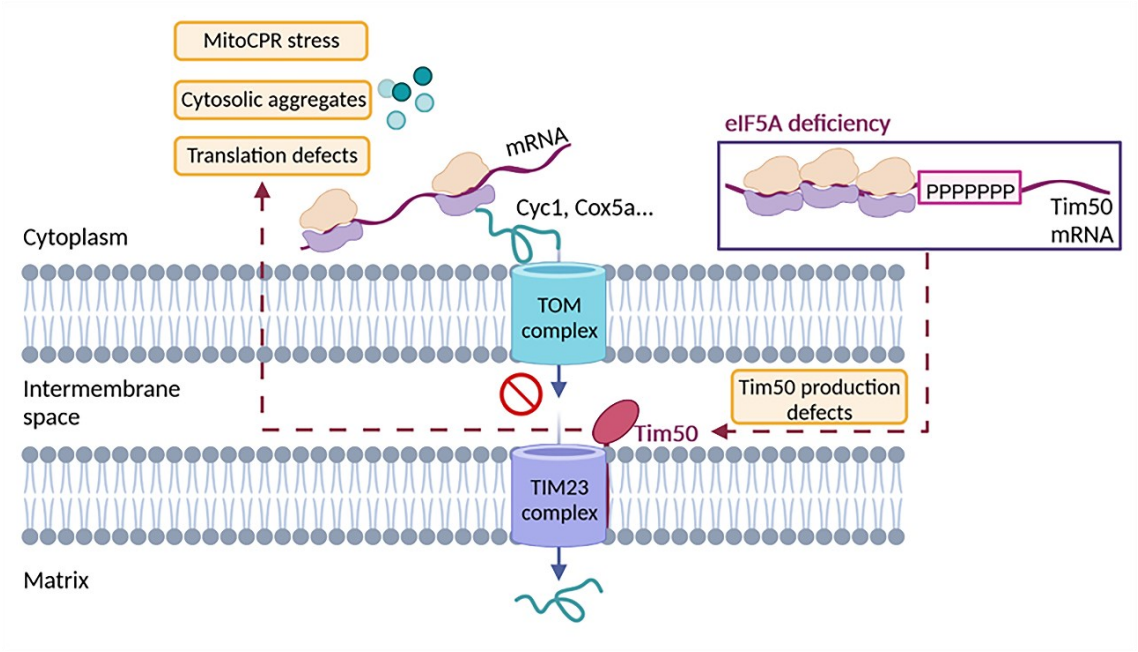

Figure 5.14. Model for eIF5A regulation of mitochondrial function via Tim50 translation regulation. eIF5A is necessary for the translation of the proline-rich region of Tim50 protein sequence. Upon eIF5A depletion, the mitochondrial import of Tim50-dependent proteins targeting the IMS, MIM and MM, is compromised. The non-imported precursors start aggregating in the cytosol and the proteins translocating in the outer membrane become stalled. Then, the mitoCPR response is induced to clear the proteins accumulating in the mitochondrial surface and the translation of RNAs encoding mitochondrial proteins is reduced, including the Tim50-dependent ones.

Chapter 6

eIF5A is involved in the transcriptional control of its target genes

Chapter 6. eIF5A is involved in transcriptional control of its target genes.

Chapter 6 is still not published in a scientific journal. Additional experiments are intended to be performed in the near future to amplify the knowledge and elaborate a manuscript for submission.

The precise control of gene expression is essential for the healthy growth and development of all cellular organisms. Although transcription and translation are considered independent processes due to their distinct molecular mechanisms, timings and sites of action, multiple crosstalk factors coordinate both processes which include the heterodimer Rpb4/Rpb7, the Ccr4-Not complex or the exonuclease Xrn1. In this line, mechanisms by which transcription influences translation of mRNAs to proteins have been widely studied in the last years (Slobodin and Dikstein, 2020). The translation factor eIF5A shows cytoplasmic and nuclear localization and this cellular distribution is regulated by post-translational modifications. Although poorly understood, several studies have described connections between nuclear eIF5A and some processes related to gene expression. Nuclear eIF5A has been found highly associated with RNA Polymerase II in precursor neurons (Rafiee *et al.*, 2023), bound to some RNAs under specific conditions, such as viral infection, to mediate their nuclear export (Ruhl *et al.*, 1993; Maier *et al.*, 2010; Balukoff *et al.*, 2020) or accumulated in the nucleus upon pro-apoptotic stimulus (Taylor *et al.*, 2007). As growing evidence indicates a role for eIF5A in the nucleus, we aimed to explore and characterize possible functions related to RNA synthesis and metabolism, and their specificity.

6.1 Global changes in synthesis rate and mRNA stability upon eIF5A depletion

As a first approach to elucidate the effects of eIF5A depletion on mRNA synthesis and metabolism, we determined the transcription rate (TR) and mRNA amount (RA) of the entire yeast genome using the genomic run-on (GRO) method (see section 2.3 of Chapter 2). We used a wild-type strain and the temperature-sensitive strain *tif51A-1* (carrying a single Pro83 to Ser mutation), since eIF5A is an essential protein (Valentini *et al.,* 2002; Li *et al.,* 2011). The two isogenic yeast strains were grown in glucose-based medium to early exponential phase at permissive temperature (25ºC) and then transferred to restrictive temperature (37ºC) for 4 hours. At this point, the growth rate was decreased in the *tif51A-1* cells at 37ºC with no big changes in cell viability (Li *et al.*, 2014), while increased for the wild-type cells, and eIF5A protein levels were almost undetectable in the mutant (Figures 6.1-A-C). A slight and statistically significant increase of 15% was observed in the cellular volume of *tif51A-1* cells at 37ºC (Figure 6.1-B). Nascent transcription rate values were then corrected by cell volume and expressed as synthesis rate (SR) hereon (Pérez-Ortín *et al.*, 2013).

We first analyzed the global RNA Pol II SR and RA by calculating the median of all the yeast protein-coding genes (4505 genes analyzed) using the fold change (FC) data between the two temperatures for each strain. First, we analyzed the SR FC data for each individual strain. As expected, the global profile of SR increased for the wild-type strain at 37ºC compared to 25ºC, since an increase in growth rate is usually accompanied by an increase in SR (García-Martínez *et al.*, 2010). In contrast, global transcription was significantly reduced in *tif51A-1* cells at 37ºC (Figure 6.1-D). This is probably because *tif51A-1* mutant grows slower than wild-type at 37ºC (duplication time of 3.7 h for the *tif51A-1* cells *vs* 1.4 h for wild-type cells). Total RA was determined by macroarray hybridization after oligo(dT)-primed cDNA labelling (see section 2.3 of Chapter 2). Contrary to SR, total RA was slightly reduced in wild-type cells while increased for *tif51A-1* cells (Figure 6.1-D). Using the SR and RA datasets we estimated the half-lives (HL) for each gene. The global profile showed a decrease in the HLs of wild-type cells, while deletion of eIF5A led to a high stabilization of most mRNAs in *tif51A-1* cells (Figure 6.1-D). To sum up, total RA is not greatly affected in wild-type cells owing to the compensatory effect between higher transcription and lower mRNA stability, while stabilization is the main contribution to increased RA observed under eIF5A deficiency. When comparing the datasets between strains, differences in the three parameters were found to be statistically significant. Hence, we can confirm that eIF5A has significant effects in the three studied parameters and upon eIF5A depletion, yeast cells experience important increases in global mRNA stability. However, these global effects are likely due to changes in growth rate and thus, indirect.

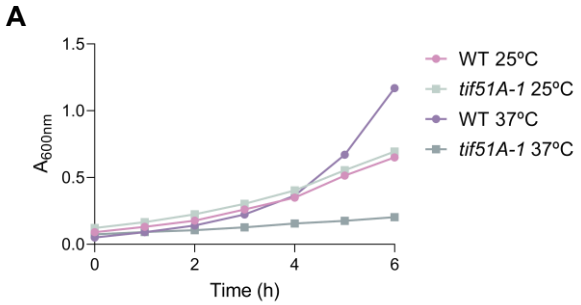

B

Growth rates and cell volumes of strains used in this study

	Strain	Duplication time (h)	Cell volume (fL)	Statistical significance
25ºC				
	WT	2.08 ± 0.04	46.15 ± 3.33	n.s
	tif51A-1	2.42 ± 0.06	45.52 ± 1.71	n.s
37ºC				
	WT	1.43 ± 0.08	49.81 ± 2.84	n.s
	tif51A-1	3.65 ± 0.19	57.43 ± 2.78	p<0.001

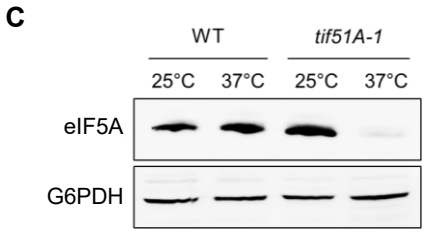

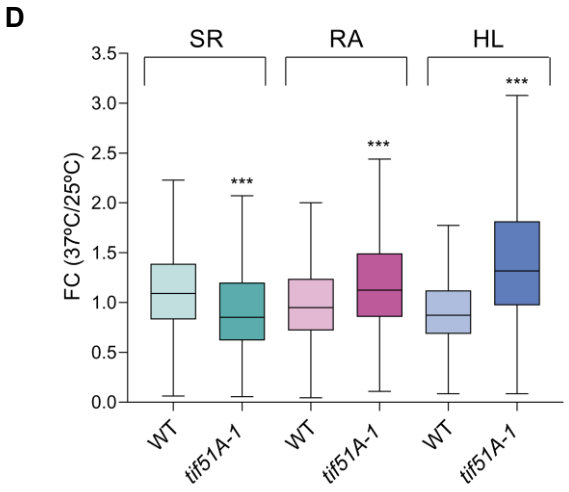

Figure 6.1. eIF5A depletion causes changes in global RNA Pol II synthesis rate (SR), mRNA amount (RA) and mRNA stability (HL). (A) Wild-type and *tif51A-1* mutant yeast strains were grown in YPD medium at 25ºC, inoculated at pre-exponential OD_{600} and transferred to 25ºC or 37ºC. The OD_{600} was measured at the indicated time points. A representative experiment is shown. (B) Doubling times were calculated from data in (A). Cell volume was measured with a counter Coulter for each strain at the corresponding temperature. Statistical significance for volume differences was determined using a two-tailed paired Student's t-test relative to wild-type cells at 25ºC. n.s indicates no significant differences. (C) A representative western blotting experiment of the eIF5A protein levels in the wild-type and *tif51A-1* cells at the indicated temperatures. G6PDH protein levels were used as loading controls. (D) Exponentially growing cultures of wild-type and *tif51A-1* mutant yeast strains were grown in YPD medium at 25ºC until exponential phase and then transferred to 25ºC or 37ºC for 4 h. Genomic data of SR, RA and HL were calculated as described in Chapter 2. Data are presented in box-plots showing the minimum, first quartile, median, third quartile and maximum from the 4505 genes analyzed. Data are presented as the fold change 37ºC *vs.* 25ºC from three independent GRO experiments. Statistical significance was determined using a two-tailed paired Student's t-test relative to corresponding wild-type cells. ***p<0.001.

6.2 SR and RA changes in target mRNAs directly correlate with their dependence on eIF5A for translation

Results shown above indicated a global mRNA stabilization in the *tif51A-1* cells, being the main contribution to the global increase in RA. The general trend previously seen represents the average over all protein-coding genes, but we were interested in studying the changes occurring in the set of eIF5A translation-dependent genes and thus, more sensitive to the presence/absence of eIF5A. Although multiple proteins have been proved to be direct eIF5A targets for their translation in *S. cerevisiae,* still the number is not so high. For this reason, we classified the yeast genes according to their putative eIF5A-dependence for translation.

First, we defined a Protein Pause Index (PPI) for each gene by using the strength pause values obtained for the top 43 eIF5A-dependent tripeptides revealed by the 5PSeq analysis (Table 1.1) (Pelechano and Alepuz, 2017). The three top tripeptides among these were KPP, PPP and PGW, with stall scores of 8.982, 7.032 and 6.410 respectively; while the rest were mostly combinations of proline, glycine and/or acid or basic amino acids (Table 1.1) (Pelechano and Alepuz, 2017). The PPI was calculated for each gene as the sum of each of these top 43 eIF5A-dependent tripeptides contained in its corresponding amino acid sequence, multiplied by its specific strength pause value. The higher the PPI for the gene, the more likely that translation of the corresponding mRNA will stall upon eIF5A deficiency. The yeast proteome (data from 6714 proteins) showed an average of 2.9 motifs/protein and an average PPI value of 10.84. We then arbitrarily established a target group of genes for subsequent analysis, as those in which their PPI was above 60 (48 genes). These genes were strong candidates to be dependent on eIF5A for their translation due to the high number of eIF5A-dependent tripeptides found in their sequences. We calculated and represented the median SR, RA and HL of these eIF5A putative targets and compared them to the global values previously analyzed in Figure 6.1-D. Additionally and to better understand the results, we also calculated the SR, RA and HL ratios between this target group and the global one for each strain. When comparing the synthesis rates, the pattern was reversed, so that genes with high eIF5A-dependence (PPI > 60) had an increased SR upon eIF5A depletion, opposite to the decreased SR observed globally (Figure 6.2-A). Besides, the analysis of the RA among this group of genes showed a more marked RA increase than the global data (Figure 6.2-B). These results suggested a specific behaviour of eIF5A-dependent genes compared to global profiles. Conversely, the analysis of the HL showed minor differences with regards to the global data, indicating that the mRNAs of these genes were also stabilized (Figure 6.2-C). The observed differences in the three parameters in this set of genes were found to be statistically significant between the two strains.

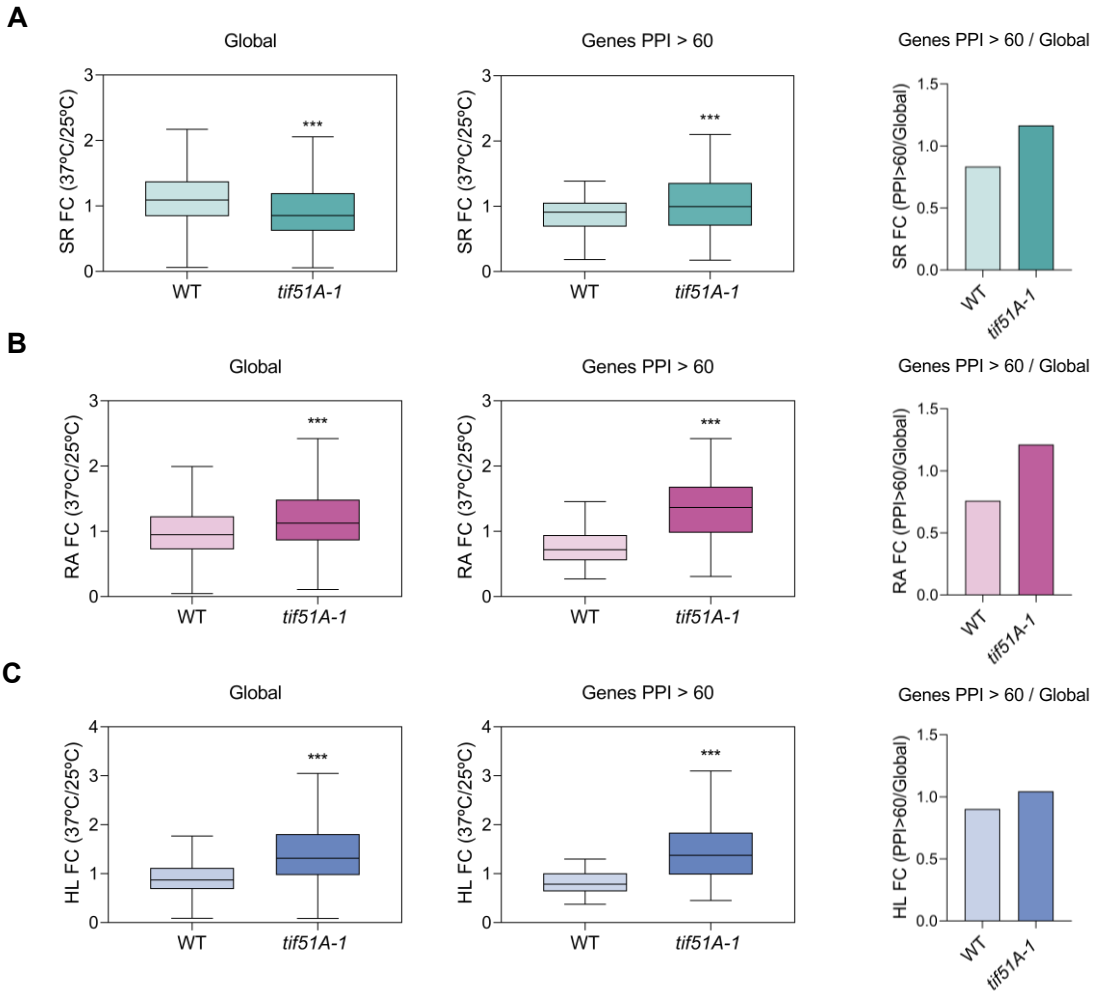

Figure 6.2. Genes with high content of eIF5A-dependent motifs (PPI > 60) show differential behavior in SR, RA and HL upon eIF5A depletion. (A-C) Genomic data of SR (A), RA (B) and HL (C) are presented in box-plots, showing the minimum, first quartile, median, third quartile and maximum from the global data (4505 genes) and genes with PPI > 60 (48 genes). Data are presented as the fold change (FC) 37ºC *vs.* 25ºC from three independent experiments. Statistical significance was determined using a two-tailed paired Student's t-test relative to the corresponding wild-type cells. ***p<0.001. The right panels of the figure show the fold change (FC) between the median values of the two groups for each strain. No statistical significance was determined due to the nature of the data.

Therefore, we identified specific trends of a group of genes predicted to behave as eIF5A-dependent, which diverged substantially from the general trend in the *tif51A-1* mutant. In particular, we found a strong and positive effect on the RNA Pol II SR of specific genes, suggesting that eIF5A depletion activates the synthesis of its targets at the transcriptional level. To shed some light into this idea, we classified the 4505 genes into 10 groups showing different PPI intervals, so that genes were ordered according to their eIF5A-dependence for translation (Table 6.1). Hence, genes showing low PPI values could be considered as non-eIF5A dependent genes while genes showing high PPI values could be considered as eIF5A-dependent genes for their translation. We calculated the mean values of SR, RA and HL for each group and plotted them against the PPI values. The analysis of this data set revealed

that the SR correlated significantly and positively with the PPI in a non-linear manner (Figure 6.3-A). Consistent with this increase, we observed an increase in RA that was strongly and positively correlated with the PPI (Figure 6.3-B). In contrast, the HL data indicated that genes with low PPI values (less eIF5A-dependent) experienced a positive correlation between HL and PPI, up to the PPI value of 30, from which no stability increase was observed (Figure 6.3-C). Hence, the responsiveness of target genes in the SR and the HL upon eIF5A depletion seems to be substantially different, being the SR the major contribution to increased RA.

On the other hand, it is known that among the 43 eIF5A-dependent tripeptides, consecutive prolines are considered to give one of the strongest pauses upon eIF5A depletion (Gutierrez *et al.*, 2013) with a specific strength pause value of 7.032 (Table 1.1) (Pelechano and Alepuz, 2017). We asked if the polyPro stretches were driving the changes in SR, RA and HL seen above. To test this, we defined a new index termed the polyPro Index (PI) for each gene. We calculated the PI as the sum of all the PPP tripeptides contained in the amino acid sequence and multiplied by its strength pause value of 7.032. Then, we ordered and divided the 4505 genes into 6 groups showing different PI intervals, so that genes were classified according to their eIF5A-dependence (Table 6.1). The general SR and RA trends resulted in linear positive correlations with the PI and therefore, the eIF5A-dependence. However, the strength of the SR correlation with the PI was lower than with the PPI and not statistically significant (Figures 6.3-D,E), indicating that non-polyPro containing eIF5A-dependent tripeptides have an additional and significant contribution to changes in SR. In addition, the HL trend was found not correlated to the PI (Figure 6.3-F).

Taken together, our results indicate that a lack of eIF5A yields specific and important effects in transcriptional induction for genes requiring eIF5A for their translation, and only minor effects in mRNA stabilization. As a result of the higher SR, the mRNA abundance of eIF5A-target genes also increases upon eIF5A depletion. Hence, the levels of overall mRNAs increase because of stabilization upon eIF5A depletion, while the levels of mRNAs with stronger eIF5A-dependence for their translation increase due to higher synthesis rather than stability.

Table 6.1. Classification of genes into groups according to their eIF5A-dependency for translation.

Protein Pause Index (PPI)	Gene number	polyPro Index (PI)	Gene number
0	975	0	4165
0-10	1812	0-10	241
10-20	1039	10-20	147
20-30	384	20-30	30
30-40	156	30-50	8
40-50	54	> 50	8
50-60	33		
60-70	23		
70-80	11		
> 80	14		

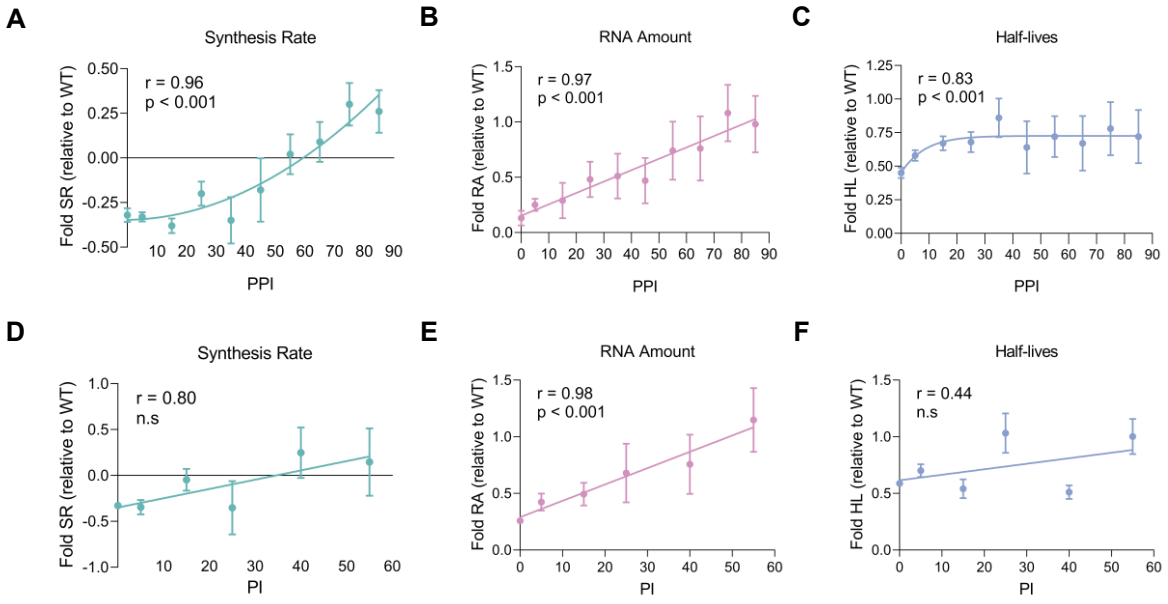

Figure 6.3. Changes in SR, RA and HL upon eIF5A depletion correlate with the degree of eIF5A-dependence for translation. (A-C) Graphs represent the average SR (A), RA (B), and HL (C) for all genes included in each group versus the protein pause index (PPI) interval from each group. (D-F) Graphs represent the average SR (D), RA (E), and HL (F) for all genes included in each group versus the polyPro Index (PI) interval from each group. (A-F) Values represent the $\log_2$ fold change (FC) at 37ºC *vs.* 25ºC ± SE, relative to the corresponding value in the wild-type strain. Experimental data were adjusted to linear (B,D-F), potential (A) or logarithmic (C) trends. Pearson's correlation coefficient and the associated significance for the plots are shown. n.s indicates no significant differences.

6.3 eIF5A depletion increases RNA Pol II transcription of its target genes

To validate our RA genome-wide data, we measured the changes in mRNA levels of several specific genes showing differences in their eIF5A translation-dependencies, according to their PPI and PI values (Figure 6.4-A). The quantification of mRNA by RT-qPCR from wild-type and *tif51A-1* cells showed a statistically significant increase in mRNA levels in *tif51A-1* cells with respect to the wild-type for most of the tested genes (Figure 6.4-B). Consistent with our previously described GRO results, this increase correlated well with the PPI and PI values, so genes showing a stronger eIF5A-dependence for their translation presented a higher abundance in their mRNA levels than genes with the lowest eIF5A-dependence.

Taken together, these results indicate and confirm that eIF5A absence boosts the induction of mRNA levels of genes requiring eIF5A for their translation in which, presumably, the translation process halts and ribosomes become stalled.

A

Genes selected for mRNA levels analysis

Gene	eIF5A-dependent motifs	PPP motifs	Protein Pause Index (PPI)	polyPro Index (PI)
GAPDH	2	0	7	0
YTA10	12	0	42	0
HAP1	12	0	46	0
TIM50	9	5	48	35
XRN1	15	4	65	28
YTA12	12	7	73	49
BNR1	34	17	188	120
BNI1	39	21	217	148
VRP1	90	37	466	260

B

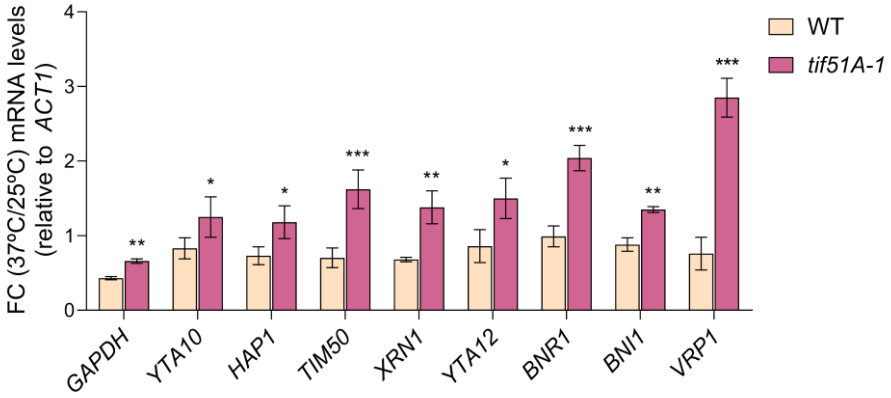

Figure 6.4. Lack of eIF5A provokes an increased mRNA expression of eIF5A-translation dependent genes. (A) Genes selected for mRNA level analysis by RT-qPCR. The number of eIF5A-dependent motifs and PPI/PI indexes are shown. (B) Exponentially growing cultures of wild-type and *tif51A-1* mutant yeast strains were grown in YPD medium at 25ºC until exponential phase and then transferred to 25ºC or 37ºC for 4 h. mRNA levels of each gene were determined by RT-qPCR using primers designed for amplification in the ORF regions (see Table A1.4). Data are presented as the mean fold change (FC) 37ºC *vs.* 25ºC ± SD from three independent experiments. Statistical significance was determined using a two-tailed paired Student's t-test relative to wild-type cells. *p<0.05, **p<0.01, ***p<0.001.

The increase in mRNA levels may be consequence of an increase in SR and/or HL. To independently corroborate that in this case this is due to an increase in SR as indicated by our genomic analysis (Figure 6.3-A), we investigated the occupancy of total RNA Pol II, as a proxy of SR, to a set of specific genes that show different eIF5A-dependencies, according to their PPI and PI values (Figure 6.5-A). We performed chromatin immunoprecipitation (ChIP) experiments using an antibody against the Rpb1 subunit of RNA Pol II (8WG16). We found that total RNA Pol II was recruited to similar levels in wild-type and *tif51A-1* cells to gene bodies which do not require eIF5A for their translation such as *ACT1* or *GAPDH.* However, and consistent to our previously described GRO results, we found a higher and significant association (2- to 4-fold increase) of the total RNA Pol II to the ORFs of genes showing a strong eIF5A-dependence for their translation in the *tif51A-1* cells (Figure 6.5-B). The higher binding

of the RNA Pol II elongation complex was in parallel to the higher mRNA levels of affected genes (Figure 6.4-B).

A

Genes selected for RNA Pol II binding analysis

Gene	eIF5A-dependent motifs	PPP motifs	Protein Pause Index (PPI)	polyPro Index (PI)
GAPDH	2	0	7	0
ACT1	2	0	7	0
TIM50	9	5	48	35
YTA12	12	7	73	49
BNR1	34	17	188	120
BNI1	39	21	217	148
VRP1	90	37	466	260

B

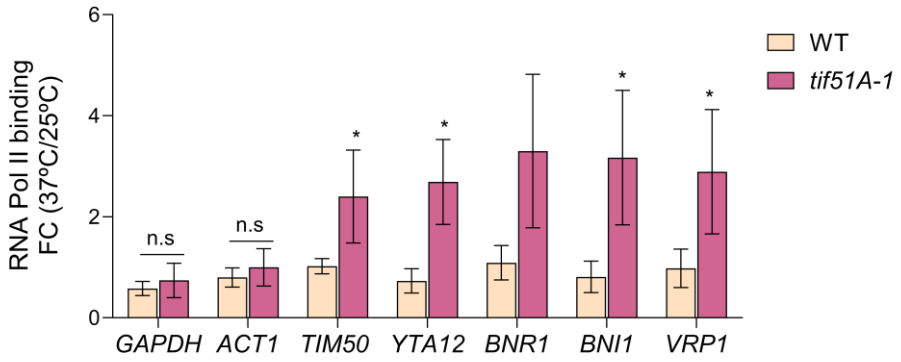

Figure 6.5. Lack of eIF5A provokes an increased association of RNA Pol II with eIF5A translation dependent genes. (A) Genes selected for RNA Pol II binding analysis by chromatin immunoprecipitation (ChIP). The number of eIF5A-dependent motifs and PPI/PI indexes are shown. (B) ChIP analysis of RNA Pol II recruitment in wild-type and *tif51A-1* cells. ChIP of RNA Pol II was performed with the 8WG16 anti-Rpb1 antibody. The immunoprecipitated DNA was used to quantify the different ORFs by qPCR (primers listed in Table A1.4). The percentage of the signal obtained in each ChIP sample with respect to the signal obtained with the DNA from the corresponding whole cell extract was calculated. Data are presented as the mean fold change (FC) 37ºC *vs.* 25ºC ± SD from three independent experiments. Statistical significance was determined using a two-tailed paired Student's t-test relative to wild-type cells. *p<0.05. n.s indicates no significant difference.

To summarize, the run-on data indicated a global decrease in the RNA Pol II transcription rate upon eIF5A depletion. However, and contrary to the overall trend, genes whose translation is highly dependent on eIF5A due to the presence of eIF5A-requiring motifs in their coding sequences, experience an increase in RNA Pol II binding and SR. This is the main cause of the significant increase in their mRNA levels, proportional to the presumed eIF5A-dependence for translation.

6.4 Removal of polyPro regions suppresses the translational and the transcriptional effects of eIF5A depletion

Proteins which require eIF5A for translation contain specific motifs in their sequences (Pelechano and Alepuz, 2017; Schuller *et al.*, 2017). Since the polyPro motifs are the strongest contributors to high eIF5A-dependence (resulting in high PPI and PI values), removal of these regions would turn eIF5A-translation dependent genes into non-dependent ones (Li *et al.*, 2014). We aimed to study the effect on mRNA levels and transcription of these mutant versions predicted to be eIF5A-translation independent. To test this, we obtained new strains targeting the genes *BNR1*, *YTA12* and *TIM50* in both wild-type and *tif51A-1* genetic backgrounds (Figure 6.6). Bnr1 is a formin involved in the formation of actin filaments; Yta12 is a component of the mitochondrial m-AAA protease and mediates the degradation of misfolded or unassembled proteins; and Tim50 is an essential component of the TIM23 complex translocase in mitochondria (see Chapter 5 for details). These three genes have high PPI and PI values and have been shown to be responsive to eIF5A depletion by increasing their TR and mRNA levels (Figures 6.4 and 6.5). For each gene, we obtained two genomic HA- or GFP-tagged versions in wild-type and *tif51A-1* cells: a full-length gene with HA or GFP after the coding region (*BNR1-HA*, *YTA12-GFP* and *TIM50-GFP*) and a mutated version in which the region containing the polyPro stretches was deleted (*BNR1ΔPro-HA*, *YTA12ΔPro-GFP*, *TIM50ΔPro-GFP*). These new strains, therefore, showed lower PPI and PI values and were predicted to behave as eIF5A-independent genes (Figure 6.6).

We first analyzed the mRNA levels by RT-qPCR in the new set of strains and found similar results for the three selected genes. Despite the modifications made in the 3'-UTR regions, which are known to influence the stability of some mRNAs (Lee and Lykke-Andersen, 2013; Geisberg *et al.*, 2014), we still found a significant increase in the mRNA levels of the three full length genes with C-terminal tags (still expressing the polyPro stretches) in the *tif51A-1* cells after the temperature shift (Figures 6.6-A-C). However, we found that this increase in the mRNA levels of the three genes was no longer present in the mutant cells expressing the mutated versions without prolines (Figures 6.6-A-C).

Next, we evaluated the recruitment of the RNA Pol II to the *YTA12* gene in the new set of strains. By performing ChIP analysis with 8WG16 antibody against the Rpb1 subunit of RNA Pol II, we found that the association of the polymerase to the *YTA12* gene body was increased in the *tif51A-1* cells carrying the *YTA12-GFP* version (Figure 6.6-D), consistent with our previous results. Conversely, we found lower RNA Pol II recruitment to the *YTA12* gene between the *tif51A-1* cells carrying the *YTA12ΔPro-GFP* version compared to the corresponding wild-type (Figure 6.6-D).

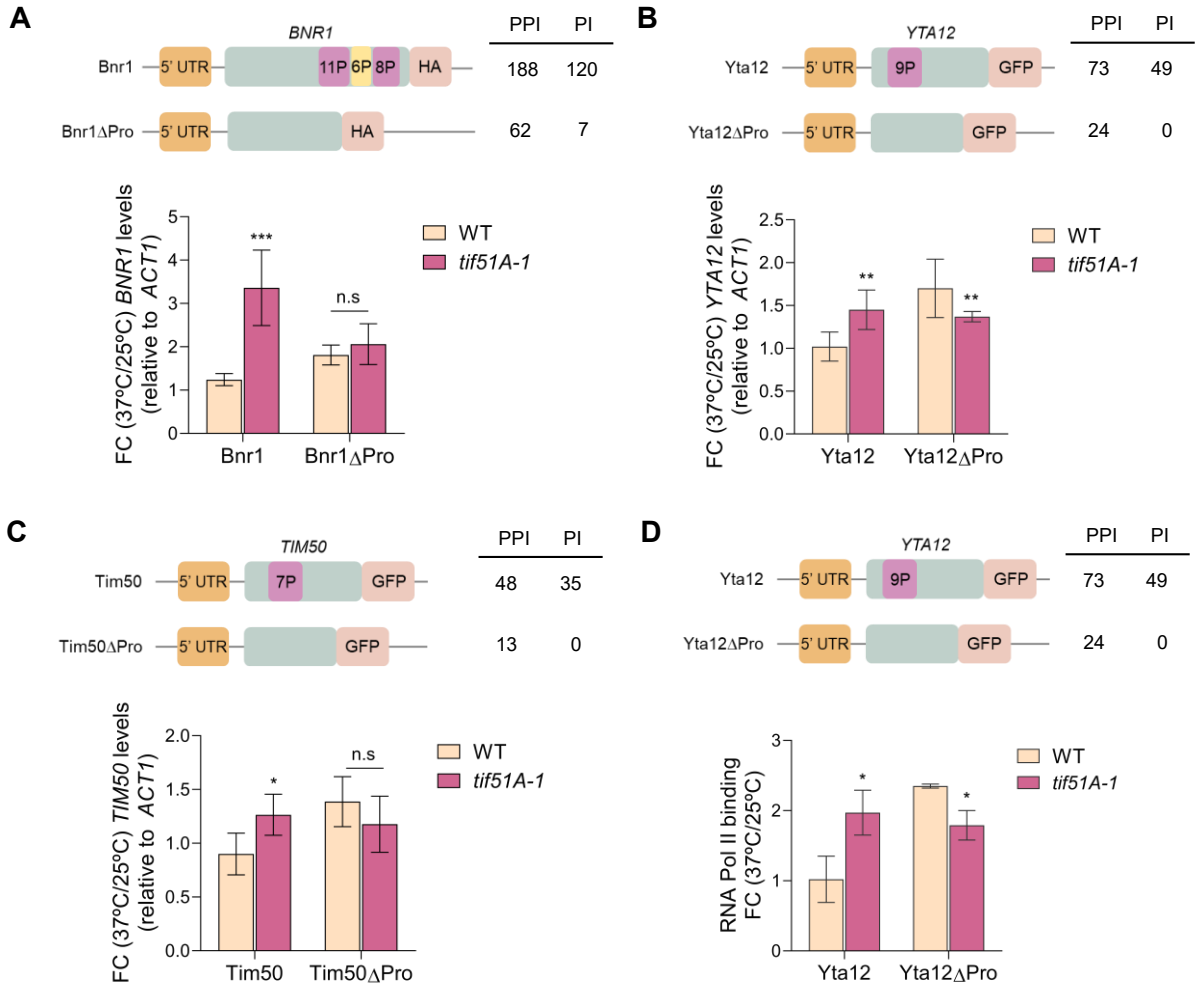

Figure 6.6. Removal of polyPro stretches rescues the eIF5A effects on RA and SR. (A-C) Schematic diagram showing the C-terminal genomic tagging of full-length *BNR1, YTA12* and *TIM50* ORFs and their polyPro-deleted versions. PolyPro stretches with the number of consecutive prolines are shown in pink, while regions containing non-consecutive prolines are shown in yellow. PPI and PI of both wild-type and mutated versions are shown (top). mRNA levels from *BNR1* (A), *YTA12* (B) and *TIM50* (C) were determined in the strains carrying the wild-type versions and the mutated versions of these genes by RT-qPCR (bottom). (D) ChIP analysis of RNA Pol II recruitment in wild-type and *tif51A-1* cells. ChIP of RNA Pol II was performed with the 8WG16 anti-Rpb1 antibody. The immunoprecipitated DNA was used to quantify the *YTA12* ORF by qPCR (primers listed in Table A1.4). The percentage of the signal obtained in each ChIP sample with respect to the signal obtained with the DNA from the corresponding whole cell extract was calculated. (A-D) Data are presented as the mean fold change (FC) 37ºC *vs.* 25ºC ± SD from three independent experiments. Statistical significance was determined using a two-tailed paired Student's t-test relative to corresponding wild-type cells. *p<0.05, **p<0.01, ***p<0.001. n.s indicates no significant difference.

In summary, the reversal of the SR and RA effects by removing eIF5A-dependent motifs highlights the idea that the presence of motifs which stall translation under eIF5A deficiency, drives the eIF5A-dependent transcriptional regulation. Thereby, the presence of these codons allows for an eIF5A-dependent regulation of transcription and translation; where eIF5A presence promotes translation and eIF5A absence promotes transcription while represses translation. On the contrary, the absence of eIF5A-dependent motifs cancels this regulation and transcription of the so-called eIF5A-dependent genes turns independent on the presence/absence of eIF5A.

6.5 eIF5A binds to chromatin with higher recruitment to its target genes

The previous results indicated that RNA Pol II binding and transcription of eIF5A-translation dependent genes was increased in the absence of eIF5A. Although different mechanisms could account for the changes in transcription, our results suggested a direct role of eIF5A in specifically repressing the binding of the RNA Pol II to genes requiring eIF5A for their translation. In fact, the nuclear localization of eIF5A has already been reported in different model organisms and related to different functions such as mRNA export, apoptosis or transcription activation of specific genes (see Ruhl *et al.,* 1993; Taylor *et al*., 2007; Li *et al*., 2014 and section 1.5.3 of Chapter 1). Interestingly, it has recently been shown in mammalian precursor neurons that RNA Pol II immunoprecipitation from chromatin enriched samples captures eIF5A as an associated protein, pointing to a possible functional interaction between the two proteins in the nucleus (Rafiee *et al.*, 2023). Nevertheless, there is lacking detailed information about eIF5A's DNA binding properties.

Therefore, due to the already known information of nuclear eIF5A, we aimed to address if eIF5A binds to DNA chromatin of specific genes. To answer this question, we performed ChIP experiments in wild-type cells exponentially grown in glucose media using a polyclonal antibody against eIF5A protein. We studied the association of eIF5A to different chromatin regions, including an intergenic region, and coding regions of a transcriptionally repressed gene (*GAL1*) and some genes with different eIF5A-dependencies for their translation (Figure 6.7-A). Our results revealed that the cross-linking procedure trapped eIF5A on the chromatin in coding regions. In fact, we found a strong and significant binding of eIF5A to all the tested gene ORFs, compared to the intergenic region, where the signal was almost absent (Figure 6.7-B). However, we did also find that eIF5A-dependent genes showed higher levels of eIF5A association compared to eIF5A-independent genes. The binding of eIF5A to non-target genes such as *ACT1* or *GAPDH* was similar to that of *GAL1*, which transcription is repressed under fermentative conditions. This suggests that certain level of eIF5A recruitment to chromatin may be independent on transcription. Interestingly, we observed a higher and significant binding of eIF5A to its target genes, such as *VRP1* or *BNR1*, compared to eIF5A-independent genes such as *ACT1* (approximately 2-fold signal).

Therefore, our results confirm that eIF5A is bound to chromatin, especially to the coding regions of target genes requiring this factor for their translation. However, we have not addressed yet if this binding is direct or indirect through other factors which might confer preferential binding over its targets.

A

Genes selected for eIF5A binding analysis

Gene	eIF5A-dependent motifs	PPP motifs	Protein Pause Index (PPI)	polyPro Index (PI)
Intergenic	0	0	0	0
GAL1	2	0	9	0
ACT1	2	0	7	0
GAPDH	2	0	7	0
BNR1	34	17	188	120
BNI1	39	21	217	148
VRP1	90	37	466	260

B

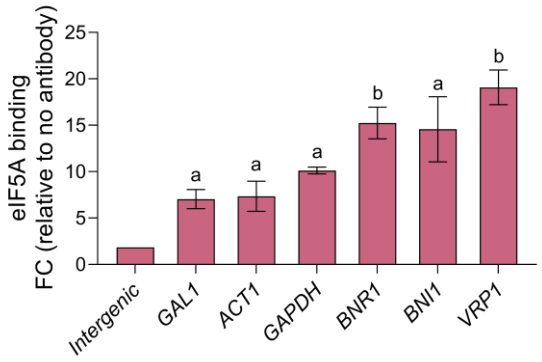

Figure 6.7. eIF5A binds to chromatin in wild-type cells. (A) Genes selected for eIF5A binding analysis by chromatin immunoprecipitation (ChIP). The number of eIF5A-dependent motifs and PPI/PI indexes are shown. (B) ChIP analysis of eIF5A recruitment in wild-type cells exponentially grown in YPD. ChIP of eIF5A was performed using an anti-eIF5A antibody. The immunoprecipitated DNA was used to quantify the different ORFs by qPCR (primers listed in Table A1.4). The percentage of the signal obtained in each ChIP sample with respect to the signal obtained with the DNA from the corresponding whole cell extract was calculated. Data are presented as the mean fold change (FC) relative to a sample without antibody ± SD from three independent experiments. Statistical significance was determined using a two-tailed paired Student's t-test relative to intergenic region-binding signal. When bars do not share any common letter (a,b), values are statistically different (p-value < 0.05).

Discussion of Chapter 6

Cytosolic translation and nuclear transcription are two major processes efficiently coordinated although separated in space and time. The intricate level of coordination allows the fine-tuning of gene expression and adaptation to changing conditions. The crosstalk between transcription and translation has been demonstrated for many cases but always in the direction from transcription to translation (Slobodin and Dikstein, 2020). This direct crosstalk is easier to understand because transcription precedes translation and can influence it by means of imprinting the transcribed mRNA by a plethora of possibilities.

Here, we have found that in addition to its widely known function in cytoplasmic translation, eIF5A also functions in transcriptional control. Our results demonstrate that the specificity of eIF5A is broad as it seems to be present on many chromatin loci. However, we found that eIF5A shows a preferential binding to those gene bodies which encode for eIF5A-dependent motifs and need this factor for their translation. eIF5A inactivation produces ribosome stalling in specific mRNAs encoding eIF5A-dependent motifs and also a substantial increase in RNA Pol II binding to target genes accompanied by a minor increase in their mRNA half-lives. This leads to an increase in the mRNA levels of genes encoding proteins requiring eIF5A for their translation (Figure 6.8). The results suggest a buffering mechanism in which eIF5A independently regulates transcription in a negative way and translation in a positive way. Thus, the nucleocytoplasmic role of eIF5A targets the same mRNAs encoding eIF5A-dependent motifs via transcription and translation to ensure right protein levels to meet cellular demands. Therefore, the new role of eIF5A in the nucleus uncovered here would avoid excess protein production of specific proteins through transcriptional attenuation. Although more evidence is needed to support this mechanism, it does reflect the need for tight mRNA synthesis for genes requiring eIF5A for their translation.

Importantly, our results identify a critical role of this translation factor in regulating mRNA synthesis in *Saccharomyces cerevisiae*. Previous connections on how translation elongation and mRNA turnover communicate have been made (Coller and Parker, 2004), but this crosstalk is incompletely understood. Features like ribosomes flux, amino acid identity, codon optimality, tRNA abundance or A site tRNA decoding kinetics have shown a direct relationship to mRNA decay in different model organisms (Presnyak *et al.*, 2015; Bazzini *et al.*, 2016; Weinberg *et al.*, 2016; Dave *et al.*, 2023). Translation elongation undergoes multiple quality control checkpoints. So, when cells encounter translation elongation difficulties the appropriate response is triggered (canonical mRNA turnover or problematic mRNA quality control). Slow or stalled ribosomes may lead to mRNA decay, ribosome rescue and nascent peptide degradation (Hanson and Coller, 2018; Collart and Weiss, 2020; Inada, 2020; D'Orazio and Green, 2021). The particular conformational state in which ribosomes are found and whether it can be resolved determines the kind of quality control pathway. Upon eIF5A depletion, the translation stalls at specific tripeptides within the ORF and leads to upstream ribosome collisions (Simms *et al.*, 2017). Here, the state of the leading ribosome involves the E site free while the P and A sites occupied by tRNAs charged with problematic amino acids which cannot form the peptide bond and the pause cannot be resolved (Figure 1.2). This unrotated state with the molecular signature of an occupied A site leads to a structural interface that seems to be non-compatible with ensuing the NGD (Buschauer *et al.*, 2020) and the RQC machineries for mRNA and peptide degradation respectively, which activate when the A site is free (Figure 1.13). In addition, eIF5A has recently been discovered as a key RQC factor necessary

to promote the elongation of the stalled peptide prior degradation (Tesina *et al.*, 2023). Therefore, these two features might explain the slight increase in mRNAs stabilities of eIF5A-dependent genes due to the absence of an upstream signal or an upstream factor that would ultimately coordinate the mRNA decay, peptide degradation and ribosome recycling.

Besides degradation, transcription of mRNAs influences the process of translation and multiple crosstalk factors coordinating both processes exist (Slobodin and Dikstein, 2020). For instance, the Rpb4/Rpb7 subunits of RNA Pol II associate with mature transcripts in the nucleus and accompany them to cytoplasm, where Rpb4 interacts with eIF3 to promote translation (Harel-Sharvit *et al.*, 2010; Dahan and Choder, 2013). From our results we cannot exclude the idea of a direct and specific crosstalk where the association of eIF5A to target genes allows eIF5A to function in translation, neither a reversal crosstalk communicating the translational status to transcriptional regulation. In a reversal crosstalk the upstream signal would be the eIF5A-dependent translation status and ribosome stalling would signal for transcription up-regulation of eIF5A-dependent genes. However, the idea that the functions of eIF5A in the cytoplasm and nucleus are dependent on each other has not been demonstrated herein and needs further research.

Our results suggest a dual and specific activity in attenuating transcription in the nucleus while promoting protein synthesis in the cytoplasm. In this line and consistent to other publications, eIF5A shuttles between the nucleus and cytoplasm in eukaryotic cells. The nuclear localization of yeast and mammalian eIF5A has been previously reported and is regulated via acetylation (Lee *et al.*, 2009). Additionally, the mammalian N-terminal extension contributes to its nuclear localization, although it does not display any structural similarity with classical nuclear localization signals (Parreiras-e-Silva *et al.*, 2007). eIF5A has been proposed to regulate the nucleocytoplasmic shuttling of retroviral Rev and Rex RNA transport factors (Hofmann *et al.*, 2001) and to interact with the exportins Xpo1 and Xpo4 in human cells (Rosorius *et al.*, 1999; Aksu *et al.*, 2016). eIF5A has also been described to specifically bind to importins KPNA1/2, KPNB1 and RanGTP in human cells (Smeltzer *et al.*, 2021). Among eukaryotic initiation factors (eIFs), eIF5A is not the only one found in the nucleus and cytoplasm. In fact, many components of the translation machinery have been found in cell nuclei in different organisms (Kachaev *et al.*, 2021). There, they are involved in genome integrity control, transcription, mRNA processing, mRNA export and cell stress response but the functional roles remain quite unclear. In human cells, the RNA Pol II has been found to interact with many eIFs (Kachaev *et al.*, 2021) and more recently with eIF5A (Rafiee *et al.*, 2023). Also, human eIF5A2 isoform binds to *HIF-1α* promoter and its overexpression is linked to higher *HIF-1α* levels under hypoxia (Li *et al.*, 2014). Hence, eIF5A arises as a moonlighting protein that may perform different nuclear and cytoplasmic roles, including transcriptional and translational control.

The structural features of eIF5A confirm its potential to interact with nucleic acids as it has a C-terminal domain which resembles an oligonucleotide-binding-fold domain, common in DNA- and RNA-binding proteins. Previous studies pointed to its function as an RNA-binding protein as it binds to extensive stem-loop RNA structures (Xu *et al.*, 2004) but also as a protein with RNAse activity in archaea (Bassani *et al.*, 2019). Although eIF5A is essential for cell survival and proliferation, its true physiological function has yet to be elucidated. Here, we proposed a function inside the nucleus as a potential transcriptional down-regulator of genes encoding proteins containing eIF5A-dependent tripeptides.

Thereby, the observed increase in transcription upon eIF5A depletion might be caused by the absence of its repressor function over the RNA Pol II elongating complex. In this line, we hypothesize that eIF5A could recognize specific regions present in the DNA or in the RNA sequences of its target genes, such as the CCn-rich sequences encoding polyPro stretches and attenuate their transcription. The presence of these sequences is the only common feature we have found among the eIF5A-dependent genes. Despite not many DNA- or RNA-binding proteins recognize specific sequences in gene (DNA or RNA) bodies, some examples have been described in the last years. This is the case with the RNA-binding proteins Nrd1 and Nab3, which recognize specific motifs in cryptic unstable transcripts and target them for premature transcription termination and RNA degradation (Arigo *et al.*, 2006; Thiebaut *et al.*, 2006). However, more evidence will be needed to clarify the molecular mechanism by which eIF5A mediates transcriptional control and if its nuclear function depends on the recruitment of other proteins to chromatin or on its post-translational modifications such as acetylation. The finding of a nuclear localization signal (NLS) in the yeast eIF5A protein and whether it binds to specific DNA or RNA consensus sequences, will shed light on the mechanism by which eIF5A works in the nucleus and modulates the transcription.

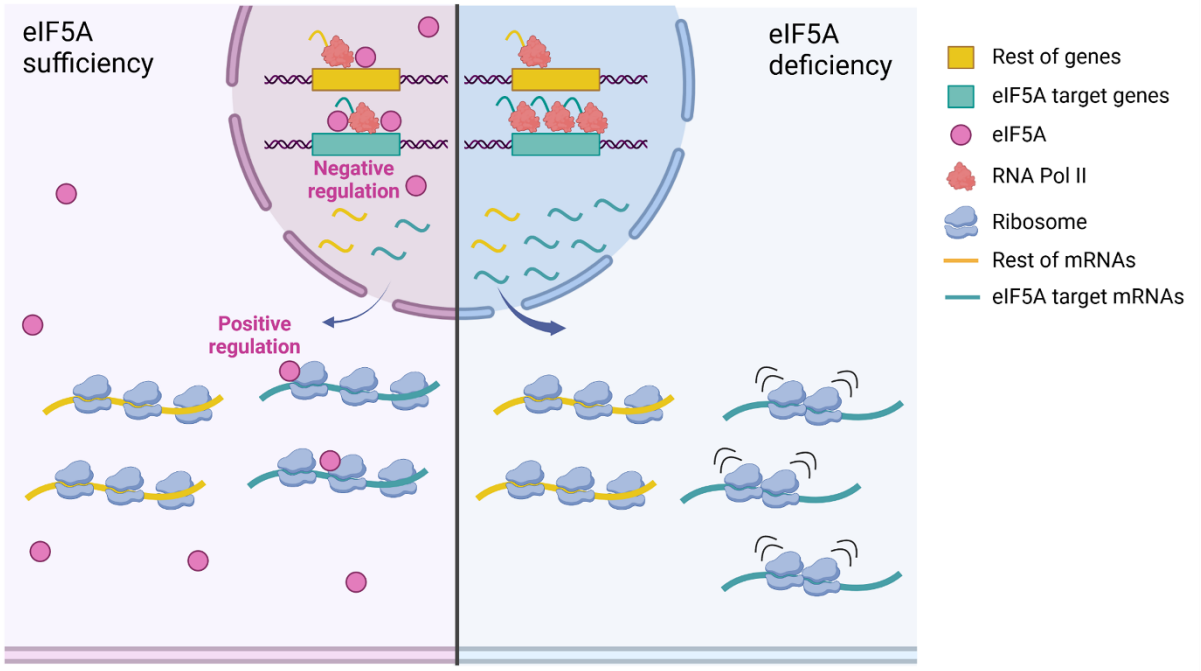

Figure 6.8. eIF5A attenuates the transcription of genes encoding eIF5A-translation dependent proteins. Under normal conditions, the translation factor eIF5A helps cytosolic translation elongation of proteins with eIF5A-dependent motifs in their sequences and rescues ribosome stalling. In addition, this factor is present in the nucleus most likely as an acetylated protein, where it binds and down-regulates transcription of eIF5A-dependent genes to tightly regulate mRNA synthesis and protein homeostasis. Under eIF5A deficiency conditions, translation of mRNAs requiring eIF5A for peptide synthesis stall. In parallel, there is a minor decrease in mRNA decay and a transcriptional induction of the so-called eIF5A-dependent genes without inducing global transcription. The transcriptional induction contributes to sustain higher mRNA levels of eIF5A-dependent genes that would try to compensate the decrease in protein synthesis.

Chapter 7

General Discussion and Conclusions

7.1 General Discussion

eIF5A is an essential and highly conserved eukaryotic translation factor with functions in the three stages of translation. eIF5A is activated by hypusination and is involved in a large number of cellular functions, most of them through its activity in translating specific peptide motifs containing combinations of proline, glycine and charged amino acids. In this thesis we have uncovered and characterized new features of eIF5A including its own gene expression regulation, novel targets and an additional basic function (Figure 7.1).

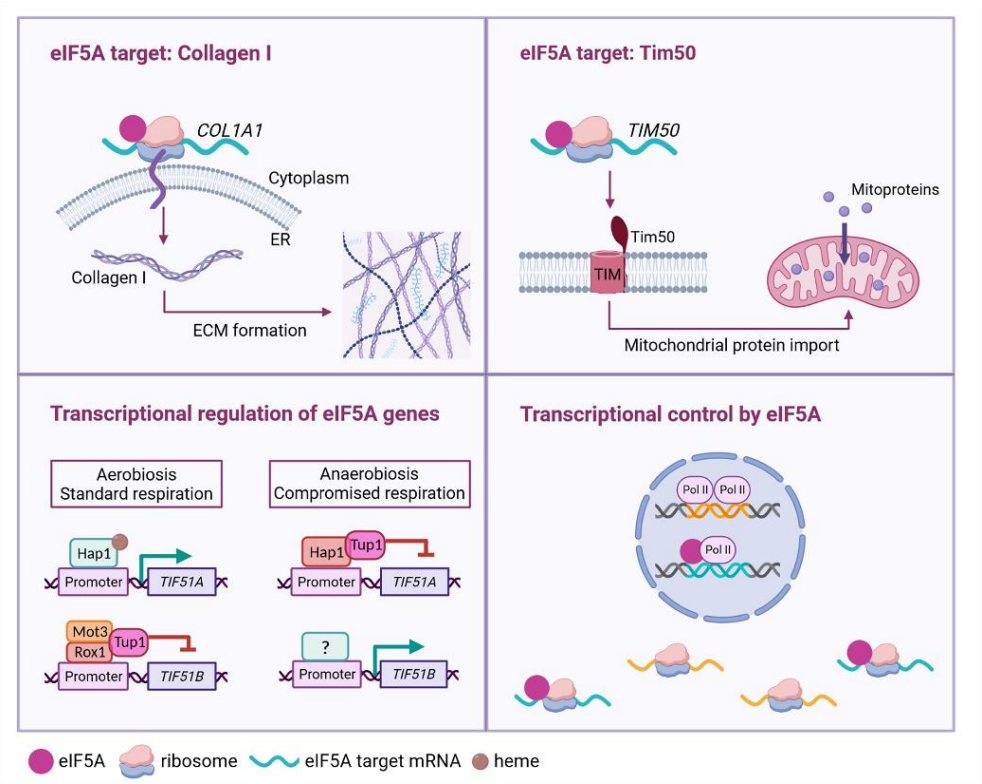

Figure 7.1. Functions of eIF5A described in this thesis. Hypusinated eIF5A is involved in the ER-coupled translation of collagenic motifs present in mammalian collagen I, which is essential for the formation of the extracellular matrix (top, left; Chapter 3). eIF5A is required for the translation of the proline-rich region of Tim50, a component of the mitochondrial inner membrane TIM23 complex, essential for the recognition of the mitochondrial precursor proteins. eIF5A impacts the mitochondrial protein import by modulating Tim50 levels (top, right; Chapter 5). The transcriptional regulation of the two yeast eIF5A isoforms has been determined under different metabolic conditions. Expression of the eIF5A genes is regulated via Hap1 in an opposite manner (bottom, left; Chapter 4). eIF5A binds to DNA in the nucleus and regulates the transcription of genes with eIF5A-dependent tripeptides. The specific molecular mechanism has not been outlined yet (bottom, right; Chapter 6).

In connection to its primary role in translation, eIF5A also localizes to the ER membrane and facilitates the co-translational translocation of some proteins into the ER (Rossi *et al.*, 2014). Here, we have described that hypusinated eIF5A is required for the translation of mammalian collagen I, the most abundant component of the extracellular matrix (Chapter 3). The interference of *eIF5A* and *DHPS* mRNAs as well as the inhibition of DHPS by GC7 treatment, causes ribosome stalling and reduces the co-translational insertion of collagen into the ER, and therefore, its synthesis. Importantly, the excessive production of collagen in a liver fibrosis human cell line is greatly reduced with GC7. However, additional *in vivo* experiments are still needed to confirm the role of eIF5A in the profibrotic progression and disease.

Fibrotic diseases contribute to one-third of human deaths worldwide (Wynn, 2008) and current treatment options are insufficient. Over the past decade, targeting the collagen biosynthesis and maturation pathway has emerged as an attractive therapy. Because collagen function depends on multiple synthesis steps from translation to secretion, there are many opportunities to intervene. The role of eIF5A as an essential factor acting in the upstream stages of collagen synthesis makes it a potential candidate to intervene in fibrotic diseases and other collagenopathies. Expanding the treatment to cancer might also be an attractive possibility as collagen is the major component of the tumour microenvironment and is extensively deposited to increase tumour stiffness and invasiveness (Yamauchi *et al.*, 2018). Overexpression of eIF5A2 isoform is common in cancer (Caraglia *et al.*, 2013; Ning *et al.*, 2020) and could be directly related to collagen production, among other functions, to promote metastasis. This could be of potential interest for future research as the control of eIF5A activity might have novel implications for therapeutic control of other diseases.

On the other hand, the gene expression regulation of eIF5A has been elucidated in this thesis (Chapter 4). We have found how the levels of the two yeast eIF5A isoforms are oppositely regulated by Hap1 to adapt to the mitochondrial functional status, with the Tif51A isoform expressed under respiration (respiratory/aerobic isoform) and the Tif51B isoform (fermentative/anaerobic isoform) expressed under fermentation. This opposite gene regulation resembles to that of the isoforms encoding the cytochrome c protein (*CYC1* and *CYC7*), in which oxygen/heme activates the expression of the aerobic isoform (*CYC1*) and represses the transcription of the hypoxic isoform (*CYC7*) (Zitomer and Lowry, 1992). In both gene pairs, there is a high degree of sequence homology between isoforms and no functional differences have been documented. The slight differences in the amino acids sequences of the two eIF5A isoforms probably gives rise to partially different cellular functions and advantages of one isoform over the other one to favour different cell metabolisms. Interestingly, the activity of the deoxyhypusine hydroxylase (DOHH) enzyme, the second enzyme of the hypusine pathway, is also regulated by oxygen. When the oxygen is limited, deoxyhypusine hydroxylation decreases and causes lower hypusinated eIF5A levels (Zhang *et al.*, 2022). Functional differences between the two eIF5A isoforms might be limited to DOHH activity so that when the oxygen concentration is low, Tif51B might behave as a more efficient substrate for hydroxylation than Tif51A. Although our preliminary oxygen consumption experiments under normoxic conditions show no differences between the two isoforms and indicate a compensatory phenomenon, it would be interesting to conduct these experiments under hypoxic conditions.

Hap1 activates *TIF51A* expression under standard respiratory conditions where the heme levels are high, while represses it when the respiratory process is compromised and heme levels drop (Chapter 4). However, humans lack an obvious Hap1 ortholog and *EIF5A1* expression is known to respond to KRas, p53 and NF-kappaB signalling pathways (Rahman-Roblick *et al.*, 2007; Chen *et al.*, 2014; Fujimura *et al.*, 2014). Nevertheless, synergistic action with other transcriptional regulators involved in mitochondrial biogenesis and respiration might be taking place. Conversely, the expression of the second isoform *TIF51B* was shown to respond to Hap1 indirectly, through the action of the two hypoxia gene repressors Rox1 and Mot3 causing in contrast to *TIF51A*, the induction of *TIF51B* expression under compromised respiratory conditions. Further studies are required to determine if additional transcription factors activate *TIF51B* in these conditions, as suggested in Chapter 4. In humans, the regulation of this second isoform, encoded by *EIF5A2*, is of particular importance, especially in the cancer context where, as mentioned above, it is often found overexpressed (Caraglia *et al.*, 2013; Ning *et al.*, 2020). *EIF5A2* is induced under hypoxia via hypoxia inducible factor 1α (HIF-1α) (Li *et al.*, 2014), and the activity of HIF-1α is, in turn, highly dependent on hypusinated eIF5A (Tariq *et al.*, 2016). In fact, eIF5A2 binds to *HIF-1α* promoter and correlates to higher mRNA levels under hypoxic conditions (Li *et al.*, 2014). Therefore, it would be an attractive possibility to explore whether eIF5A2 is acting as a direct transcriptional activator of RNA Pol II to induce *HIF-1α* expression or if it is controlling HIF-1α at the translation level as suggested by Tariq *et al.*, 2016. The presence of only two non-polyPro eIF5A-dependent tripeptide in its sequence makes its translational dependence less feasible. If demonstrated, the direct transcriptional regulation would prove that cancer cells partly employ the overexpression of *EIF5A2* to promote the adaptation to a hypoxic environment, a critical feature of the tumour microenvironment. These findings suggest an interdependence of the *EIF5A2* and HIF-1α proteins to function in hypoxia similar to the *EIF5A1* and p53 interdependence, where eIF5A translates p53 and p53 regulates *EIF5A1* transcription (Rahman-Roblick *et al.*, 2007; Martella *et al.*, 2020). According to our results and connected to this, the preferential use of *EIF5A2* over *EIF5A1* by cancer cells (Cao *et al.*, 2017) would support the use of fermentation instead of respiration for energy production, adapting in this way to the hypoxic conditions. Exploring whether the transcription factor Hap1 is regulated at translational level by eIF5A is of interest as well as it contains putative eIF5A-dependent tripeptides in its sequence. If confirmed, these results would point to common mechanisms for yeast and human cells in regard to the differential regulation of the two eIF5A isoforms to adapt to the oxygen content, although using transcription factors, Hap1 and HIF-1α, respectively, non-homologous in their amino acid sequence.

Findings from Chapter 4 highlight the relevance of eIF5A (Tif51A isoform) in maintaining the mitochondrial function. In the last years it has been proposed that eIF5A is necessary for the translation of specific mitoproteins with the specificity residing in the amino acid sequences at their N-terminal/MTS sequences, especially those ones with weak interactions with the peptide exit tunnel (Puleston *et al.*, 2019; Zhang *et al.*, 2022). In this thesis, we have deciphered a molecular mechanism by which eIF5A controls the mitochondrial activity (Chapter 5). eIF5A specifically impacts mitochondrial protein import by modulating Tim50 translation and thus, the activity of the TIM23 complex. In addition, translation of mitochondrial proteins was reduced upon eIF5A inactivation, which suggests the highly likely connection of the import status to the translation of mitoproteins that need to be translocated. Therefore, this novel mechanism of import control might be acting complementarily to

the already described ones, where the primary signal might be the decreased Tim50 activity. Then, the lower capacity for N-terminal/MTS recognition would cause a defective import and a decrease in the translation of proteins containing MTSs that need to be translocated into mitochondria. However, more work will be needed to decipher which are the specific molecular changes linking the clogging status of TIM23 complex and translation, which proteins act as sensors mediating this response or whether the import failure is the only and primary cause. The uniform translational attenuation of mitoproteins observed under eIF5A deficiency implies the driving of this effect by a common feature such as targeting signals, mRNA localization and/or translation in the mitochondrial surface or by a common factor such as the nascent chain-associated heterotrimeric complex (NAC), which binds to ribosomal exit tunnel during translation near the mitochondria (Gamerdinger *et al.*, 2019).

Recovery of Tim50 and TIM23 complex functionality using the eIF5A-independent Tim50ΔPro version was not sufficient to rescue the growth of eIF5A mutant in respiratory media nor to recover mitochondrial membrane potential. These results suggest that additional mechanisms involve eIF5A in maintaining the mitochondrial activity, so it is of interest to explore other putative mitochondrial targets with eIF5A-dependent motifs in their sequences. For instance, the protein Yta12 is part of the m-AAA protease located in the MIM and is a potential eIF5A target gene due to the presence of nine consecutive prolines in its sequence. Translation downregulation of this protein would cause defects in the assembly and degradation of proteins from complexes of the ETC and could also contribute to the observed phenotypes upon eIF5A depletion.

Human Tim50 has more prolines than yeast, but these are found scattered throughout the sequence rather than being consecutive. Thus, it would be of interest to address if this sequence organization is a true target for eIF5A. Besides, eIF5A deficiency and Tim50 down-regulation clogs translocases and generates cytosolic mitoprotein aggregates that cannot be translocated into the mitochondria (Chapter 5). Clogging of translocases and cytosolic deposition of mitochondrial precursors have been implicated in some neurodegenerative disorders. Aggregation of mitoproteins in cytosol increases misfolding of α-synuclein and amyloid precursor proteins, which are involved in Parkinson's and Alzheimer's diseases, as they can co-aggregate together, engage translocases and further increase the clogging hazard (Devi *et al.*, 2006; Cenini *et al.*, 2016; Di Maio *et al.*, 2016; Nowicka *et al.*, 2021). Therefore, human-derived samples from malignant tissues affected by neurodegenerative disorders could be tested to analyse the eIF5A levels and see if these are reduced. If this is the case, overexpression of eIF5A or spermidine supplementation could be beneficial to improve the mitochondrial protein import.

Finally, Chapter 6 uncovers a new basic function of eIF5A taking place in a different cellular organelle, the nucleus. Our findings show that eIF5A absence enhances transcription of genes carrying eIF5A-dependent motifs and that eIF5A itself binds to these genes ORFs. The details of the specific role that eIF5A may play in such transcription attenuation remain to be elucidated yet and many questions arise from these findings. eIF5A's structural features suggest its potential to interact with nucleic acids and its RNA-binding properties have already been described (Xu *et al.*, 2004). Therefore, further studies would be required to address whether eIF5A could specifically recognize specific regions present in the DNA or RNA sequences of its target genes, such as the CCn-rich sequences encoding polyPro stretches, and whether the action of eIF5A in the nucleus is through direct binding to RNA Pol II or if accessory proteins are required. Whether the nuclear function of eIF5A in transcriptional control is regulated via

acetylation is of interest as well and could be addressed by using a mutant version of the acetylation residue (Lys47).

Hence, eIF5A is confirmed as a moonlighting protein which, through its actions in the nucleus and cytoplasm, manages to tightly control the final protein levels to meet cellular demands (Chapter 6). Although our findings suggest independent roles of eIF5A in the nucleus and the cytoplasm, we cannot rule out the possibility of a crosstalk between transcription and translation. Up to now, most identified crosstalk factors have been described to connect the two processes in the direction of nuclear transcription to cytoplasmic translation (Slobodin and Dikstein, 2020). Our results, however, might suggest the possibility of a reverse direction where the translational state of some mRNAs would signal a specific repression of their nuclear genes. This is reminiscent of the attenuation mechanism found in bacteria for amino acid synthesis operons where the translational state of the mRNA controls the transcription elongation of the RNA polymerase (Yanofsky, 1981, 2000).

Furthermore, as the association of nuclear eIF5A to RNA Pol II has already been demonstrated in human cells (Rafiee *et al.*, 2023), it seems highly likely that eIF5A also binds to its target genes to control their transcription. As previously mentioned, the mammalian isoform eIF5A2 binds to *HIF-1α* promoter region under hypoxic conditions, whose expression activates target genes associated with hypoxia, angiogenesis, invasion and metastasis (Li *et al.*, 2014). According to the already described opposite regulation of the two yeast eIF5A isoforms (Chapter 4), studying whether Tif51B isoform is also nuclear when induced under hypoxic/anaerobic conditions, and if so, whether it affects transcription of target genes, perhaps of those involved in fermentative metabolism, is of relevance.

In conclusion, in this thesis we have described novel pleiotropic functions of the translation factor eIF5A. We have observed a plastic modulation of the two eIF5A isoforms by the cell to meet energy demands and to produce proteins with essential functions in metabolism and other cell processes. Beyond translation, eIF5A has a novel function to precisely control protein homeostasis through transcription and translation regulation.

7.2 Conclusions of this thesis

1. Hypusinated eIF5A is essential for collagen I synthesis as it is required for the translation of the Pro-Gly containing tripeptide motifs present in its amino acid sequence. Moreover, eIF5A facilitates collagen I co-translational translocation into the ER.
2. GC7 blockade of eIF5A greatly reduces the production of collagen I of human hepatic stellate cells (HSCs) under TGF-β1 activation *in vitro*. Hence, eIF5A emerges as a potential target to control the excessive collagen production in human fibrotic diseases.
3. The cellular metabolic status oppositely regulates the gene expression of the two yeast eIF5A isoforms through TORC1 signalling and Hap1-mediated mechanisms. Tif51A isoform is essential for the mitochondrial function and is therefore positively regulated to be the dominant form under respiratory conditions, whereas Tif51B is the abundant form under compromised respiration.
4. Hap1 is the master transcription factor regulating the expression of the two yeast eIF5A genes. Hap1 is constitutively bound to the *TIF51A* promoter to activate its expression under respiratory conditions and to repress it by recruiting the co-repressors Tup1/Ssn6 when respiration is compromised. Hap1 indirectly regulates *TIF51B* by directly activating *ROX1* and *MOT3* repressors under respiratory conditions. Under respiratory inhibition, Hap1 represses *ROX1* and *MOT3* using the Tup1 co-repressor and *TIF51B* becomes activated.
5. eIF5A impacts mitochondrial activity through the control of the mitochondrial protein import by modulating Tim50 translation and TIM23 complex activity. Under eIF5A deficiency, translocases become clogged and non-imported mitochondrial precursors aggregate in the cytosol.
6. Translation of mitochondrial proteins is attenuated when eIF5A levels are reduced. This overall decrease in translation suggests a mechanism linking the mRNA translation to the import of the corresponding proteins into the mitochondria.
7. eIF5A localizes to the nucleus where it is found engaged to chromatin to attenuate the transcription of genes encoding eIF5A-dependent tripeptides. Upon eIF5A inactivation, the transcription of these eIF5A-translation dependent genes is increased. Therefore, eIF5A functions as a moonlighting protein acting in the nucleus and cytoplasm to precisely control the final protein levels of its targets.

References

Aksu, M., Trakhanov, S., & Görlich, D. (2016). Structure of the exportin Xpo4 in complex with RanGTP and the hypusine-containing translation factor eIF5A. *Nature Communications, 7*, 11952.

Aoki, H., Xu, J., Emili, A., Chosay, J. G., Golshani, A., & Ganoza, M. C. (2008). Interactions of elongation factor EF-P with the Escherichia coli ribosome. *The FEBS journal, 275*, 671-681.

Arigo, J. T., Eyler, D. E., Carroll, K. L., & Corden, J. L. (2006). Termination of cryptic unstable transcripts is directed by yeast RNA-binding proteins Nrd1 and Nab3. *Molecular cell, 23*, 841-851.

Arseni, L., Lombardi, A., & Orioli, D. (2018). From structure to phenotype: impact of collagen alterations on human health. *International journal of molecular sciences, 19*, 1407.

Balaban, R. S., Nemoto, S., & Finkel, T. (2005). *Mitochondria, oxidants, and aging. cell, 120*, 483-495.

Balukoff, N. C., Ho, J. D., Theodoridis, P. R., Wang, M., Bokros, M., Llanio, L. M., & Lee, S. (2020). A translational program that suppresses metabolism to shield the genome. *Nature communications, 11*, 5755.

Barba-Aliaga, M., & Alepuz, P. (2022). Role of eIF5A in mitochondrial function. *International Journal of Molecular Sciences, 23*, 1284.

Barba-Aliaga, M., & Alepuz, P. (2022). The activator/repressor Hap1 binds to the yeast eIF5A-encoding gene TIF51A to adapt its expression to the mitochondrial functional status. *FEBS letters, 596*, 1809-1826.

Barba-Aliaga, M., Mena, A., Espinoza, V., Apostolova, N., Costell, M., & Alepuz, P. (2021). Hypusinated eIF5A is required for the translation of collagen. *Journal of Cell Science, 134*, jcs258643.

Barba-Aliaga, M., Villarroel-Vicente, C., Stanciu, A., Corman, A., Martínez-Pastor, M. T., & Alepuz, P. (2020). Yeast translation elongation factor eIF5A expression is regulated by nutrient availability through different signalling pathways. *International Journal of Molecular Sciences, 22*, 219.

Bassani, F., Zink, I. A., Pribasnig, T., Wolfinger, M. T., Romagnoli, A., Resch, A., & La Teana, A. (2019). Indications for a moonlighting function of translation factor aIF5A in the crenarchaeum Sulfolobus solfataricus. *RNA biology, 16*, 675-685.

Bazzini, A. A., Del Viso, F., Moreno-Mateos, M. A., Johnstone, T. G., Vejnar, C. E., Qin, Y., & Giraldez, A. J. (2016). Codon identity regulates mRNA stability and translation efficiency during the maternal-to-zygotic transition. *The EMBO journal, 35*, 2087-2103.

Begley, V., Corzo, D., Jordán-Pla, A., Cuevas-Bermudez, A., Miguel-Jiménez, L. D., Pérez-Aguado, D., Machuca-Ostos, M., Navarro, F., Chávez, M.J., Pérez-Ortín, J.E., & Chávez, S. (2019). The mRNA degradation factor Xrn1 regulates transcription elongation in parallel to Ccr4. *Nucleic Acids Research, 47*, 9524-9541.

Bengtson, M. H., & Joazeiro, C. A. (2010). Role of a ribosome-associated E3 ubiquitin ligase in protein quality control. *Nature, 467*, 470-473.

Benito-Jardon, M., Klapproth, S., Gimeno-LLuch, I., Petzold, T., Bharadwaj, M., Müller, D. J., Zuchtriegel, G., Reichel, C. A. & Costell, M. (2017). The fibronectin synergy site re-enforces cell adhesion and mediates a crosstalk between integrin classes. *Elife, 6*, e22264.

Benne, R., Brown-Luedi, M. L., & Hershey, J. W. (1978). Purification and characterization of protein synthesis initiation factors eIF-1, eIF-4C, eIF-4D, and eIF-5 from rabbit reticulocytes. *Journal of Biological Chemistry, 253*, 3070-3077.

Blasco-Moreno, B., de Campos-Mata, L., Böttcher, R., García-Martínez, J., Jungfleisch, J., Nedialkova, D. D., Chattopadhyay, S., Gas, M., Oliva, B., Pérez-Ortín, J. E., Leidel, S. A., Choder, M., & Díez, J. (2019). The exonuclease Xrn1 activates transcription and translation of mRNAs encoding membrane proteins. *Nature communications, 10*, 1298.

Boengler, K., Kosiol, M., Mayr, M., Schulz, R., & Rohrbach, S. (2017). Mitochondria and ageing: role in heart, skeletal muscle and adipose tissue. *Journal of cachexia, sarcopenia and muscle, 8*, 349-369.

Boon, K., Caron, H. N., Van Asperen, R., Valentijn, L., Hermus, M. C., Van Sluis, P., & Versteeg, R. (2001). N-myc enhances the expression of a large set of genes functioning in ribosome biogenesis and protein synthesis. *The EMBO journal, 20*, 1383-1393.

Boos, F., Krämer, L., Groh, C., Jung, F., Haberkant, P., Stein, F., Gackstatter, A., Zöller, E., Van der Laan, M., Savitski, M. M., Benes, V., & Herrmann, J. M. (2019). Mitochondrial protein-induced stress triggers a global adaptive transcriptional programme. *Nature cell biology, 21*, 442-451.

Boos, F., Labbadia, J., & Herrmann, J. M. (2020). How the mitoprotein-induced stress response safeguards the cytosol: a unified view. *Trends in cell biology, 30*, 241-254.

Borst, P., & Grivell, L. A. (1978). The mitochondrial genome of yeast. *Cell, 15*, 705-723.

Bouchez, C. L., Yoboue, E. D., de la Rosa Vargas, L. E., Salin, B., Cuvellier, S., Rigoulet, M., & Devin, A. (2020). "Labile" heme critically regulates mitochondrial biogenesis through the transcriptional co-activator Hap4p in Saccharomyces cerevisiae. *Journal of Biological Chemistry, 295*, 5095-5109.

Brandman, O., & Hegde, R. S. (2016). Ribosome-associated protein quality control. *Nature structural & molecular biology, 23*, 7-15.

Brodsky, B., & Persikov, A. V. (2005). Molecular structure of the collagen triple helix. *Advances in protein chemistry, 70,* 301-339.

Brodsky, B., & Ramshaw, J. A. (2017). Bioengineered collagens. *Fibrous Proteins: Structures and Mechanisms*, 601-629.

Buschauer, R., Matsuo, Y., Sugiyama, T., Chen, Y. H., Alhusaini, N., Sweet, T., Ikeuchi, K., Cheng, J., Matsuki, Y., Nobuta, R., Gilmozzi, A., Berninghausen, O., Tesina, P., Becker, T., Coller, J., Inada, T., & Beckmann, R. (2020). The Ccr4-Not complex monitors the translating ribosome for codon optimality. *Science, 368,* eaay6912.

Buttgereit, F., & Brand, M. D. (1995). A hierarchy of ATP-consuming processes in mammalian cells. *Biochemical Journal, 312*, 163-167.

Bykov, Y. S., Rapaport, D., Herrmann, J. M., & Schuldiner, M. (2020). Cytosolic events in the biogenesis of mitochondrial proteins. *Trends in biochemical sciences, 45*, 650-667.

Cao, T. T., Lin, S. H., Fu, L., Tang, Z., Che, C. M., Zhang, L. Y., & Guan, X. Y. (2017). Eukaryotic translation initiation factor 5A2 promotes metabolic reprogramming in hepatocellular carcinoma cells. *Carcinogenesis, 38*, 94-104.

Caraglia, M., Park, M. H., Wolff, E. C., Marra, M., & Abbruzzese, A. (2013). eIF5A isoforms and cancer: two brothers for two functions?. *Amino acids, 44*, 103-109.

Cardenas, M. E., Cutler, N. S., Lorenz, M. C., Di Como, C. J., & Heitman, J. (1999). The TOR signaling cascade regulates gene expression in response to nutrients. *Genes & development, 13*, 3271-3279.

Cenini, G., Rüb, C., Bruderek, M., & Voos, W. (2016). Amyloid β-peptides interfere with mitochondrial preprotein import competence by a coaggregation process. *Molecular biology of the cell, 27*, 3257-3272.

Charneski, C. A., & Hurst, L. D. (2013). Positively charged residues are the major determinants of ribosomal velocity. *PLoS biology, 11*, e1001508.

Chatterjee, I., Gross, S. R., Kinzy, T. G., & Chen, K. Y. (2006). Rapid depletion of mutant eukaryotic initiation factor 5A at restrictive temperature reveals connections to actin cytoskeleton and cell cycle progression. *Molecular genetics and genomics, 275*, 264-276.

Chattopadhyay, M. K., Park, M. H., & Tabor, H. (2008). Hypusine modification for growth is the major function of spermidine in Saccharomyces cerevisiae polyamine auxotrophs grown in limiting spermidine. *Proceedings of the National Academy of Sciences, 105*, 6554-6559.

Chaudhuri, M., Tripathi, A., & Gonzalez, F. S. (2021). Diverse functions of Tim50, a component of the mitochondrial inner membrane protein translocase. *International Journal of Molecular Sciences, 22*, 7779.

Chen, D. J., Xu, Y. M., Du, J. Y., Huang, D. Y., & Lau, A. T. (2014). Cadmium induces cytotoxicity in human bronchial epithelial cells through upregulation of eIF5A1 and NF-kappaB. *Biochemical and biophysical research communications, 445*, 95-99.

Chen, Z. P., Yan, Y. P., Ding, Q. J., Knapp, S., Potenza, J. A., Schugar, H. J., & Chen, K. Y. (1996). Effects of inhibitors of deoxyhypusine synthase on the differentiation of mouse neuroblastoma and erythroleukemia cells. *Cancer letters, 105*, 233-239.

Christiano, R., Nagaraj, N., Fröhlich, F., & Walther, T. C. (2014). Global proteome turnover analyses of the yeasts S. cerevisiae and S. pombe. *Cell reports, 9*, 1959-1965.

Chu, D., Barnes, D. J., & Von Der Haar, T. (2011). The role of tRNA and ribosome competition in coupling the expression of different mRNAs in Saccharomyces cerevisiae. *Nucleic acids research, 39*, 6705-6714.

Clement, P. M., Johansson, H. E., Wolff, E. C., & Park, M. H. (2006). Differential expression of eIF5A-1 and eIF5A-2 in human cancer cells. *The FEBS journal, 273*, 1102-1114.

Collart, M. A. (2016). The Ccr4-Not complex is a key regulator of eukaryotic gene expression. *Wiley Interdisciplinary Reviews: RNA, 7*, 438-454.

Collart, M. A., & Weiss, B. (2020). Ribosome pausing, a dangerous necessity for co-translational events. *Nucleic acids research, 48*, 1043-1055.

Coller, H. A., Grandori, C., Tamayo, P., Colbert, T., Lander, E. S., Eisenman, R. N., & Golub, T. R. (2000). Expression analysis with oligonucleotide microarrays reveals that MYC regulates genes involved in growth, cell cycle, signaling, and adhesion. *Proceedings of the National Academy of Sciences, 97*, 3260-3265.

Coller, J., & Parker, R. (2004). Eukaryotic mRNA decapping. *Annual review of biochemistry, 73*, 861-890.

Coni, S., Serrao, S. M., Yurtsever, Z. N., Di Magno, L., Bordone, R., Bertani, C., & Canettieri, G. (2020). Blockade of EIF5A hypusination limits colorectal cancer growth by inhibiting MYC elongation. *Cell death & disease, 11*, 1045.

Conrad, M., Schothorst, J., Kankipati, H. N., Van Zeebroeck, G., Rubio-Texeira, M., & Thevelein, J. M. (2014). Nutrient sensing and signaling in the yeast Saccharomyces cerevisiae. *FEMS microbiology reviews, 38*, 254-299.

Cracchiolo, B. M., Heller, D. S., Clement, P. M., Wolff, E. C., Park, M. H., & Hanauske-Abel, H. M. (2004). Eukaryotic initiation factor 5A-1 (eIF5A-1) as a diagnostic marker for aberrant proliferation in intraepithelial neoplasia of the vulva. *Gynecologic oncology, 94*, 217-222.

Dahan, N., & Choder, M. (2013). The eukaryotic transcriptional machinery regulates mRNA translation and decay in the cytoplasm. *Biochimica et Biophysica Acta (BBA)-Gene Regulatory Mechanisms, 1829*, 169-173.

Dave, P., Roth, G., Griesbach, E., Mateju, D., Hochstoeger, T., & Chao, J. A. (2023). Single-molecule imaging reveals translation-dependent destabilization of mRNAs. *Molecular Cell, 83*, 589-606.

De Minicis, S., Seki, E., Uchinami, H., Kluwe, J., Zhang, Y., Brenner, D. A., & Schwabe, R. F. (2007). Gene expression profiles during hepatic stellate cell activation in culture and in vivo. *Gastroenterology, 132*, 1937-1946.

DeRisi, J. L., Iyer, V. R., & Brown, P. O. (1997). Exploring the metabolic and genetic control of gene expression on a genomic scale. *Science, 278*, 680-686.

Devi, L., Prabhu, B. M., Galati, D. F., Avadhani, N. G., & Anandatheerthavarada, H. K. (2006). Accumulation of amyloid precursor protein in the mitochondrial import channels of human Alzheimer's disease brain is associated with mitochondrial dysfunction. *Journal of Neuroscience, 26*, 9057-9068.

Dever, T. E., Dinman, J. D., & Green, R. (2018). Translation elongation and recoding in eukaryotes. *Cold Spring Harbor perspectives in biology, 10*, a032649.

Di Maio, R., Barrett, P. J., Hoffman, E. K., Barrett, C. W., Zharikov, A., Borah, A., & Greenamyre, J. T. (2016). α-Synuclein binds to TOM20 and inhibits mitochondrial protein import in Parkinson's disease. *Science translational medicine, 8*, 342ra78-342ra78.

Dimmer, K. S. (2014). Fluorescence Staining of Mitochondria for morphology analysis in Saccharomyces cerevisiae. *Yeast Protocols*, 131-152.

Doerfel, L. K., Wohlgemuth, I., Kothe, C., Peske, F., Urlaub, H., & Rodnina, M. V. (2013). EF-P is essential for rapid synthesis of proteins containing consecutive proline residues. *Science, 339*, 85-88.

Doma, M. K., & Parker, R. (2006). Endonucleolytic cleavage of eukaryotic mRNAs with stalls in translation elongation. *Nature, 440*, 561-564.

D'Orazio, K. N., & Green, R. (2021). Ribosome states signal RNA quality control. *Molecular cell, 81*, 1372-1383.

D'Orazio, K. N., Wu, C. C. C., Sinha, N., Loll-Krippleber, R., Brown, G. W., & Green, R. (2019). The endonuclease Cue2 cleaves mRNAs at stalled ribosomes during No Go Decay. *Elife, 8*, e49117.

Eisenberg, T., Knauer, H., Schauer, A., Büttner, S., Ruckenstuhl, C., Carmona-Gutierrez, D., Ring, J., Schroede, S., Magnes, C., Antonacci, L., Fussi, H., Deszcz, L., Hartl, R., Schraml. E., Criollo, A., Megalou, E., Weiskopf, D., Laun, P., Heeren, G., Breitenbach, M., Grubeck-Loebenstein, B., Herker, E., Fahrenkrog, B., Sinner, F., Tavernarakis, N., Minois, N., Kroemer, G., & Madeo, F. (2009). Induction of autophagy by spermidine promotes longevity. *Nature cell biology, 11*, 1305-1314.

Eisenberg, T., Abdellatif, M., Schroeder, S., Primessnig, U., Stekovic, S., Pendl, T., & Madeo, F. (2016). Cardioprotection and lifespan extension by the natural polyamine spermidine. *Nature medicine, 22*, 1428-1438.

Eliyahu, E., Pnueli, L., Melamed, D., Scherrer, T., Gerber, A. P., Pines, O., & Arava, Y. (2010). Tom20 mediates localization of mRNAs to mitochondria in a translation-dependent manner. *Molecular and cellular biology, 30*, 284-294.

Esteves, P., Dard, L., Brillac, A., Hubert, C., Sarlak, S., Rousseau, B., & Rossignol, R. (2020). Nuclear control of lung cancer cells migration, invasion and bioenergetics by eukaryotic translation initiation factor 3F. *Oncogene, 39*, 617-636.

Fang, L., Gao, L., Xie, L., & Xiao, G. (2018). Eukaryotic translation initiation factor 5A-2 involves in doxorubicin-induced epithelial-mesenchymal transition in oral squamous cell carcinoma cells. *Journal of Cancer, 9*, 3479.

Faundes, V., Jennings, M. D., Crilly, S., Legraie, S., Withers, S. E., Cuvertino, S., & Banka, S. (2021). Impaired eIF5A function causes a Mendelian disorder that is partially rescued in model systems by spermidine. *Nature communications, 12*, 833.

Fazal, F. M., Han, S., Parker, K. R., Kaewsapsak, P., Xu, J., Boettiger, A. N., & Ting, A. Y. (2019). Atlas of subcellular RNA localization revealed by APEX-Seq. *Cell, 178*, 473-490.

Fendt, S. M., & Sauer, U. (2010). Transcriptional regulation of respiration in yeast metabolizing differently repressive carbon substrates. *BMC systems biology, 4*, 1-11.

Filipuzzi, I., Steffen, J., Germain, M., Goepfert, L., Conti, M. A., Potting, C., Cerino, R., Pfeifer, M., Krastel, P., Hoepfner, P., Bastien, J., Koehler, C., & Helliwell, S. B. (2017). Stendomycin selectively inhibits TIM23-dependent mitochondrial protein import. *Nature chemical biology, 13*, 1239-1244.

Fleming, A. B., Beggs, S., Church, M., Tsukihashi, Y., & Pennings, S. (2014). The yeast Cyc8–Tup1 complex cooperates with Hda1p and Rpd3p histone deacetylases to robustly repress transcription of the subtelomeric FLO1 gene. *Biochimica et Biophysica Acta (BBA)-Gene Regulatory Mechanisms, 1839*, 1242-1255.

Forlino, A., & Marini, J. C. (2016). Osteogenesis imperfecta. *The Lancet, 387*, 1657-1671.

Forsburg, S. L., & Guarente, L. (1989). Identification and characterization of HAP4: a third component of the CCAAT-bound HAP2/HAP3 heteromer. *Genes & development, 3*, 1166-1178.

Frantz, C., Stewart, K. M., & Weaver, V. M. (2010). The extracellular matrix at a glance. *Journal of cell science, 123*, 4195-4200.

Friedman, S. L., Sheppard, D., Duffield, J. S., & Violette, S. (2013). Therapy for fibrotic diseases: nearing the starting line. *Science translational medicine, 5*, 167sr1-167sr1.

Fujimura, K., Choi, S., Wyse, M., Strnadel, J., Wright, T., & Klemke, R. (2015). Eukaryotic translation initiation factor 5A (EIF5A) regulates pancreatic cancer metastasis by modulating RhoA and Rho-associated kinase (ROCK) protein expression levels. *Journal of Biological Chemistry, 290*, 29907-29919.

Fujimura, K., Wright, T., Strnadel, J., Kaushal, S., Metildi, C., Lowy, A. M., & Klemke, R. L. (2014). A hypusine–eIF5A–PEAK1 switch regulates the pathogenesis of pancreatic cancer. *Cancer research, 74*, 6671-6681.

Galdieri, L., Mehrotra, S., Yu, S., & Vancura, A. (2010). Transcriptional regulation in yeast during diauxic shift and stationary phase. *Omics: a journal of integrative biology, 14*, 629-638.

Gamerdinger, M., Kobayashi, K., Wallisch, A., Kreft, S. G., Sailer, C., Schlömer, R., & Deuerling, E. (2019). Early scanning of nascent polypeptides inside the ribosomal tunnel by NAC. *Molecular cell, 75*, 996-1006.

Ganapathi, M., Padgett, L. R., Yamada, K., Devinsky, O., Willaert, R., Person, R., Au, P.-Y. B., Tagoe, J., McDonald, M., Karlowicz, D. & Chung, W. K. (2019). Recessive rare variants

in deoxyhypusine synthase, an enzyme involved in the synthesis of hypusine, are associated with a neurodevelopmental disorder. The American Journal of Human *Genetics, 104*, 287-298.

Gancedo, J. M. (1998). Yeast carbon catabolite repression. *Microbiology and molecular biology reviews, 62*, 334-361.

Gao, S. P., Sun, H. F., Jiang, H. L., Li, L. D., Hu, X., Xu, X. E., & Jin, W. (2016). Loss of TIM50 suppresses proliferation and induces apoptosis in breast cancer. *Tumor Biology, 37*, 1279-1287.

García-Martínez, J., Aranda, A., & Pérez-Ortın, J. E. (2004). Genomic run-on evaluates transcription rates for all yeast genes and identifies gene regulatory mechanisms. *Molecular cell, 15*, 303-313.

García-Martínez, J., Delgado-Ramos, L., Ayala, G., Pelechano, V., Medina, D. A., Carrasco, F., González, R., Andrés-León, E., Steinmetz, L., Warringer, J., Chávez, S., & Pérez-Ortín, J. E. (2016). The cellular growth rate controls overall mRNA turnover, and modulates either transcription or degradation rates of particular gene regulons. *Nucleic acids research, 44*, 3643-3658.

García-Martínez, J., Pérez-Martínez, M. E., Pérez-Ortín, J. E., & Alepuz, P. (2021). Recruitment of Xrn1 to stress-induced genes allows efficient transcription by controlling RNA polymerase II backtracking. *RNA biology, 18*, 1458-1474.

García-Rodríguez, L. J., Gay, A. C., & Pon, L. A. (2007). Puf3p, a Pumilio family RNA binding protein, localizes to mitochondria and regulates mitochondrial biogenesis and motility in budding yeast. *The Journal of cell biology, 176*, 197-207.

Garzia, A., Jafarnejad, S. M., Meyer, C., Chapat, C., Gogakos, T., Morozov, P., & Sonenberg, N. (2017). The E3 ubiquitin ligase and RNA-binding protein ZNF598 orchestrates ribosome quality control of premature polyadenylated mRNAs. *Nature communications, 8*, 16056.

Gardin, J., Yeasmin, R., Yurovsky, A., Cai, Y., Skiena, S., & Futcher, B. (2014). Measurement of average decoding rates of the 61 sense codons in vivo. *Elife, 3*, e03735.

Garí, E., Piedrafita, L., Aldea, M., & Herrero, E. (1997). A set of vectors with a tetracycline-regulatable promoter system for modulated gene expression in Saccharomyces cerevisiae. *Yeast, 13*, 837-848.

Garre, E., Romero-Santacreu, L., De Clercq, N., Blasco-Angulo, N., Sunnerhagen, P., & Alepuz, P. (2012). Yeast mRNA cap-binding protein Cbc1/Sto1 is necessary for the rapid reprogramming of translation after hyperosmotic shock. *Molecular biology of the cell, 23*, 137-150.

Garre, E., Romero-Santacreu, L., Barneo-Munoz, M., Miguel, A., Perez-Ortin, J. E., & Alepuz, P. (2013). Nonsense-mediated mRNA decay controls the changes in yeast ribosomal protein pre-mRNAs levels upon osmotic stress. *PLoS One, 8*, e61240.

Gates, S. N., Yokom, A. L., Lin, J., Jackrel, M. E., Rizo, A. N., Kendsersky, N. M., & Southworth, D. R. (2017). Ratchet-like polypeptide translocation mechanism of the AAA+ disaggregase Hsp104. *Science, 357*, 273-279.

Gawron, K. (2016). Endoplasmic reticulum stress in chondrodysplasias caused by mutations in collagen types II and X. *Cell Stress and Chaperones, 21*, 943-958.

Geisberg, J. V., Moqtaderi, Z., Fan, X., Ozsolak, F., & Struhl, K. (2014). Global analysis of mRNA isoform half-lives reveals stabilizing and destabilizing elements in yeast. *Cell, 156*, 812-824.

Gevorkyan-Airapetov, L., Zohary, K., Popov-Čeleketić, D., Mapa, K., Hell, K., Neupert, W., & Mokranjac, D. (2009). Interaction of Tim23 with Tim50 is essential for protein translocation by the mitochondrial TIM23 complex. *Journal of Biological Chemistry, 284*, 4865-4872.

Gietz, D., St Jean, A., Woods, R. A., & Schiestl, R. H. (1992). Improved method for high efficiency transformation of intact yeast cells. *Nucleic acids research, 20*, 1425.

Giraud, S., Kerforne, T., Zely, J., Ameteau, V., Couturier, P., Tauc, M., & Hauet, T. (2020). The inhibition of eIF5A hypusination by GC7, a preconditioning protocol to prevent brain death-induced renal injuries in a preclinical porcine kidney transplantation model. *American Journal of Transplantation, 20*, 3326-3340.

Gold, V. A., Chroscicki, P., Bragoszewski, P., & Chacinska, A. (2017). Visualization of cytosolic ribosomes on the surface of mitochondria by electron cryo-tomography. *EMBO reports, 18*, 1786-1800.

Gregio, A. P., Cano, V. P., Avaca, J. S., Valentini, S. R., & Zanelli, C. F. (2009). eIF5A has a function in the elongation step of translation in yeast. *Biochemical and biophysical research communications, 380*, 785-790.

Guan, X. Y., Sham, J. S., Tang, T. C., Fang, Y., Huo, K. K., & Yang, J. M. (2001). Isolation of a novel candidate oncogene within a frequently amplified region at 3q26 in ovarian cancer. *Cancer research, 61*, 3806-3809.

Gutierrez, E., Shin, B. S., Woolstenhulme, C. J., Kim, J. R., Saini, P., Buskirk, A. R., & Dever, T. E. (2013). eIF5A promotes translation of polyproline motifs. *Molecular cell, 51*, 35-45.

Haastrup, M. O., Vikramdeo, K. S., Singh, S., Singh, A. P., & Dasgupta, S. (2023). The Journey of Mitochondrial Protein Import and the Roadmap to Follow. *International Journal of Molecular Sciences, 24*, 2479.

Hach, A., Hon, T., & Zhang, L. (1999). A new class of repression modules is critical for heme regulation of the yeast transcriptional activator Hap1. *Molecular and cellular biology, 19*, 4324-4333.

Haimovich, G., Medina, D. A., Causse, S. Z., Garber, M., Millán-Zambrano, G., Barkai, O., Chávez, S., Pérez-Ortín, J.E., Darzacq, X., & Choder, M. (2013). Gene expression is circular: factors for mRNA degradation also foster mRNA synthesis. *Cell, 153*, 1000-1011.

Han, P., Shichino, Y., Schneider-Poetsch, T., Mito, M., Hashimoto, S., Udagawa, T., & Iwasaki, S. (2020). Genome-wide survey of ribosome collision. *Cell Reports, 31*, 107610.

Hanauske-Abel, H. M., Park, M. H., Hanauske, A. R., Popowicz, A. M., Lalande, M., & Folk, J. E. (1994). Inhibition of the G1-S transition of the cell cycle by inhibitors of deoxyhypusine hydroxylation. *Biochimica et Biophysica Acta (BBA)-Molecular Cell Research, 1221*, 115-124.

Hanawa-Suetsugu, K., Sekine, S. I., Sakai, H., Hori-Takemoto, C., Terada, T., Unzai, S., & Yokoyama, S. (2004). Crystal structure of elongation factor P from Thermus thermophilus HB8. *Proceedings of the National Academy of Sciences, 101*, 9595-9600.

Hansen, K. G., & Herrmann, J. M. (2019). Transport of proteins into mitochondria. *The Protein Journal, 38*, 330-342.

Hanson, G., & Coller, J. (2018). Codon optimality, bias and usage in translation and mRNA decay. *Nature reviews Molecular cell biology, 19*, 20-30.

Hardwick, J. S., Kuruvilla, F. G., Tong, J. K., Shamji, A. F., & Schreiber, S. L. (1999). Rapamycin-modulated transcription defines the subset of nutrient-sensitive signaling pathways directly controlled by the Tor proteins. *Proceedings of the National Academy of Sciences, 96*, 14866-14870.

Harel-Sharvit, L., Eldad, N., Haimovich, G., Barkai, O., Duek, L., & Choder, M. (2010). RNA polymerase II subunits link transcription and mRNA decay to translation. *Cell, 143*, 552-563.

Harigaya, Y., & Parker, R. (2016). Analysis of the association between codon optimality and mRNA stability in Schizosaccharomyces pombe. *BMC genomics, 17*, 1-16.

Hazra, S., Miyahara, T., Rippe, R. A., & Tsukamoto, H. (2004). PPAR gamma and hepatic stellate cells. *Comparative Hepatology, 3*, 1-3.

Healy, S. J., Gorman, A. M., Mousavi-Shafaei, P., Gupta, S., & Samali, A. (2009). Targeting the endoplasmic reticulum-stress response as an anticancer strategy. *European journal of pharmacology, 625*, 234-246.

Hedbacker, K., & Carlson, M. (2008). SNF1/AMPK pathways in yeast. *Frontiers in bioscience: a journal and virtual library, 13*, 2408.

Hetz, C., Zhang, K., & Kaufman, R. J. (2020). Mechanisms, regulation and functions of the unfolded protein response. *Nature reviews Molecular cell biology, 21*, 421-438.

Hickman, M. J., & Winston, F. (2007). Heme levels switch the function of Hap1 of Saccharomyces cerevisiae between transcriptional activator and transcriptional repressor. *Molecular and cellular biology, 27*, 7414-7424.

Hill, S. M., Hanzén, S., & Nyström, T. (2017). Restricted access: spatial sequestration of damaged proteins during stress and aging. *EMBO reports, 18*, 377-391.

Hofer, S. J., Liang, Y., Zimmermann, A., Schroeder, S., Dengjel, J., Kroemer, G., Eisenberg, T., Sigrist, S., & Madeo, F. (2021). Spermidine-induced hypusination preserves mitochondrial and cognitive function during aging. *Autophagy, 17*, 2037-2039.

Hofmann, W., Reichart, B., Ewald, A., Müller, E., Schmitt, I., Stauber, R. H., & Dabauvalle, M. C. (2001). Cofactor requirements for nuclear export of rev response element (RRE)–and constitutive transport element (CTE)–containing retroviral RNAs: an unexpected role for actin. *The Journal of cell biology*, *152*, 895-910.

Hon, T., Lee, H. C., Hach, A., Johnson, J. L., Craig, E. A., Erdjument-Bromage, H., & Zhang, L. (2001). The Hsp70-Ydj1 molecular chaperone represses the activity of the heme activator protein Hap1 in the absence of heme. *Molecular and Cellular Biology*, *21*, 7923-7932.

Hudson, D. M., & Eyre, D. R. (2013). Collagen prolyl 3-hydroxylation: a major role for a minor post-translational modification?. *Connective tissue research, 54*, 245-251.

Hukelmann, J. L., Anderson, K. E., Sinclair, L. V., Grzes, K. M., Murillo, A. B., Hawkins, P. T., & Cantrell, D. A. (2016). The cytotoxic T cell proteome and its shaping by the kinase mTOR. *Nature immunology, 17*, 104-112.

Hussmann, J. A., Patchett, S., Johnson, A., Sawyer, S., & Press, W. H. (2015). Understanding biases in ribosome profiling experiments reveals signatures of translation dynamics in yeast. *PLoS genetics, 11*, e1005732.

Hyvönen, M. T., Keinänen, T. A., Khomutov, M., Simonian, A., Vepsäläinen, J., Park, J. H., & Park, M. H. (2012). Effects of novel C-methylated spermidine analogs on cell growth via hypusination of eukaryotic translation initiation factor 5A. *Amino acids, 42*, 685-695.

Igarashi, K., & Kashiwagi, K. (2015). Modulation of protein synthesis by polyamines. *IUBMB life, 67*, 160-169.

Ikeuchi, K., Izawa, T., & Inada, T. (2019). Recent progress on the molecular mechanism of quality controls induced by ribosome stalling. *Frontiers in Genetics, 9*, 743.

Inada, T. (2020). Quality controls induced by aberrant translation. *Nucleic acids research, 48*, 1084-1096.

Ingolia, N. T. (2014). Ribosome profiling: new views of translation, from single codons to genome scale. *Nature reviews genetics, 15*, 205-213.

Ishfaq, M., Maeta, K., Maeda, S., Natsume, T., Ito, A., & Yoshida, M. (2012). Acetylation regulates subcellular localization of eukaryotic translation initiation factor 5A (eIF5A). *FEBS letters, 586*, 3236-3241.

Ito, S., & Nagata, K. (2019). Roles of the endoplasmic reticulum–resident, collagen-specific molecular chaperone Hsp47 in vertebrate cells and human disease. *Journal of Biological Chemistry, 294*, 2133-2141.

Iwaisako, K., Jiang, C., Zhang, M., Cong, M., Moore-Morris, T. J., Park, T. J., & Kisseleva, T. (2014). Origin of myofibroblasts in the fibrotic liver in mice. *Proceedings of the National Academy of Sciences, 111*, E3297-E3305.

Jakus, J., Wolff, E. C., Park, M. H., & Folk, J. E. (1993). Features of the spermidine-binding site of deoxyhypusine synthase as derived from inhibition studies. Effective inhibition by bis- and mono-guanylated diamines and polyamines. *Journal of Biological Chemistry, 268*, 13151-13159.

Jao, D. L. E., & Chen, K. Y. (2006). Tandem affinity purification revealed the hypusine-dependent binding of eukaryotic initiation factor 5A to the translating 80S ribosomal complex. *Journal of cellular biochemistry, 97*, 583-598.

Jenkins, Z. A., Hååg, P. G., & Johansson, H. E. (2001). Human eIF5A2 on chromosome 3q25–q27 is a phylogenetically conserved vertebrate variant of eukaryotic translation initiation factor 5A with tissue-specific expression. *Genomics, 71*, 101-109.

Joazeiro, C. A. (2019). Mechanisms and functions of ribosome-associated protein quality control. *Nature Reviews Molecular Cell Biology, 20*, 368-383.

Jobling, R., D'Souza, R., Baker, N., Lara-Corrales, I., Mendoza-Londono, R., Dupuis, L., Savarirayan, R., Ala-Kokko, L. & Kannu, P. (2014). The collagenopathies: review of clinical phenotypes and molecular correlations. *Current rheumatology reports*, 16, 1-13.

Jordá, T., Barba-Aliaga, M., Rozès, N., Alepuz, P., Martínez-Pastor, M. T., & Puig, S. (2022). Transcriptional regulation of ergosterol biosynthesis genes in response to iron deficiency. *Environmental microbiology, 24*, 5248-5260.

Joska, T. M., Mashruwala, A., Boyd, J. M., & Belden, W. J. (2014). A universal cloning method based on yeast homologous recombination that is simple, efficient, and versatile. *Journal of microbiological methods, 100*, 46-51.

Juszkiewicz, S., Chandrasekaran, V., Lin, Z., Kraatz, S., Ramakrishnan, V., & Hegde, R. S. (2018). ZNF598 is a quality control sensor of collided ribosomes. *Molecular cell, 7*, 469-481.

Juszkiewicz, S., & Hegde, R. S. (2017). Initiation of quality control during poly (A) translation requires site-specific ribosome ubiquitination. *Molecular cell, 65*, 743-750.

Kachaev, Z. M., Ivashchenko, S. D., Kozlov, E. N., Lebedeva, L. A., & Shidlovskii, Y. V. (2021). Localization and functional roles of components of the translation apparatus in the eukaryotic cell nucleus. *Cells, 10*, 3239.

Kadler, K. E., Baldock, C., Bella, J., & Boot-Handford, R. P. (2007). Collagens at a glance. *Journal of cell science, 120*, 1955-1958.

Kaiser, A., Heiss, K., Mueller, A. K., Fimmers, R., Matthes, J., & Njuguna, J. T. (2020). Inhibition of EIF-5A prevents apoptosis in human cardiomyocytes after malaria infection. *Amino Acids, 52*, 693-710.

Kang, Y., Fielden, L. F., & Stojanovski, D. (2018). Mitochondrial protein transport in health and disease. *Seminars in cell & developmental biology, 76*, 142-153

Kastaniotis, A. J., Mennella, T. A., Konrad, C., Torres, A. M. R., & Zitomer, R. S. (2000). Roles of transcription factor Mot3 and chromatin in repression of the hypoxic gene ANB1 in yeast. *Molecular and cellular biology, 20*, 7088-7098.

Kayikci, Ö., & Nielsen, J. (2015). Glucose repression in Saccharomyces cerevisiae. *FEMS yeast research, 15*, fov068.

Kellems, R. E., & Butow, R. A. (1972). Cytoplasmic-type 80 S Ribosomes Associated with Yeast Mitochondria: I. EVIDENCE FOR RIBOSOME BINDING SITES ON YEAST MITOCHONDRIA. *Journal of Biological Chemistry, 247*, 8043-8050.

Kemper, W. M., Berry, K. W., & Merrick, W. C. (1976). Purification and properties of rabbit reticulocyte protein synthesis initiation factors M2Balpha and M2Bbeta. *Journal of Biological Chemistry, 251*, 5551-5557.

Kim, K. K., Hung, L. W., Yokota, H., Kim, R., & Kim, S. H. (1998). Crystal structures of eukaryotic translation initiation factor 5A from Methanococcus jannaschii at 1.8 Å resolution. *Proceedings of the National Academy of Sciences, 95*, 10419-10424.

Kisseleva, T., Cong, M., Paik, Y., Scholten, D., Jiang, C., Benner, C., & Brenner, D. A. (2012). Myofibroblasts revert to an inactive phenotype during regression of liver fibrosis. *Proceedings of the National Academy of Sciences, 109*, 9448-9453.

Klier, H., Wöhl, T., Eckerskorn, C., Magdolen, V., & Lottspeich, F. (1993). Determination and mutational analysis of the phosphorylation site in the hypusine-containing protein Hyp2p. *FEBS letters, 334*, 360-364.

Klinkenberg, L. G., Mennella, T. A., Luetkenhaus, K., & Zitomer, R. S. (2005). Combinatorial repression of the hypoxic genes of Saccharomyces cerevisiae by DNA binding proteins Rox1 and Mot3. *Eukaryotic cell, 4*, 649-660.

Kocabayoglu, P., & Friedman, S. L. (2013). Cellular basis of hepatic fibrosis and its role in inflammation and cancer. *Frontiers in Bioscience-Scholar, 5*, 217-230.

Koehler, C. M., Merchant, S., Oppliger, W., Schmid, K., Jarosch, E., Dolfini, L., & Tokatlidis, K. (1998). Tim9p, an essential partner subunit of Tim10p for the import of mitochondrial carrier proteins. *The EMBO journal, 17*, 6477-6486.

Koide, T., Nishikawa, Y., Asada, S., Yamazaki, C. M., Takahara, Y., Homma, D. L., & Kitagawa, K. (2006). Specific recognition of the collagen triple helix by chaperone HSP47: II. The HSP47-binding structural motif in collagens and related proteins. *Journal of Biological Chemistry, 281*, 11177-11185.

Krakowiak, J., Zheng, X., Patel, N., Feder, Z. A., Anandhakumar, J., Valerius, K., & Pincus, D. (2018). Hsf1 and Hsp70 constitute a two-component feedback loop that regulates the yeast heat shock response. *Elife, 7*, e31668.

Krämer, L., Dalheimer, N., Räschle, M., Storchová, Z., Pielage, J., Boos, F., & Herrmann, J. M. (2023). MitoStores: chaperone-controlled protein granules store mitochondrial precursors in the cytosol. *The EMBO Journal, 42*, e112309.

Kroemer, G., & Pouyssegur, J. (2008). Tumor cell metabolism: cancer's Achilles' heel. *Cancer cell, 13*, 472-482.

Kulak, N. A., Pichler, G., Paron, I., Nagaraj, N., & Mann, M. (2014). Minimal, encapsulated proteomic-sample processing applied to copy-number estimation in eukaryotic cells. *Nature methods, 11*, 319-324.

Lan, C., Lee, H. C., Tang, S., & Zhang, L. (2004). A novel mode of chaperone action: heme activation of Hap1 by enhanced association of Hsp90 with the repressed Hsp70-Hap1 complex. *Journal of Biological Chemistry, 279*, 27607-27612.

Lee, S. B., Park, J. H., Kaevel, J., Sramkova, M., Weigert, R., & Park, M. H. (2009). The effect of hypusine modification on the intracellular localization of eIF5A. *Biochemical and biophysical research communications, 383*, 497-502.

Lee, S. R., & Lykke-Andersen, J. (2013). Emerging roles for ribonucleoprotein modification and remodeling in controlling RNA fate. *Trends in cell biology, 23*, 504-510.

Lee, U. E., & Friedman, S. L. (2011). Mechanisms of hepatic fibrogenesis. *Best practice & research Clinical gastroenterology, 25*, 195-206.

Lenkiewicz, A. M., Krakowczyk, M., & Bragoszewski, P. (2022). Cytosolic quality control of mitochondrial protein precursors—the early stages of the organelle biogenesis. *International Journal of Molecular Sciences, 23*, 7.

Letzring, D. P., Dean, K. M., & Grayhack, E. J. (2010). Control of translation efficiency in yeast by codon–anticodon interactions. *Rna, 16*, 2516-2528.

Levasseur, E. M., Yamada, K., Piñeros, A. R., Wu, W., Syed, F., Orr, K. S., & Mirmira, R. G. (2019). Hypusine biosynthesis in β cells links polyamine metabolism to facultative cellular proliferation to maintain glucose homeostasis. *Science signaling, 12*, eaax0715.

Li, A. L., Li, H. Y., Jin, B. F., Ye, Q. N., Zhou, T., Yu, X. D., & Zhang, X. M. (2004). A novel eIF5A complex functions as a regulator of p53 and p53-dependent apoptosis. *Journal of Biological Chemistry, 279*, 49251-49258.

Li, C. H., Ohn, T., Ivanov, P., Tisdale, S., & Anderson, P. (2010). eIF5A promotes translation elongation, polysome disassembly and stress granule assembly. *PloS one, 5*, e9942.

Li, J., & Sha, B. (2015). The structure of Tim50 (164–361) suggests the mechanism by which Tim50 receives mitochondrial presequences. *Acta Crystallographica Section F: Structural Biology Communications, 71*, 1146-1151.

Li, T., Belda-Palazón, B., Ferrando, A., & Alepuz, P. (2014). Fertility and polarized cell growth depends on eIF5A for translation of polyproline-rich formins in Saccharomyces cerevisiae. *Genetics, 1974*, 1191-1200.

Li, Y., Fu, L., Li, J. B., Qin, Y., Zeng, T. T., Zhou, J., & Guan, X. Y. (2014). Increased expression of EIF5A2, via hypoxia or gene amplification, contributes to metastasis and angiogenesis of esophageal squamous cell carcinoma. *Gastroenterology, 146*, 1701-1713.

Li, Z., Vizeacoumar, F. J., Bahr, S., Li, J., Warringer, J., Vizeacoumar, F. S., Min, R., Vandersluis, B., Bellay, J., Devit, M. & Boone, C. (2011). Systematic exploration of essential yeast gene function with temperature-sensitive mutants. *Nature biotechnology, 29*, 361-367.

Liang, Y., Piao, C., Beuschel, C. B., Toppe, D., Kollipara, L., Bogdanow, B., & Sigrist, S. J. (2021). eIF5A hypusination, boosted by dietary spermidine, protects from premature brain aging and mitochondrial dysfunction. *Cell reports, 35*, 108941.

Lin, X., Zhang, C. Y., Bai, X. W., Song, H. Y., & Xiao, D. G. (2014). Effects of MIG1, TUP1 and SSN6 deletion on maltose metabolism and leavening ability of baker's yeast in lean dough. *Microbial Cell Factories, 13*, 1-9.

Lindquist, J. N., Marzluff, W. F., & Stefanovic, B. (2000). III. Posttranscriptional regulation of type I collagen. *American Journal of Physiology-Gastrointestinal and Liver Physiology, 279*, G471-G476.

Lipowsky, G., Bischoff, F. R., Schwarzmaier, P., Kraft, R., Kostka, S., Hartmann, E., Kutay, U., & Görlich, D. (2000). Exportin 4: a mediator of a novel nuclear export pathway in higher eukaryotes. *The EMBO journal, 19*, 4362-4371.

Liu, J., Zhan, X., Li, M., Li, G., Zhang, P., Xiao, Z., & Chen, Z. (2012). Mitochondrial proteomics of nasopharyngeal carcinoma metastasis. *BMC medical genomics, 5*, 1-17.

Liu, Y., Peng, L., Chen, J., Chen, L., Wu, Y., Cheng, M., & Jin, Y. (2023). EIF5A2 specifically regulates the transcription of aging-related genes in human neuroblastoma cells. *BMC geriatrics, 23*, 1-13.

Longtine, M. S., Mckenzie III, A., Demarini, D. J., Shah, N. G., Wach, A., Brachat, A., & Pringle, J. R. (1998). Additional modules for versatile and economical PCR-based gene deletion and modification in Saccharomyces cerevisiae. *Yeast, 14*, 953-961.

Lowry, C. V., & Lieber, R. H. (1986). Negative regulation of the Saccharomyces cerevisiae ANB1 gene by heme, as mediated by the ROX1 gene product. *Molecular and Cellular Biology, 6*, 4145-4148.

Lowry, C. V., & Zitomer, R. S. (1988). ROX1 encodes a heme-induced repression factor regulating ANB1 and CYC7 of Saccharomyces cerevisiae. *Molecular and cellular biology, 8*, 4651-4658.

Lubas, M., Harder, L. M., Kumsta, C., Tiessen, I., Hansen, M., Andersen, J. S., Lund, A. H., & Frankel, L. B. (2018). eIF 5A is required for autophagy by mediating ATG 3 translation. *EMBO reports, 19*, e46072.

Luchessi, A. D., Cambiaghi, T. D., Alves, A. S., Parreiras-E-Silva, L. T., Britto, L. R., Costa-Neto, C. M., & Curi, R. (2008). Insights on eukaryotic translation initiation factor 5A (eIF5A) in the brain and aging. *Brain research, 1228*, 6-13.

Maier, B., Ogihara, T., Trace, A. P., Tersey, S. A., Robbins, R. D., Chakrabarti, S. K., & Mirmira, R. G. (2010). The unique hypusine modification of eIF5A promotes islet β cell inflammation and dysfunction in mice. *The Journal of clinical investigation, 120*, 2156-2170.

Maiers, J. L., Kostallari, E., Mushref, M., deAssuncao, T. M., Li, H., Jalan-Sakrikar, N., & Shah, V. H. (2017). The unfolded protein response mediates fibrogenesis and collagen I secretion through regulating TANGO1 in mice. *Hepatology, 65*, 983-998.

Malhotra, V., & Erlmann, P. (2015). The pathway of collagen secretion. *Annual review of cell and developmental biology, 31*, 109-124.

Mandal, A., Mandal, S., & Park, M. H. (2014). Genome-wide analyses and functional classification of proline repeat-rich proteins: potential role of eIF5A in eukaryotic evolution. *PloS one, 9*, e111800.

Mandal, A., Mandal, S., & Park, M. H. (2016). Global quantitative proteomics reveal up-regulation of endoplasmic reticulum stress response proteins upon depletion of eIF5A in HeLa cells. *Scientific reports, 6*, 25795.

Mao, X., Tey, S. K., Yeung, C. L. S., Kwong, E. M. L., Fung, Y. M. E., Chung, C. Y. S., Mak, L. Y., Wong, D. K. H., Yuen, M. F., Ho, J. C. M., & Yam, J. W. P. (2020). Nidogen 1-enriched extracellular vesicles facilitate extrahepatic metastasis of liver cancer by activating pulmonary fibroblasts to secrete tumor necrosis factor receptor 1. *Advanced Science, 7*, 2002157.

Mao, Y., & Chen, C. (2019). The hap complex in yeasts: structure, assembly mode, and gene regulation. *Frontiers in Microbiology, 10*, 1645.

Marini, J. C., & Cabral, W. A. (2018). Osteogenesis imperfecta. *Genetics of bone biology and skeletal disease*, 397-420.

Martella, M., Catalanotto, C., Talora, C., La Teana, A., Londei, P., & Benelli, D. (2020). Inhibition of eukaryotic translation initiation factor 5A (eIF5A) hypusination suppress p53 translation and alters the association of eIF5A to the ribosomes. *International Journal of Molecular Sciences, 21*, 4583.

Mårtensson, C. U., Priesnitz, C., Song, J., Ellenrieder, L., Doan, K. N., Boos, F., Floerchinger, A., Zufall, N., Oeljeklaus, S., Warscheid, B., & Becker, T. (2019). Mitochondrial protein translocation-associated degradation. *Nature, 569*, 679-683.

Masser, A. E., Kandasamy, G., Kaimal, J. M., & Andréasson, C. (2016). Luciferase NanoLuc as a reporter for gene expression and protein levels in Saccharomyces cerevisiae. *Yeast, 33*, 191-200.

Mathews, M. B., & Hershey, J. W. (2015). The translation factor eIF5A and human cancer. *Biochimica et Biophysica Acta (BBA)-Gene Regulatory Mechanisms, 1849*, 836-844.

Matsuo, Y., Tesina, P., Nakajima, S., Mizuno, M., Endo, A., Buschauer, R., & Inada, T. (2020). RQT complex dissociates ribosomes collided on endogenous RQC substrate SDD1. *Nature structural & molecular biology, 27*, 323-332.

McNabb, D. S., & Pinto, I. (2005). Assembly of the hap2p/hap3p/hap4p/hap5p-DNA complex in Saccharomyces cerevisiae. *Eukaryotic cell, 4*, 1829-1839.

Medina, D. A., Jordán-Pla, A., Millán-Zambrano, G., Chávez, S., Choder, M., & Pérez-Ortín, J. E. (2014). Cytoplasmic 5′-3′ exonuclease Xrn1p is also a genome-wide transcription factor in yeast. *Frontiers in genetics, 5*, 1.

Melis, N., Rubera, I., Cougnon, M., Giraud, S., Mograbi, B., Belaid, A., & Tauc, M. (2017). Targeting eIF5A hypusination prevents anoxic cell death through mitochondrial silencing and improves kidney transplant outcome. *Journal of the American Society of Nephrology, 28*, 811-822.

Melnikov, S., Mailliot, J., Shin, B. S., Rigger, L., Yusupova, G., Micura, R., & Yusupov, M. (2016). Crystal structure of hypusine-containing translation factor eIF5A bound to a rotated eukaryotic ribosome. *Journal of molecular biology, 428*, 3570-3576.

Meng, X. M., Nikolic-Paterson, D. J., & Lan, H. Y. (2016). TGF-β: the master regulator of fibrosis. *Nature Reviews Nephrology, 12*, 325-338.

Mense, S. M., & Zhang, L. (2006). Heme: a versatile signaling molecule controlling the activities of diverse regulators ranging from transcription factors to MAP kinases. *Cell research, 16*, 681-692.

Meydan, S., & Guydosh, N. R. (2020). Disome and trisome profiling reveal genome-wide targets of ribosome quality control. *Molecular cell, 79*, 588-602.

Minois, N., Rockenfeller, P., Smith, T. K., & Carmona-Gutierrez, D. (2014). Spermidine feeding decreases age-related locomotor activity loss and induces changes in lipid composition. *PloS one, 9*, e102435.

Miyake, T., Pradeep, S., Wu, S. Y., Rupaimoole, R., Zand, B., Wen, Y., & Sood, A. K. (2015). XPO1/CRM1 Inhibition Causes Antitumor Effects by Mitochondrial Accumulation of eIF5AIGF2BP1 Regulates eIF5A and Apoptosis. *Clinical Cancer Research, 21*, 3286-3297.

Mokranjac, D., Sichting, M., Popov-Čeleketić, D., Mapa, K., Gevorkyan-Airapetov, L., Zohary, K., & Neupert, W. (2009). Role of Tim50 in the transfer of precursor proteins from the outer to the inner membrane of mitochondria. *Molecular biology of the cell, 20*, 1400-1407.

Morgenstern, M., Stiller, S. B., Lübbert, P., Peikert, C. D., Dannenmaier, S., Drepper, F., & Warscheid, B. (2017). Definition of a high-confidence mitochondrial proteome at quantitative scale. *Cell reports, 19*, 2836-2852.

Münch, C., & Harper, J. W. (2016). Mitochondrial unfolded protein response controls matrix pre-RNA processing and translation. *Nature, 534*, 710-713.

Muñoz-Soriano, V., Domingo-Muelas, A., Li, T., Gamero, E., Bizy, A., Fariñas, I., Alepuz, P., & Paricio, N. (2017). Evolutionary conserved role of eukaryotic translation factor eIF5A in the regulation of actin-nucleating formins. *Scientific reports, 7*, 9580.

Myllyharju, J., & Kivirikko, K. I. (2001). Collagens and collagen-related diseases. *Annals of medicine, 33*, 7-21.

Nakanishi, S., & Cleveland, J. L. (2016). Targeting the polyamine-hypusine circuit for the prevention and treatment of cancer. *Amino acids, 48*, 2353-2362.

Nguyen, S., Leija, C., Kinch, L., Regmi, S., Li, Q., Grishin, N. V., & Phillips, M. A. (2015). Deoxyhypusine modification of eukaryotic translation initiation factor 5A (eIF5A) is essential for Trypanosoma brucei growth and for expression of polyprolyl-containing proteins. *Journal of Biological Chemistry, 290*, 19987-19998.

Nicolas, E., Tricarico, R., Savage, M., Golemis, E. A., & Hall, M. J. (2019). Disease-associated genetic variation in human mitochondrial protein import. *The American Journal of Human Genetics, 104*, 784-801.

Ning, L., Wang, L., Zhang, H., Jiao, X., & Chen, D. (2020). Eukaryotic translation initiation factor 5A in the pathogenesis of cancers. *Oncology Letters, 20*, 1-1.

Nishimura, K., Lee, S. B., Park, J. H., & Park, M. H. (2012). Essential role of eIF5A-1 and deoxyhypusine synthase in mouse embryonic development. *Amino acids, 42*, 703-710.

Nowicka, U., Chroscicki, P., Stroobants, K., Sladowska, M., Turek, M., Uszczynska-Ratajczak, B., Kundra, R., Goral, T., Perni, M., Dobson, C. M., Vendruscolo, M., & Chacinska, A.

(2021). Cytosolic aggregation of mitochondrial proteins disrupts cellular homeostasis by stimulating the aggregation of other proteins. *Elife, 10*, e65484.

Okamoto, H., Miyagawa, A., Shiota, T., Tamura, Y., & Endo, T. (2014). Intramolecular disulfide bond of Tim22 protein maintains integrity of the TIM22 complex in the mitochondrial inner membrane. *Journal of Biological Chemistry, 289*, 4827-4838.

Oliverio, S., Corazzari, M., Sestito, C., Piredda, L., Ippolito, G., & Piacentini, M. (2014). The spermidine analogue GC7 (N1-guanyl-1, 7-diamineoheptane) induces autophagy through a mechanism not involving the hypusination of eIF5A. *Amino Acids, 46*, 2767-2776.

Olsen, M. E., Filone, C. M., Rozelle, D., Mire, C. E., Agans, K. N., Hensley, L., & Connor, J. H. (2016). Polyamines and hypusination are required for ebolavirus gene expression and replication. *MBio, 7*, e00882-16.

Oyadomari, S., & Mori, M. (2004). Roles of CHOP/GADD153 in endoplasmic reticulum stress. *Cell Death & Differentiation, 11*, 381-389.

Padgett, L. R., Robertson, M. A., Anderson-Baucum, E. K., Connors, C. T., Wu, W., Mirmira, R. G., & Mastracci, T. L. (2021). Deoxyhypusine synthase, an essential enzyme for hypusine biosynthesis, is required for proper exocrine pancreas development. *The FASEB Journal, 35*.

Park, M. H. (2006). The post-translational synthesis of a polyamine-derived amino acid, hypusine, in the eukaryotic translation initiation factor 5A (eIF5A). *Journal of biochemistry, 139*, 161-169.

Park, M. H., Cooper, H. L., & Folk, J. E. (1981). Identification of hypusine, an unusual amino acid, in a protein from human lymphocytes and of spermidine as its biosynthetic precursor. *Proceedings of the National Academy of Sciences, 78*, 2869-2873.

Park, M. H., Kar, R. K., Banka, S., Ziegler, A., & Chung, W. K. (2021). Post-translational formation of hypusine in eIF5A: Implications in human neurodevelopment. *Amino acids*, 1-15.

Park, M. H., Lee, Y. B., & Joe, Y. A. (1997). Hypusine is essential for eukaryotic cell proliferation. *Neurosignals, 6*, 115-123.

Park, M. H., & Wolff, E. C. (2018). Hypusine, a polyamine-derived amino acid critical for eukaryotic translation. *Journal of Biological Chemistry, 293*, 18710-18718.

Park, M. H., Wolff, E. C., Lee, Y. B., & Folk, J. E. (1994). Antiproliferative effects of inhibitors of deoxyhypusine synthase. Inhibition of growth of Chinese hamster ovary cells by guanyl diamines. *Journal of Biological Chemistry, 269*, 27827-27832.

Parreiras-e-Silva, L. T., Gomes, M. D., Oliveira, E. B., & Costa-Neto, C. M. (2007). The N-terminal region of eukaryotic translation initiation factor 5A signals to nuclear localization of the protein. *Biochemical and Biophysical Research Communications, 362*, 393-398.

Pavlov, M. Y., Watts, R. E., Tan, Z., Cornish, V. W., Ehrenberg, M., & Forster, A. C. (2009). Slow peptide bond formation by proline and other N-alkylamino acids in translation. *Proceedings of the National Academy of Sciences, 106*, 50-54.

Peat, J. K., Dickerson, J., & Li, J. (1998). Effects of damp and mould in the home on respiratory health: a review of the literature. *Allergy, 53*, 120-128.

Pechmann, S., Willmund, F., & Frydman, J. (2013). The ribosome as a hub for protein quality control. *Molecular cell, 49*, 411-421.

Pelechano, V., & Alepuz, P. (2017). eIF5A facilitates translation termination globally and promotes the elongation of many non polyproline-specific tripeptide sequences. *Nucleic acids research, 45*, 7326-7338.

Pereira, K. D., Tamborlin, L., Meneguello, L., de Proença, A. R. G., Almeida, I. C. D. P. A., Lourenço, R. F., & Luchessi, A. D. (2016). Alternative start codon connects eIF5A to mitochondria. *Journal of Cellular Physiology, 231*, 2682-2689.

Pérez-Ortín, J. E., Medina, D. A., Chávez, S., & Moreno, J. (2013). What do you mean by transcription rate? The conceptual difference between nascent transcription rate and mRNA synthesis rate is essential for the proper understanding of transcriptomic analyses. *BioEssays, 35*, 1056-1062.

Pérez-Ortín, J. E., Tordera, V., & Chávez, S. (2019). Homeostasis in the Central Dogma of molecular biology: the importance of mRNA instability. *RNA biology, 16*, 1659-1666.

Pickrell, A. M., & Youle, R. J. (2015). The roles of PINK1, parkin, and mitochondrial fidelity in Parkinson's disease. *Neuron, 85*, 257-273.

Presnyak, V., Alhusaini, N., Chen, Y. H., Martin, S., Morris, N., Kline, N., & Coller, J. (2015). Codon optimality is a major determinant of mRNA stability. *Cell, 160*, 1111-1124.

Proshkin, S. A., Shematorova, E. K., Souslova, E. A., Proshkina, G. M., & Shpakovski, G. V. (2011). A minor isoform of the human RNA polymerase II subunit hRPB11 (POLR2J) interacts with several components of the translation initiation factor eIF3. *Biochemistry, 76*, 976-980.

Proud, C. G. (2002). Regulation of mammalian translation factors by nutrients. *European journal of biochemistry, 269*, 5338-5349.

Puleston, D. J., Buck, M. D., Geltink, R. I. K., Kyle, R. L., Caputa, G., O'Sullivan, D., & Pearce, E. L. (2019). Polyamines and eIF5A hypusination modulate mitochondrial respiration and macrophage activation. *Cell metabolism, 30*, 352-363.

Puleston, D. J., Zhang, H., Powell, T. J., Lipina, E., Sims, S., Panse, I., Watson, A. S., Cerundolo, V., Townsend, A. RM., Klenerman, P., & Simon, A. K. (2014). Autophagy is a critical regulator of memory CD8+ T cell formation. *Elife, 3*, e03706.

Qin, W., Myers, S. A., Carey, D. K., Carr, S. A., & Ting, A. Y. (2021). Spatiotemporally-resolved mapping of RNA binding proteins via functional proximity labeling reveals a mitochondrial mRNA anchor promoting stress recovery. *Nature communications, 12*, 4980.

Quirós, P. M., Prado, M. A., Zamboni, N., D'Amico, D., Williams, R. W., Finley, D., & Auwerx, J. (2017). Multi-omics analysis identifies ATF4 as a key regulator of the mitochondrial stress response in mammals. *Journal of Cell Biology, 216*, 2027-2045.

Rafiee, M. R., Rohban, S., Davey, K., Ule, J., & Luscombe, N. M. (2023). RNA polymerase II-associated proteins reveal pathways affected in VCP-related amyotrophic lateral sclerosis. *Brain*, awad046.

Rahman-Roblick, R., Johannes Roblick, U., Hellman, U., Conrotto, P., Liu, T., Becker, S., & Wiman, K. G. (2007). p53 targets identified by protein expression profiling. *Proceedings of the National Academy of Sciences, 104*, 5401-5406.

Ramos-Alonso, L., Romero, A. M., Martínez-Pastor, M. T., & Puig, S. (2020). Iron regulatory mechanisms in Saccharomyces cerevisiae. *Frontiers in Microbiology, 11*, 582830.

Reis, M. D., Savva, R., & Wernisch, L. (2004). Solving the riddle of codon usage preferences: a test for translational selection. *Nucleic acids research, 32*, 5036-5044.

Ricard-Blum, S., Baffet, G., & Théret, N. (2018). Molecular and tissue alterations of collagens in fibrosis. *Matrix Biology, 68*, 122-149.

Robbins, R. D., Tersey, S. A., Ogihara, T., Gupta, D., Farb, T. B., Ficorilli, J., & Mirmira, R. G. (2010). Inhibition of deoxyhypusine synthase enhances islet β cell function and survival in the setting of endoplasmic reticulum stress and type 2 diabetes. *Journal of Biological Chemistry, 285*, 39943-39952.

Roger, A. J., Muñoz-Gómez, S. A., & Kamikawa, R. (2017). The origin and diversification of mitochondria. *Current Biology, 27*, R1177-R1192.

Rolland, F., Winderickx, J., & Thevelein, J. M. (2002). Glucose-sensing and-signalling mechanisms in yeast. *FEMS yeast research, 2*, 183-201.

Rolland, S. G., Schneid, S., Schwarz, M., Rackles, E., Fischer, C., Haeussler, S., & Conradt, B. (2019). Compromised mitochondrial protein import acts as a signal for UPRmt. *Cell reports, 28*, 1659-1669.

Ron, D., & Walter, P. (2007). Signal integration in the endoplasmic reticulum unfolded protein response. *Nature reviews Molecular cell biology, 8*, 519-529.

Rosorius, O., Reichart, B., Kratzer, F., Heger, P., Dabauvalle, M. C., & Hauber, J. (1999). Nuclear pore localization and nucleocytoplasmic transport of eIF-5A: evidence for direct interaction with the export receptor CRM1. *Journal of Cell Science, 112*, 2369-2380.

Rossi, D., Barbosa, N. M., Galvão, F. C., Boldrin, P. E., Hershey, J. W., Zanelli, C. F., & Valentini, S. R. (2016). Evidence for a negative cooperativity between eIF5A and eEF2 on binding to the ribosome. *PloS one, 11*, e0154205.

Rossi, D., Galvão, F. C., Bellato, H. M., Boldrin, P. E., Andrews, B. J., Valentini, S. R., & Zanelli, C. F. (2014). eIF5A has a function in the cotranslational translocation of proteins into the ER. *Amino Acids, 46*, 645-653.

Ruhl, M., Himmelspach, M., Bahr, G. M., Hammerschmid, F., Jaksche, H., Wolff, B., & Bevec, D. (1993). Eukaryotic initiation factor 5A is a cellular target of the human immunodeficiency virus type 1 Rev activation domain mediating trans-activation. *The Journal of cell biology, 123*, 1309-1320.

Saha, I., & Shamala, N. (2012). Investigating diproline segments in proteins: occurrences, conformation and classification. *Biopolymers, 97*, 54-64.

Saikia, M., Wang, X., Mao, Y., Wan, J., Pan, T., & Qian, S. B. (2016). Codon optimality controls differential mRNA translation during amino acid starvation. *Rna, 22*, 1719-1727.

Saini, P., Eyler, D. E., Green, R., & Dever, T. E. (2009). Hypusine-containing protein eIF5A promotes translation elongation. *Nature, 459*, 118-121.

Saint-Georges, Y., Garcia, M., Delaveau, T., Jourdren, L., Le Crom, S., Lemoine, S., Tanty, V., Devaux, F., & Jacq, C. (2008). Yeast mitochondrial biogenesis: a role for the PUF RNA-binding protein Puf3p in mRNA localization. *PloS one, 3*, e2293.

Saito, K., Chen, M., Bard, F., Chen, S., Zhou, H., Woodley, D., & Malhotra, V. (2009). TANGO1 facilitates cargo loading at endoplasmic reticulum exit sites. *Cell, 136*, 891-902.

San-Millán, I., & Brooks, G. A. (2017). Reexamining cancer metabolism: lactate production for carcinogenesis could be the purpose and explanation of the Warburg Effect. *Carcinogenesis, 38*, 119-133.

Sanchez, Y., & Lindquist, S. L. (1990). HSP104 required for induced thermotolerance. *Science, 248*, 1112-1115.

Sankala, H., Vaughan, C., Wang, J., Deb, S., & Graves, P. R. (2011). Upregulation of the mitochondrial transport protein, Tim50, by mutant p53 contributes to cell growth and chemoresistance. *Archives of biochemistry and biophysics, 512*, 52-60.

Santangelo, G. M. (2006). Glucose signaling in Saccharomyces cerevisiae. *Microbiology and Molecular Biology Reviews, 70*, 253-282.

Sarkadi, B., Homolya, L., Szakács, G., & Váradi, A. (2006). Human multidrug resistance ABCB and ABCG transporters: participation in a chemoimmunity defense system. *Physiological reviews, 86*, 1179-1236.

Scarpulla, R. C. (2002). Nuclear activators and coactivators in mammalian mitochondrial biogenesis. *Biochimica et biophysica acta (BBA)-gene structure and expression, 1576*, 1-14.

Schäfer, J. A., Bozkurt, S., Michaelis, J. B., Klann, K., & Münch, C. (2022). Global mitochondrial protein import proteomics reveal distinct regulation by translation and translocation machinery. *Molecular cell, 82*, 435-446.

Schleif, R., Hess, W., Finkelstein, S., & Ellis, D. (1973). Induction kinetics of the L-arabinose operon of Escherichia coli. *Journal of bacteriology, 115*, 9-14.

Schmidt, C., Becker, T., Heuer, A., Braunger, K., Shanmuganathan, V., Pech, M., & Beckmann, R. (2016). Structure of the hypusinylated eukaryotic translation factor eIF-5A bound to the ribosome. *Nucleic acids research, 44*, 1944-1951.

Schmidt, O., Pfanner, N., & Meisinger, C. (2010). Mitochondrial protein import: from proteomics to functional mechanisms. *Nature reviews Molecular cell biology, 11*, 655-667.

Schnier, J., Schwelberger, H. G., Smit-McBride, Z., Kang, H. A., & Hershey, J. W. (1991). Translation initiation factor 5A and its hypusine modification are essential for cell viability in the yeast Saccharomyces cerevisiae. *Molecular and cellular biology, 11*, 3105-3114.

Schröder, M., & Kaufman, R. J. (2005). The mammalian unfolded protein response. *Annu. Rev. Biochem., 74*, 739-789.

Schroeder, S., Hofer, S. J., Zimmermann, A., Pechlaner, R., Dammbrueck, C., Pendl, T., & Madeo, F. (2021). Dietary spermidine improves cognitive function. *Cell reports, 35*, 108985.

Schuller, A. P., Wu, C. C. C., Dever, T. E., Buskirk, A. R., & Green, R. (2017). eIF5A functions globally in translation elongation and termination. *Molecular cell, 66*, 194-205.

Schüller, H. J. (2003). Transcriptional control of nonfermentative metabolism in the yeast Saccharomyces cerevisiae. *Current genetics, 43*, 139-160.

Schulz, J. N., Nüchel, J., Niehoff, A., Bloch, W., Schönborn, K., Hayashi, S., & Eckes, B. (2016). COMP-assisted collagen secretion–a novel intracellular function required for fibrosis. *Journal of cell science, 129*, 706-716.

Schwelberger, H. G., Kang, H. A., & Hershey, J. W. (1993). Translation initiation factor eIF-5A expressed from either of two yeast genes or from human cDNA. Functional identity under aerobic and anaerobic conditions. *Journal of Biological Chemistry, 268*, 14018-14025.

Semenza, G. L. (2007). HIF-1 mediates the Warburg effect in clear cell renal carcinoma. *Journal of bioenergetics and biomembranes, 39*, 231.

Sertil, O., Kapoor, R., Cohen, B. D., Abramova, N., & Lowry, C. V. (2003). Synergistic repression of anaerobic genes by Mot3 and Rox1 in Saccharomyces cerevisiae. *Nucleic acids research, 31*, 5831-5837.

Shahrour, M. A., Staretz-Chacham, O., Dayan, D., Stephen, J., Weech, A., Damseh, N., & Malicdan, M. C. (2017). Mitochondrial epileptic encephalopathy, 3-methylglutaconic aciduria and variable complex V deficiency associated with TIMM50 mutations. *Clinical genetics, 91*, 690-696.

Shakya, V. P., Barbeau, W. A., Xiao, T., Knutson, C. S., Schuler, M. H., & Hughes, A. L. (2021). A nuclear-based quality control pathway for non-imported mitochondrial proteins. *Elife, 10*, e61230.

Shao, S., Brown, A., Santhanam, B., & Hegde, R. S. (2015). Structure and assembly pathway of the ribosome quality control complex. *Molecular cell, 57*, 433-444.

Sharma, U., Carrique, L., Vadon-Le Goff, S., Mariano, N., Georges, R. N., Delolme, F., & Hulmes, D. J. (2017). Structural basis of homo-and heterotrimerization of collagen I. *Nature communications, 8*, 14671.

Shashkova, S., Welkenhuysen, N., & Hohmann, S. (2015). Molecular communication: crosstalk between the Snf1 and other signaling pathways. *FEMS yeast research, 15*.

Shi, X. P., Yin, K. C., Zimolo, Z. A., Stern, A. M., & Waxman, L. (1996). The subcellular distribution of eukaryotic translation initiation factor, eIF-5A, in cultured cells. *Experimental cell research, 225*, 348-356.

Shiba, T., Mizote, H., Kaneko, T., Nakajima, T., & Yasuo, K. (1971). Hypusine, a new amino acid occurring in bovine brain: Isolation and structural determination. *Biochimica et Biophysica Acta (BBA)-General Subjects, 244*, 523-531.

Sievert, H., Pällmann, N., Miller, K. K., Hermans-Borgmeyer, I., Venz, S., Sendoel, A., & Balabanov, S. (2014). A novel mouse model for inhibition of DOHH-mediated hypusine modification reveals a crucial function in embryonic development, proliferation and oncogenic transformation. *Disease models & mechanisms, 7*, 963-976.

Simms, C. L., Yan, L. L., & Zaher, H. S. (2017). Ribosome collision is critical for quality control during no-go decay. *Molecular cell, 68*, 361-373.

Slobodin, B., & Dikstein, R. (2020). So close, no matter how far: multiple paths connecting transcription to mRNA translation in eukaryotes. *EMBO reports, 21*, e50799.

Smeltzer, S., Quadri, Z., Miller, A., Zamudio, F., Hunter, J., Stewart, N. J., & Selenica, M. L. B. (2021). Hypusination of Eif5a regulates cytoplasmic TDP-43 aggregation and accumulation in a stress-induced cellular model. *Biochimica et Biophysica Acta (BBA)-Molecular Basis of Disease, 1867*, 165939.

Song, J., Herrmann, J. M., & Becker, T. (2021). Quality control of the mitochondrial proteome. *Nature reviews Molecular cell biology, 22*, 54-70.

Stouthamer, A. H. (1973). A theoretical study on the amount of ATP required for synthesis of microbial cell material. *Antonie van Leeuwenhoek, 39*, 545-565.

Sugiyama, S., Moritoh, S., Furukawa, Y., Mizuno, T., Lim, Y. M., Tsuda, L., & Nishida, Y. (2007). Involvement of the mitochondrial protein translocator component tim50 in growth, cell proliferation and the modulation of respiration in Drosophila. *Genetics, 176*, 927-936.

Sun, Z., Cheng, Z., Taylor, C. A., McConkey, B. J., & Thompson, J. E. (2010). Apoptosis induction by eIF5A1 involves activation of the intrinsic mitochondrial pathway. *Journal of cellular physiology, 223*, 798-809.

Tan, X., Wang, D. B., Lu, X., Wei, H., Zhu, R., Zhu, S. S., & Yang, Z. J. (2010). Doxorubicin induces apoptosis in H9c2 cardiomyocytes: role of overexpressed eukaryotic translation initiation factor 5A. *Biological and Pharmaceutical Bulletin, 33*, 1666-1672.

Tang, D. J., Dong, S. S., Ma, N. F., Xie, D., Chen, L., Fu, L., & Guan, X. Y. (2010). Overexpression of eukaryotic initiation factor 5A2 enhances cell motility and promotes tumor metastasis in hepatocellular carcinoma. *Hepatology, 51*, 1255-1263.

Tariq, M., Ito, A., Ishfaq, M., Bradshaw, E., & Yoshida, M. (2016). Eukaryotic translation initiation factor 5A (eIF5A) is essential for HIF-1α activation in hypoxia. *Biochemical and biophysical research communications, 470,* 417-424.

Taylor, C. A., Sun, Z., Cliche, D. O., Ming, H., Eshaque, B., Jin, S., & Thompson, J. E. (2007). Eukaryotic translation initiation factor 5A induces apoptosis in colon cancer cells and associates with the nucleus in response to tumour necrosis factor α signalling. *Experimental cell research*, 313, 437-449.

Tersey, S. A., Colvin, S. C., Maier, B., & Mirmira, R. G. (2014). Protective effects of polyamine depletion in mouse models of type 1 diabetes: implications for therapy. *Amino acids, 46,* 633-642.

Tesina, P., Ebine, S., Buschauer, R., Thoms, M., Matsuo, Y., Inada, T., & Beckmann, R. (2023). Molecular basis of eIF5A-dependent CAT tailing in eukaryotic ribosome-associated quality control. *Molecular Cell, 83,* 607-621.

Thiebaut, M., Kisseleva-Romanova, E., Rougemaille, M., Boulay, J., & Libri, D. (2006). Transcription termination and nuclear degradation of cryptic unstable transcripts: a role for the nrd1-nab3 pathway in genome surveillance. *Molecular cell, 23,* 853-864.

Tong, Y., Park, I., Hong, B. S., Nedyalkova, L., Tempel, W., & Park, H. W. (2009). Crystal structure of human eIF5A1: insight into functional similarity of human eIF5A1 and eIF5A2. *Proteins: Structure, Function, and Bioinformatics, 75*, 1040-1045.

Topf, U., Suppanz, I., Samluk, L., Wrobel, L., Böser, A., Sakowska, P., & Warscheid, B. (2018). Quantitative proteomics identifies redox switches for global translation modulation by mitochondrially produced reactive oxygen species. *Nature communications, 9,* 324.

Troeger, J. S., Mederacke, I., Gwak, G. Y., Dapito, D. H., Mu, X., Hsu, C. C., & Schwabe, R. F. (2012). Deactivation of hepatic stellate cells during liver fibrosis resolution in mice. *Gastroenterology, 143,* 1073-1083.

Tsuboi, T., Viana, M. P., Xu, F., Yu, J., Chanchani, R., Arceo, X. G., Tutucci, E., Choi, J., Chen, Y. S., Singer, R. H., Rafelski, S. M., & Zid, B. M. (2020). Mitochondrial volume fraction and translation duration impact mitochondrial mRNA localization and protein synthesis. *Elife, 9,* e57814.

Tsuchida, T., & Friedman, S. L. (2017). Mechanisms of hepatic stellate cell activation. *Nature reviews Gastroenterology & hepatology, 14,* 397-411.

Ude, S., Lassak, J., Starosta, A. L., Kraxenberger, T., Wilson, D. N., & Jung, K. (2013). Translation elongation factor EF-P alleviates ribosome stalling at polyproline stretches. *Science, 339,* 82-85.

Vakifahmetoglu-Norberg, H., Ouchida, A. T., & Norberg, E. (2017). The role of mitochondria in metabolism and cell death. *Biochemical and biophysical research communications, 482*, 426-431.

Valentini, S. R., Casolari, J. M., Oliveira, C. C., Silver, P. A., & McBride, A. E. (2002). Genetic interactions of yeast eukaryotic translation initiation factor 5A (eIF5A) reveal connections to poly (A)-binding protein and protein kinase C signaling. *Genetics, 160*, 393-405.

Vander Heiden, M. G., Cantley, L. C., & Thompson, C. B. (2009). Understanding the Warburg effect: the metabolic requirements of cell proliferation. *Science, 324*, 1029-1033.

Vera, M., Pani, B., Griffiths, L. A., Muchardt, C., Abbott, C. M., Singer, R. H., & Nudler, E. (2014). The translation elongation factor eEF1A1 couples transcription to translation during heat shock response. *Elife, 3*, e03164.

Vögtle, F. N., Wortelkamp, S., Zahedi, R. P., Becker, D., Leidhold, C., Gevaert, K., & Meisinger, C. (2009). Global analysis of the mitochondrial N-proteome identifies a processing peptidase critical for protein stability. *Cell, 139*, 428-439.

Volpon, L., Culjkovic-Kraljacic, B., Sohn, H. S., Blanchet-Cohen, A., Osborne, M. J., & Borden, K. L. (2017). A biochemical framework for eIF4E-dependent mRNA export and nuclear recycling of the export machinery. *Rna, 23*, 927-937.

Wang, X., & Chen, X. J. (2015). A cytosolic network suppressing mitochondria-mediated proteostatic stress and cell death. *Nature, 524*, 481-484.

Warburg, O., Wind, F., & Negelein, E. (1927). The metabolism of tumors in the body. *The Journal of general physiology, 8*, 519.

Weidberg, H., & Amon, A. (2018). MitoCPR—A surveillance pathway that protects mitochondria in response to protein import stress. *Science, 360*, eaan4146.

Weinberg, D. E., Shah, P., Eichhorn, S. W., Hussmann, J. A., Plotkin, J. B., & Bartel, D. P. (2016). Improved ribosome-footprint and mRNA measurements provide insights into dynamics and regulation of yeast translation. *Cell reports, 14*, 1787-1799.

Weir, B. A., & Yaffe, M. P. (2004). Mmd1p, a novel, conserved protein essential for normal mitochondrial morphology and distribution in the fission yeast Schizosaccharomyces pombe. *Molecular biology of the cell, 15*, 1656-1665.

Weiskirchen, R., Weiskirchen, S., & Tacke, F. (2019). Organ and tissue fibrosis: Molecular signals, cellular mechanisms and translational implications. *Molecular aspects of medicine, 65*, 2-15.

Westermann, B., & Neupert, W. (2000). Mitochondria-targeted green fluorescent proteins: convenient tools for the study of organelle biogenesis in Saccharomyces cerevisiae. *Yeast, 16*, 1421-1427.

Wiedemann, N., & Pfanner, N. (2017). Mitochondrial machineries for protein import and assembly. *Annual review of biochemistry, 86*, 685-714.

Wieser, W., & Krumschnabel, G. (2001). Hierarchies of ATP-consuming processes: direct compared with indirect measurements, and comparative aspects. *Biochemical Journal, 355*, 389-395.

Williams, C. C., Jan, C. H., & Weissman, J. S. (2014). Targeting and plasticity of mitochondrial proteins revealed by proximity-specific ribosome profiling. *Science, 346*, 748-751.

Wolff, E. C., Kang, K. R., Kim, Y. S., & Park, M. H. (2007). Posttranslational synthesis of hypusine: evolutionary progression and specificity of the hypusine modification. *Amino acids, 33*, 341.

Wong, M. Y., & Shoulders, M. D. (2019). Targeting defective proteostasis in the collagenopathies. *Current opinion in chemical biology, 50*, 80-88.

Wrobel, L., Topf, U., Bragoszewski, P., Wiese, S., Sztolsztener, M. E., Oeljeklaus, S., & Chacinska, A. (2015). Mistargeted mitochondrial proteins activate a proteostatic response in the cytosol. *Nature, 524*, 485-488.

Wu, J., Suka, N., Carlson, M., & Grunstein, M. (2001). TUP1 utilizes histone H3/H2B–specific HDA1 deacetylase to repress gene activity in yeast. *Molecular cell, 7*, 117-126.

Wynn, T. (2008). Cellular and molecular mechanisms of fibrosis. *The Journal of Pathology: A Journal of the Pathological Society of Great Britain and Ireland, 214*, 199-210.

Xie, D., Ma, N. F., Pan, Z. Z., Wu, H. X., Liu, Y. D., Wu, G. Q., & Guan, X. Y. (2008). Overexpression of EIF-5A2 is associated with metastasis of human colorectal carcinoma. *Human pathology, 39*, 80-86.

Xu, A., Jao, D. L. E., & Chen, K. Y. (2004). Identification of mRNA that binds to eukaryotic initiation factor 5A by affinity co-purification and differential display. *Biochemical Journal, 384*, 585-590.

Xu, G. D., Shi, X. B., Sun, L. B., Zhou, Q. Y., Zheng, D. W., Shi, H. S., & Shao, G. F. (2013). Down-regulation of eIF5A-2 prevents epithelial-mesenchymal transition in non-small-cell lung cancer cells. *Journal of Zhejiang University SCIENCE B, 14*, 460-467.

Xu, G., Yu, H., Shi, X., Sun, L., Zhou, Q., Zheng, D., & Shao, G. (2014). Cisplatin sensitivity is enhanced in non-small cell lung cancer cells by regulating epithelial-mesenchymal

transition through inhibition of eukaryotic translation initiation factor 5A2. *BMC pulmonary medicine, 14*, 1-10.

Xu, X., Liu, H., Zhang, H., Dai, W., Guo, C., Xie, C., & Xu, X. (2015). Sonic Hedgehog–GLI Family Zinc Finger 1 Signaling Pathway Promotes the Growth and Migration of Pancreatic Cancer Cells by Regulating the Transcription of Eukaryotic Translation Initiation Factor 5A2. *Pancreas, 44*, 1252-1258.

Yamauchi, M., Barker, T. H., Gibbons, D. L., & Kurie, J. M. (2018). The fibrotic tumor stroma. *The Journal of clinical investigation, 128*, 16-25.

Yan, X., Hoek, T. A., Vale, R. D., & Tanenbaum, M. E. (2016). Dynamics of translation of single mRNA molecules in vivo. *Cell, 165*, 976-989.

Yang, G. F., Xie, D., Liu, J. H., Luo, J. H., Li, L. J., Hua, W. F., & Guan, X. Y. (2009). Expression and amplification of eIF-5A2 in human epithelial ovarian tumors and overexpression of EIF-5A2 is a new independent predictor of outcome in patients with ovarian carcinoma. *Gynecologic oncology, 112*, 314-318.

Yano, H., Baranov, S. V., Baranova, O. V., Kim, J., Pan, Y., Yablonska, S., & Friedlander, R. M. (2014). Inhibition of mitochondrial protein import by mutant huntingtin. *Nature neuroscience, 17*, 822-831.

Yanofsky, C. (1981). Attenuation in the control of expression of bacterial operons. *Nature, 289*, 751-758.

Yanofsky, C. (2000). Transcription attenuation: once viewed as a novel regulatory strategy. *Journal of bacteriology, 182*, 1-8.

Yao, M., Ohsawa, A., Kikukawa, S., Tanaka, I., & Kimura, M. (2003). Crystal structure of hyperthermophilic archaeal initiation factor 5A: a homologue of eukaryotic initiation factor 5A (eIF-5A). *Journal of biochemistry, 133*, 75-81.

Yu, C. H., Dang, Y., Zhou, Z., Wu, C., Zhao, F., Sachs, M. S., & Liu, Y. (2015). Codon usage influences the local rate of translation elongation to regulate co-translational protein folding. *Molecular cell, 59*, 744-754.

Zaman, Z., Ansari, A. Z., Koh, S. S., Young, R., & Ptashne, M. (2001). Interaction of a transcriptional repressor with the RNA polymerase II holoenzyme plays a crucial role in repression. *Proceedings of the National Academy of Sciences, 98*, 2550-2554.

Zaman, S., Lippman, S. I., Schneper, L., Slonim, N., & Broach, J. R. (2009). Glucose regulates transcription in yeast through a network of signaling pathways. *Molecular systems biology, 5*, 245.

Zaman, S., Lippman, S. I., Zhao, X., & Broach, J. R. (2008). How Saccharomyces responds to nutrients. *Annual review of genetics, 42*, 27-81.

Zanelli, C. F., Maragno, A. L., Gregio, A. P., Komili, S., Pandolfi, J. R., Mestriner, C. A., & Valentini, S. R. (2006). eIF5A binds to translational machinery components and affects translation in yeast. *Biochemical and biophysical research communications, 348*, 1358-1366.

Zanelli, C. F., & Valentini, S. R. (2005). Pkc1 acts through Zds1 and Gic1 to suppress growth and cell polarity defects of a yeast eIF5A mutant. *Genetics, 171*, 1571-1581.

Zanelli, C. F., & Valentini, S. R. (2007). Is there a role for eIF5A in translation?. *Amino acids, 33*, 351.

Zeisberg, M., & Kalluri, R. (2013). Cellular mechanisms of tissue fibrosis. 1. Common and organ-specific mechanisms associated with tissue fibrosis. *American Journal of Physiology-Cell Physiology, 304*, C216-C225.

Zhang, H., Alsaleh, G., Feltham, J., Sun, Y., Napolitano, G., Riffelmacher, T., Charles, P., Frau, L., Hublitz, P., Yu, Z., Mohammed, S., Ballabio, A., Balabanov, S., Mellor, J., & Simon, A. K. (2019). Polyamines control eIF5A hypusination, TFEB translation, and autophagy to reverse B cell senescence. *Molecular cell, 76*, 110-125.

Zhang, L., & Guarente, L. (1994). The yeast activator HAP1--a GAL4 family member--binds DNA in a directly repeated orientation. *Genes & Development, 8*, 2110-2119.

Zhang, L., & Hach, A. (1999). Molecular mechanism of heme signaling in yeast: the transcriptional activator Hap1 serves as the key mediator. *Cellular and Molecular Life Sciences, 56*, 415-426.

Zhang, T., Bu, P., Zeng, J., & Vancura, A. (2017). Increased heme synthesis in yeast induces a metabolic switch from fermentation to respiration even under conditions of glucose repression. *Journal of Biological Chemistry, 292*, 16942-16954.

Zhang, X., Han, S., Zhou, H., Cai, L., Li, J., Liu, N., & Miao, Y. (2019). TIMM50 promotes tumor progression via ERK signaling and predicts poor prognosis of non-small cell lung cancer patients. Molecular Carcinogenesis, 58, 767-776.

Zhang, Y., Chen, Y., Gucek, M., & Xu, H. (2016). The mitochondrial outer membrane protein MDI promotes local protein synthesis and mt DNA replication. *The EMBO journal, 35*, 1045-1057.

Zhang, Y., & Stefanovic, B. (2016). LARP6 meets collagen mRNA: specific regulation of type I collagen expression. *International journal of molecular sciences, 17*, 419.

Zhang, Y., Su, D., Zhu, J., Wang, M., Zhang, Y., Fu, Q., Zhang, S., & Lin, H. (2022). Oxygen level regulates N-terminal translation elongation of selected proteins through deoxyhypusine hydroxylation. *Cell reports*, *39*, 110855.

Zhu, M., Dai, X., & Wang, Y. P. (2016). Real time determination of bacterial in vivo ribosome translation elongation speed based on LacZα complementation system. *Nucleic acids research*, *44*, e155-e155.

Zitomer, R. S., Carrico, P., & Deckert, J. (1997). Regulation of hypoxic gene expression in yeast. *Kidney international*, *51*, 507-513.

Zitomer, R. S., & Lowry, C. V. (1992). Regulation of gene expression by oxygen in Saccharomyces cerevisiae. *Microbiological reviews*, *56*, 1-11.

Zuk, D., & Jacobson, A. (1998). A single amino acid substitution in yeast eIF-5A results in mRNA stabilization. *The EMBO journal*, *17*, 2914-2925.

Annex I

Supplementary Information

Table A1.1. *Saccharomyces cerevisiae* strains used in this study.

Name	Genotype	Source
BY4741	MATa *ura3Δ0 leu2Δ0 his3Δ1 met15Δ0*	Euroscarf
***hap1*Δ**	BY4741 MATa *ura3Δ0leu2Δ0 his3Δ1 met15Δ0 hap1::kanMX6*	This study
***hap4*Δ**	BY4741 MATa *ura3Δ0 leu2Δ0 his3Δ1 met15Δ0 hap4::kanMX4*	Euroscarf
***lia1*Δ**	BY4741 MATa *ura3Δ0 leu2Δ0 his3Δ1 met15Δ0 lia1::kanMX4*	Euroscarf
***mpc1*Δ**	BY4741 MATa *ura3Δ0 leu2Δ0 his3Δ1 met15Δ0 mpc1::kanMX4*	Euroscarf
***msn2*Δ**	BY4741 MATa *ura3Δ0 leu2Δ0 his3Δ1 met15Δ0 msn2::kanMX4*	Euroscarf
***pda1*Δ**	BY4741 MATa *ura3Δ0 leu2Δ0 his3Δ1 met15Δ0 pda1::kanMX4*	Euroscarf
***snf1*Δ**	BY4741 MATa *ura3Δ0 leu2Δ0 his3Δ1 met15Δ0 snf1::kanMX4*	Euroscarf
***ssn6*Δ**	BY4741 MATa *ura3Δ0 leu2Δ0 his3Δ1 met15Δ0 ssn6::kanMX4*	Euroscarf
***tup1*Δ**	BY4741 MATa *ura3Δ0 leu2Δ0 his3Δ1 met15Δ0 tup1::kanMX4*	Euroscarf
FY2609	MATa *ura3Δ0 leu2Δ0 his3Δ200 lys2-128δ HAP1*	(Hickman & Winston, 2007)
FY2613	MATa *ura3Δ0 leu2Δ0 his3Δ200 lys2-128δ* 3myc-*HAP1*	(Hickman & Winston, 2007)
J697	MATα *trp1-Δ63 ura3-52 leu2-3 leu2-112 gcn2Δ tif51b::NAT tif51a::kanMX4 + p[TIF51A, LEU2]*	(Saini *et al.*, 2009)
J699	MATα *trp1-Δ63 ura3-52 leu2-3 leu2-112 gcn2Δ tif51b::NAT tif51a::kanMX4 + p[tif51a-S149P, LEU2]*	(Saini *et al.*, 2009)
PAY780	MATα *ura3Δ0 leu2Δ0 his3Δ200 trp1Δ1 tif51A::LEU2 tif51B::HIS3 (pBM-TIF51A)*	(Schwelberger *et al.*, 1993)
PAY859	BY4741 MATa *ura3Δ0 leu2Δ0 his3Δ1 met15Δ0 YTA12-13myc-his3MX6*	This study
PAY860	BY4741 MATa *ura3Δ0 leu2Δ0 his3Δ1 met15Δ0 tif51A-1::kanR YTA12-13myc-his3MX6*	This study
PAY864	BY4741 MATa *ura3Δ0 leu2Δ0 his3Δ1 met15Δ0 TIM50-3HA-his3MX6*	This study
PAY866	BY4741 MATa *ura3Δ0 leu2Δ0 his3Δ1 met15Δ0 tif51A-1::kanR TIM50-3HA-his3MX6*	This study
PAY888	BY4741 MATa *ura3Δ0 leu2Δ0 his3Δ1 met15Δ0 TIM50-GFP-his3MX6*	This study
PAY890	BY4741 MATa *ura3Δ0 leu2Δ0 his3Δ1 met15Δ0 tif51A-1::kanR TIM50-GFP-his3MX6*	This study
PAY892	BY4741 MATa *ura3Δ0 leu2Δ0 his3Δ1 met15Δ0 YTA12-GFP-his3MX6*	This study
PAY893	BY4741 MATa *ura3Δ0 leu2Δ0 his3Δ1 met15Δ0 tif51A-1::kanR YTA12-GFP-his3MX6*	This study
PAY896	BY4741 MATa *ura3Δ0 leu2Δ0 his3Δ1 met15Δ0 BNR1-3HA-his3MX6*	This study
PAY898	BY4741 MATa *ura3Δ0 leu2Δ0 his3Δ1 met15Δ0 tif51A-1::kanR BNR1-3HA-his3MX6*	This study
PAY899	BY4741 MATa *ura3Δ0 leu2Δ0 his3Δ1 met15Δ0 BNR1ΔPro-3HA-his3MX6*	This study
PAY901	BY4741 MATa *ura3Δ0 leu2Δ0 his3Δ1 met15Δ0 tif51A-1::kanR BNR1ΔPro-3HA-his3MX6*	This study
PAY915	BY4741 MATa *ura3Δ0 leu2Δ0 his3Δ1 met15Δ0 TUP1-13myc-his3MX6*	This study
PAY916	BY4741 MATa *ura3Δ0 leu2Δ0 his3Δ1 met15Δ0 hap1::kanMX6 TUP1-13myc-his3MX6*	This study
PAY937	BY4741 MATa *ura3Δ0 leu2Δ0 his3Δ1 met15Δ0 PDR5-GFP-his3MX6*	This study
PAY938	BY4741 MATa *ura3Δ0 leu2Δ0 his3Δ1 met15Δ0 tif51A-1::kanR PDR5-GFP-his3MX6*	This study
PAY983	BY4741 MATa *ura3Δ0 leu2Δ0 his3Δ1 met15Δ0 SSN6-13myc-his3MX6*	This study
PAY984	BY4741 MATa *ura3Δ0 leu2Δ0 his3Δ1 met15Δ0 hap1::kanMX6 SSN6-13myc-his3MX6*	This study
PAY1066	BY4741 MATa *ura3Δ0 leu2Δ0 his3Δ1 met15Δ0 TOM70-GFP-his3MX6 SU9-mCherry-URA3*	This study
PAY1067	BY4741 MATa *ura3Δ0 leu2Δ0 his3Δ1 met15Δ0 tif51A-1::kanR TOM70-GFP-his3MX6 SU9-mCherry-URA3*	This study
PAY1068	BY4741 MATa *ura3Δ0 leu2Δ0 his3Δ1 met15Δ0 CYC1-GFP-his3MX6 SU9-mCherry-URA3*	This study
PAY1069	BY4741 MATa *ura3Δ0 leu2Δ0 his3Δ1 met15Δ0 tif51A-1::kanR CYC1-GFP-his3MX6 SU9-mCherry-URA3*	This study
PAY1072	BY4741 MATa *ura3Δ0 leu2Δ0 his3Δ1 met15Δ0 ILV2-GFP-his3MX6 SU9-mCherry-URA3*	This study

Table A1.1. *Saccharomyces cerevisiae* strains used in this study (continued).

Name	Genotype	Source
PAY1073	BY4741 MATa *ura3Δ0 leu2Δ0 his3Δ1 met15Δ0 tif51A-1::kanR ILV2-GFP-his3MX6 SU9-mCherry-URA3*	This study
PAY1078	BY4741 MATa *ura3Δ0 leu2Δ0 his3Δ1 met15Δ0 TIM50-GFP-his3MX6 SU9-mCherry-URA3*	This study
PAY1079	BY4741 MATa *ura3Δ0 leu2Δ0 his3Δ1 met15Δ0 tif51A-1::kanR TIM50-GFP-his3MX6 SU9-mCherry-URA3*	This study
PAY1080	BY4741 MATa *ura3Δ0 leu2Δ0 his3Δ1 met15Δ0 YTA12-GFP-his3MX6 SU9-mCherry-URA3*	This study
PAY1081	BY4741 MATa *ura3Δ0 leu2Δ0 his3Δ1 met15Δ0 tif51A-1::kanR YTA12-GFP-his3MX6 SU9-mCherry-URA3*	This study
PAY1085	BY4741 MATa *ura3Δ0 leu2Δ0 his3Δ1 met15Δ0 TIM50Δ7Pro-GFP-his3MX6*	This study
PAY1086	BY4741 MATa *ura3Δ0 leu2Δ0 his3Δ1 met15Δ0 tif51A-1::kanR TIM50Δ7Pro-GFP-his3MX6*	This study
PAY1087	BY4741 MATa *ura3Δ0 leu2Δ0 his3Δ1 met15Δ0 YTA12Δ9Pro-GFP-his3MX6*	This study
PAY1088	BY4741 MATa *ura3Δ0 leu2Δ0 his3Δ1 met15Δ0 tif51A-1::kanR YTA12Δ9Pro-GFP-his3MX6*	This study
PAY1105	BY4741 MATa *ura3Δ0 leu2Δ0 his3Δ1 met15Δ0 TIM50-GFP-his3MX6 HSP42-RFP-clonNAT*	This study
PAY1107	BY4741 MATa *ura3Δ0 leu2Δ0 his3Δ1 met15Δ0 TIM50-GFP-his3MX6 HSP104-RFP-clonNAT*	This study
PAY1111	BY4741 MATa *ura3Δ0 leu2Δ0 his3Δ1 met15Δ0 tif51A-1::kanR TIM50-GFP-his3MX6 HSP42-RFP-clonNAT*	This study
PAY1113	BY4741 MATa *ura3Δ0 leu2Δ0 his3Δ1 met15Δ0 tif51A-1::kanR TIM50-GFP-his3MX6 HSP104-RFP-clonNAT*	This study
PAY1139	MATa *trp1Δ0 leu2Δ0* pRS306-pADH1-OsTIR1 *TIM23-IAA17-kanMX6*	This study
PAY1142	BY4741 MATa *ura3Δ0 leu2Δ0 his3Δ1 met15Δ0 CYC1-GFP-his3MX6 HSP104-RFP-clonNAT*	This study
PAY1144	BY4741 MATa *ura3Δ0 leu2Δ0 his3Δ1 met15Δ0 tif51A-1::kanR CYC1-GFP-his3MX6 HSP104-RFP-clonNAT*	This study
tif51A-1	BY4741 MATa *ura3Δ0 leu2Δ0 his3Δ1 met15Δ0 tif51A-1::kanR*	(Li *et al.*, 2011)
tif51A-3	BY4741 MATa *ura3Δ0 leu2Δ0 his3Δ1 met15Δ0 tif51A-3::kanR*	(Li *et al.*, 2011)
yMC805	MATa *trp1Δ0 leu2Δ0* pRS306-pADH1-OsTIR1	M. Choder

Table A1.2. Chemical composition of media, buffers and solutions used in this study.

Solution	Chemical composition
Culture media	
Drop-Out complete	18 mg/L adenine, 380 mg/L L-leucine, 76 mg/L for rest of amino acids
LB	1% NaCl, 1% tryptone, 0.5% yeast extract
SC	2% glucose, 0.7% yeast nitrogen base, Drop-Out complete
SGal	2% galactose, 0.7% yeast nitrogen base, Drop-Out complete
YEP	2% bacteriological peptone, 1% yeast extract
YPD	2% glucose, 2% bacteriological peptone, 1% yeast extract
YPEtOH	2% ethanol, 2% bacteriological peptone, 1% yeast extract
YPGal	2% galactose, 2% bacteriological peptone, 1% yeast extract
YPGly	2% glycerol, 2% bacteriological peptone, 1% yeast extract
General buffers and solutions	
10 Prep Buffer	2% Triton X-100, 1% SDS, 0.1 M NaCl, 10 mM Tris-HCl pH 8.0, 1 mM EDTA pH 8.0
AGC mix	10 mM each of ATP, CTP, and GTP
ChIP Lysis Buffer	50 mM HEPES pH 7.5, 140 mM NaCl, 1 mM EDTA pH 8.0, 1% Triton X-100, 0.1% sodium deoxycholate, 1 mM PMSF, 1 mM benzamidine, protease inhibitor cocktail
ChIP Elution Buffer	50 mM Tris-HCl pH 8.0, 10 mM EDTA pH 8.0, 1% SDS
Complete Lysis Buffer	20 mM HEPES pH 7.4, 400 mM NaCl, 20% glycerol, 0.1 mM EDTA, 10 μM Na_2MoO_4, 10 mM NaF
DNA Gel loading dye	3x TBE buffer, 30% glycerol, 0.25% bromophenol blue
dNTP mix	16 mM dATP, dTTP, dGTP and 0.1 mM dCTP
Dual-luciferase Lysis Buffer	50 mM Tris-HCl pH 7.5, 150 mM NaCl, 5 mM $MgCl_2$, 5% NP-40, protease inhibitor cocktail
Hybridization solution	0.5 M phosphate buffer, 1 mM EDTA, 7% SDS, pH 7.2
LETS	0.1 M LiCl, 10 mM EDTA pH 8.0, 10 mM Tris-HCl pH 7.4, 0.2% SDS
PBS	137 mM NaCl, 2.7 mM KCl, 10 mM Na_2HPO_4, 1.8 mM KH_2PO_4
PBS/Tween	1x PBS, 0.02% Tween
Polysome Lysis Buffer	20 mM Tris-HCl pH 8, 140 mM KCl, 5 mM $MgCl_2$, 0.5 mM DTT, 1% Triton X-100, 0.1 mg/mL CHX, and 0.5 mg/mL heparin
Protein loading buffer	24 mM Tris-HCl pH 6.8, 10% glycerol, 0.8% SDS, 5.76 mM β-mercaptoethanol, 0.04% bromophenol blue
RIPA Buffer	150 mM NaCl, 0.05 M Tris-HCl pH 8.0, 0.005 mM EDTA, 0.1% SDS, 0.5% sodium deoxycholate, 1% NP-40, protease inhibitor cocktail
SDS Running Buffer	25 mM Tris Base, 192 mM glycine, 0.1% SDS, pH: 8.1-8.5
SSC	3M NaCl, 0.3M sodium citrate
TBE 0.5x	40 mM Tris-HCl, 45 mM boric acid, 1 mM EDTA pH 8
TBS	25 mM Tris Base, 15 mM NaCl, pH 7.5
TE 1x	10 mM Tris-HCl pH 7.5, 1 mM EDTA pH 8.0
Transcription Buffer	50 mM Tris-HCl pH 7.7, 500 mM KCl, 80 mM MgCl2
Transfer Buffer	25 mM Tris Base, 192 mM glycine, 0.1% SDS, 20% methanol, pH: 8.1-8.5
TBS-T	20 mM Tris Base, 150 mM NaCl 15 mM, 0.1% Tween 20
Z Buffer	60 mM Na2HPO4, 40 mM NaH_2PO_4, 10 mM KCl, 1 mM $MgSO_4$, 50 mM β-mercaptoethanol

Table A1.3. Reagents used in this study.

Chemical	Working concentration	Stock concentration	Solvent	Source
Culture supplements				
Ampicillin	50 µg/mL	50 mg/mL	H_2O	Sigma-Aldrich (A8351)
ALA	300 µg/mL	100 mg/mL	H_2O	Sigma-Aldrich (A3785)
Antimycin A	10 µg/mL	1 mg/mL	Ethanol	Sigma-Aldrich (A8674)
Auxin	0.5 mM	0.5 M	Ethanol	Sigma-Aldrich (I2886)
Bacteriological agar	2%	100%	H_2O	Condalab (1800)
BPS	100 µM	100 mM	H_2O	Sigma-Aldrich (B1357)
CCCP	1 µM	1 mM	Ethanol	Sigma-Aldrich (C2759)
Cyclohexamide	0.1 mg/mL	10 mg/mL	H_2O	Sigma-Aldrich (C7698)
Doxycycline	2 or 10 µg/mL	1 mg/mL	Ethanol	Sigma-Aldrich (D5207)
Drop-Out	0.1%	100%	H_2O	Kaiser, Formedium
Furimazine	5 µM	10 mM	DMSO	Promega
Galactose	2%	100%	H_2O	Sigma-Aldrich (15522)
GC7	30 µM	10 mM	PBS	Calbiochem (150333-69-0)
Geneticin	200 µg/mL	20 mg/mL	H_2O	Gibco (G418)
Glucose	2%	100%	H_2O	Condalab (1900)
Glycerol	2%	100%	H_2O	Sigma-Aldrich (G5516)
Hemin	25 µg/mL	10 mg/mL	DMSO	Sigma-Aldrich (H9039)
Nourseothricin	100 µg/mL	10 mg/mL	H_2O	Goldbio (N-500-100)
ONPG	0.8 mg/mL	4 mg/mL	H_2O	Sigma-Aldrich (N1127)
Peptone	2%	100%	H_2O	Condalab (1616)
Rapamycin	200 ng/mL	0.5 mg/mL	Ethanol	LC Laboratories (R-500)
TGFβ-1	2.5 ng/mL	20 µg/mL	DMSO	Myltenyi Biotec
Tryptone	1%	100%	H_2O	Condalab (1612)
Yeast extract	1%	100%	H_2O	Condalab (1702)
YNB	0.7%	100%	H_2O	Fisher Scientific (11387809)
Commercial Kits				
Dual-luciferase Assay	-	-	-	Promega (E1910)
GeneJet Gel extraction	-	-	-	Thermo Fisher Scientific (K0691)
GeneJet Plasmid MiniPrep	-	-	-	Thermo Fisher Scientific (K0503)
GeneJet Purification	-	-	-	Thermo Fisher Scientific (K0702)
PureLink RNA Mini	-	-	-	Invitrogen (12183018A)
SpeedTools Total RNA Extraction	-	-	-	Biotools B&M Labs (21.212-4210)
Microscopy probes				
DAPI	1 µg/mL	1 mg/mL	H_2O	Thermo Fisher Scientific (62248)
MitoTracker	0.5 µM	1 mM	DMSO	Thermo Fisher Scientific (M7512)
Nile Red	3.5 µM	3.5 mM	DMSO	Thermo Fisher Scientific (N1142)

Table A1.3. Reagents used in this study (continued).

Chemical	Working concentration	Stock concentration	Solvent	Source
Other				
Acrylamide:bisacrylamide	-	30%	-	PanReac Applichem (A3626)
Benzamidine	1 mM	-	H_2O	Sigma-Aldrich (B6506)
DMSO	-	-	-	Sigma-Aldrich (D8418)
DNA Ladder	-	-	-	Thermo Fisher Scientific (SM0332)
DNAse	1 U/µL	10 U/µL	-	Roche (04716728001)
DTT	0.1M	1M	H_2O	Sigma-Aldrich (DTT-RO)
FCS	10%	100%	DMEM	Gibco (A5256701)
Formaldehyde	1%	37%	H_2O	Sigma-Aldrich (F1635)
Laminin	10 ug/mL	0.5 mg/mL	PBS	Roche (11243217001)
Maxima RT	-	-	-	Thermo Fisher Scientific (EP0741)
NP-40	1%	100%	H_2O	Sigma-Aldrich (I3021)
Pfu Ultra Polymerase	-	-	-	Agilent (600380)
Penicillin-streptomycin	1%	100%	DMEM	Gibco (15070063)
PMSF	1 mM	0.1M	Ethanol	Sigma-Aldrich (PMSF-RO)
PNK	-	-	-	Roche (PNK-RO)
Protease Inhibitor cocktail cOmplete	-	-	H_2O	Roche (11836153001)
Protein ladder	-	-	-	Thermo Fisher Scientific (26617)
Proteinase K	0.5 mg/mL	18.5 mg/mL	-	Roche (RPROTKSOL-RO)
Red Ponceau	0.5%	100%	5% acetic acid	Sigma-Aldrich (B6008)
RNAse	0.1 mg/mL	10 mg/mL	H_2O	Roche (10109134001)
RNase OUT	-	-	-	Invitrogen (10777019)
SafeView	-	-	-	NBS Biologicals (NBS-SV1)
SDS	1%	100%	H_2O	Sigma-Aldrich (L3771)
Skimmed milk	5%	100%	TBS-T	Thermo Fisher Scientific (LP0033B)
Sodium deoxycholate	1%	100%	H_2O	Sigma-Aldrich (30970)
SYBR Green	-	-	-	Takara (RR820W)
Subcloning Efficiency™ DH5α	-	-	-	Invitrogen (18265017)
Taq DNA Polymerase	-	-	-	Biotools (10.002)
Triton X-100	1%	100%	H_2O	Sigma-Aldrich (T9284)
Trypsin-EDTA	0.25X	10X	PBS	Gibco (15400054)
Tween	0.02%	100%	H_2O	Sigma-Aldrich (P7949)
Transfection reagents				
Control siRNA	-	-	-	Santa Cruz Biotechnology (sc-36869)
Control siRNA	-	-	-	Sigma-Aldrich (SIC001)
DHPS siRNA	-	-	-	Sigma-Aldrich (EMU150671)
eIF5A siRNA	-	-	-	Santa Cruz Biotechnology (sc-40560)
Lipofectamine 3000	-	-	-	Thermo Fisher Scientific (L3000015)
Opti-Mem I	-	-	-	Thermo Fisher Scientific (31985062)
Transfection medium	-	-	-	Santa Cruz Biotechnology (sc-36868)
Transfection reagent	-	-	-	Santa Cruz Biotechnology (sc-29528)

Table A1.4. Oligonucleotides used in this study.

Primer	Sequence (5'-3')
Oligonucleotides for *S. cerevisiae* gene expression analysis by RT-qPCR	
ACT1-F	TCGTTCCAATTTACGCTGGTT
ACT1-R	CGGCCAAATCGATTCTCAA
ARF1-F	AGATCGCGTATTGGTGAAGC
ARF1-R	ACACGTGGCTTGGATAAACC
BNI1-F	ACATGTGGAAAACGGAAAGC
BNI1-R	AGATCTTCTGCGCCATCTGT
BNR1-F	CCAGCTCCACCTTTACCAAA
BNR1-R	CCCAGTGGATTTGCTTCAAT
CDC48-F	GCTGCTGAAACACACGGTTA
CDC48-R	AGAATCGAGCACCTCTGCAT
CIS1-F	TGCAGAGTGGGTAGCATGTC
CIS1-R	TGGGCAGCCTTGAGTAAATC
COX5A-F	ATCCAGATGGGAGAACATGC
COX5A-R	AGCTTGCTTTTCAGGCTCAG
CYC1-F	AGATGTCTACAATGCCACACC
CYC1-R	CCCTTCAGCTTGACCAGAGT
EFT2-F	TGTTCATCAAGGCCATTCAA
EFT2-R	GTTACCGGCTGGACAGTCAT
eIF2A-F	ATTCTACTCCGGCCCCATCT
eIF2A-R	TCTAGTTTGTCACCGACGGC
GAL1-F	TGGTGTTAACAATGGCGGTA
GAL1-R	GGGCGGTTTCAAACTTGTTA
GAPDH-F	ATGACCGCCACTCAAAAGAC
GAPDH-R	CTTAGCAGCACCGGTAGAGG
GIS2-F	GTAACAAACCCGGTCACGTT
GIS2-R	TTCTTTGGTTCAGGGCATTC
GRE2-F	GCCTTCCAAAAGAGGGAAAC
GRE2-R	ATGGGTAGCACCAGAACCTG
HAP1-F	TTGGACCTTCCTCACGAATC
HAP1-R	CAGGATCTTCACTGCCCATT
HSP10-F	CCGGGCTTTACTGATGCTAA
HSP10-R	TCAGCGTCCCTGAAAAGAAT
HSP104-F	AGCAGGCTCGTCAAGGTAAA
HSP104-R	TTACCGATACCTGGCTCACC
Intergen-F	GGCTGTCAGAATATGGGGCCGTAGTA
Intergen-R	CACCCCGAAGCTGCTTTCACAATAC
NLUC-F	AGAACAAGGTGGTGTTTCTTCT
NLUC-R	CCCATTTGATCACCAGATAAACCT
MSP1-F	ACGGCAACCTTAAAAGCTGA
MSP1-R	CCTCCTCAAAAAACGCATCAT
MOT3-F	CCCCATCATCAGACCATAAA
MOT3-R	CACCAAGGGCATAGAAAATG
NOG2-F	TTCAGAAGTGCATTGGGTGA
NOG2-R	CTGCGTCCTTTTCTTCCAAC

Table A1.4. Oligonucleotides used in this study (continued).

Primer	Sequence (5'-3')
Oligonucleotides for *S. cerevisiae* gene expression analysis by RT-qPCR	
PDR1-F	TCCAAATGCGAGATTTTTCC
PDR1-R	CGAAGATGGGGTTGAAGGTA
PDR3-F	AGATGGGATTGTCTCGTTGG
PDR3-R	CTGAAATCCTTCGGCAAGAG
PDR5-F	GTACCGTGGTTGGAGCTGTT
PDR5-R	GAAACCACGCCATTTGTCTT
PDR15-F	CCAAGGTCGGAAACGATCTA
PDR15-R	CAATGTCAGCCTGGGTTTTT
PET9-F	AGGCCATGTTTGGTTTCAAG
PET9-R	TCAAACCGTTGAATTGACGA
ROX1-F	AGGGCTTACAACCGGAAGAT
ROX1-R	GCTGTTGCTCGATTTCCTTC
RPN6-F	TTGTGTGCGAGAAAAGCATC
RPN6-R	CGTCCAGCTTTTTGAACTCC
RPP2B-F	GGAAGGTAAGGGCTCTTTGG
RPP2B-R	TTCTTCAGCAGCATCACCAC
RPT1-F	AAGTTGTCGAGCTGCCCTTA
RPT1-R	GCTCAGACCCAATGACCCTA
RPT5-F	GCTAAACTAGTCCGCGATGC
RPT5-R	ATTCCAGCATGGTTCTTTGC
SCL1-F	ATACCGGATGCAAGAAATGC
SCL1-R	AACCTGCAGGGTCAGTTTTG
SDH1-F	CTCCAAGTTGACTTTGCTCAGAA
SDH1-R	ACGCGGAACCGTTTACAGA
SDH2-F	ATTGAGAAGGAAGGCCTTTTGT
SDH2-R	AGTTTTCAATCTGGGGGTATGC
SDH8-F	GCCTGAATTTTCCAAGACCA
SDH8-R	AAACGAATAATCGCCGTGTC
SSB1-F	TGTTCGGTATCGTTGTTCCA
SSB1-R	TGGTTTGGTTGTCAGCACAT
SSB2-F	CCAGAATTCCAAAGGTCCAA
SSB2-R	GTGGATTGGCCAGTCAAGAT
TIF51-1	TCGACAATCTTACATGGTCT
TIF51A-1	CGATTCTACTTCTGTAGCCA
TIF51B-1	CTACACTTTAGTTCCCTTAC
TIM50-F	TCTGCGTTGACAGGTACTGC
TIM50-R	AATCAGGGAAAGGTGGCTCT
TOM20-F	CCGCAATTCAGGAAAGTGTT
TOM20-R	CCTTTTGCAGCTTCACTTCC
TOM70-F	GACCCAAGAAGTGAGCAAGC
TOM70-R	AGCGGCTTCAGCAAAAGTAA
UBX2-F	AAGTGGTGGCGGTAATTCAG
UBX2-R	AAATGCATCCTTGTCCTTCG

Table A1.4. Oligonucleotides used in this study (continued).

Primer	Sequence (5'-3')
Oligonucleotides for *S. cerevisiae* gene expression analysis by RT-qPCR	
VRP1-F	GGCAGAAATTAATGCCAGGA
VRP1-R	GTGGTGCAGTAGGCGGTAAT
XRN1-F	AATCGCCAAAGTCACAAAGC
XRN1-F	CCTTTGACAATCCCCATTTG
YTA10-F	TTTCTGGGAAATTGGCTACG
YTA10-R	TCAATGGCTTGCTCAAAGTG
YTA12-F	GTTTGTTGGTGTTGGTGCAG
YTA12-R	TCATCATTGGCACCTGAAAA
Oligonucleotides for *Mus musculus* gene expression analysis by RT-qPCR	
ATF6-F	AGCTGTCTGTGTGATGATAG
ATF6-R	GTGATCATAGCTGTAACTGTC
BIP-F	CATGGTTCTCACTAAAATGAAGG
BIP-R	GCTGGTACAGTAACAACT
CHOP-F	TGTTGAAGATGAGCGGGTGG
CHOP-R	CGTGGACCAGGTTCTGCTTT
COL I α1-F	GAAGCACGTCTGGTTTGG
COL I α1-F	ACTCGAACGGGAATCCAT
eIF5A1-F	TGGTTTAGGTTCCCCTCTCC
eIF5A1-R	GCTTGGGGGTGAAGGACTAT
GAPDH-F	AGGTCGGTGTGAACGGATTTG
GAPDH-R	GGGGTCGTTGATGGCAACA
Oligonucleotides for PCR-mediated disruption in *S. cerevisiae*	
HAP1-F1	GAAATAGAAGAAAAAGAAAAAAAAAAAAAGGGAACAATAGGTTAGCGGATCCCCGGGTTAATTAA
HAP1-R1	TTACATTATCAATCCTTGCGTTTCAGCTTCCACTAATTTAGATGAGAATTCGAGCTCGTTTAAAC
Oligonucleotides for PCR-mediated gene tagging in *S. cerevisiae*	
BNR1-F2	TTACTAGAGAGAACGCATGCTATGCTGAACGATATTCAAAATATACGGATCCCCGGGTTAATTAA
BNR1-R1	TTTCTTTATATAAGCTCCACAACTACATAAAATACTAAGTCTTCAGAATTCGAGCTCGTTTAAAC
CYC1-F2	AAAGACAGAAACGACTTAATTACCTACTTGAAAAAAGCCTGTGAGCGGATCCCCGGGTTAATTAA
CYC1-R1	TGACATAACTAATTACATGATATCGACAAAGGAAAAGGGGCCTGTGAATTCGAGCTCGTTTAAAC
HSP42-RFP-F	GAAGAATTGGGAGTTTGAAGAAAATCCCAACCCTACGGTAGAAAATCGTACGCTGCAGGTCGAC
HSP42-RFP-R	TTATAAATATAAATGTATGTATGTGTGTATAAACAGATACGATATTCAATCGATGAATTCGAGCTCG
HSP104-RFP-F	GATGACGATAATGAGGACAGTATGGAAATTGATGATGACCTAGATCGTACGCTGCAGGTCGAC
HSP104-RFP-R	TACTGCTTCTTGTTCGAAAGTTTTTTAAAAATCACACTATATTAAATCAATCGATGAATTCGAGCTCG
ILV2-F2	AGACAACAGACTGAATTACGTCATAAGCGTACAGGCGGTAAGCACCGGATCCCCGGGTTAATTAA
ILV2-R1	TGCATTTTTTACTGAAAATGCTTTTGAAATAAATGTTTTTGAAATGAATTCGAGCTCGTTTAAAC

Table A1.4. Oligonucleotides used in this study (continued).

Primer	Sequence (5'-3')
Oligonucleotides for PCR-mediated gene tagging in *S. cerevisiae*	
PDR5-F2	TGGTTAGCAAGAGTGCCTAAAAAGAACGGTAAACTCTCCAAGAAACGGATCCCCGGGTTAATTAA
PDR5-R1	GTCCATCTTGGTAAGTTTCTTTTCTTAACCAAATTCAAAATTCTAGAATTCGAGCTCGTTTAAAC
SSN6-F2	GAAAATGTAGTAAGGCAAGTGGAAGAAGATGAAAACTACGACGACCGGATCCCCGGGTTAATTAA
SSN6-R1	TCGTTGATTATAAATTAGTAGATTAATTTTTTGAATGCAAACTTTGAATTCGAGCTCGTTTAAAC
TIM23-F	GCGTGCGCCGTCTGGTGTAGTGTCAAGAAAAGACTACTTGAAAAAAATGATGGGCAGTGTCGAG
TIM23-R	GAGAGAGAGAGAGAAAGAGAGAGAGAGTAGGTTCTTGTGTTGCCCGGCAGATCCGCGGCCGC
TIM50-F2	TTATTTGAAGAGGAAAAGAAAAAAGAAGAAGATTGCTGAATCCAAACGGATCCCCGGGTTAATTAA
TIM50-R1	CACACATAGATACGTAGATACATGAGAAGAGGGTTTACATGAAAAGAATTCGAGCTCGTTTAAAC
TOM70-F2	AAGATTCAAGAAACTTTAGCTAAATTACGCGAACAGGGTTTAATGCGGATCCCCGGGTTAATTAA
TOM70-R1	TAGTTTTTGTCTTCTCCTAAAAGTTTTTAAGTTTATGTTTACTGTGAATTCGAGCTCGTTTAAAC
TUP1-F2	GATTGTAAAGCAAGGATTTGGAAGTATAAAAAATAGCGCCAAATCGGATCCCCGGGTTAATTAA
TUP1-R1	GTTTAGTTAGTTACATTTGTAAAGTGTTCCTTTTGTGTTCTGTTCGAATTCGAGCTCGTTTAAAC
YTA12-F2	GAAGAAAAAAAACGAAAAACGTAATGAGCCTAAGCCATCTACAAACCGGATCCCCGGGTTAATTAA
YTA12-R1	ATATGTAGAACAGTCTTCCTCCATTTCTTTGTATTGTGAAATATCGAATTCGAGCTCGTTTAAAC
Oligonucleotides for PCR-mediated prolines deletion in *S. cerevisiae*	
BNR1-delPro-F	AGTCTTGATAATGGAATCCAACTAGTACCTGAAGTTGTTAAACTATCCTTGTCGATGAACAAA
BNR1-delPro-R	TTTCTTTATATAAGCTCCACAACTACATAAAATACTAAGTCTTCAGAATTCGAGCTCGTTTAAAC
TIM50-delPro-F	CCTACTTCCAAGAGCCACCTTTCCCTGATTTACTACCAAAGGCCATTAACTCTTG
TIM50-delPro-R	CACACATAGATACGTAGATACATGAGAAGAGGGTTTACATGAAAA
YTA12-delPro-F	GCTACTTTGAAGGTAACAATAGCAGAAATATTCCACTAAATGATCCTAGTAATCC
YTA12-delPro-R	TTTCTTTATATAAGCTCCACAACTACATAAAATACTAAGTCTTCA
Oligonucleotides for cloning into pCM179 plasmid	
COL I-α1-F	ACGCAAACACAAATACACACACTAAATTACCGGATCAATTCGGGGATGTTCAGCTTTGTGGAC
COL I-α1-F	CGACGTTGTAAAACGACGGCCAGTGAATCCGTAATCATGGTCATACCCTTGGGACCTGGAGG
BNI 1-F	ACGCAAACACAAATACACACACTAAATTACCGGATCAATTCGGGGATGTTGAATACAGATGGCG CAGAAGAT
BNI 1-R	CGACGTTGTAAAACGACGGCCAGTGAATCCGTAATCATGGTCATTTTCTTGTGTGGACGAGGATA
Oligonucleotides for cloning into pDL202 plasmid	
Primary sequences	
Collagen IV-α1	GCTGCTGCTGCTGCTTGTCCTCCGGGATTTACTGGACCACCGGGTCCTCCAGGCCCTCCTGGACCT CCTGGATACCGATGCGATCAAACG
3PPP	GCTGCTGCTGCTGCTTGTCCACCACCATACGCTTGTCCACCACCATACGCTTGTCCACCACCATAC CGATGCGATCAAACG
3PGP	GCTGCTGCTGCTGCTTGTCCAGGTCCATACGCTTGTCCAGGTCCATACGCTTGTCCAGGTCCATAC AGATGTGACCAAACT
3EPG	GCTGCTGCTGCTGCTTGTGAACCAGGTTACGCTTGTGAACCAGGTTACGCTTGTGAACCAGGTTA CAGATGTGACCAAACT
3TQA	GCTGCTGCTGCTGCTTGTACTCAGGCTTACGCTTGTACTCAGGCTTACGCTTGTACTCAGGCTTAC AGATGTGACCAAACT
Secondary sequences	
pDL202 5'	AAATCGTTCGTTGAGCGAGTTCTCAAAAATGAACAAATGTCGACGGCTGCTGCTGCTGCTTGT
pDL202/303 3'	TTCGAGCTCAGGGAAGTTGAAGGATCCGAACGTTTGATCGCATCGGTA

Table A1.4. Oligonucleotides used in this study (continued).

Primer	Sequence (5'-3')
Oligonucleotides for cloning into ZP446 plasmid	
ZP446-F	ATGGTTTTTACTTTAGAAGATTTTG
ZP446-R	TGCAAGCGGGTGATTTTTGGAAGTTTATTCTAGC
CYC1-F	CCAAAAATCACCCGCTTGCAATGACTGAATTCAAGGCCGGTTCTGCTAAG
CYC1-R	CAACAAAATCTTCTAAAGTAAAAACCATCTCACAGGCTTTTTTCAAGTAGGTAAT
COX5A-F	CCAAAAATCACCCGCTTGCAATGTTACGTAACACTTTTACTAGAGCTGGT
COX5A-R	CAACAAAATCTTCTAAAGTAAAAACCATTTTAGATTGGACCTGAGAATAACCAC
TOM70-F	CCAAAAATCACCCGCTTGCAATGAAGAGCTTCATTACAAGGAACAAGACA
TOM70-R	CAACAAAATCTTCTAAAGTAAAAACCATCATTAAACCCTGTTCGCGTAATTTA

Table A1.5. Oligonucleotides used for *S. cerevisiae* chromatin immunoprecipitation.

Primer	Sequence (5'-3')	Hap1 consensus binding sequence (CGGNNNTANCGG)	PCR amplicon*
CYC1-F	ATCTAAAATTCCCGGGAGCA	CGGGGTTTACGG	-397 to -195
CYC1-R	ACTAAAGTTGCCTGGCCATC		
MOT3-F	GGCGCGACTCGAATCCTTGA	TGGCGATAACGG	-528 to -374
MOT3-R	AGAAGAAAATCAAGAAGAAAAACGA		
ROX1-F	CCTGGATATCATTGGCCTGT	TGGAACTACCGG	-526 to -216
ROX1-R	AGGAAAATGCAAGAGCGAAA		
TIF51A-1-F	TGAGCCCGGTTCATTTCTAT	CGGATATATCCGG	-737 to -586
TIF51A-1-R	CAGCCAAACGAGAAGGGTAG		
TIF51A-2-F	TTACCCTTTCTTGCCGCTAC	CGGATATATCCGG	-621 to -471
TIF51A-2-R	GTTCCCGTTTTGCTGTTCTC		
TIF51A-3-F	CCAAGGCCGGTAAAATTCTG	CGGATATATCCGG	-427 to -273
TIF51A-3-R	CGGCGTTTCTTTTAGCTCCT		
TIF51B-F	TTTCCATTGTTCGTTCGTTG	-------	-790 to -650
TIF51B-R	TGAGTTCCGACAACAATGAGTT		

* With respect to transcription start site (+1) position

Table A1.6. Plasmids used in this study.

Name	Plasmid description	Source
pCM179	ptetO$_7$-lacZ-URA3	(Garí *et al.*, 1997)
pDL202	pPGK1-Fluc-Rluc-URA3	(Letzring *et al*., 2010)
PA201	pFA6a-3HA-his3MX6	(Longtine *et al.*, 1998)
PA231	pFA6a-kanMX6	(Longtine *et al.*, 1998)
PA239	pFA6a-13myc-kanMX6	(Longtine *et al.*, 1998)
PA242	pFA6a-GFP-his3MX6	(Longtine *et al.*, 1998)
PA321	p414-pGAL-CEN-TRP1	Dr. Jesús de la Cruz
PA329	pCM179 ptetO$_7$-Col1a1(1-420 aa)-lacZ-URA3	This study
PA332	pDL202 pPGK1-Fluc-PPP(10)-Rluc-URA3	(Letzring *et al*., 2010)
PA347	pCM179 ptetO$_7$-Bni1(1221-1360 aa)-lacZ-URA3	This study
PA349	pDL202 pPGK1-ColIVa1-URA3	This study
PA352	pDL202 pPGK1-Fluc-PPP(3)-Rluc-URA3	This study
PA354	pMK46-IAA17-kanMX6	Dr. Ethel Queralt
PA357	pDL202 pPGK1-Fluc-EPG(3)-Rluc-URA3	This study
PA360	pDL202 pPGK1-Fluc-PGP(3)-Rluc-URA3	This study
PA362	pDL202 pPGK1-Fluc-TQA(3)-Rluc-URA3	This study
PA367	pYM43-Redstar2-clonNAT	Euroscarf (P30255)
PA383	pVT100U-mtGFP-URA3	Addgene (45054)
TTP76	pRS406-pGPD-Su9-mCherry-URA3	Dr. Brian Zid
ZP446	pAG306-ptetO$_7$-Tim50 5'UTR-nLuc-CYC1term-URA3	Dr. Brian Zid
ZP447	pAG306-ptetO$_7$-Tim50 5'UTR-Tim50-nLuc-CYC1term-URA3	Dr. Brian Zid
ZP448	pAG306-ptetO$_7$-Tim50 5'UTR-Tim50Δ7Pro-nLuc-CYC1term-URA3	Dr. Brian Zid
ZP449	pAG306-ptetO$_7$-Tim50 5'UTR-Tim50Δ14Pro-nLuc-CYC1term-URA3	Dr. Brian Zid
ZP603	pAG306-ptetO7-Tim50 5'UTR-CYC1-nLuc-CYC1term-URA3	This study
ZP604	pAG306-ptetO7-Tim50 5'UTR-TOM70-nLuc-CYC1term-URA3	This study
ZP605	pAG306-ptetO7-Tim50 5'UTR-COX5A-nLuc-CYC1term-URA3	This study

Table A1.7. Antibodies used in this study.

Primary Antibody	Working organism	Working dilution	Source	Secondary Antibody	Working dilution	Source
Protein detection by Western blotting						
α-eIF2α	*S. cerevisiae*	1:2000	Thomas Dever Lab	α-rabbit	1:10000	Promega
α-tubulin	Mouse	1:5000	Proteintech (66031-1)	α-mouse	1:10000	Promega
Collagen 1	Mouse fibroblasts	1:500	Merck (AB765P)	α-rabbit	1:10000	Promega
Collagen 1	Mouse LX2	1:1000	Cell Signaling (84336)	α-rabbit	1:10000	Promega
eIF5A	*S. cerevisiae*/Mouse	1:500	Abcam (Ab32407)	α-rabbit	1:10000	Promega
G6PDH	*S. cerevisiae*	1:15000	Roche (10127671001)	α-rabbit	1:10000	Promega
Gadd153/CHOP	Mouse fibroblasts	1:200	Santa Cruz (sc-7351)	α-mouse	1:10000	Promega
GAPDH	Mouse fibroblasts	1:5000	Invitrogen (PA1-987)	α-rabbit	1:10000	Promega
GAPDH	Mouse LX2	1:5000	Sigma-Aldrich (G8795)	α-mouse	1:10000	Promega
HA	*S. cerevisiae*	1:5000	Roche (12013819001)	-	-	-
hyp-eIF5A	*S. cerevisiae*	1:600	Genentech (FabHpu)	α-rabbit	1:10000	Promega
Myc	*S. cerevisiae*	1:1000	Invitrogen (13-2500)	α-mouse	1:10000	Promega
Chromatin immunoprecipitation						
eIF5A	*S. cerevisiae*	1:4	Abcam (Ab32407)	Dynabeads anti-rabbit IgG		Invitrogen (11203D)
Myc	*S. cerevisiae*	1:5	Invitrogen (13-2500)	Dynabeads Pan Mouse IgG		Invitrogen (11041)
Rpb1 (8WG16)	*S. cerevisiae*	1:7	Invitrogen (MA1-10882)	Dynabeads Pan Mouse IgG		Invitrogen (11041)
Protein detection by immunofluorescence						
Collagen 1	Mouse fibroblasts	1:250	Merch (AB765P)	Alexa Fluor 488-anti-rabbit	1:2000	Invitrogen (A-11094)
Gadd 153/CHOP	Mouse fibroblasts	1:40	Santa Cruz (sc-7351)	Alexa Fluor 546-anti-mouse	1:800	Invitrogen (A-21143)
HSP47	Mouse fibroblasts	1:50	Santa Cruz (sc-5293)	Alexa Fluor 546-anti-mouse	1:800	Invitrogen (A-21143)
Nidogen-1	Mouse fibroblasts	1:500	Rupert Timpl lab	Alexa Fluor 488-anti-rabbit	1:2000	Invitrogen (A-11094)

Resumen

Introducción

La traducción es el proceso por el cual la información contenida en moléculas de ARN mensajero (mRNA) es leída por los ribosomas para producir nuevas proteínas. El proceso de traducción se divide en tres fases: inicio, elongación y terminación. Los factores de traducción asisten las tres fases de síntesis de proteínas, aunque algunos de ellos tienen funciones especializadas para traducir mRNAs específicos, como el factor de inicio de traducción de eucariotas 5A (eIF5A). Aunque inicialmente fue descrito como un factor de inicio, eIF5A tiene funciones en las tres fases del proceso de traducción. En la actualidad, eIF5A es principalmente conocido por favorecer la elongación de la traducción en secuencias enriquecidas en prolinas y otros aminoácidos problemáticos que dificultan la formación del enlace peptídico y atascan al ribosoma.

eIF5A es una proteína esencial y uno de los pocos factores de traducción conservados universalmente. La mayoría de los organismos eucariotas expresan dos isoformas de eIF5A que se encuentran altamente conservadas y se expresan en condiciones diferentes. En levadura, las dos isoformas de eIF5A están codificadas por los genes *TIF51A* y *TIF51B. TIF51A* se expresa en condiciones de aerobiosis mientras que *TIF51B* lo hace en condiciones de anaerobiosis. En mamíferos, las dos isoformas de eIF5A están codificadas por los genes *EIF5A1* y *EIF5A2*. *EIF5A1* se expresa de forma constitutiva en todas las células y tejidos, mientras que *EIF5A2* aunque es generalmente indetectable, se encuentra sobreexpresado en diversos tipos de células cancerosas. De hecho, debido a la correlación directa entre una elevada expresión de *EIF51A2* y una mala prognosis y mayor riesgo a metástasis, *EIF5A2* es un biomarcador tumoral.

eIF5A es la única proteína conocida en la naturaleza que contiene el aminoácido hipusina. La hipusinación ocurre de forma posttraduccional y exclusivamente en un residuo específico de lisina (Lys51 en levadura y Lys50 en humanos) mediante la acción consecutiva de dos enzimas: deoxihipusina sintasa (DHPS) y deoxihipusina hidroxilasa (DOHH). La forma biológica de eIF5A que contiene hipusina es la forma madura y biológicamente activa de eIF5A. La hipusinación ocurre de forma irreversible y es esencial para la función de eIF5A y la viabilidad celular.

La función molecular más conocida de eIF5A es su participación en la fase de elongación de la traducción en aminoácidos específicos. Algunos aminoácidos se clasifican como dadores o aceptores pobres porque sus enlaces peptídicos se forman de manera poco eficiente. Entre estos, la prolina (Pro) se considera un donador y un aceptor pobre con baja reactividad debido a su estructura geométrica rígida. Cuando los ribosomas encuentran estos residuos problemáticos pueden pararse y atascar la traducción, generando colisiones con los ribosomas que se encuentran traduciendo aguas arriba. Para evitar esta situación, eIF5A se une a los ribosomas de forma dependiente de su residuo hipusina y se coloca en el sitio E. Aquí, extiende su dominio desestructurado donde reside la hipusina cerca del brazo aceptor del peptidil-tRNA ubicado en el sitio P. La aproximación del residuo de hipusina estabiliza la conformación del peptidil-tRNA y favorece el correcto alineamiento de sustratos para la formación del enlace peptídico. eIF5A favorece la formación del enlace peptídico en residuos de prolina consecutivos y otros aminoácidos como glicina y aminoácidos con carga, y así alivia el atascamiento de ribosomas y la parada de traducción.

Por lo tanto, eIF5A participa en la traducción de una parte de la población global de mRNAs, los cuales contienen aminoácidos críticos en sus secuencias, denominados tripéptidos o motivos dependientes de eIF5A. Debido al amplio espectro de funciones celulares en las que participan sus dianas directas, eIF5A juega un papel esencial en diversos procesos celulares. Estos procesos incluyen la proliferación, formación de gránulos de estrés, organización del citoesqueleto, autofagia y migración celular entre otros. Sin embargo, existen múltiples estudios que relacionan eIF5A con otras funciones moleculares no directamente relacionadas con la síntesis de proteínas. Entre éstas destacan la unión a moléculas de RNA y exporte de éstas del núcleo a citoplasma. Debido al papel esencial que eIF5A juega en los diversos procesos celulares mencionados, esta proteína está implicada en la patogénesis de diferentes enfermedades humanas como infección retroviral, diabetes, cáncer, envejecimiento y trastornos del neurodesarrollo.

La clasificación de categorías funcionales de proteínas de humanos con los niveles más altos de motivos dependientes de eIF5A para su traducción, señala diferentes procesos celulares entre los que se incluyen el metabolismo del colágeno y la organización de la matriz extracelular. El colágeno es el componente mayoritario de la matriz extracelular y contiene abundantes repeticiones de motivos dependientes de eIF5A de tipo no poliPro como PGP, PPG, DPG y EPG. Por tanto, aunque la función de eIF5A en el metabolismo del colágeno es desconocida, la presencia de estos motivos de pausa en su secuencia sugiere su papel como posible diana de eIF5A.

El colágeno es esencial para las interacciones célula-célula, para mantener la estructura mecánica del tejido y para otras funciones como reparación de heridas, adhesión y migración celular. Los colágenos contienen repeticiones abundantes del conocido motivo colagénico (X-Y-Gly), donde la primera y segunda posiciones están normalmente ocupadas por prolina o hidroxiprolina y la tercera siempre por glicina. La repetición de este motivo permite la formación de la triple hélice característica de los colágenos. De entre todos los colágenos existentes, el colágeno I es el más estudiado y consiste en dos cadenas α1 idénticas y una tercera cadena α2, codificadas por los genes *COL1A1* y *COL1A2* respectivamente. La síntesis del colágeno es compleja y requiere diferentes pasos que incluyen su translocación cotraduccional en el retículo endoplásmico, plegamiento, transporte a través de vesículas de Golgi y secreción al espacio extracelular. En este proceso participan múltiples proteínas con funciones esenciales. El colágeno I en concreto, constituye más del 25% del peso del cuerpo humano y es el principal constituyente de la piel, ligamentos, tendones y huesos donde proporciona fuerza mecánica y elasticidad. La presencia de mutaciones en los genes que codifican a los colágenos o en proteínas implicadas en su metabolismo producen enfermedades denominadas colagenopatías. Cuando la síntesis de colágeno se produce de forma excesiva y descontrolada, la deposición de colágeno en la matriz extracelular culmina en un proceso de fibrosis. La fibrosis hepática es la fibrosis más común y afecta a millones de personas en el mundo. Esta enfermedad se caracteriza por una producción excesiva de colágeno I y puede derivar en el desarrollo de enfermedades crónicas hepáticas. En el Capítulo 3 de esta tesis se pretende abordar cuál es la relevancia de eIF5A en la síntesis de colágeno en condiciones normales y en el contexto de fibrosis hepática.

La levadura *Saccharomyces cerevisiae* es un organismo aerobio facultativo e incluso en presencia de oxígeno, prefiere utilizar un metabolismo de tipo fermentativo en lugar de uno respiratorio. Durante el proceso de fermentación la glucosa se metaboliza a etanol y CO_2 y los genes de glucólisis y fermentación se encuentran inducidos, mientras que los genes que codifican enzimas respiratorias del ciclo de Krebs, cadena de transporte de electrones y fosforilación oxidativa se reprimen por glucosa. Por el contrario, cuando el sustrato es de tipo no fermentable (glicerol, etanol, lactato…), se produce un cambio de metabolismo a uno de tipo respiratorio, lo que implica una reprogramación masiva de la expresión génica para inducir genes implicados en procesos respiratorios. Esta reprogramación implica diferentes rutas de señalización, así como diversos factores de transcripción.

Los factores de transcripción Hap1 y el complejo HAP (Hap2/3/4/5) juegan un papel esencial en la desrepresión de los genes de respiración, y sus actividades dependen de los niveles de hemo celular, cuya síntesis depende, a su vez, de la presencia de oxígeno. Hap1 se activa mediante su unión al grupo hemo y activa la transcripción de diversos genes implicados en respiración. En deficiencia de hemo, Hap1 es capaz de funcionar como represor de la transcripción de algunos genes mediante el reclutamiento de correpresores como el complejo Ssn6/Tup1. Además de Hap1, el complejo HAP es considerado el regulador principal de la respiración mitocondrial y está implicado en activar la expresión de numerosos genes del ciclo de Krebs, la cadena de transporte de electrones y la fosforilación oxidativa. Su actividad se regula también mediante hemo, que induce la transcripción y estabilidad de la subunidad coactivadora Hap4.

Tal y como se ha mencionado antes, la mayoría de los organismos eucariotas expresan dos genes parálogos que codifican las dos isoformas de eIF5A. En *S. cerevisiae*, la expresión de estos dos genes está regulada por oxígeno de forma recíproca. En condiciones aerobias se expresa *TIF51A* de forma abundante, mientras que los niveles de *TIF51B* son prácticamente indetectables. La represión de *TIF51B* ocurre a través de los represores Rox1 y Mot3 que, a su vez, se encuentran activados por Hap1. Por el contrario, en condiciones de anaerobiosis, la expresión de *TIF51B* pasa a ser muy elevada mientras que *TIF51A* se reprime. En estas condiciones, Hap1 funciona como represor de Rox1 y Mot3, lo que desencadena la inducción de *TIF51B*. Aunque el mecanismo de regulación de *TIF51B* por oxígeno es conocido, la regulación de la expresión de *TIF51A* es desconocida tanto en aerobiosis como en anaerobiosis. La regulación diferencial de la expresión de ambas isoformas parece sugerir que la isoforma Tif51A favorecería un metabolismo de tipo respiratorio mientras que la isoforma Tif51B favorecería uno de tipo fermentativo. En el Capítulo 4 de esta tesis, se estudia la regulación transcripcional de las dos isoformas de eIF5A de *S. cerevisiae* en respuesta a diferentes condiciones metabólicas y se describe el papel que ejerce Hap1 como activador/represor.

Las mitocondrias son esenciales para la producción de energía en el metabolismo respiratorio porque sostienen procesos metabólicos esenciales como la fosforilación oxidativa, la cadena de transporte electrónico, ciclo de Krebs, β-oxidación y síntesis de lípidos. Además de esta función primaria, participan en otros procesos celulares y su función es crítica para la salud. El 99% del proteoma mitocondrial se encuentra codificado en el genoma nuclear y, por tanto, estas proteínas mitocondriales son sintetizadas por ribosomas en el citosol pero han de ser transportadas y translocadas al interior de la mitocondria, lugar donde ejercen sus funciones. La translocación de estas proteínas puede ocurrir de forma posttraduccional y asistida por chaperonas, o de forma cotraduccional. La translocación

cotraduccional ocurre para aquellos mRNAs que se localizan en la superficie mitocondrial, los cuales codifican mayoritariamente proteínas localizadas en la membrana interna mitocondrial. Para ello, existen diferentes factores que participan en la localización de estos mRNAs como, por ejemplo, Puf3.

Las proteínas mitocondriales contienen señales de localización mitocondrial en sus secuencias que son reconocidas por receptores específicos en la superficie de la mitocondria para llevar a cabo su importe. Alrededor de un 60% de proteínas mitocondriales contienen esta señal en su extremo N-terminal, que se caracteriza por ser de longitud variable y por formar una hélice α anfipática con un lado con carga positiva y otro lado hidrófobo. Dichas secuencias sufren un corte proteolítico una vez alcanzan la matriz mitocondrial. El resto de las proteínas mitocondriales presentan otras señales internas que carecen de patrones consistentes.

Los sistemas de translocación ubicados en la membrana externa y membrana interna mitocondrial llevan a cabo el importe de proteínas al interior de la mitocondria. Existen siete maquinarias conectadas que definen cinco rutas de importe y que reconocen proteínas con características y señales de localización diferentes. El complejo translocasa de la membrana externa TOM es la entrada universal de la gran mayoría de proteínas mitocondriales. TOM reconoce diferentes precursores en el citosol y los transfiere a través de la membrana externa. Entonces, las proteínas se distribuyen a través de diferentes rutas de importe dependiendo de cuál es su destino final. La translocasa de la membrana interna TIM23 media el importe de todas las proteínas de la matriz mitocondrial y de la mayoría de la membrana interna. TIM23 reconoce las secuencias de localización ubicadas en el extremo N-terminal y se ayuda del complejo motor PAM para el aporte de energía necesario para el proceso de translocación. Otros complejos translocadores como TIM22, MIA40, SAM o la insertasa de la membrana externa reconocen otras señales internas en las secuencias de proteínas y median el importe a otros destinos como la membrana interna, el espacio intermembrana y la membrana externa mitocondrial. Situaciones de estrés que disminuyen el potencial de membrana mitocondrial, así como mutaciones en los componentes de las translocasas, proteínas defectuosas o de sobrecarga, pueden obstruir los sistemas translocadores y generar un fallo de importe de proteínas. El fallo de importe de proteínas altera las funciones mitocondriales y está asociado con diferentes enfermedades. Sin embargo, la célula cuenta con diferentes respuestas de estrés para aumentar la actividad de chaperonas y del proteasoma y así eliminar las proteínas acumuladas y no importadas.

En los últimos años se han publicado diversos estudios que relacionan eIF5A y las enzimas responsables de la hipusinación con la función mitocondrial, aunque el mecanismo molecular todavía no se conoce. Además, la localización de eIF5A en la mitocondria ha sido demostrada y en humanos existe una variante de *EIF5A1* que contiene una señal de localización mitocondrial. Hasta la fecha, se han descrito dos mecanismos alternativos, aunque relacionados, que conectan la actividad de eIF5A con la función mitocondrial. El primero sugiere que eIF5A regula la respiración mitocondrial al favorecer la traducción de señales de localización del N-terminal de algunas proteínas mitocondriales. El segundo propone que eIF5A y su residuo hipusina favorecen una correcta interacción entre aminoácidos del N-terminal de proteínas mitocondriales y el túnel de salida del ribosoma. Sin embargo, los detalles del mecanismo molecular todavía no se han descrito. El Capítulo 5 de esta tesis caracteriza un mecanismo molecular específico mediante el cual eIF5A regula el importe y la síntesis de proteínas mitocondriales, y así, la función mitocondrial.

El control preciso de la expresión génica es esencial para el crecimiento y desarrollo de todos los organismos celulares. Además, la integración de los distintos eventos de la expresión génica es fundamental para alcanzar las demandas celulares y permitir adaptarse a los estímulos ambientales. La síntesis de proteínas representa el proceso de mayor consumo energético celular y está íntimamente conectado a la síntesis y degradación de mRNA. Aunque la transcripción y la traducción se consideran procesos independientes debido a sus distintos mecanismos y lugares de acción, existen factores comunes que coordinan ambos procesos como el heterodímero Rpb4/Rpb7, el complejo Ccr4-Not o la exonucleasa Xrn1.

Diversos factores de traducción de eucariotas se encuentran en el núcleo en varios organismos donde participan en diferentes procesos asociados al control de integridad del genoma y a etapas nucleares de la expresión génica (transcripción, procesamiento y exporte de mRNAs). La acumulación nuclear de eIF5A se ha descrito en diferentes organismos y en mamíferos se regula por acetilación y requiere el uso de dos exportinas (Xpo4 y Xpo1). En el núcleo, eIF5A se ha visto asociada con la RNA polimerasa II en neuronas y también se ha descrito su unión al promotor del factor inducible de hipoxia (HIF-1). Por otro lado, se ha demostrado su capacidad de unión a diferentes mRNAs, incluyendo algunos del virus del VIH, para facilitar su exporte al citoplasma. Aunque estos resultados son difíciles de entender, sí sugieren una comunicación entre los procesos de transcripción y traducción. El Capítulo 6 de esta tesis aborda la relevancia de eIF5A como una proteína que no solo funciona en traducción sino también en el control de la transcripción.

Objetivos de esta tesis

La finalidad de esta tesis doctoral es dilucidar nuevas funciones moleculares de eIF5A en el metabolismo celular y el control transcripcional, utilizando *Saccharomyces cerevisiae* y *Mus musculus* como organismos modelo. Para ello, esta tesis ha sido dividida en cuatro capítulos que se corresponden con los siguientes objetivos propuestos:

1. Determinar si eIF5A es necesario para la síntesis del colágeno en células de mamífero y describir a nivel molecular las causas de la parada en traducción de colágeno producida en ausencia de eIF5A.
2. Dilucidar si la regulación de la expresión génica de las dos isoformas eucarióticas que codifican eIF5A responden al estado metabólico celular y los mecanismos a cargo de dicha regulación en *S. cerevisiae*.
3. Descifrar el mecanismo molecular por el cual eIF5A es esencial para la respiración celular en *S. cerevisiae* y analizar cómo afecta a la síntesis de proteínas mitocondriales.
4. Investigar si eIF5A nuclear participa en el control transcripcional e identificar genes diana, mecanismos y su supuesta participación en el "crosstalk" general entre transcripción y traducción en *S. cerevisiae*.

Materiales y Métodos

La metodología empleada (Capítulo 2) para llevar a cabo el estudio de estos objetivos propuestos incluye: (i) técnicas microbiológicas para la construcción de cepas de levadura y plásmidos; (ii) técnicas moleculares para el estudio y cuantificación del DNA, como la inmunoprecipitación de cromatina; para el estudio del RNA y su traducción (RT-qPCR y fraccionamiento de polisomas); y para el estudio de proteínas como western blotting y microscopía de fluorescencia; (iii) ensayos de actividad β-galactosidasa, actividad luciferasa y de consumo de oxígeno; y (iv) análisis de tasa de transcripción y vidas medias a nivel ómico mediante genomic run-on.

Resultados y Discusión

Los resultados del Capítulo 3 se centran en estudiar el papel de eIF5A en la traducción de colágenos, que son proteínas con repeticiones abundantes de motivos enriquecidos en Pro-Gly (denominados motivos colagénicos) y, por tanto, son considerados como posibles dianas de eIF5A para su traducción. En primer lugar, utilizando un sistema reportero de doble luciferasa en levadura, se confirmó que eIF5A es necesario para la síntesis heteróloga de colágeno tipo I α1. Estos experimentos demostraron una parada de traducción en ausencia de eIF5A en los motivos colagénicos enriquecidos en Pro-Gly como PPG, PPG o EPG. En segundo lugar, nuestros resultados mostraron que la inactivación de eIF5A mediante RNAs de silenciamiento e inhibición de DHPS con GC7 en fibroblastos de ratón, reducían de forma drástica los niveles de proteína de colágeno tipo I α1. Los niveles de mRNA de colágeno no se vieron afectados en deficiencia de eIF5A, por lo que la reducción de colágeno se debía a una parada en su traducción. Por otro lado, el análisis de proteína de colágeno I α1 mediante técnicas de inmunofluorescencia y microscopía reveló su localización alrededor del núcleo. También se observó la inducción de marcadores de estrés de retículo endoplásmico, sugiriendo la retención de colágeno I α1 parcialmente sintetizado en el retículo, lugar donde se produce su inserción cotraduccional. Por último, se utilizó una línea celular humana de células estrelladas hepáticas, esenciales en el desarrollo del proceso fibrótico de hígado, para determinar hasta qué punto la sobreproducción de colágeno dependía de la expresión de eIF5A. En ausencia de eIF5A y al tratar con la citoquina profibrótica TGF-β1, se observó una drástica bajada de los niveles de colágeno I α1. Por lo tanto, nuestros resultados mostraron que el mantenimiento de la homeostasis de colágeno I requiere eIF5A e implican su potencial como diana para la regulación de la producción de colágeno en enfermedades fibróticas.

Por otro lado, para profundizar en el papel de eIF5A en la función mitocondrial, determinamos la regulación transcripcional de las dos isoformas de eIF5A de *S. cerevisiae* en respuesta al estado metabólico (Capítulo 4). Nuestros primeros resultados indicaron que la isoforma Tif51A, pero no Tif51B, es necesaria para el crecimiento bajo fuentes de carbono no fermentables como glicerol o etanol. Bajo fuentes de carbono respirables y tras el cambio diáuxico, la expresión a nivel de mRNA y de proteína de la isoforma Tif51A se inducía, mientras que la de la isoforma Tif51B disminuía. Además, la inactivación de la isoforma Tif51A generaba defectos de crecimiento en fuentes de carbono respirables, reducción del consumo de oxígeno y del potencial de membrana mitocondrial. Por el contrario, el análisis mediante microscopía de fluorescencia de la cantidad y distribución de mitocondrias, reveló que no había cambios críticos en deficiencia de eIF5A. Por tanto, estos resultados

indicaban la esencialidad de la isoforma Tif51A en el metabolismo respiratorio. Experimentos adicionales realizados con concentraciones de glucosa variables y el uso de mutantes de factores de transcripción implicados en respiración, indicaron que la expresión de Tif51A seguía una doble regulación positiva: a través de la ruta TORC1 en condiciones de alta concentración de glucosa para favorecer el crecimiento, y a través del factor de transcripción Hap1 en condiciones de respiración para asegurar una correcta función mitocondrial.

A continuación, se examinó el mecanismo molecular de dicha regulación. Mediante ensayos de inmunoprecipitación de cromatina se determinó la unión constitutiva y directa de Hap1 a la región promotora de *TIF51A*, en concreto cerca de la zona que contiene la secuencia consenso de unión de Hap1 CGGataTAttcGG. La unión de Hap1 activad la trascripción de *TIF51A* bajo condiciones de respiración. Sin embargo, la unión de Hap1 al promotor de *TIF51A*, incluso en condiciones de inhibición de respiración donde la expresión de *TIF51A* se reprime, sugerían la posibilidad de que Hap1 actuara como represor en estas condiciones. Los experimentos de inmunoprecipitación del complejo represor general Ssn6/Tup1 confirmaron el papel represor de Hap1 mediado por el reclutamiento de Ssn6/Tup1 para reprimir la expresión de *TIF51A* en situaciones donde el proceso de respiración se ve inhibido, como la deficiencia de hierro o el tratamiento con antimicina A, que inhibe la cadena de transporte de electrones.

En cuanto a la regulación de la expresión de la isoforma Tif51B, se observó una inducción de sus niveles de mRNA en deficiencia de hierro y tras suplementar los cultivos con antimicina A, indicando el papel de esta proteína en condiciones donde la respiración resulta inhibida. Estos resultados señalaban una regulación de la expresión opuesta entre las dos isoformas de eIF5A. La unión de Hap1 a las secuencias consenso previamente descritas en las regiones promotoras de *ROX1* y *MOT3* en condiciones normales de respiración sugería una regulación indirecta de *TIF51B*. De este modo, Hap1 activa la expresión de Rox1 y Mot3 que son represores generales de genes de hipoxia entre los que se incluye *TIF51B*. Rox1 y Mot3 reprimen la expresión de *TIF51B* mediante el reclutamiento del correpresor Tup1. Por el contrario, en condiciones de inhibición de respiración, Hap1 pasa a ser represor y mediante el reclutamiento de Tup1 reprime la expresión de *ROX1* y *MOT3*, lo que desencadena la activación de *TIF51B*. Por tanto, Hap1 surge como un sensor mitocondrial para modular la expresión de eIF5A en levadura. En conclusión, los resultados del Capítulo 4 describen el mecanismo molecular por el cual se regula de forma opuesta la expresión de los dos genes de eIF5A en respuesta al estado metabólico y a la demanda energética celular.

Los resultados del Capítulo 5 se centran en descifrar el mecanismo molecular por el cual eIF5A es esencial para la función mitocondrial en *S. cerevisiae*. Estudios proteómicos llevados a cabo en nuestro laboratorio revelaron la mitocondria como una de las categorías funcionales más afectadas en deficiencia de eIF5A. Además, proteínas del ciclo de Krebs, cadena de transporte de electrones, sistemas transportadores y subunidades de la ATP sintasa se vieron reducidas significativamente. Al analizar posibles dianas de eIF5A por la presencia de motivos dependientes de eIF5A en sus secuencias, resultó de interés el análisis de Tim50. Tim50 es una proteína esencial y la subunidad receptora del complejo translocador TIM23, ubicado en la membrana mitocondrial interna. Tim50 reconoce de forma específica la región N-terminal de proteínas mitocondriales y favorece su importe al interior de la mitocondria. El interés de Tim50 como posible diana de eIF5A para su traducción radica en la presencia de una región

rica en 14 prolinas, 7 de las cuales son consecutivas. En primer lugar, y mediante el uso de reporteros de nanoluciferasa fusionados a diferentes versiones de Tim50, se analizó con un mutante termosensible de la isoforma *TIF51A* (*tif51A-1*), la síntesis de proteína producida en presencia y ausencia de eIF5A. Los resultados mostraron una bajada muy pronunciada de los niveles de Tim50 en deficiencia de eIF5A y una recuperación de dichos niveles al eliminar la región de prolinas, sugiriendo así que la traducción disminuye porque los ribosomas se atascan a lo largo de la región de prolinas en ausencia de eIF5A.

A continuación, se planteó el determinar si a través de la regulación de Tim50, eIF5A regula el importe de proteínas mitocondriales. Mediante el uso de microscopía de fluorescencia, se analizó la localización celular de Tim50 y de otras proteínas mitocondriales cuyo importe dependía o no de su reconocimiento por Tim50. En deficiencia de eIF5A, se observó la formación de agregados de Tim50 fuera de la mitocondria. Además, el análisis de proteínas mitocondriales con diferentes localizaciones indicó que las proteínas Cyc1, Yta12 e Ilv2, localizadas en el espacio intermembrana, la membrana mitocondrial interna y la matriz mitocondrial respectivamente, dependían de Tim50 y del complejo TIM23 para su correcto importe. En deficiencia de eIF5A, se observó la agregación de estas proteínas fuera de la mitocondria, señalando su defecto de importe. Sin embargo, proteínas como Tom70 que se localiza en la membrana mitocondrial externa parecía comportarse como independiente de Tim50 ya que su distribución celular no se vio afectada en deficiencia de eIF5A. Para confirmar estos resultados, se utilizó CCCP, un desacoplador del potencial de membrana mitocondrial e inhibidor del importe, y se analizaron algunas de las mismas proteínas mitocondriales analizadas antes por microscopía. Los resultados obtenidos fueron similares entre células tratadas con CCCP y el mutante de eIF5A, lo que confirmó que eIF5A modula el proceso de importe de proteínas a la mitocondria. A continuación, se investigó la localización celular de los agregados de proteínas mitocondriales no importadas y se determinó su colocalización con la chaperona Hsp104 en el citosol. La activación de la respuesta al estrés por defectos de importe, denominada mitoCPR, en ausencia de eIF5A se describe también en este capítulo.

Por último, se investigó si el fallo en el importe causado por una menor actividad del complejo TIM23 en ausencia de eIF5A podía desencadenar un efecto en la traducción de proteínas dependientes de Tim50 como Cyc1. En primer lugar, se utilizaron reporteros de nanoluciferasa para el análisis de síntesis de proteínas mitocondriales y se determinó que en ausencia de eIF5A la síntesis de proteínas con dependencia por Tim50 estaba afectada de forma significativa. Los niveles de mRNA y la velocidad de degradación de estas proteínas no se vieron alterados en el mutante de eIF5A, por lo que los resultados sugerían que la deficiencia de eIF5A afectaba a la traducción de estas proteínas. Para confirmar estos resultados, se estudió la traducción de mRNAs específicos mediante el uso de fraccionamiento de polisomas. Se escogió un amplio grupo de mRNAs para su estudio con características diferentes en cuanto a localización de proteína codificada, dependencia por Tim50 o localización de mRNA en la superficie de la mitocondria entre otros. Aunque la traducción a nivel global del mutante no se vio alterada respecto a la cepa silvestre, todos los mRNAs que codifican para proteínas mitocondriales se vieron desplazados hacia fracciones de menos ribosomas. Sin embargo, la traducción de mRNAs que codifican para proteínas constitutivas del citosol no se vio afectada. Estos resultados indicaban una bajada general de la traducción de proteínas mitocondriales ya que la asociación de múltiples ribosomas a todos los mRNAs testados se vio disminuida en ausencia de eIF5A de manera uniforme. Por otro lado, estos resultados sugieren, aunque no confirman, la capacidad de la célula de acoplar el estado funcional

o actividad del complejo TIM23 y el importe a la traducción de proteínas mitocondriales que deben ser importadas.

En último lugar, en el Capítulo 6 se pretendió abordar cual es la contribución de eIF5A en el núcleo y si está relacionada con el control transcripcional. Como primera aproximación, se determinó la tasa de transcripción, cantidad de mRNA y vidas medias del genoma completo de levadura mediante el método de genomic run-on (GRO), utilizando la cepa silvestre y el mutante termosensible *tif51A-1*. Los resultados señalaban que eIF5A tiene efectos significativos en los tres parámetros estudiados y que, en su ausencia las células experimentan, en global, una ligera disminución de la tasa de transcripción, un aumento de la cantidad de mRNA y un aumento considerable de la estabilidad de mRNAs. Sin embargo, el interés de este estudio radicaba en los cambios que ocurren en los genes que dependen de eIF5A para su traducción y son, por tanto, más sensibles a la presencia/ausencia de eIF5A. Para realizar dicho análisis, se clasificaron los genes en función de su supuesta dependencia de eIF5A para su traducción (basada en el número de motivos dependientes de eIF5A de sus secuencias). Tras analizar los datos utilizando esta clasificación, se confirmó que en ausencia de eIF5A existía una correlación fuerte y positiva entre la tasa de síntesis de mRNA y dependencia por eIF5A para su traducción. Del mismo modo, la cantidad de mRNA también se vio correlacionada de forma positiva con la dependencia por eIF5A. Sin embargo, la correlación entre estabilidad y dependencia de eIF5A era más ligera. Estos datos indicaban que en deficiencia de eIF5A, aquellos genes con mayor sensibilidad a eIF5A para su traducción se transcriben más que aquellos que no requieren eIF5A para su traducción. Mediante ensayos de RT-qPCR e inmunoprecipitación de cromatina de RNA polimerasa II, se confirmó que la ausencia de eIF5A inducía los niveles de mRNA y la unión de polimerasa a genes cuya traducción depende de eIF5A debido a la presencia de tripéptidos dependientes de eIF5A en sus secuencias. Estos resultados sugerían un papel de eIF5A como represor de la transcripción.

A continuación, se estudió si la eliminación de regiones enriquecidas en prolinas de genes específicos dependientes de eIF5A produciría que el efecto en los niveles de mRNA y de transcripción se volviera independiente de eIF5A. Para ello se generaron versiones mutantes mediante la eliminación de regiones poliPro de los genes *BNR1, YTA12* y *TIM50*, y se analizaron sus niveles de mRNA y la unión de RNA polimerasa II. Los resultados de estos experimentos indicaron una pérdida de los efectos en transcripción en ausencia de eIF5A tras la eliminación de motivos dependientes de eIF5A de sus secuencias. Esto sugería la idea de que la presencia de codones dependientes de eIF5A es lo que permite una regulación dependiente de eIF5A de transcripción y traducción; donde la presencia de eIF5A favorece la traducción mientras que reprime la transcripción y la ausencia de eIF5A favorece la transcripción, pero reprime la traducción. Por último, debido a que la localización nuclear de eIF5A se ha descrito en diferentes organismos, se planteó la hipótesis de que eIF5A regulase de forma directa la transcripción de sus genes diana en el núcleo. Para comprobar dicha hipótesis, se llevó a cabo una inmunoprecipitación de cromatina de eIF5A en una cepa silvestre y se estudió la asociación de este factor a diferentes regiones. Los resultados indicaron que eIF5A se unía a todas las regiones génicas estudiadas, aunque la asociación a genes dependientes de eIF5A era significativamente mayor que a los genes independientes. Aunque todavía no se ha determinado si dicha asociación es directa o indirecta, si es a DNA o RNA, o si depende de la RNA polimerasa II, sí que se ha confirmado una tendencia a ocupar aquellos genes que requieren de este factor para su traducción.

En conclusión, esta tesis añade información sobre el factor de traducción eIF5A, incluyendo la regulación transcripcional de sus dos isoformas, nuevas dianas de traducción y una función nuclear. Así, se ha descrito una modulación plástica de las dos isoformas de eIF5A que permite responder a las demandas energéticas de la célula, y se ha determinado que eIF5A es necesario para producir proteínas con funciones esenciales en el metabolismo y otros procesos celulares. Más allá de la traducción, se ha encontrado una nueva función de eIF5A, la regulación de la transcripción, que permite controlar de forma precisa la síntesis de los mRNAs y la homeostasis de sus proteínas diana.

CONCLUSIONES

1. eIF5A hipusinado es esencial para la síntesis de colágeno, ya que es necesario para la traducción de motivos tripeptídicos enriquecidos en Pro-Gly presentes en su secuencia de aminoácidos. Además, eIF5A facilita la translocación cotraduccional del colágeno en el retículo endoplásmico.
2. El bloqueo de la actividad de eIF5A con el inhibidor GC7 reduce de forma considerable la producción de colágeno en células hepáticas estrelladas de humano tratadas con el activador profibrótico TGF-β1. De este modo, eIF5A surge como una diana potencial para el control de la producción excesiva de colágeno en enfermedades fibróticas.
3. El estado metabólico celular regula de manera opuesta la expresión génica de las dos isoformas de eIF5A a través de la señalización por TORC1 y de mecanismos mediados por Hap1. La isoforma Tif51A es esencial para la función mitocondrial y se regula de forma positiva para ser la forma abundante en condiciones respiratorias, mientras que Tif51B es la forma abundante en condiciones donde la respiración se encuentra inhibida.
4. Hap1 es el principal factor de transcripción que regula la expresión de los dos genes de eIF5A. Hap1 se une de forma constitutiva al promotor de *TIF51A* para activar su expresión en condiciones de respiración y para reprimirlo, mediante el reclutamiento de los correpresores Tup1/Ssn6, cuando la respiración está inhibida. Hap1 regula de forma indirecta *TIF51B,* mediante la activación directa de los represores *ROX1* y *MOT3,* en condiciones de respiración. Cuando la respiración está inhibida, Hap1 reprime a *ROX1* y *MOT3* usando el correpresor Tup1 y así, la expresión de *TIF51B* se activa.
5. eIF5A controla la actividad mitocondrial a través de su efecto en el importe de proteínas mitocondriales mediante la regulación de la traducción de Tim50 y del estado funcional del complejo Tim23. En condiciones de deficiencia de eIF5A, este complejo translocasa se atasca y los precursores mitocondriales no importados agregan en el citosol.
6. La traducción de las proteínas mitocondriales se reduce cuando los niveles de eIF5A son bajos. Esta bajada general de traducción sugiere un mecanismo que conecta la traducción con el importe de las proteínas correspondientes a la mitocondria.

7. eIF5A se localiza en el núcleo donde se une a la cromatina para atenuar la transcripción de genes que codifican tripéptidos dependientes de eIF5A. Cuando eIF5A se inactiva, la transcripción de estos genes cuya traducción dependen de eIF5A, aumenta. Por tanto, eIF5A funciona como una proteína en el citoplasma y en el núcleo para controlar de forma precisa los niveles de proteína de sus genes diana.